



# Università degli Studi di Ferrara

DOTTORATO DI RICERCA IN  
"SCIENZE e TECNOLOGIE per l'ARCHEOLOGIA e i BENI CULTURALI"

CICLO XXIII

COORDINATORE Prof. Carlo Peretto

## Non-invasive spectroscopic study of 19<sup>th</sup> century artists' materials

Settore Scientifico Disciplinare FIS/01

**Dottorando**

Dott. [Lara Boselli](#)

---

(firma)

**Tutore**

Prof. [Ferruccio Petrucci](#)

---

(firma)

**Co-tutore**

Prof. [Marcello Picollo](#)

---

(firma)

Anni 2008/2010

---

Corso di Dottorato in convenzione con



UNIVERSITA'  
DEGLI STUDI  
DI  
SIENA



UNIVERSITÀ DEGLI STUDI  
DI MODENA E REGGIO EMILIA

Borsa di studio finanziata da:  
Università degli Studi di Ferrara

# TABLE OF CONTENTS

<b>INTRODUCTION</b>	<b>1</b>
<b>CHAPTER 1</b>	<b>3</b>
<b>UV-VIS-NIR SPECTROSCOPY</b>	<b>3</b>
<b>1.1- RADIATION-MATTER INTERACTION</b>	<b>7</b>
1.1.1- ABSORPTION	7
1.1.2- TRANSMISSION	8
1.1.3- REFLECTION	9
1.1.4- REFRACTION	9
<b>1.2- THE KUBELKA-MUNK THEORY</b>	<b>10</b>
<b>1.3- ELECTRON SPECTROSCOPY</b>	<b>12</b>
1.3.1- TRANSITION BETWEEN DELOCALISED MOLECULAR ORBITALS	12
1.3.2- CHARGE-TRANSFER TRANSITIONS	14
1.3.3- LIGAND FIELD TRANSITION (D-D)	15
1.3.4- BAND-BAND TRANSITIONS	16
<b>1.4- UV-VIS-NIR FORS</b>	<b>16</b>
<b>1.5- MULTISPECTRAL IMAGE REFLECTANCE SPECTROSCOPY</b>	<b>19</b>
REFERENCES	23
<b>CHAPTER 2</b>	<b>25</b>
<b>INSTRUMENTAL SET-UP</b>	<b>25</b>
<b>2.1- ZEISS SPECTROANALYSERS</b>	<b>27</b>
<b>2.2- SPECTROPHOTOMETER BENCH (PERKIN ELMER <math>\lambda</math> 1050)</b>	<b>29</b>
<b>2.3- HYPERSPECTRAL SCANNER</b>	<b>30</b>
REFERENCES	33
<b>CHAPTER 3</b>	<b>35</b>
<b>SPECTROSCOPIC ANALYSIS OF MACCHIAIOLI PAINTINGS</b>	<b>35</b>
<b>3.1- THE MACCHIAIOLI AND THE MACCHIA</b>	<b>37</b>
<b>3.2- FEDERICO ZANDOMENEGHI (VENICE, 1841 – PARIS, 1917)</b>	<b>38</b>
3.2.1- BASTIMENTO ALLO SCALO	39
3.2.2- RITRATTO DI DIEGO MARTELLI ALLO SCRITTOIO	45
3.2.3- LUNA DI MIELE	50
3.2.4- A LETTO	60
<b>3.3- SILVESTRO LEGA (MODIGLIANA, 1826 – FLORENCE, 1895)</b>	<b>74</b>
3.3.1- PASSEGGIATA IN GIARDINO	75
<b>3.4- CONCLUSIONS</b>	<b>85</b>
REFERENCES	87

<b>CHAPTER 4</b>	<b>89</b>
<b>NON-INVASIVE SPECTROSCOPIC ANALYSIS OF GREEN PIGMENTS</b>	<b>89</b>
<b>4.1- ANALYSIS AND SPECTROSCOPIC CHARACTERIZATION OF REFLECTANCE SPECTRA OF GREEN PIGMENT</b>	<b>90</b>
4.1.1- CANVAS	92
4.1.2- VIRIDIAN	94
4.1.3- CHROMIUM OXIDE	95
4.1.4- COBALT GREEN	96
4.1.5- CINNABAR GREEN	97
4.1.6- MALACHITE	98
4.1.7- VERDIGRIS	99
4.1.8- SCHWEINFURT GREEN	100
4.1.9- ULTRAMARINE GREEN	101
<b>4.2- COMPARISON OF GREEN PIGMENTS</b>	<b>102</b>
<b>4.3- GREEN PIGMENTS IN MIXTURES</b>	<b>105</b>
4.3.1- MALACHITE AND VERDIGRIS	106
4.3.2- CHROMIUM OXIDE GREEN	117
<b>CONCLUSIONS</b>	<b>128</b>
REFERENCES	132
<b>CHAPTER 5</b>	<b>133</b>
<b>SPECTROSCOPIC ANALYSIS OF 19<sup>TH</sup> CENTURY WINSOR &amp; NEWTON WATERCOLOURS</b>	<b>133</b>
<b>5.1- BRIEF HISTORY OF WINSOR &amp; NEWTON WATERCOLOURS</b>	<b>135</b>
<b>5.2- FORS ANALYSIS</b>	<b>137</b>
<b>5.3- RESULTS</b>	<b>138</b>
<b>5.4- CONCLUSIONS</b>	<b>169</b>
REFERENCES	170
<b>CONCLUSIONS</b>	<b>173</b>
<b>ACKNOWLEDGMENTS</b>	<b>175</b>

# Introduction

In recent years, several studies have been conducted on 19<sup>th</sup> century works of art mainly from a cognitive or conservation point of view. Paintings of that period were usually made with new, as opposed to non traditional, pigments, a result of the fast development of chemical manufacturing processes. As a consequence, it can be particularly difficult to retrieve information needed to plan effective interventions for the proper conservation of these objects due to the lack of knowledge of the original materials used. The goal of this thesis is to provide information on 19<sup>th</sup> century painting materials, mainly pigments and dyes, through the spectroscopic study of works of art, by analysing laboratory mock-ups expressly prepared, and by analysing original pigments (in this specific case watercolours). The investigation of works of art and precious objects often present problems due to necessity of non destructive examination techniques. However, noninvasive analysis usually provides less information than that achievable by sampling. In order to improve the results obtainable with noninvasive investigations, a multidisciplinary approach based on the data's complementarities must be developed. In this thesis, point by point spectroscopic information using Fibre Optics Reflectance Spectroscopy (FORS) was integrated with High Hyperspectral Image Spectroscopy (HHIS) and, in a few selected cases, X-ray Fluorescence (XRF) spectroscopy, to better frame the case studies. The present work can be divided into two main sections:

- 1) introduction about spectroscopy and description of the instrumental set-ups (Chapters 1 and 2);
- 2) FORS results obtained on different case studies of 19<sup>th</sup> century objects and painting materials:
  - a) a selection of paintings from the Galleria d'arte moderna of Florence in Palazzo Pitti (Chapter 3);
  - b) a green pigment database (Chapter 4);
  - c) Winsor & Newton watercolour database (Chapter 5).

The analysis of the Winsor & Newton watercolours would not have been possible without the courtesy of the Victoria & Albert Museum, London, UK.

The present thesis was possible thanks to a mutual collaboration between the University of Ferrara and the "Nello Carrara" Institute of Applied Physics of the National Research Council (IFAC-CNR, Florence).



## **Chapter 1**

### **UV-Vis-NIR Spectroscopy**

Spectroscopy was originally the study of the interaction between radiation and matter as a function of wavelength. This science was born when Isaac Newton performed his experiment using visible light dispersed by a triangular glass prism. Subsequently, the concept of spectroscopy was expanded to include any measurement of a quantity as a function of wavelength.

In the case of artists' materials, the first spectrophotometric studies were conducted in 1938 by N.F. Barnes, who wanted to characterise many artists' pigments by means of their spectral features and colorimetric values [1]. Around the same time, F. I. G. Rawlins, the first scientific adviser at the National Gallery in London, UK, performed visible spectrophotometric measurements on paintings, in order to verify variations in colour of the paint layer [2]. The first infrared (IR) spectroscopic analysis of materials of interest for fine arts can be traced back to J. M. Hunt in his 1950s studies [3], while the first reference in the literature is attributed to Feller, Abrahams and Edelstein, Gettens and Stout, Afremow and Vandenberg in the 1960s.

Spectroscopy describes the interaction between radiation and matter. Before delving into the details of spectroscopic techniques, it is necessary to define what radiation is, introducing two theoretical models: in the first one radiation is described as a wave, while in the second radiation is a fast-moving particle. This dichotomy or dual behaviour is generally referred to as wave-corpucle duality [4, 5].

In the wave model formulated by Maxwell, radiations are described as electromagnetic waves made up of electric and magnetic fields, perpendicular but in phase with one another and perpendicular to the direction of the energy propagation. The electromagnetic waves are characterised by the wavelength ( $\lambda$ ), the peak-to-peak distance in the wave, and by the frequency: the number of occurrences of a repeating

point of the wave per unit time or the number of cycles of oscillation the wave completes per second ( $\nu$ ).

The velocity ( $c$ ) of a wave is calculated using the formula

$$c = \lambda \nu$$

where  $c$  is a physical constant used to indicate the speed of light in a vacuum and its value is 299.792.458 meters per second.

In the corpuscle (or particle) model formulated by Einstein in an attempt to explain the photoelectric effect, radiation is formed by small energy “quanta”, called *photons*, that possess energy and momentum in discrete packets. The energy ( $E$ ) of the emitted radiation is calculated using the formula

$$E = h\nu$$

where  $h$  is Planck’s constant. The measurement unity of Planck’s constant is an energy multiplied by time. In the International System of Units, Planck’s constant is expressed in joule seconds ( $J\cdot s$ ) and its value is  $6.626 \times 10^{-34} J\cdot s$ .

The modern theory combines the electromagnetic theory introduced by Maxwell with the corpuscular theory of Einstein: the link between these two model lies in Planck’s fundamental postulate of quantum theory expressed in the previous formula. In fact  $E = h\nu$  means that the energy of photons is directly proportional to the frequency and inversely proportional to the wavelength, and

$$E = hc/\lambda$$

the frequency determines the wavelengths, so that different energies can be expressed in terms of wavelengths; from Plank’s equation, the energy of quanta is a function of the wavelength as well, because the energy of quanta depends on the frequency.

Depending on the subject matter, it is more appropriate to use one model instead of the other: for example, topics such as polarisation and interference are explained using the wave model, while photochemistry requires the corpuscle model.

Electromagnetic waves are classified by frequency (Hertz,  $\text{sec}^{-1}$ ) as: radio waves, microwaves, infrared radiation, visible light, ultraviolet radiation, X-rays and gamma rays. The whole of these radiations constitutes the electromagnetic spectrum (Figure 1).

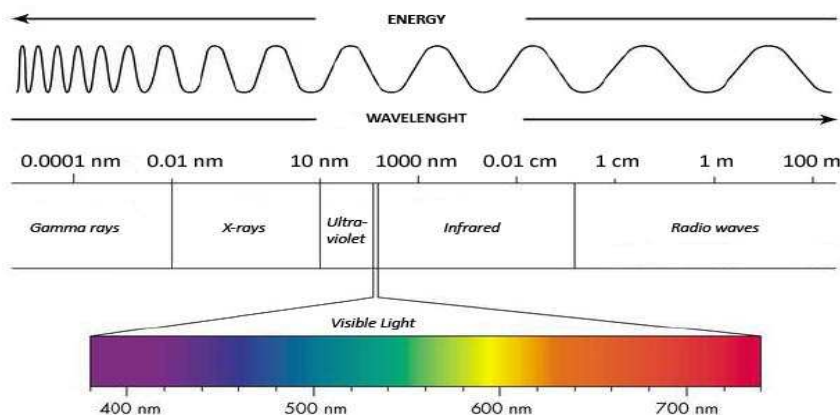


Figure 1: Electromagnetic spectrum with the spectral regions and the corresponding wavelengths (energies). Visible range was expanded for further detail (image from <http://www.antonine-education.co.uk>).



This chapter will be focused on ultraviolet, visible and infrared radiation, because this is the spectral range used for the analysis performed in the present work.

Ultraviolet (UV) radiation (10-380 nm) can be subdivided into: 10-180 nm or vacuum ultraviolet; 180-280 nm or far-ultraviolet (UVC); 280-300 nm or middle-ultraviolet (UVB); 300-380 nm or long-ultraviolet (UVA) (Table 1). UV radiation in the 200-380 nm range can cause photochemical reactions and bond ruptures in organic compounds; this may result in, for example, fading of paint layers. However, UV radiation is widely used in the conservation field. UV-induced luminescence is commonly used to characterise, for example, the presence of varnish layers and, in specific conditions, highlight recent retouches [6, 7].

Visible (Vis) radiation (380 nm to 780 nm) is defined as the radiation that can be perceived by the retina of the human eye. The radiation-retina interaction involves the human brain and determines the sensation called 'colour'. A spectral colour is a colour that can be produced by visible light of a single frequency. Therefore, every wavelength of light is perceived as a spectral colour, in a continuous spectrum with no clear boundaries between one colour and the next [8]. Keeping in mind that any division is arbitrary, spectral ranges may be used as an approximation in order to classify spectral colours (Table 1). Starting from short wavelengths to long wavelengths, the succession is violet, indigo, blue, green, yellow, orange and red and may be seen by just letting solar light pass through a prism. This phenomenon is known as light dispersion and was discovered by Newton in 1672. Newton's experiment shows that, except for the empty space, light does not travel at the same velocity for all the wavelengths and therefore a separation occurs. As it is possible to see from Figure 2 the red light, characterised by the longest wavelength, has the greatest velocity and least dispersion, while the opposite is true for violet light [5, 6].

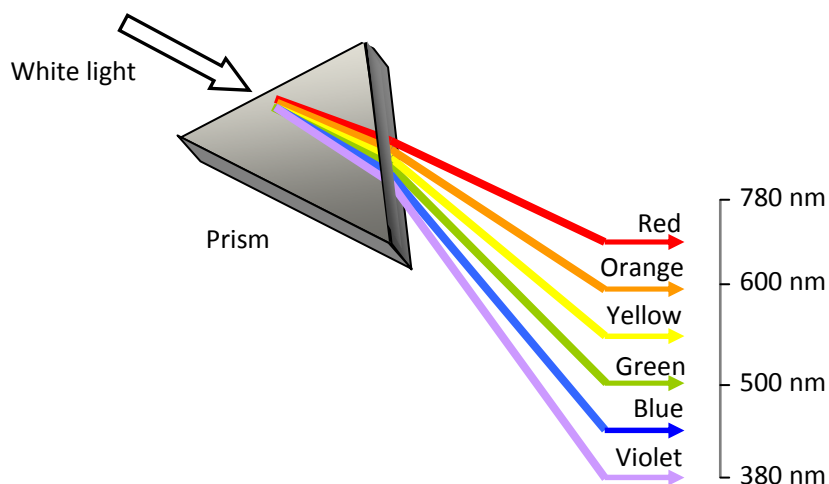


Figure 2 : Visible range expanded for further detail. For the colours the corresponding wavelengths are reported.

IR radiation is usually divided into three sub-categories (Table 1) and the International Organization for Standardization (ISO) recommends the following division of IR radiation [9]: Near Infrared (NIR) from 0.78  $\mu\text{m}$  to 3  $\mu\text{m}$  (780 nm – 3000 nm), Mid Infrared (MIR) from 3  $\mu\text{m}$  to 50  $\mu\text{m}$  (3000 nm – 50,000 nm) and Far Infrared (FAR) from 50  $\mu\text{m}$  to 1000  $\mu\text{m}$  (50,000 nm – 1 mm). This kind of division is usually made on the

basis of the working range of infrared detectors; other distinctions concern radiation properties, for example NIR radiation is known to be the range of electronic transitions and combination/overtone vibrational transitions.

A commonly used sub-division scheme is also reported [10]: NIR from 0.75  $\mu\text{m}$  to 1.4  $\mu\text{m}$ , mainly used in fiber optic-telecommunication because of low attenuation losses in the SiO<sub>2</sub> glass (silica) medium; Short-Wavelength Infrared (SWIR) from 1.4  $\mu\text{m}$  to 3  $\mu\text{m}$ ; Mid-Wavelength Infrared (MWIR) also called Intermediate Infrared (IIR) from 3  $\mu\text{m}$  to 8  $\mu\text{m}$ ; Long-Wavelength Infrared (LWIR) from 8  $\mu\text{m}$  to 15  $\mu\text{m}$  and Far Infrared (FIR) from 15  $\mu\text{m}$  to 1000  $\mu\text{m}$ . NIR and SWIR are sometimes called "reflected infrared" while MWIR and LWIR are sometimes referred to as "thermal infrared." In fact LWIR is also defined as the "thermal imaging" region, in which sensors can obtain a passive picture of objects based on thermal emissions only and requiring no external light or thermal source.

In this thesis the chemical division of Infrared was taken into account, where the NIR is from about 780 nm to 2500 nm, while the MIR is from 2.5  $\mu\text{m}$  to 25  $\mu\text{m}$  (or 4000-400  $\text{cm}^{-1}$ ). In the MIR particularly attention is usually paid to a well-defined spectral region called the 'fingerprint' region (1500-500  $\text{cm}^{-1}$ ), because the spectra acquired in this range are typical for each compound.

UV-Vis-IR spectral ranges		Type of radiation
UV radiation (10-380 nm)	10-180 nm	Vacuum UV
	180-280 nm	Far-ultraviolet (UVc)
	280-300 nm	Middle-ultraviolet (UVb)
	300-380 nm	Long-ultraviolet (UVa).
Visible radiation (380-760 nm)	380-430 nm	Violet
	430-490 nm	Blue
	490-560 nm	Green
	560-580 nm	Yellow
	580-620 nm	Orange
	620-760 nm	Red
IR radiation (780 nm – 1 mm)	780-3000 nm	Near Infrared (NIR)
	3000-50,000 nm	Middle Infrared (MIR)
	50,000 nm – 1 mm	Far Infrared (FIR)

Table 1: A subdivision proposed for the UV-Vis-IR spectral ranges in the corresponding type of radiation.

### 1.1- Radiation-matter interaction

When UV-Vis-NIR radiation enters in contact with an interface (matter), three kinds of interactions can be observed: (1) the total or partial absorption of the radiation by the object, (2) the reflection and/or scattering of the radiation from the surface and (3) the transmission and/or refraction of the radiation.

As energy is conserved, the sum of the intensity of radiation involved in these three phenomena must be equal to the intensity of the incident radiation. While interactions 1 and 2 depend on the surface characteristics, the composition of the incident beam and the chemical composition of the material, interaction 3 is strictly linked to the transparency of the sample investigated, which depends upon the composition, the concentration and the absorption coefficient of the material.

If it is assumed that the refraction is a phenomenon not relevant, transmission, absorption, and reflection due to the varnish and the pictorial layers influence the final behaviour of the painting surface, at various wavelengths [6]. In Figure 3 all the phenomena previously listed are represented and some theoretical information will be given in the following paragraphs

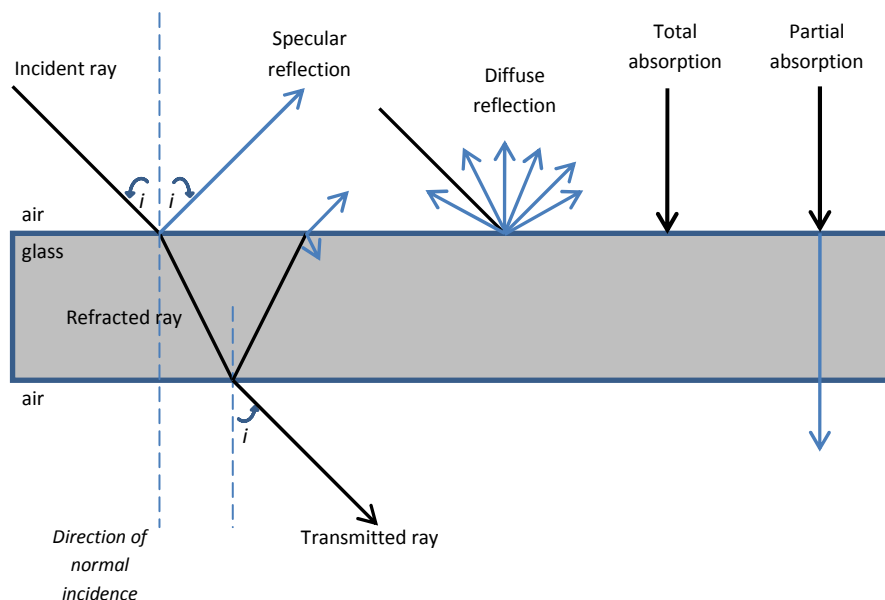


Figure 3: A pictorial summary of the radiation-matter interactions.

#### 1.1.1- Absorption

The energy of a molecule is calculated by its movement through space (translational energy), its rotatory motion (rotational energy), the oscillatory movements of atoms with respect to each other (vibrational energy), and the distribution of its electron density. This last energy and the vibrational energy as combinations or overtones of fundamental vibrations are those investigated in UV-Vis-NIR spectral range.

The phenomenon of absorption happens when the electromagnetic field of the incident beam induces a transition between two different energy levels of the molecules or ions constituting the material [11]. In the UV-Vis-NIR region this happens when the radiation causes a variation in the electron density distribution within the molecules [12] and transitions between different electronic levels can be observed. Vibrational

transition can be also observed as *overtones* and combinations of the fundamental absorptions in the NIR range [11].

In general, the radiation absorbed by the matter has a frequency that corresponds to the energy gap between two discrete atomic or molecular energy levels, as expressed by Bohr's law

$$\Delta E = E_2 - E_1 = h\nu = \frac{hc}{\lambda}$$

Bohr's law is a relation between the energetic atomic or molecular levels involved and the energy of the incident beam.

When absorption occurs the matter becomes 'excited'. This condition is not permanent and the substance will come back to its initial equilibrium by means of deactivation processes. Depending on the molecular environment and pathways of deactivation, the excited states can exist for  $10^{-13}$  to  $10^{-3}$  seconds [12].

### 1.1.2- Transmission

Radiation transmission is calculated by the amount of incident radiation that passes through a material. When a monochromatic radiation incident to the surface at  $i=0^\circ$  interacts penetrating in a homogeneous medium, an attenuation of the transmitted radiation occurs. The transmittance ( $T$ ), or the ratio between the transmitted radiation ( $I$ ) and the incident radiation ( $I_0$ ), is relative to the absorption coefficient of the substance  $\alpha$  and the dimension of the sample (path length)  $\ell$ . The absorption coefficient is the product of both the molar absorptivity of a sample  $\varepsilon$  and the concentration of absorbing species in the material  $c$ .

All these parameters are linked to each other by the Lambert-Beer Law:

$$T = \frac{I}{I_0} = 10^{-\alpha\ell} = 10^{-\varepsilon\ell c}$$

$$\text{Log}T = \log \frac{I}{I_0} = -\varepsilon\ell c$$

and if transmittance is expressed in terms of absorbance ( $A$ ), it is possible to obtain a linear dependence among absorbance, and the parameters  $\varepsilon$ ,  $\ell$  and  $c$ .

$$A = -\log \frac{I}{I_0} = \log \left( \frac{I_0}{I} \right) = \varepsilon\ell c$$

As a consequence, if the path length and the molar absorptivity are known and the absorbance is measured, the concentration of the substance (or the number density of absorption centres) can be deduced.

### 1.1.3- Reflection

If the frequency of incident radiation does not coincide with the energy difference between two electronic levels no absorption can be observed but reflection and refraction can.

The reflection is defined as specular if the reflected beam creates an angle with the normal surface equal to the incident angle. The volume reflection is the radiation that penetrates into the material, interacts with it, and finally resurfaces (Figure 4). Because of this interaction with the matter, the volume reflection 'contains' the most information about the surface material and it is the most interesting to analyse from a spectroscopic point of view. This reflection is diffuse because there are multiple reflected beams forming different angles with the normal: in this case there is not a preferential direction of reflection (scattering). It is then possible to summarise that specular reflection is due to superficial smoothness, while diffuse reflection is typical of rough surfaces (such as clothing or papers). It is also important to explain that diffuse reflection is a function of the wavelength of the radiation used and it depends on the average granulometry of the pigment.

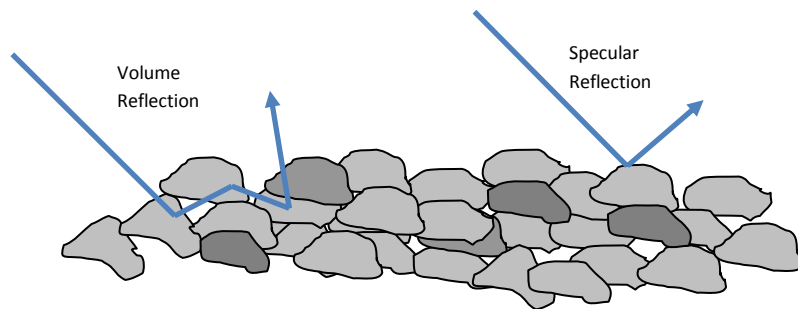


Figure 4: A pictorial summary of different types of reflection.

### 1.1.4- Refraction

When an incident beam moves from one medium, characterised by a refractive index  $n_1$ , to another medium with refractive index  $n_2$ , both reflection and refraction of the light may occur (Figure 5).

The refraction index of a substance is a measure of the velocity of a selected wavelength radiation in that substance and it is expressed as a ratio of the speed of light in a vacuum relative to that in the considered medium or as a ratio between the incident angle  $\sin$  and the refraction angle  $\sin$  [5, 6].

$$n_r = \frac{\sin \theta_i}{\sin \theta_t} = \frac{v_i}{v_t}$$

The fraction of the incident radiation reflected from the interface is given by the reflectance  $R$  (%) and is formulated using the Fresnel equation. If the incident beam is normal to the surface and the medium 1 is transparent, the reflectance for each wavelength is calculated by:

$$R = \frac{R_r}{R_i} = \left[ \frac{n_2 - n_1}{n_2 + n_1} \right]^2$$

If the medium 1 is air the refraction index begins at 1 and the Fresnel equation is:

$$R = \frac{R_r}{R_i} = \left[ \frac{n_2 - 1}{n_2 + 1} \right]^2$$

Materials with a high refractive index are more opaque than materials with a low refractive index.

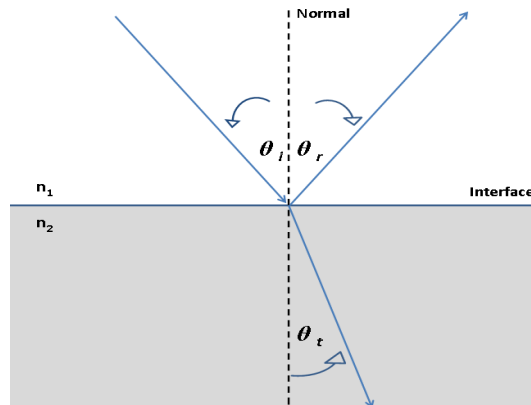


Figure 5: A pictorial summary of the refraction, with  $n_2 > n_1$ .

The radiation beam that enters a transparent/semitransparent material with a refractive index higher than the first medium will follow the reflection laws when it is inside the material. If this radiation strikes the interface with an angle to the normal greater than  $\theta_c$ , the *critical angle of incidence*, it is reflected back into the material without the possibility of escaping. This phenomenon is called *total internal reflection* and the critical angle is the angle of incidence above which total internal reflection occurs. The angle of incidence is measured with respect to the normal at the refractive boundary. The critical angle is given by the relation:

$$\sin \theta_c = \frac{n_1}{n_2} = \arcsin \left( \frac{n_1}{n_2} \right)$$

where  $n_1$  is the refractive index of the less optically dense medium, and  $n_2$  is the refractive index of the more optically dense medium. If the incident ray is precisely at the critical angle, the refracted ray is tangent to the interface at the point of incidence. For example, in a glass-air interface, with the refractive index of glass at 1.50 and the refractive index of air at 1.00, the calculation would result in the critical angle for light from glass into air, which is  $41.8^\circ$ .

## 1.2- The Kubelka-Munk theory

The Kubelka-Munk (K-M) theory (1931) [13] and its modifications [14], provides a good and simple approach to spectroscopy of an opaque material because they are based on single absorption and scattering coefficients. The basic assumptions of this theory are that radiation that interacts with the matter could be just scattered or absorbed and the spectral behaviour of the sample depends upon the wavelength of the incident radiation. The scattering and absorbing material should be homogeneous with an infinite thickness. A paint layer, for example, could be a good example because even if its thickness is not infinite, it is possible to assume that it is not transparent in the visible range. Thus, the radiation that interacts with the surface can be just scattered or absorbed.

When a layer of the absorbing and scattering material is so thick that no radiation penetrates through the layer the relationship given by Kubelka-Munk (K-M) for each wavelength is:

$$F(R_\infty) = \frac{(1 - R_\infty)^2}{2R_\infty} = \frac{K}{S} \quad \text{and} \quad R_\infty = 1 + \left(\frac{K}{S}\right) - \sqrt{\frac{K^2}{S^2} + 1}$$

Where  $R_\infty$  is the reflectance for a material with infinite thickness,  $K$  is the absorption coefficient and  $S$  is the scattering coefficient.

The simple K-M theory can be applied to materials that are completely opaque, when a pigmented material is transparent, other forms of the K-M must be used that take into account the colour of the background.

In this simple equation it is possible to see that changing just one of the coefficients causes the reflectance of the sample to increase or decrease (Figure 6), so if  $K$  increases  $R$  decreases and vice versa if  $S$  increases  $R$  increases as well [15, 16].

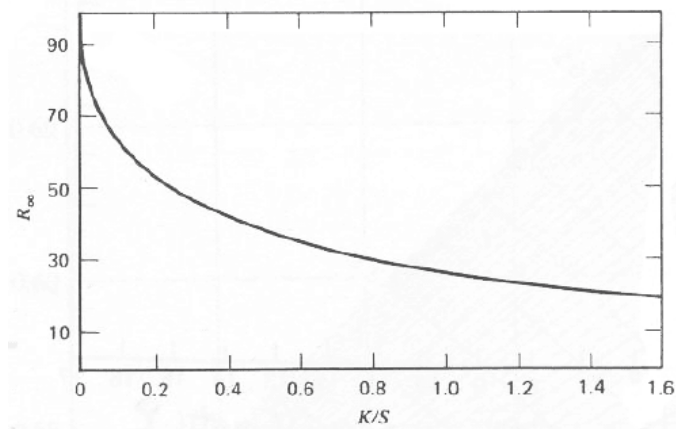


Figure 6: Theoretical plot showing inverse relationship between reflectivity  $R$  and the ratio  $K/S$  (Image from [16]).

In 1962 Duncan demonstrated that the absorption-scattering ratio of a system made as a mixture of pigments  $m$  is given by the additivity of the individual contributions of absorption and scattering from each pigment present at each wavelength [17]:

$$F(R_\infty)_m = \left[ \frac{(1 - R_\infty)^2}{2R_\infty} \right]_m = \left( \frac{K}{S} \right)_m = \frac{C_1 K_1 + C_2 K_2 + \dots + C_n K_n}{C_1 S_1 + C_2 S_2 + \dots + C_n S_n}$$

$C$  indicates the relative fraction concentration for each pigment ( $n$ ), the subscript number indicates the single pigment present in the mixture and  $K$  and  $S$  are the coefficients for unit concentration. This formula is widely used in pigment and varnish industrial manufacturing in order to predict the colour of a mixture. This means that the reflectance spectrum measured on a painting layer depends on the number of pigments and their concentration in the point analysed.

### 1.3- Electron Spectroscopy

UV-Vis-NIR spectroscopy mainly concerns the study of transitions that involve electronic states [12]. An electron is excited when the frequency of the incident radiation is equal to the energy difference between two electronic states. This energy difference depends on the specific molecule and its environment.

In the next paragraphs transitions concerning dyes, organic and inorganic pigments will be discussed: transition between delocalised molecular orbitals (MO), charge-transfer transition, ligand field transition and energy band transition.

In order for a transition to occur, some rules have to be respected:

*-The Laporte selection rule:* since transitions occur thanks to an interaction between the electric field of the radiation (energy) and the dipole moment of the atom or the molecule involved, it requires that the two states involved have a symmetric and antisymmetric wave function, respectively. In other words, electronic transitions conserving either symmetry or asymmetry with respect to an inversion centre are forbidden. La Porte selection rule may be expressed in the formula  $\Delta l = \pm 1$ , where  $l$  is the orbital angular momentum quantum number. If  $s$  and  $d$  are centrosymmetric orbitals while  $p$  and  $f$  are antisymmetric, then electronic transition between  $s$  and  $p$  and  $p$  and  $d$  are allowed while transitions between  $d$  and  $s$  orbitals and between two different  $d$  orbitals are forbidden [18].

*-Spin-forbidden selection rule:* allowed transitions must involve the promotion of electrons without a change in their spin.

However, forbidden transition can take place because of the electromagnetic spin interactions due to the presence of close cations in the lattice. On the basis of these rules, the intensity of the absorption band can vary: for example spin and Laporte-forbidden transitions have a lower molar extinction coefficient (from  $10^3$  to  $10$ ) than spin and Laporte-allowed transitions (from  $10^2$  to  $10^5$ ) [19].

#### 1.3.1- Transition between delocalised Molecular Orbitals

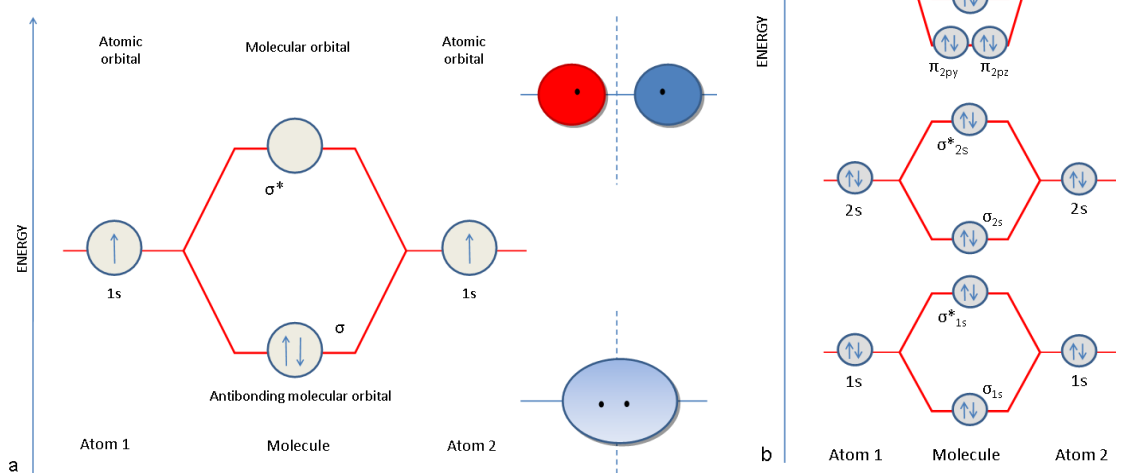
Before discussing these transitions, some details about Molecular Orbitals (MO) will be introduced, such as bonding and antibonding orbitals. Taking into account the example of the hydrogen molecule, the two atomic orbitals of the atoms 1 and 2, each with just one electron, will combine in order to form two molecular orbitals (Figure 7-a). When isolated, the atoms have identical energy levels. However, as the spacing between the two atoms becomes smaller the electron, wave functions (atomic orbitals) begin to overlap. Owing to this interaction two molecular orbitals at different energies are created: The first orbital is lower in energy than the original atomic orbitals of the separate atoms so it is more stable and promotes the bonding of the two H atoms into  $H_2$ . In fact, the two  $1s$  electrons are shared by the two atoms and, therefore, the molecule is more stable than the separate H atoms. According to the Pauli principle, since no two electrons in an interacting system may have the same quantum state, the two electrons must have opposite spin or, in other terms, a spin paired state occurs. This is the bonding orbital ( $\sigma$ ). The second orbital is higher in energy than the original atomic orbitals and is less stable, and therefore opposes the bonding. For this reason it is called antibonding orbital and is usually labelled with an asterisk ( $\sigma^*$ ). By a



symmetry point of view ( $\sigma$ ) bonds occur when the region of overlap is a figure of revolution about the line between the two nuclei (Figure 7-a) [20].

Instead, the term  $\pi$  bond applies to a bonding overlap where there is a node along the bonding axis (*i.e.* the electron density is zero along the axis connecting the two atoms). To clarify the matter the interaction between atomic  $p$  orbitals in the oxygen molecule ( $O_2$ ) is considered (Figure 7-b). In this case,  $\sigma$ -bonding and  $\sigma$ -antibonding molecular orbitals ( $\sigma_{1s}$ ,  $\sigma_{1s}^*$ ,  $\sigma_{2s}$ , and  $\sigma_{2s}^*$ ) are formed by their  $s$  orbitals as shown in Figure 7. It is also possible for a  $p$  orbital on each atom to interact producing a pair of  $\sigma_{2p}$ -bonding and  $\sigma_{2p}$ -antibonding orbitals. Each atom has still available two  $p$  orbitals perpendicular to the  $\sigma$  bond connecting the oxygen atoms. These  $p$  orbitals can interact laterally in order to give two  $\pi$ -bonding molecular orbitals ( $\pi_{2py}$  and  $\pi_{2pz}$ ) and  $\pi$ -antibonding ( $\pi_{2py}^*$  and  $\pi_{2pz}^*$ ) (Figure 7-b) [20].

Figure 7: Electronic energy levels in ground and excited states. This scheme is used in order to explain the meaning of bonding and antibonding  $\sigma$  and  $\pi$  orbitals by means of Pauli exclusion Principle. In the first example (a) two hydrogen atoms are taken into account, while in the second it was considered the oxygen molecule (b).



Transitions between delocalised molecular orbitals are typical of organic pigments and dyes. In order to be coloured, organic molecules must contain specific groups: for instance a chromophore and an auxochrome group divided by a polyene. The chromophore is an organic functional group (nitro-, nitroso-, azo- and carbonyl-groups) that has an electron-acceptor function. Molecules having these groups are called chromogens because they can develop a colour even if they are not themselves intensely coloured [6,7].

In order to develop colour, the presence of an auxochrome group is necessary, as is an electron-donor group, typically a polar group, which does not produce colour by itself but is capable of increasing the intensity of a colour. For example, the auxochrome group can produce a hypsochromic effect (a shift of the absorption band toward a shorter wavelength), a bathochromic effect (a shift of the absorption band toward a longer wavelength), a hyperchromic effect (an increase of the colour intensity) or a hypochromic effect (a decrease of the colour intensity) [7]. Chromophore and auxochrome groups are linked in the same

molecule by a polyene system, which is a conjugated system of double or triple bonds, where single bonds are alternated by double or triple bonds connected in an unsaturated chain or a ring of carbon atoms. Saturated organic hydrocarbons contain no double or triple bonds and are not able to absorb energy in the visible range, so they cannot produce colour.

The absorption bands in unsaturated hydrocarbons are very broad and occur in near UV and visible ranges [11]. Compounds in which all the valency electrons are involved in  $\sigma$ -bond formation, such as the saturated hydrocarbons, only show absorption due to excitation of an electron to a  $\sigma^*$ -antibonding or higher orbital ( $\sigma \rightarrow \sigma^*$ ).

Compounds containing an atom with a lone pair of electrons (O; N or S) not used in bonding can present  $n \rightarrow \pi^*$  transitions that cause absorption bands at longer wavelengths than those linked with  $\sigma \rightarrow \sigma^*$ . Finally  $\pi \rightarrow \pi^*$  transitions occur in molecules containing double bonds in which there is overlap of p-orbitals causing formation of  $\pi$ -bonds. The overlap of the p-orbitals is not so great as in  $\sigma$ -bonding so the  $\pi \rightarrow \pi^*$  transitions generally happen at intermediate energy between  $\sigma \rightarrow \sigma^*$  and  $n \rightarrow \pi^*$  transitions [21] at about 330 nm [6].

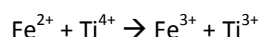
### 1.3.2- Charge-transfer transitions

Charge-transfer transitions occur between molecular orbitals located in different positions of the molecule or crystal. This means that during the transition a real transfer of electrons happens [11]. This process can produce strong energy absorptions because the transitions are allowed by the selection rules.

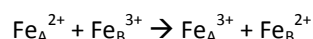
Depending on the nature of atoms/atomic groups involved, it is possible to classify charge-transfer transition in different categories:

*-heteronuclear intervalence charge transfer*, when the transition happens between two different metals [7].

For example, in the blue sapphire gem ( $\text{Al}_2\text{O}_3$ ), two close  $\text{Al}^{3+}$  ions are substituted by  $\text{Fe}^{2+}$  and  $\text{Ti}^{4+}$  ions. The deep gem coloration is due to the charge transfer from iron to titanium [11]. This kind of process could be read like a photochemical oxidation-reduction reaction:



*-homonuclear intervalence charge transfer*, when the transition happens between two atoms of the same element in different sites or valence states. The most common example is given by iron, present as  $\text{Fe}^{2+}$  and  $\text{Fe}^{3+}$ . If these two ions occupy adjacent identical sites in a crystal, then the charge transfer from  $\text{Fe}^{2+}$  to  $\text{Fe}^{3+}$  does not determine any change in the energy, since the final state would be the same as the initial state. So this process does not result from absorption of light. The other way round, if the two iron ions are located in different sites, then there will be an energy difference between the two arrangements [7]. In Prussian blue  $\text{Fe}_4[\text{Fe}(\text{CN})_6]_3 \cdot n\text{H}_2\text{O}$  the charge transfer occurs among two non equivalent iron ions both in octahedral sites [11].



The valence of the ions is due to the different environments: the  $\text{Fe}^{2+}$  ions are surrounded by six carbon ligands, belonging to  $\text{CN}^-$  cyanide groups, while the  $\text{Fe}^{3+}$  are surrounded by six carbon ligands ( $\text{CN}^-$  groups and oxygens of water molecules) [7].

-*metal/ligand charge transfer*, when the electronic transition occurs between a cation (metal) and a generic anion (ligand) or as it could be found in a chromate. In the chrome yellow  $\text{PbCrO}_4$  the group  $[\text{CrO}_4]^{2-}$  is made up of the cation  $\text{Cr}^{6+}$  and two anions  $\text{O}^{2-}$ . The  $\text{Cr}^{6+}$  is not favoured energetically, so more stable arrangements are obtained when electrons move from the oxygens thus determining the yellow colour of the pigment. For hematite  $\text{Fe}_2\text{O}_3$  the process involved is the same: the red colour of the mineral is due to the movement of electrons from  $\text{O}^{2-}$  to  $\text{Fe}^{3+}$  [7]. In both the cases analysed the electrons move from the ligands to the metal ( $\text{L} \rightarrow \text{M}$ ).

The inverse process ( $\text{M} \rightarrow \text{L}$ ), so the movement of electrons from the metal to the ligand is not so common but it can occur in specific substances, such as in  $\text{Fe}(\text{CO})_5$  where the low energy  $\pi$ -orbitals of the carbonyl can accept electron from the metal [7].

-*anion-anion charge transfer*, when the transition involves two anions. This process can be observed in ultramarine blue  $\text{Na}_{8-10}\text{Al}_6\text{Si}_6\text{O}_{24}\text{S}_{2-4}$  and it is responsible for the deep colour of the pigment. The transitions happen among the molecular orbitals of anions  $\text{S}_3^-$ , which has 19 outer electrons, causing the absorption of energy in the yellow region corresponding to 2.1 eV [7].

### 1.3.3- Ligand field transition (d-d)

Transition elements with unpaired electrons in  $d$  orbitals can absorb light by means of a process that involves levels localised mainly on metal ions. The metal ion is surrounded by ligands that produce a field able to act upon the central ion orbitals and the splitting of the  $d$  orbitals of the transition-metal ion can be caused [11]. The new arrangement of  $d$  orbitals will produce a shift in the energy levels of the individual orbitals. The size of the splitting is a measure of the magnitude of the field [7].

The energies of the radiation absorbed during these transitions depend on the number and symmetry of the ligands and the strength of the ligand field. In any case, since the ligand-field transitions are not allowed by the selection rules, the absorption bands are weak and the colour of the pigments used in these processes are normally pale [7]. Nevertheless, absorption intensities can be increased thanks to the coupling interactions with nearest-neighbour cations: for example in ferric oxide minerals the couple of  $\text{Fe}^{3+}$  ions ( $\text{Fe}^{3+} - \text{Fe}^{3+}$ ) has different selection rules from the isolated ions and the related transition may be present in the visible spectra region. The energy of spin-forbidden transitions can also be intensified by magnetic interactions with cations in adjacent sites or by cations occupying acentric coordination sites [19]. A typical  $d-d$  absorption is observed in chromium oxide  $\text{Cr}_2\text{O}_3$  where two absorption bands at 600 and 460 nm due to the Cr (III) ion in octahedral environment can be detected [11]. Also blue pigments containing Co(II) are characterised by  $d-d$  transitions that cause an absorption in the 550 nm – 650 nm range divided into three sub-bands. Moreover, depending on the behaviour of the spectra in the NIR region it is possible to identify the cobalt ion geometry. If three sub-bands in the 1200nm -1800 nm range are detected, the cobalt ion is in tetrahedral geometry as in Thénards blue  $\text{CoO Al}_2\text{O}_3$ ; if a single absorption band is detected around 860 nm the cobalt ion is in a octahedral geometry as in cobalt violet  $\text{Co}_3(\text{PO}_4)_2$  [22].

### **1.3.4- Band-band transitions**

Band-band transitions are observed in pigments constituted by semiconductors, such as cinnabar, cadmium yellow, minium, Naples yellow etc. In these systems, the molecular orbitals are displaced so close to one another that they create a continuum, an energy band. In conductor materials this band is partially filled with electrons and is called a conduction band. Semiconductors are characterised by two bands separated by an energy gap. The first band, at low energy, is filled and is called a valence band, the second band, displaced at high energy is the conduction band and it is empty. In such materials, a transition occurs when the energy absorbed coincides with the energy gap. The resulting reflectance spectrum is characterised by a typical 'S' shape, corresponding to the gap. The energy of the gap corresponds to the wavelengths absorbed and causes the specific colour. For example Zinc white (ZnO) has a band gap of 3.0 eV which determines the absorption of the UV component, while the visible light is reflected causing a white effect. Differently, cinnabar HgS, which has a 2.0 eV band gap, absorbs the violet-blue and green component resulting in a red colour. When the energy gap is less than the energy corresponding to the limit of the visible spectrum (700 nm, 1.77 eV), all the visible radiation is absorbed resulting in a black colour [7].

### **1.4- UV-Vis-NIR FORS**

UV-Vis-NIR FORS is a noninvasive methodology and a useful technique for analysing works of art. In this spectral range, electronic and vibrational transitions can be observed. In the latter case, the transitions are multiple or combinations of transitions that are commonly observed in the mid-IR [11].

FORS is primarily used in order to identify pigments and dyes [23, 24, 25, 26, 27], evaluate colour and colour changes [28, 29, 30], and to detect alteration products [31]. Depending on the instrumental set-up, these aims can be achieved with just a unique measurement. FORS can also be a very useful tool to inform a sampling strategy: when used in conjunction with imaging spectroscopy, it may aid in the location of micro-sampling areas, while, when extending local data to a broader scale it may help in reducing the extent of micro-sampling [32].

UV-Vis-NIR reflectance spectroscopy is based on the analysis of the radiation diffused by the surface when compared with a highly reflecting reference standard, such as Spectralon® or barium sulphate plates. The reflectance spectrum of the polychrome surface (painting) is reported as the percentage of reflected radiation versus the wavelength.

With specific reference to pigment identification, FORS can be applied mainly in order to identify inorganic materials, such as synthetic or natural compounds. The UV, Vis, NIR spectroscopic features can be due to numerous different processes, which have either electronic or vibrational origins and a transition between the electronic energy levels determines absorption bands in the UV, Vis and NIR regions. As reported in the previous paragraph, in inorganic pigments the absorption bands are mainly related to Ligand-Field, Charge Transfer, and Valence-Conduction band transitions. In many cases, the spectral features make it possible to identify the nature of the compounds analysed and, in detail, to recognise inorganic pigments. As a consequence, FORS can be applied also to discern pigments of the same colour, if characterised by specific

absorptions. For instance, by using FORS it is easy to distinguish between blue pigments, such as lapis lazuli and azurite. In fact the first pigment presents a strong absorption band at about 600 nm, as reported before, whereas azurite has a strong, broad, and structured electronic absorption band in the red-NIR region, and a characteristic absorption band at 1498 nm due to the first overtone of the OH<sup>-</sup> ion.

On the other hand, pigments having the same colour and characterised by strong absorption S-shaped bands are difficult to distinguish. In these cases, derivative spectroscopy can be of help for a correct assignment. For example, minium can be distinguished from vermilion and cadmium red thanks to a displacement of 20 nm in the positions of the inflection point [11]. However, vermilion and cadmium red cannot be distinguished, because their reflectance spectra match each other closely. Furthermore, pigments that do not exhibit characteristic absorptions, such as black pigments, are impossible to identify. FORS is also sensitive to dyes. Indeed, detection of dyes through other techniques, such as FTIR, is hampered by the typical low concentration of the dyestuff and by interference from the substrate or binder. To be economically convenient, a dye has to have a rather large extinction coefficient; that is it must impart a strong coloration, even when used in small quantities. UV-Vis-NIR spectroscopy, compared to other techniques, exploits the only physical property of the pigment not shared by extenders and binding media: its electronic spectrum which is the cause of colour [26, 27, 33].

FORS does not produce very accurate results when complex mixtures are investigated: in these cases, the position of the absorption bands may be shifted a few nanometres or be reduced in intensity (weakened). In addition, the effect of yellowing of the binder or of the varnish may significantly move their curves and inflection points, particularly when the pigments or dyes are present in low concentrations.

Although widely accepted by the scientific community, UV, Vis, and NIR reflectance techniques have so far had only limited use, in spite of their ability to identify pigments and dyes without sampling. A useful 'instrument' for pigment identification is to use a database of spectra of artist's materials for comparison. Indeed, the interpretation and/or identification of spectra are usually conducted by correlating the unknown data to a suitable spectroscopic database. These reference spectra must be acquired on mock-up paintings prepared following the techniques and pictorial materials used by artists as closely as possible. For instance, the database created and hosted by IFAC-CNR is a collection of reflectance spectra in the 270-820 nm, 350-1000 nm, and 980-1700 nm ranges. They were acquired from several paint layer structures that were built with materials selected from those most commonly used, both in the past and at present. This database is a part of the continuing collaboration between the Restoration Laboratory of the "Opificio delle Pietre Dure" and the Applied Spectroscopy Laboratory of IFAC-CNR [34].

FORS instrumentation includes spectrophotometers and spectroanalysers. Thanks to a spectroanalyser, the radiation can be sent to the sample by means of a fibre optic bundle. The backscattered light is then collected using fibre optics and is directed first to a dispersive element (grating) and subsequently to a suitable detector. The fibre optic bundles consist of two extended coaxial cylinders: the inner one ("core") has a high refractive index, while the exterior one ("cladding") has a lower refractive index. Light is reflected through the fibre optics because of the difference in the refractive index. The optical fibres are usually

coated for the sake of protection with a jacket of a non-optical material, such as metal or plastic. Fused silica fibres are able to transmit the entire range of UV-Vis-NIR [11]. A probe head connected to the fibre optics is placed on the painted surface. Depending on the design of the probe head, different geometries for illumination and acquisition can be used. One of the most widely used probe heads has three apertures on the dome of a hemisphere with a  $2 \times 45^\circ / 0^\circ$  geometry. This means that the probe has two apertures placed at a  $45^\circ$  angle symmetrically with respect to the vertical axis of the dome. They direct the radiation on the investigated area while the third one, positioned at the top of the dome, receives the back-scattered light from the sample. This configuration makes it possible to work in diffuse reflectance (by taking into consideration the radiation reflected by the surface in any direction) by collecting the light scattered at  $45^\circ$  with respect to the incident light, thus avoiding specular reflected light. This is the radiation that is reflected without interacting with the bulk of the material analysed, so it does not carry any information on chemical composition. The spot size can vary with the type of probe head. For instance, the probe head usually used at IFAC analyses an area of about 2 mm in diameter at a working distance of approximately 4.5 mm from the surface.

The depth of penetration of the radiation into the painted layers is related to several factors, and depends on the material's chemical composition, refractive index, density and particle size (if applicable), as well as on the wavelength of the light used in the analysis. Hence, in the UV region the depth of penetration into the paint layers can be of a few microns while in the NIR region it can easily reach one hundred microns.

Another important aspect is the definition of a reliable method for identifying the exact location of investigated areas, particularly when the analysis is repeated at a later date. For example, positioning the optical-fibre probe-head on exactly the same area is crucial to evaluate colour changes resulting from cleaning procedures or caused by natural aging. During monitoring related to colour changes it is necessary to compare reflectance spectra recorded at different times in order to determine the variations. One of the most reliable and simple procedures in studying paintings is the use of a transparent film of Mylar®. The areas to be investigated are selected and indicated with a marker on the Mylar sheet. Several references are drawn on the film in correspondence with clear and sharp contours, in order to facilitate the repositioning of the film in the exact position for acquiring spectra. Subsequently, the Mylar® film is removed and circular holes are made that correspond to the marks previously drawn; to facilitate the matching between the hole on the film and the probe head, crosses are also drawn on the latter. Lastly, the film is fitted back on the painting, and the spectra are recorded [35].

The development of easily transportable devices has made it possible to perform measurements in situ, on totally unmovable objects (i.e. wall-paintings, large paintings, etc.). Moreover, the acquired spectra can be visualized on a PC monitor and analysed in real time. FORS measurements can be performed using relatively inexpensive instrumentations, however, for more accurate measurements that cover wider spectral ranges, expensive devices might be more appropriate.

### 1.5- Multispectral Image Reflectance Spectroscopy

In the field of conservation of cultural heritages, image reflectance spectroscopy (commonly abbreviated as IS) is a powerful non-invasive diagnostic tool for extracting extended spectral information over a bidimensional surface. Unlike FORS, IS provides information which is not localised, but it is spatial: i.e. mapping vs point analysis.

One of the most common imaging techniques is wide-band Near Infrared reflectography, mainly applied on paintings in order to study the preparation layer and to discover *pentimenti*, or changes in intentions of the artist. By increasing the wavelength of the radiation from visible to NIR, the superficial scattering phenomena due to the particles of the paint layer decrease. As a consequence, a reduction of the hiding power of the paint layer occurs and it is possible to detect the radiation reflected by the preparatory layer.

Initially, reflectographs were obtained by analog cameras, using a NIR sensitive photographic film, such as IR Kodak Ektachrome. Since the mid-1960's, the development of lead sulphide (PbS) vidicon video-cameras allowed to extend the spectral range from 0.9  $\mu\text{m}$  to around 2  $\mu\text{m}$ , improving the amount of information achievable from the underlying materials [36, 37]. At present, large matrix arrays of sensors made with new photo-detector materials allow high resolution IR digital images to be acquired [38, 39, 40, 41, 42, 43, 44]. Thanks to these technological developments, it has become possible to record digital images directly without the need of acquisition systems such as a scanner. The production of large area sensor arrays allowed an improvement of the spatial resolution of the image. However, when the resolution of the detector is not sufficient, it is necessary to record smaller frames with good resolution and reconstruct the image of the whole surface by means of mosaicing [45]. Such an acquisition scheme is usually implemented by means of a scanning device capable of recording the whole surface frame by frame (or even line by line, depending on the detector).

A multispectral imaging system acquires a sequence of narrow-band images taken at different wavelengths. It provides images of the surface under investigation as well as point-by-point spectral information. The first applications of multispectral imaging systems, such as the VASARI (Visual Art System for Archiving and Retrieval of Images) project in 1998, focused on digitising works of art in order to record the state of the objects at a given time. The crucial point of the project was to achieve higher colour accuracy by means of a multispectral approach which can provide better colourimetric values than a conventional red-green-blue (RGB) colour separation. [46]. At the same time, when the spectral sampling is sufficiently accurate, reflectance spectra of the points/pixels analysed can be achieved in order to characterise the superficial materials and to map them by means of different data processing methods [47, 48, 49, 50].

Generally, multispectral scanning devices can be subdivided into two categories depending on the scanning mechanism: the focal-plane [43, 44] and the object-plane scanner. A scanner of the second type, operating in the 400–900 nm range, was developed and built at IFAC-CNR.

The device used for the present thesis is based on a prism-grating-prism line-spectrograph ImSpector V10E (Speclm Ltd) connected to a camera (Hamamatsu ORCA-ERG). The characteristics of the scanner are

approximately 0.1 mm spatial sampling over a  $1 \times 1 \text{ m}^2$  surface and about 1 nm spectral sampling in the 400–900 nm range. These high-performance characteristics allow to obtain several well-defined images of the surface and well-resolved reflectance spectra, very useful for a first material identification. The data acquired with the hyperspectral scanner are organised in a single file called file-cube. The data can be described as a cube in a three-dimensional space, defined by the two spatial dimensions of the scan and by the wavelength dimension. Therefore, the cube can be imagined as a set of monochromatic images at different wavelengths or as a set of reflectance data of each point of the painting (Figure 8).

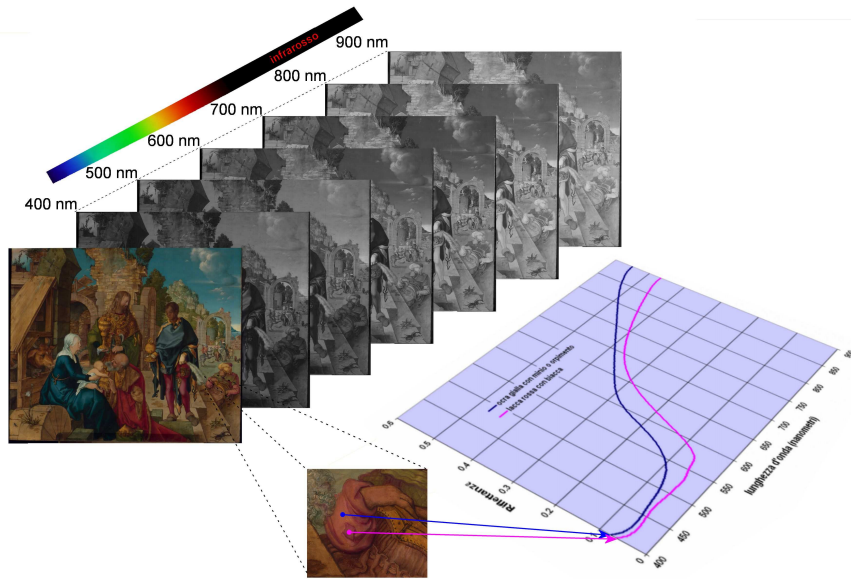


Figure 8: Visualisation of the data acquired by means of the hyperspectral scanner developed at IFAC laboratories on the painting “Adorazione dei Magi” by Albrecht Dürer.

From the file-cube, single images referring to a specific wavelength or to a spectral range can be extracted. Depending on the detector’s working spectral range, infrared images can be studied. In this case of the Inspector system, NIR images until about 900 nm can be extracted. Moreover, multispectral data allow false-colour IR images to be generated. False-colour IR images can be very useful in a preliminary study of a paint layer. For IR, red (R) and blue (B) images an average of the monochromatic images respectively contained in the NIR region (751-9000 nm), red region (581-750 nm), and blue region (520-580 nm) is calculated. The IR, R and G channels are assigned to the R, G and B channels, respectively.

Data analysis can be applied to study the distribution of a specific material on the surface. Some examples include: Spectral Angle Mapper (SAM), Euclidean minimum distance (EMD), curvature mapper and Principal Component analysis (PCA).

- Spectral Angle Mapper (Figure 9) treats the reflectance spectra as vectors and it calculates the spectral angle between them. Considering a vector ( $x$ ) as a reference, a second vector ( $y$ ) can be considered similar to the reference when the angular difference is smaller than a predefined threshold (usually 5-6°). If  $N$  is the number of the considered spectral bands, the angle between  $x$  and  $y$  is calculated according to the following equation:



$$\theta(x, y) = \arccos\left(\frac{\langle x, y \rangle}{\|x\| \|y\|}\right) \quad \text{with } 0 \leq \theta \leq \pi/2$$

where  $\langle x, y \rangle$  is the dot product operator and  $\| \bullet \|$  is the 2-norm.

From its mathematical definition, SAM uses just the vector direction and not the vector length, so the algorithm is not sensitive to scale changes [48, 51, 52].

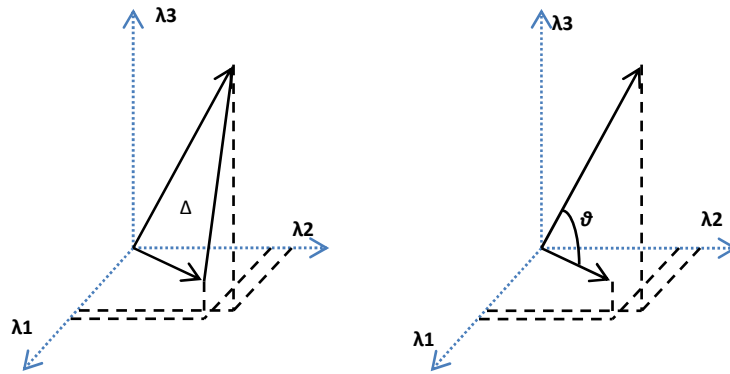


Figure 9 and Figure 10 : SAM and EMD used in hyperspectral processing.

-Euclidean Minimum Distance (Figure 10) measures the shortest distance between two vectors  $x$  and  $y$  with the following equation:

$$EDM(xy) = \|x - y\| = \sqrt{\sum_{i=1}^N (x_i - y_i)^2}$$

By imposing a threshold on the EMD output, the similarity between two considered spectra can be evaluated. Differently from SAM, EDS is sensitive to illumination changes; this means that spectra characterised by identical absorption bands but translated into reflectance can show a high euclidean distance and not be recognised as similar.

- A simple least squares parabolic fit of a wavelength interval may often be a quick and effective tool to test the presence of a candidate absorption band. If the absorption band is locally present, the spectrum is locally concave and the sign of the 2<sup>nd</sup> coefficient of the fitting parabola is positive, otherwise the “curvature” is negative or null (convex or straight spectrum). After a normalisation, the 2<sup>nd</sup> order coefficients are reported in grey levels on the image, thus providing an understandable curvature map [32]. Obviously, this simple method contains the defect of producing false results when the chosen interval is focused on a ‘shoulder’ of the spectral curve instead an absorption band. It can be appropriately used only by specialist with a good knowledge of the possible reflectance spectra of the materials, who can discard false alarm signals on the basis of a priori information, taking at the same time advantage of its prompt response.

- PCA can be defined as a transformation that rotates the space of data to a new one whose first axis is along the direction of largest variance, the second axis is along the direction of largest variance among the directions which are orthogonal to the first one, and so on. Usually, the contribution due to the first four or

five dimensions includes all the statistical variance of the data. However the images obtained have not got a physical meaning, but they can be read as degrees of freedom of the information contained. Thanks to this informative synthesis, principal component images can underline details not visible by just examining spectral images [47].

These elaborations require a lot of computing time depending also on the dimension of the processed file-cube. As a consequence, a reduction of the spatial resolution is desirable. Furthermore, the PCA algorithm may be limited to a specific region of interest.

## References

1. N. Barnes, *Technical Studies in the Field of the Fine Arts*, 7, 1939, 120.
2. F. I. G. Rawlins, *Technical studies in the Field of Fine Arts*, 10, 1942, 230.
3. J. M. Hunt, M. P. Whisher, and L.C. Bonham, *Analytical Chemistry*, 22, 1950, 1478.
4. R. Eisberg, and R. Resnick, *Quantum Physics of atoms, molecules, solids, nuclei, and particles*, 2<sup>nd</sup> Edition, John Wiley & Sons, USA, 1985.
5. A. Bettini, *Le onde e la luce*, Decibel press, Padova, 1993.
6. T. B. Brill, *Light, Its Interaction with Art and Antiquities*, Plenum Press, New York, 1980.
7. K. Nassau, *The Physics and chemistry of Color*, J. W. Goodman (Ed.), John Wiley & Sons, New York, 1983.
8. T. J. Bruno, and Paris D. N. Svoronos, *CRC Handbook of Fundamental Spectroscopic Correlation Charts*, CRC Press, 2005.
9. ISO 20473:2007 - Optics and photonics - Spectral bands.
10. IPAC Staff. Near, mid and Far-Infrared, NASA ipac. Retrieved 2007-04-04.
11. M. Bacci, *Modern Analytical Methods in Art and Archaeology*, Chemical Analysis Series, E. Ciliberto, and G. Spoto (Eds.), John Wiley & Sons Inc., New York, 155, 2000, 321.
12. H. Gunzler, and A. Williams, *Handbook of Analytical Techniques*, Wiley-Vch, Weinheim, 2001.
13. P. Kubelka, and F. Munk, *Technische Physik*, 12, 1931, 593.
14. P. Kubelka, *Journal of Optical Society of America*, 38, 1948, 448.
15. R. Johnston-Feller, *Color science in Examination of Museum Objects, non Destructive Procedures*, The Getty Conservation Institute, Los Angeles, 2001.
16. P. B. Mitton, *Pigment Handbook vol. III Characterization and Physical relationships*, T.C. Patton (Ed.), Wiley & Sons, New York, 1973.
17. D.R. Duncan, *Journal of the Oil and Colour Chemist Association*, 42, 1965, 300.
18. R. J. Lancashire, *Selection Rules for Electronic Spectra of Transition Metal Complexes*, University of the West Indies, Mona, 2006.
19. R.G. Burns, *Mineralogical applications of crystal field theory*, 2<sup>nd</sup> edition, Cambridge University Press, Cambridge, 1993.
20. W. H. Brown, C. S. Foote, and B. L. Iverson, *Organic chemistry*, 5<sup>th</sup> edition, L. Lockwood, and K. Kiselika (Eds.), Brooks/Cole Cengage Learning, Belmont, 2009.
21. D. Patterson, *Pigments, an introduction to their Physical Chemistry*, Elsevier Publishing Co. England, 1967.
22. M. Bacci, and M. Picollo, *Studies in Conservation*, 42 (3), 1996, 136.
23. M. Bacci, F. Baldini, R. Carlà, and R. Linari, *Applied Spectroscopy*, 45 (1), 1991, 26.
24. M. Leona, and J. Winter, *Studies in Conservation*, 46, 2001, 153.
25. G. Dupuis, M. Elias, and L. Simonot, *Applied Spectroscopy*, 56 (10), 2002, 1329.
26. M. Bacci, I. Cazenobe, M. Picollo, S. Porcinai, and B. Radicati, *Proc. of the 3<sup>rd</sup> International Conference on Science and Technology for the safeguard of cultural heritage in the Mediterranean Basin*, Alcalà de Henares, Spain, 2001, 267.
27. I. Cazenobe, M. Bacci, M. Picollo, B. Radicati, G. Bacci, S. Conti, G. Lanterna, and S. Porcinai, *Proc. of 13<sup>th</sup> ICOM*, Rio de Janeiro, 2002, 238.

28. M. Bacci, M. Picollo, S. Porcinai, and B. Radicati, *Techne* 5, 1997, 28.
29. M. Picollo, and S. Porcinai, *Applied Spectroscopy*, 2, 1999, 125.
30. M. Bacci, C. Cucci, M. Picollo, S. Porcinai, B. Pretzel, and B. Radicati, *Proc. of the 10<sup>th</sup> Congress of the International Colour Association, Granada, 2005*, 623.
31. M. Bacci, S. Baronti, A. Casini, P. Castagna, R. Linari A. Orlando, M. Picollo, and B. Radicati, *Proc. of Materials Research Society Symposium*, 352, 1995, 153.
32. A. Casini, F. Lotti, M. Picollo, L. Stefani, and E. Buzzegoli, *Studies in Conservation*, 44, 1999, 39.
33. C. Miliani, F. Rosi, A. Burnstock, B. G. Brunetti, and A. Sgamellotti, *Applied Physics A*, 89, 2007, 849.
34. <http://fors.ifac.cnr.it> last accessed 30<sup>th</sup> November 2010.
35. M. Bacci, A. Casini, C. Cucci, M. Picollo, B. Radicati, and M. Vervat, *Journal of Cultural Heritage*, 4, 2003, 329.
36. J. R. J. Van Asperen De Boer, *Studies in Conservation*, 19, 1974, 97.
37. D. Saunders, and J. Cupitt, *National Gallery Technical Bulletin*, 16, 1995, 61.
38. A. Aldrovandi, D. Bertani, M. Cetica, M. Matteini, A. Moles, P. Poggi, and P. Tiano, *Studies in Conservation*, 33, 1988, 154.
39. E. Walmsley, C. Fletcher, and J. Delaney, *Studies in conservation*, 37, 1992, 120.
40. D. Saunders, and J. Cupitt, *National Gallery Bulletin*, 14 (1), 1993, 72.
41. E. Walmsley, C. Metzger, J. K. Delaney, and C. Fletcher, *Studies in Conservation*, 33, 1994, 217.
42. J. Coddington, and S. Siano, *Proc. of the ICC Melbourne Congress*, A. Roy, and P. Smith (Eds.); London, 2000, 39.
43. D. Bertani, and L. Consolandi, *Digital Heritage*, L. Mac Donald (Ed.), Oxford, 2006, 211.
44. D. Saunders, J. Cupitt, and J. Padfield, *Digital Heritage*, L. Mac Donald (Ed.), Oxford, 2006, 521.
45. R. Billinge, J. Cupitt, N. Dessipris, and D. Saunders, *Studies in Conservation*, 38, 1993, 92.
46. K. Martinez, J. Cupitt, D. Saunders, and R. Pillay, *Proc. of the IEEE*, 90, 1, 2002,
47. S. Baronti, A. Casini, F. Lotti, and S. Porcinai, *Applied Optics*, 37 (8), 1998, 1299.
48. A. Pelagotti, A. Del Mastio, A. De Rosa, and A. Piva, *IEEE Signal Processing*, 25 (4), 2008, 27.
49. H. Maitre, F. Schmitt, and C. Lahanier, *Proc. of the International Conference on Image Processing, Thessaloniki, 2001*, 557.
50. Y. Zhao, R. S. Berns, L. A. Taplin, and J. Coddington, *Proc. of SPIE-IS&T electronic Imaging*, 6810.
51. N. Keshava, and J. F. Mustard, *IEEE Signal Processing*, 19, 2002, 44.
52. N. Keshava, *IEE Transactions on Geosciences and remote sensing*, 42 (7), 2004, 1552.

## Chapter 2

### Instrumental set-up

Spectroscopic analysis can be conducted with different methodologies depending on the subjects and the aims of the investigations. In the present thesis three non-invasive acquisition systems were used:

- UV-Vis-NIR Reflectance Spectroscopy with ZEISS spectroanalysers to characterise the pictorial layers of *Macchiaioli* paintings;
- UV-Vis-NIR Reflectance Spectroscopy with Lambda 1050 bench spectrophotometer to analyse laboratory green mock-ups;
- Multispectral Image Spectroscopy with hyperspectral scanner to analyse a selected number of the *Macchiaioli* paintings investigated in this work.

Before discussing the technical details of the instrument, a brief and general introduction on spectrophotometric systems will be given.

A spectrometer is a device used to measure a spectrum, which can be defined as a plot of a (unknown) value in function of a specific parameter, such as time, frequency, etc. Spectrophotometers are spectrometer which record the intensity of a radiation as a function of the wavelength and are generally used to measure the reflectance (or transmittance) of radiation in specific spectral ranges in order to identify materials. Reflectance spectrophotometers, like those used in this thesis, measure the reflectance factor  $I/I_0$  of a sample (where  $I$  is the radiation reflected by the surface and  $I_0$  is the incident radiation). This is usually done by comparing the reflectance spectrum of a 99% Spectralon® diffuse reflectance standard with the reflectance spectrum of the sample maintaining the same experimental conditions. Spectrophotometers usually consist of one (or more) incoherent source which provides the incident radiation beam, wavelength selectors positioned before or after the sample to separate the radiation's

components, and the detection systems. Generally, spectrophotometers which present the wavelength selector positioned between the sample and the detector are called spectroanalysers. In these devices, the sample is reached by all the radiation that subsequently is dispersed by the monochromator and revealed by the detector.

Spectrophotometers can be divided into the categories of single and double beam devices. Single beam spectrophotometers make use of a single beam of radiation which interacts with the sample (Figure 1). In order to calculate the ratio  $I/I_0$  it is necessary to record the relative ray intensity twice: the energy of the beam striking the detector would first be measured with a reference reflectance standard, then the sample would be placed in the optical path and a second measurement would be taken. If there are any fluctuations between these two measurements in the energy of the lamp, the result would be inaccurate.

In double beam instruments, a beam splitter (or chopper) is used to obtain two beams of equal energy with equivalent optical paths (Figure 2). One of these beams reaches and interacts with the sample, while the other reaches the reference standard. These types of equipment are usually more expensive than single beam spectrophotometers, but they present some advantages, such as more stability and efficiency in the outcome.

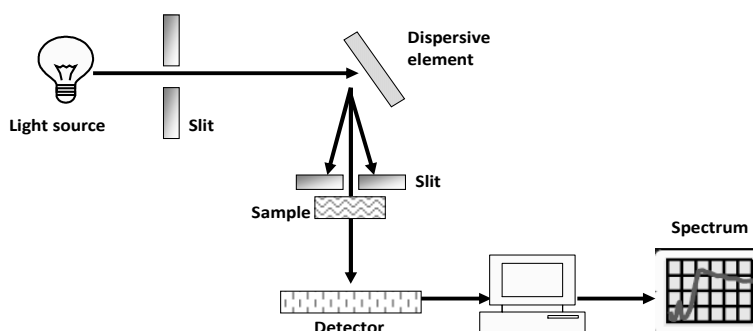


Figure 1: Optical configuration of a single beam spectrophotometer.

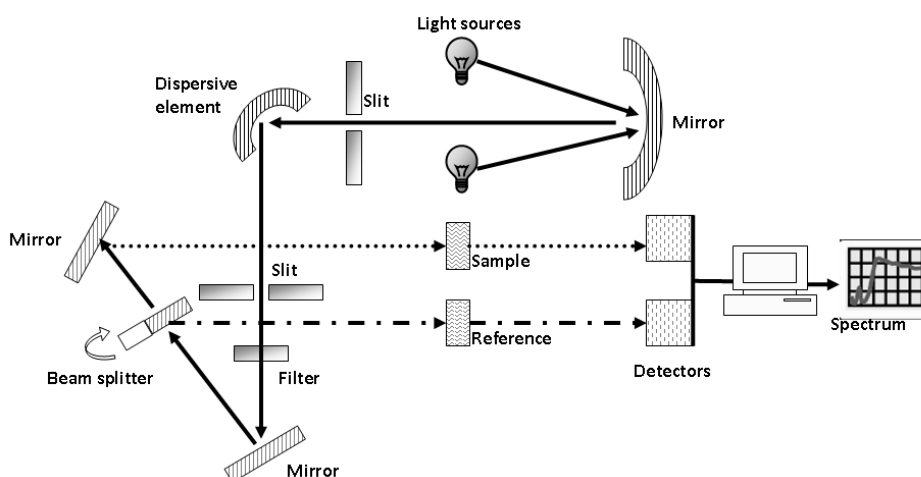


Figure 2: Optical configuration of a double beam spectrophotometer.

As shown in Figures 1 and 2, the dispersive device can be located between or before the sample and the detector. In the first case, the sample is hit by the radiation that subsequently is dispersed by a

monochromator. The split radiation can be quickly revealed by a suitable multiplex detector, capable of recording the whole reflectance spectra in fractions of second, as with the Zeiss spectroanalyser.

Differently, in bench spectrophotometers the dispersive element is usually positioned before the sample and, through suitable slits, each wavelength is well selected. As a consequence, the sample is hit one at a time by electromagnetic radiation with increasing (or decreasing) wavelengths.

As far as the acquisition geometry is concerned, several configurations are possible depending on the specific instrument and on the aim of the measurement. The  $45^\circ/0^\circ$  illumination geometry is the most commonly used: the beam hits the sample forming a  $45^\circ$  angle with the normal at the surface and the diffuse radiation is collected along the normal ( $0^\circ$ ). In the case of non-perfectly level surfaces, in order to guarantee a homogeneous illumination and to avoid the presence of shadows, a second beam at  $45^\circ$  can be added obtaining a  $2 \times 45^\circ/0^\circ$  geometry. Integrating spheres [1] offers an alternative to directional geometries. These devices are hollow cavities with their interior coated for high diffuse reflectivity that allows for measurements of diffuse light to be made by collecting the signal after multiple reflections on the inner sides of the sphere.

### 2.1- Zeiss spectroanalysers

UV-Vis-NIR FORS analysis in the 350-2100 nm range were performed on paintings by using the single beam Zeiss MCS601 (200-1000 nm range) and MCS611 NIR 2.2WR (900-2200 nm range) spectroanalysers (Figures 3 and 4) [2]. These two devices are hosted in a single and transportable chassis ideal for in-situ analysis. The data acquisition range is 0.8 nm/pixel for 1024-elements silicon photodiode array detector (MCS601) and approximately of 6.0 nm/pixel for the 256-elements InGaAs diode array detector (MCS611 NIR 2.2WR). The radiation between 320-2700 nm, provided by a tungsten-halogen lamp (module Model CLH500), is carried to the sample by bundles of optical quartz fibres which also transport the reflected radiation into the detectors. A dark hemispheric probe head, terminating in a flat base (described in Chapter 1), is connected to the fibre optics and placed on the surface of the painting. The reflectance spectra were recorded on an area of about 2 mm in diameter.

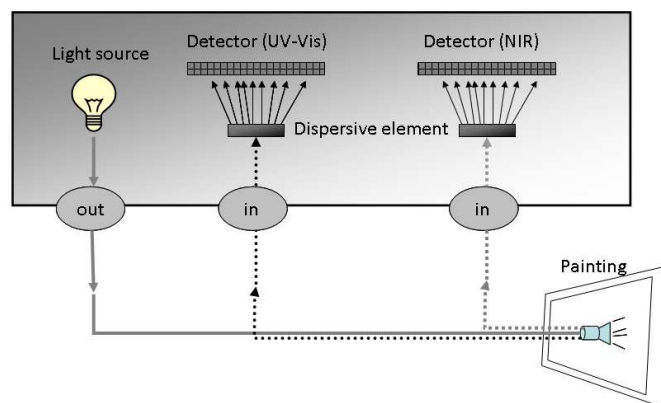


Figure 3: Optical configuration of Zeiss spectroanalysers.

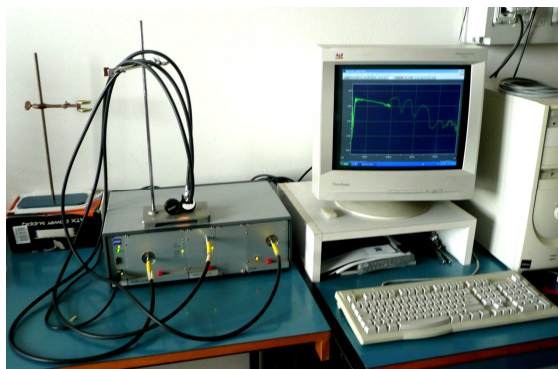


Figure 4: Zeiss spectroanalysers mod. MCS 601 and mod. MCS 611.

The probe head has three apertures on the dome. Such apertures are connected to the fibre bundles and allow the passage of radiation from the radiation source and to the detectors (Figure 5); in the  $0^\circ/2 \times 45^\circ$  acquisition geometry, the top bundle directs the incoming radiation towards the sample, while the other two collect the scattered radiation at  $45^\circ$  with respect to the incident light and send the information to the detectors. As a reference, a 99% Spectralon<sup>®</sup> diffuse reflectance standard is used.

For some spectra, a discontinuity, such as a sharp increase/decrease in reflectance, can be observed at about 980 nm. This happens when the measurement transitions between the two detectors occurs. Because of the low emissivity of the lamp in the UV region and the decreased sensitivity of the detectors at the end of the spectral sensitivity, the spectra are usually recorded in the 350-2100 nm range. The acquisition time for each measurement is fractions of second.

During the acquisition, the spectra are displayed on the monitor of a personal computer connected with the instrument as shown in Figure 4. By means of the software Aspect Plus<sup>®</sup> from Zeiss, it is possible to control the instrument and to visualise, compare and analyse the acquired spectra.

For the analysis of *'Il Ritratto di Diego Martelli'* by F. Zandomenighi, the Zeiss MCS 501 (200-1000 nm range) and MCS 511 NIR 1.7 (900-1700 nm range) spectroanalysers were used (Figure 6) with a  $0^\circ/2 \times 45^\circ$  acquisition geometry [2]. The spectroanalysers, housed in two different cases, can be connected to each other in order to obtain one reflectance spectrum for the whole 200-1700 nm range. The data acquisition intervals were of 0.8 nm/pixel for the 1024-elements silicon photodiode array detector and approximately of 6.0 nm/pixel for the 128-elements InGaAs diode array detector, respectively. The radiation source and the probe used for this set of measurements were the same as previously introduced.

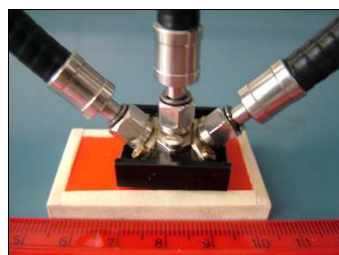


Figure 5: Probe used for FORS analyses. The top fibre bundle directs the incoming radiation towards the surface, while the other two collect the scattered radiation at  $45^\circ$  with respect to the incident light and send the information to the CCD and InGaAs detectors respectively.





Figure 6: Zeiss spectroanalyzers mod. MCS501 and mod. MCS511.

## 2.2- Spectrophotometer bench (Perkin Elmer $\lambda$ 1050)

UV-Vis-NIR analysis in the 350-2500 nm range were performed on green pigment mock-ups by using a Perkin Elmer  $\lambda$  1050 spectrophotometer [3]. In this thesis, it was used in order to characterise, by means of accurate and highly spectral resolved spectra, a selected range of green pigments. The high performance of this device makes it one of the most suitable for material characterisation in the spectral range considered. The Perkin Elmer  $\lambda$  1050 spectrophotometer is a double beam and double monochromator bench instrument capable of working in the 200-3300 nm range (Figure 7 and 8).

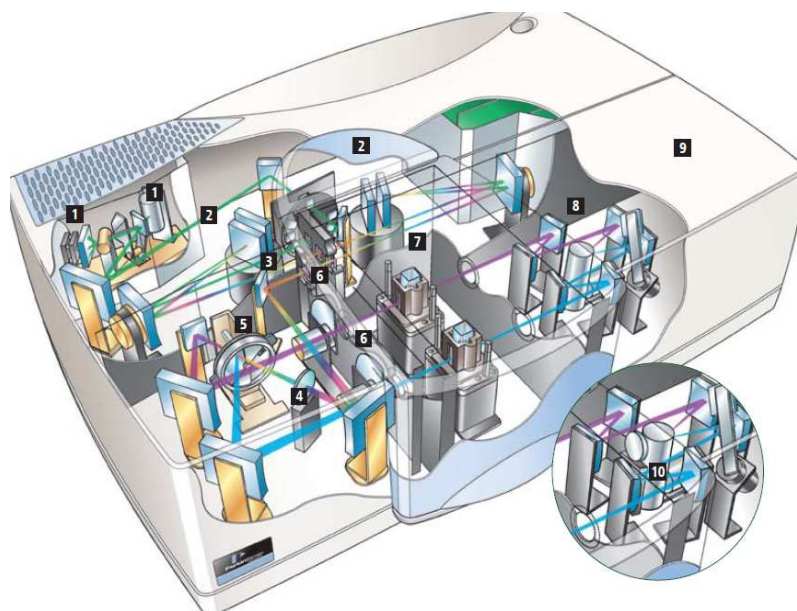


Figure 7: Optical Configuration of the UV-Vis-NIR Lambda 1050 spectrophotometer: 1) light sources; 2) monochromators; 3) common beam mask; 4) common beam depolarizer; 5) chopper; 6) sampler and reference beam attenuators; 7) sample compartment; 8) detectors; 9) sample compartment for reflectance measurements; 10) detectors (image from [4]).

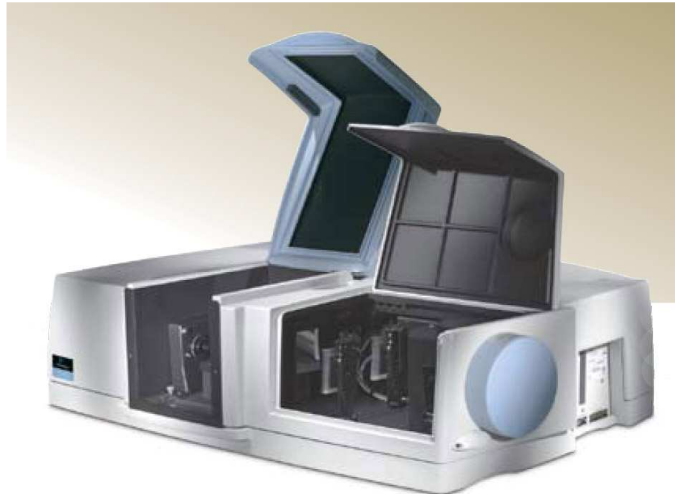


Figure 8: UV-Vis-NIR Perkin Elmer  $\lambda$  1050 spectrophotometer.

In the configuration used, two detectors are present: a photomultiplier (175-860 nm range) and a PbS sensor (860-3300 nm range); the data resolution are 0.05nm/pixel and approximately 0.20 nm/pixel, respectively. The incident beam is generated by a pre-aligned deuterium lamp (in the UV-Vis) and a halogen-tungsten lamp (in the VIS-NIR). A 60 mm integrating sphere positioned in the second sample compartment of the instrument (at the end of the optical path) allows reflectance measurements of the diffuse reflectance (excluding the specular component) with a  $0^\circ/d$  geometry [4].

The reflectance spectra are recorded on an area of about 1 cm x 0.5 cm, using 99% Spectralon<sup>®</sup> diffuse reflectance standard. The junction point of the two detectors was selected at 860 nm. The acquisition software UV WinLab<sup>™</sup> allows the instrument to be controlled and to visualise and analyse the acquired spectra.

The acquisition time for each measurement depends on the spectral range selected for the investigation. As previously mentioned, in spectrophotometers the beam separation in wavelengths is done through monochromators positioned before the sample. In this way, the sample is each time hit by a single wavelength radiation. This system results in longer acquisition times than those recorded with multiplex spectroanalysers.

### 2.3- Hyperspectral scanner

The hyperspectral scanner used to analyse the *Macchiaioli* paintings operates in the 400–1000 nm range and it was designed and built at the IFAC-CNR. The mechanical layout is based on two orthogonal linear movements that cover a  $1 \times 1 \text{ m}^2$  area with spectrograph and fibre-optic illuminators fixed to the vertical movement and positioned to analyse a horizontal line-segment (Figure 9 and Figure 10). The length of the line-segment depends on the geometric reduction factor of the lens/objective used. Moreover, the line-segment analysed is usually focused on the entrance slit of the spectrograph by means of a telecentric lens (Opto-Engineering with a 3 cm telecentric zone). The latter is normally used in order to limit distortion due to the surface when not perfectly planar. The vertical movement of the device provides a uniform

illumination and limited exposure of the work of art to the incident radiation which flashes radiation each second just on the measured line [5, 6].

The acquisition system is based on a prism-grating-prism line-spectrograph ImSpector V10 (SpecIm Ltd) connected to a medium-speed, high-sensitivity interline-transfer CCD Hamamatsu ORCA-ERG cooled with a single Peltier stage (Figure 11). The acquisition occurs line-by-line, so the spectra of the light coming from all the points of a 5,6 cm line-segment are dispersed together and focused onto the area sensor of the camera. The result is a 2D matrix of spectral intensities with wavelengths along one axis and spatial positions along the orthogonal one. This spectral scanning scheme is expressively defined “push-broom” in the jargon of remote sensing, because the line-segment “sweeps” the surface along the scan direction. The vertical scan occurs for adjacent, slightly overlapping vertical strips which are put back together with a specific conjunction software[7, 8].

The characteristics of the scanner are approximately 0.1 mm spatial sampling over a  $1 \times 1 \text{ m}^2$  surface and about 1 nm spectral sampling in the wavelength range 400–900 nm. Actually, the spectrograph should cover the entire wavelength range from 400 nm to 1000 nm by using a special filter that avoids the superposition of the near infrared part of the spectrum with the second diffraction order of the visible spectrum. This order-blocking filter has resulted to be the most critical component of the assemblage: in practice, with current cameras and lights, the residues of the second order spectrum over  $\sim 880 \text{ nm}$  are not negligible, resulting in deterioration of the measurement. The configuration of this object-plane scanner covers a maximum area of about  $1 \times 1 \text{ m}^2$ , with 20 vertical line-scan stripes and a 10-point/mm (approximately 254 ppi) scan density in both directions. Illumination is provided by a 3200 K 150-Watt QTH-lamp, and the beam is sent to the surface under investigation by means of two Schott-Fostec optic line-lights fibres with cylindrical focusing lenses. The latter are fixed to the scan-head, and symmetrically project their beams forming  $45^\circ$  angles with the normal to the surface, guarantying a  $2 \times 45^\circ/0^\circ$  geometry.

Before each vertical scan, a measurement on a standard target of diffuse reflectance Spectralon® is carried out in order to calibrate the whole system and to compensate possible variations of emission of the QTH lamp.



Figure 9 and Figure 10: Instrumental apparatus of the hyperspectral scanner; detail of the acquisition system .

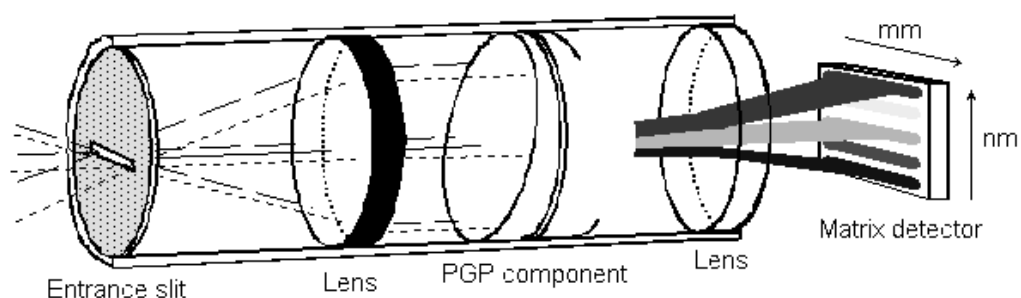


Figure 11: Experimental apparatus of the prism-grating-prism line-spectrograph ImSpector V10 (SpecIm Ltd) [ image from <http://www.vinci.it>].

For the analysis performed, the speed of the vertical movement was selected at 1.5 mm/sec, while the acquisition of the camera images proceeded independently at a constant rate of 15 frames/sec. In this way, the whole  $1 \times 1 \text{ m}^2$  area can be scanned in less than four hours.

Regarding possible damages due to the illumination system, it was calculated that in the free-run scanning mode, the maximum illumination value was measured as being about 25000 lux when the white reflectance standard is viewed at the upper limit of the camera dynamic range. The UVA fraction in the light from the optic fibre illuminator was about  $73 \mu\text{W}/\text{lumen}$ . The total exposure amounts to no more than about 1000 lux hours, that corresponds to the light dose received during approximately six hours of standard museum illumination [9].

Spectra Viewer is the program developed and written in Visual C++ for Windows in order to control the acquisition, edit and display the data. The visualisation system shows an image of the surface acquired on which the mouse cursor is pointed and with a click of the left mouse-button the spectrum of the pointed pixel is displayed in a graph. By choosing one of these spectra as a reference, the software can calculate a divergence map on the whole 2D-acquisition. Other computational elaboration can be managed with Spectra Viewer, such as curvature maps and PCA. In these cases, the software allows for the definition of the working spectral range and for the delineation of the area of interest.

**References**

1. D. K. Edwards, J. T. Gier, K. E. Nelson, and R. D. Roddick, *Journal of Optical Society. Am.*, 51, 1961, 1279
2. Hellma International, Inc., Sales Modules, 80 Skyline Drive, Plainview, NY 11803, USA.
3. Perkin Elmer, Corporate Headquarters, 940 Winter Street, Waltham, Massachusetts 02451, USA
4. Brochure – Lambda UV/Vis and UV/Vis /NIR spectrophotometers ([http://las.perkinelmer.com/content/RelatedMaterials/Brochures/BRO\\_LAMBDA8509501050.pdf](http://las.perkinelmer.com/content/RelatedMaterials/Brochures/BRO_LAMBDA8509501050.pdf) last accessed 18<sup>th</sup> January 2011)).
5. Casini, M. Bacci, C. Cucci, F. Lotti, S. Porcinai, M. Picollo, B. Radicati, M. Poggesi, and L. Stefani, SPIE Conf. 5857 “Optical Methods for Arts and Archaeology”, Munich, 2005.
6. Casini, F. Lotti, M. Picollo, L. Stefani, and E. Buzzegoli, *Studies in Conservation*, 44, 1999, 39.
7. Specim – Spectral imaging Ltd., POB 110, Teknologiantie 18 A, FIN-90571 Oulu, Finland ([www.specim.fi](http://www.specim.fi)).
8. Brochure – Imspector Imaging Spectrographs (<http://www.specim.fi/media/imspector-series-ver2-10.pdf> last accessed 18<sup>th</sup> January 2011).
9. Atto di indirizzo sui criteri tecnico scientifici e sugli standard di funzionamento dei musei. D.L. 112/1998 – art 150 comma 6



## Chapter 3

### Spectroscopic analysis of *Macchiaioli* paintings

*“The macchia was initially an accentuation of chiaroscuro in painting; a way of freeing oneself from the basic fault of the old school, which by excessive transparency of form sacrificed the solidity and sense of perspective in the painting”*

T. Signorini

This section presents the results of spectroscopic analyses performed on five paintings by Macchiaioli artists, belonging to the permanent collection of the Galleria d’arte moderna of Florence in Palazzo Pitti.

Four paintings by Federico Zandomenghi and one by Silvestro Lega were analysed:

- Bastimento allo scalo* (1869), Federico Zandomenighi – FORS analysis,
- Ritratto di Diego Martelli allo Scrittoio* (1870), Federico Zandomenighi - FORS analysis,
- Luna di miele* (1877), Federico Zandomenighi – FORS and IS analysis,
- A letto* (1878), Federico Zandomenighi – FORS and IS analysis,
- Passeggiata in Giardino* (1864), Silvestro Lega – FORS, FORS and IS analysis.

The paintings analysed showed no signs of a conservation problem, except for the presence of a degraded varnish that altered the whole chromatic perception of the pictorial layer. The removal of the varnish gave us the opportunity to study the artistic technique of the painters using non-invasive methodologies and identify the materials (pigments) used.

X-ray fluorescence (XRF) analyses were also performed on some of the paintings listed by using an Assing Lithos portable spectrometer equipped with a Mo X-ray tube. The spectra were acquired with the tube operating at 24 Kv and 0.3 mA in the 0-25 KeV range, and a resolution of 158 ev on the Fe<sup>55</sup> line. The

measurements on the *Ritratto di Diego Martelli allo Scrittoio* were conducted by Mr. Dario Vaudan and Dr. Anna Piccirillo, affiliated with the *Dipartimento Soprintendenza per i Beni e le Attività Culturali, Regione autonoma Val d'Aosta* at the time of the analysis, and by Dr. Alessandro Migliori from the Istituto Nazionale di Fisica Nucleare from Florence for the paintings *Luna di miele* and *A letto*.

It is necessary to underline some aspects concerning the FORS spectra shown here. Firstly, it is possible to recognise the presence of a step centred at 980 nm due to the changing of the detector. In this case no corrections were made in order to avoid possible alterations of the spectral shape. Moreover, since the reflectance curves are in general particularly noisy in the 320-350 nm range because of the low emissivity in the UV region of the halogen source lamp used (CHL500), it was decided to take into account only values above 350 nm. The identification of materials was made by comparing FORS spectra collected from the paintings with the new IFAC spectral database, which will be available on-line soon. This database was built by collecting spectra from laboratory standard (mock-painting) samples with a Perkin-Elmer Lambda 1050 spectrophotometer in the 200-2500 nm range. The samples were prepared by Dr. Masahiko Tsukada, during his stay at the IFAC institute.

Finally, it is important to say that some of the images reconstructed by hyperspectral data and exhibited in this section show a lateral shadow due to a component of the easel which intercepts one of the light beams of the scanner's illumination system.



### 3.1- The *Macchiaioli* and the *macchia*

The *Macchiaioli* were a group of 19<sup>th</sup> century Tuscan painters who chose the *macchia* as the main instrument of their reaction against rule-bound art academies.

Among the exponents of this trend, Giovanni Fattori from Livorno, Silvestro Lega from Modigliana, and Telemaco Signorini from Florence are probably the best known.

The word *macchiaioli* was first used in 1862 in Florence in the newspaper *Gazzetta del popolo* to describe despairingly the new group of artists who painted with a strong chiaroscuro. The *macchiaioli's* aim was to obtain more realistic effects and to reconstruct the pictures as their visual impression. Shapes were obtained just by using chromatic patches (*macchie*) while the realistic effect was achieved by means of the strong contrast between dark areas and illuminated areas. Also called the “painters of the Risorgimento”, they hoped to capture the “effect” of a particular moment in nature, working quickly and spontaneously in order to catch the caprices of the fleeting light with all its hues.

At the end of 1850, this group of young artists started to meet at the Caffè Michelangelo in Florence to discuss the new trends in art and republican ideals. One of the most important personalities was Diego Martelli, art collector and theorist of the group. After the unification of Italy in 1861, there was a need to represent the new Italian identity, and the *Macchiaioli* were well suited to this necessity as they painted exclusively thematic material of everyday life, local landscapes, customs of local people and life in the country as well as in the city. For these reasons the 1860s were the most important and creative years for the *Macchiaioli*, who usually painted outside in small groups together from different Italian regions like Costa, Cabianca, De Nittis, Boldini and Zandomeneghi. Very important for the movement was the presence in Italy of the French painter Degas, who spent time in Florence in 1858.

Historical places of meetings were Staggia, in the countryside close to Siena, Piagentina, a neighbourhood on the outskirts of Florence, and Castiglioncello, near Livorno. After 1861 Abbati, Sernesi, Fattori and Signorini started to attend Castiglioncello at Martelli's holiday home. This period, known as that of the Castiglioncello School, ended in 1867 and was characterised by a prolific production of works and by a total immersion in natural surroundings. Lega was the first of this company who retired to Piagentina, followed by Signorini, Abbati and Sernesi. Here the *Macchiaioli* began to paint sweet and melancholy pictures of interiors [1, 2, 3, 4].

### 3.2- Federico Zandomeneghi (Venice, 1841 – Paris, 1917)

Federico Zandomeneghi is considered a transitional personality between Impressionists and *Macchiaioli*. Born of a family of artists, he attended the Accademia di Belle Arti of Venice. In 1860 he took part in Garibaldi's Expedition in Sicily. In 1862 he moved to Florence and started to work with Abbati in the Santa Maria Novella church. At the beginning he was not interested in the *Macchiaioli's* movement because of his academic background, but later he was able to understand their artistic language and appreciate their need for reality as well as their new artistic technique. In fact, Zandomeneghi's name is among the signatories of a document called *Statuto della Nuova Società di Belle Arti* (1° October 1863) signed also by Abbati, D'Ancona, Banti, Cabianca, Fattori, Lega, and Signorini.

In 1865 Zandomeneghi, Abbati, and Martelli rented a flat in Florence, close to Porta San Gallo and in the summer of that same year Zandomeneghi was a guest at Martelli's home in Castiglioncello where he painted *La lettrice*. In 1869 he lived in Martelli's home where he started work on the *Ritratto di Martelli allo scrittoio*.

In 1872, Zandomeneghi was living in Rome and in Florence, which he left unexpectedly for Paris where he started to attend the Caffè Nouvelle Athènes in Pigalle. Here he got in contact with Manet, Renoir, Pissarro, and Degas. Unfortunately the distance between the *macchia* and Impressionism made his French works not be fully appreciated; they remained unsold until they entered Martelli's collection. In November 1879, Zandomeneghi was working on the painting *Ritratto di Diego Martelli* and the collector went to the painter's home in Paris to pose.

In the first half of the 1880s, Zandomeneghi moved closer to Impressionism both in the subjects he painted (mainly from metropolitan and domestic life) and for the pictorial technique more and more similar to that of Renoir, Degas and Toulouse-Lautrec.

On May 3, 1883 his first personal exhibition was inaugurated at the Durand-Ruel Gallery and in 1914 Ugo Ojetti organised at the 11th Biennale di Venezia a show of Zandomeneghi's paintings in order to summarise his artistic path. Federico Zandomeneghi died in his home in Rue Torlaque on December 30, 1917 [1, 2, 3, 5].

### 3.2.1- *Bastimento allo Scalo*

Oil on canvas, 96x41 cm

Signed and dated "Z.F 1869"

Provenience: Diego Martelli's collection, Galleria d'arte moderna of Florence

Exhibited at the *Promotrice Fiorentina* in 1869, this painting represents a shipyard in the lagoon of Venice. Since it was not taken into account by contemporary critics it entered Martelli's collection and in 1912 was acquired by the Galleria d'arte moderna of Florence [5] .

FORS measurements were performed on 28 spots by means of Zeiss spectroanalysers MCS 501 and MCS511 NIR 1.7 in the 350-1700 nm spectral range (Figure 1). Table 1 shows for the analysed points the number of FORS measurements, the exhibited colour, the description, and the tentative pigment identification.

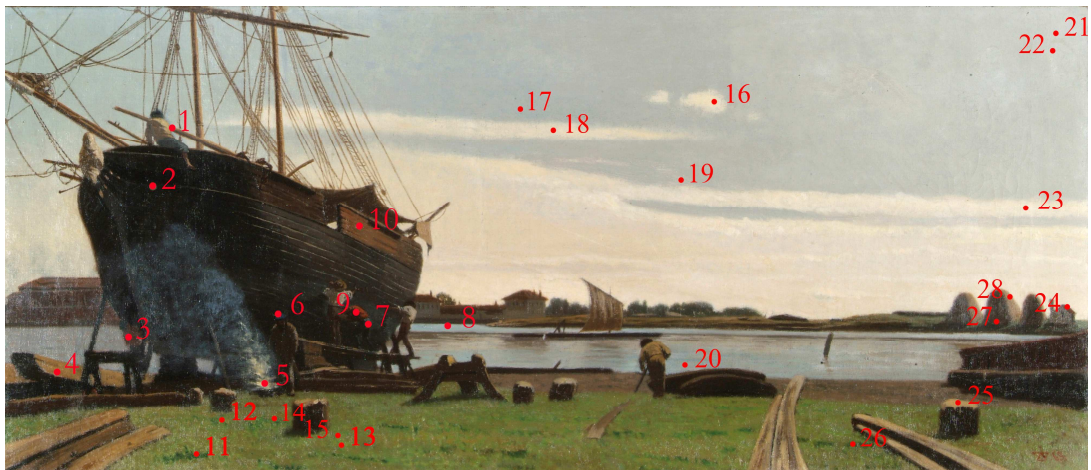


Figure 1: *Bastimento allo Scalo*, F. Zandomenighi. Points of FORS measurements.

Name Place	Bastimento allo scalo, Zandomeneghi Private Conservation Laboratory – Muriel Vervat Restauero			
Device	Zeiss MCS501 and Zeiss MCS511 NIR 1.7			
Light source	Zeiss CHL500			
Fibre	n.1 visible optical fibre and n. 2 near infrared optical fibres			
Probe	AC3 0°/2x45°			
Range	350-1700 nm			
Point	Description	Colour		Hypothesis of Pigment
1	Sailboat	Brown		Zinc white, iron oxides/hydroxides (raw Sienna earth/yellow ochre)
2	Boat	White		Lead white, zinc white, iron oxides/hydroxides
3	Sailor's shirt	Brown		Vermilion/cadmium red, iron oxides/hydroxides, black pigment
4	Floorboard	Brown	Light	Zinc white, iron oxides/hydroxides (raw Sienna earth /raw umber earth)
5	Shiny boat	White	Blue-violet	Zinc white, iron oxides/hydroxides, cobalt blue
6	Hat	Blue		Prussian blue
7	Man's trousers	Blue		Prussian blue, yellow pigment
8	Sea	Blue	Light	Lead white, Prussian blue yellow pigment
9	Shirt	Red		Vermilion/cadmium red on black layer
10	Boat	Brown	Light	Iron oxides/hydroxides (raw Sienna earth /raw umber earth), vermilion/cadmium red
11	Meadow on the left	Green	Dark	Prussian blue, chrome yellow
12	Meadow - left side, in front of the box	Green		Prussian blue, chrome yellow
13	Meadow - left side, in front of the box	Green	Light	Prussian blue, chrome yellow
14	Meadow behind the box	Green	Dark	Prussian blue, chrome yellow
15	Meadow - left side, in front of the box	Green	Light	Prussian blue, chrome yellow
16	Little clouds in the middle of the sky	White		Lead white, iron oxides/hydroxides
17	Sky	Blue	Light	Lead white, Prussian blue, black pigment
18	Cloud	White		Lead white, zinc white, iron oxides/hydroxides
19	Sky	Blue	Light	Lead white, Prussian blue
20	Sea	Blue	Light	Lead white, Prussian blue
21	Sky - right side, on the top	Blue	Light	Lead white, cobalt blue, black pigment
22	Sky - left side, on the top	Blue	Light	Lead white, cobalt blue, black pigment
23	Cloud	White		Lead white, zinc white
24	Roof – left side	Red		Lead white, iron oxides/hydroxides (burnt earth)
25	Close-up box – right side	Brown	Light	Lead white, zinc white, iron oxides/hydroxides (raw Sienna earth/yellow ochre)
26	Meadow - left side	Green	Light	Prussian blue, yellow pigment
27	Haystack	Brown	Dark	Zinc white, iron oxides/hydroxides, black pigment
28	Haystack	Brown	Light	Zinc white, iron oxides/hydroxides

Table 1: Points analysed with the descriptions, the colour and the hypothesis of pigment reported.

White areas were obtained by using lead white and zinc white (points 16, 18, 23, Figure 2). Lead white,  $2\text{PbCO}_3 \cdot \text{Pb}(\text{OH})_2$ , can be detected thanks to the absorption band at 1450 nm due to the first overtone of the OH group, while zinc white, ZnO, is detectable thanks to a strong absorption in the UV, which starts from about 380 nm due to a band-band transition (Figure 3). Lead white was in blue areas mixed with Prussian blue for the representation of the clouds, the sea (points 8 and 20, Figure 3), and the sky (points 17 and 19, Figure 3). Prussian blue,  $\text{Fe}_4[\text{Fe}(\text{CN})_6]_3 \cdot n\text{H}_2\text{O}$ , is characterised by a strong absorption centred at 700 nm due to a charge transfer transition between the two oxidation states of iron [6]. The shift recorded in the reflectance maxima of points 17 and 19 can be due to a yellow pigment.

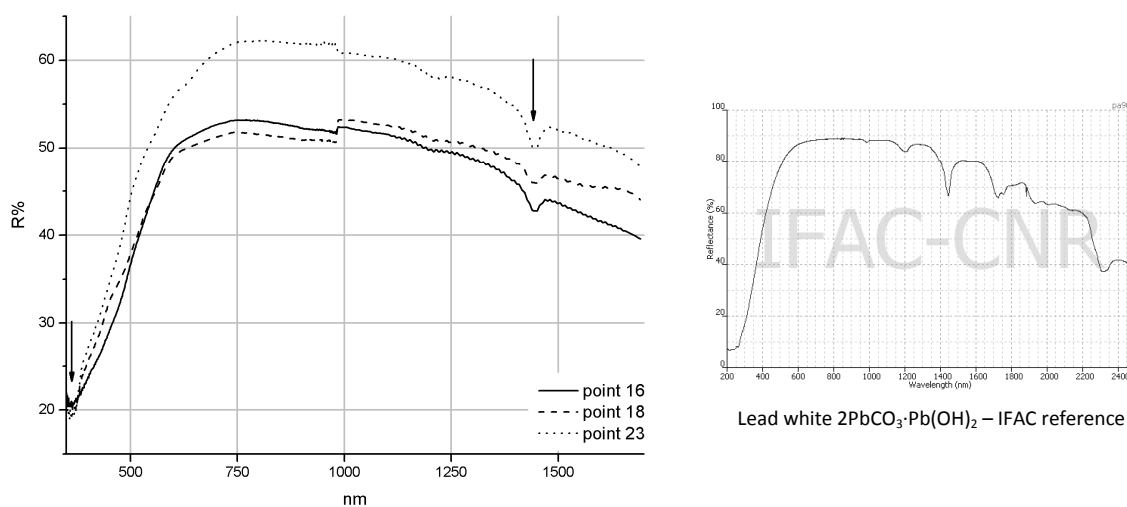


Figure 2: Reflectance spectra of white areas.

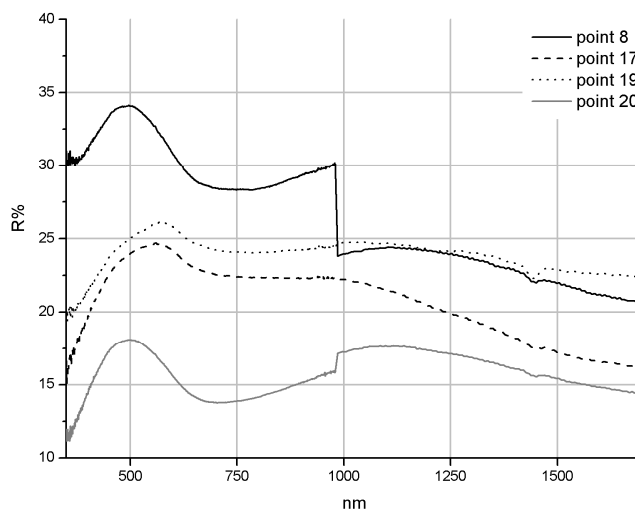


Figure 3: Reflectance spectra of blue areas.

Zinc white was used in order to lighten the dark-brown colour of the floorboards (point 4, Table 1), of the boat and some bucolic details of the landscape (points 10, 25, 27, and 28, Figure 4). The brown tone is created using earth-based pigments, which are usually a mixture of goethite ( $\alpha\text{-FeOOH}$ ) and hematite ( $\alpha\text{-Fe}_2\text{O}_3$ ), recognisable by the presence of a shoulder at 650, the absorption band at 950 nm, and a maximum at 450 nm visible only in point 25. These features are due to Fe (III)–Fe (III) pair excitations and  $d-d$  Fe (III)

transitions, while a charge-transfer transition is responsible for the absorption in the UV spectral range [6, 7]. In any raw earth, such as yellow ochre, raw Sienna and raw umber, a small reflectance maximum at 450 nm is present, which usually disappears in burnt earth and in red ochres. In fact, in goethite and hematite minerals two absorptions are present between 400 and 550 nm: the first absorption at 430 nm is probably due to d-d transition and it is very intense in hematite, the second between 480-550 nm is due to Fe (III)–Fe (III) pair excitations and is well defined for hematite as well, while in goethite it is weaker and located at about 480 nm. As a consequence, in hematite it is possible to see only one absorption in the 400-550 nm range, whereas goethite shows two small and differentiated reflectance minima [8, 9]. Obviously, this spectral behaviour influences earth-based pigments based on the amount of hematite present, more frequently in red or burnt ochre, and goethite present, more so in yellow ochres and raw earth-based pigments.

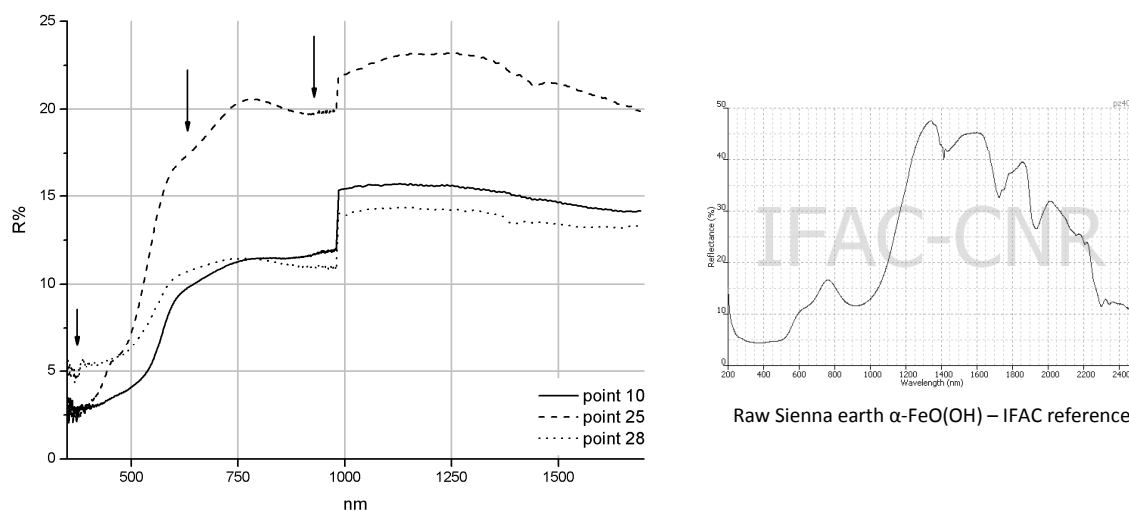


Figure 4: Reflectance spectra of brown areas.

Prussian blue is one of the pigments most utilised by Zandomenighi in this painting. It was applied for the sky and the sea (points 8, 17, 19 e 20, Figure 3), and also for the sailors' clothes (caps and trousers) (points 6 and 7, Table 1). Various mixed with a modern yellow, probably a chrome yellow ( $\text{PbCrO}_4$ ), it was used for the different greens of the meadow (points 11, 13, and 14, Figure 5). In fact, starting in the early 19<sup>th</sup> century a mixture made up of Prussian blue and chrome yellow, called chrome green or cinnabar green was traded and made available to painters.

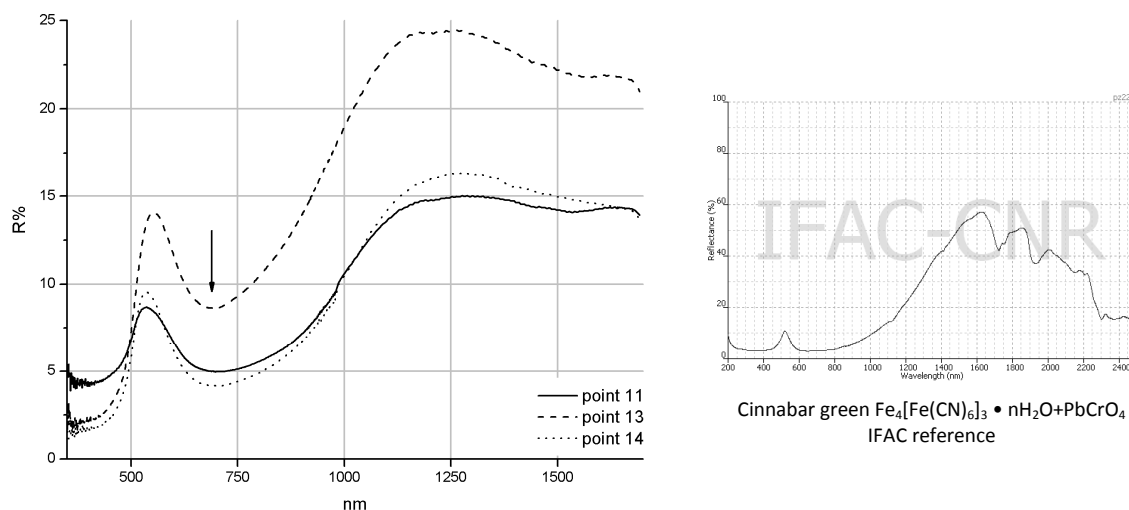


Figure 5: Reflectance spectra of green areas.

A cobalt blue, or Thenard's blue,  $\text{Co} \cdot \text{Al}_2\text{O}_4$ , was detected in some spots localised in the sky (points 21 and 22, Figure 6) and in point 5 (Table 1) thanks to its typical absorption band in the 500-650 nm range due to  $d-d$  transitions of to the Co (II). Since a black pigment which absorbs in the NIR is present in points 21 and 22, no confirmations can be achieved about the coordination number of the cobalt ion [10].

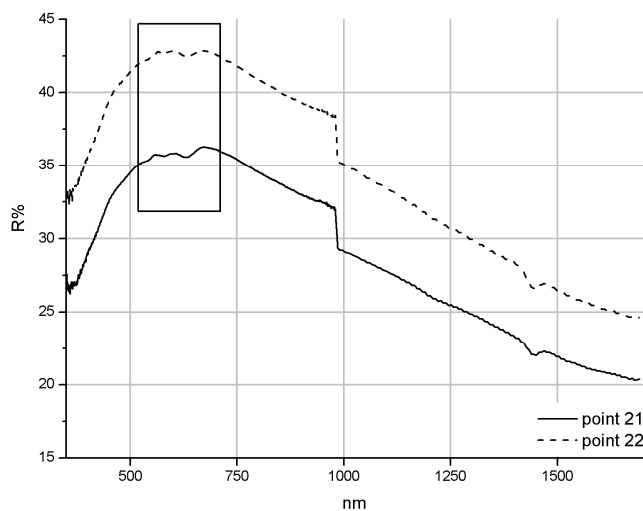


Figure 6: Reflectance spectra of light blue areas.

Finally, a red pigment such as vermilion ( $\text{HgS}$ ) or cadmium red ( $\text{CdS}$ ), was detected on the sailors' shirts (points 3 and 9, Figure 7), which are the only red areas of the painting together with the roof of a house in the background (point 24, Figure 7). Unfortunately vermilion and cadmium red cannot be distinguished with FORS because both present an S-shape band due to a band-to-band transition with the inflection points localised at around 600 nm [6].

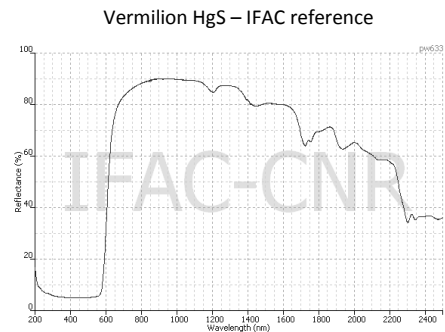
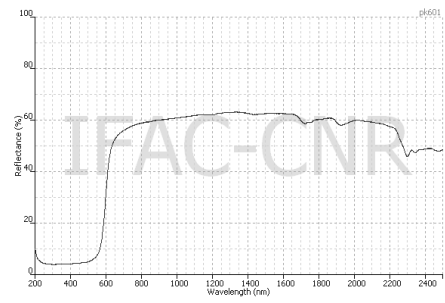
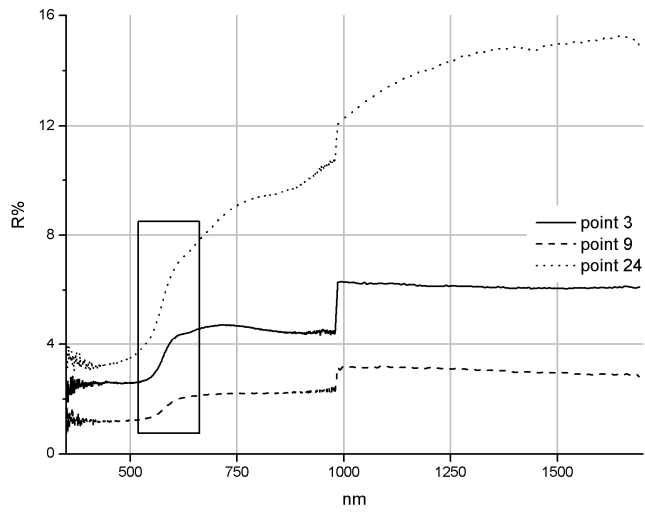


Figure 7: Reflectance spectra of red areas.



### 3.2.2- *Ritratto di Diego Martelli allo scrittoio*

Oil on canvas, 63 cm x 41 cm

Signed and dated "Firenze '70"

Provenience: Diego Martelli's collection, Galleria d'arte moderna of Florence

The portrait was made in 1870 during the painter's stay at Martelli's house in Florence. After Diego Martelli's death, the painting entered the National Collection in 1912.

Martelli is depicted at his desk, in a home environment. The composition is contained between two crooked planes, which make the painting free of traditional construction schemes and from conventionalities characteristic of works made for official exhibitions [3, 5].

FORS measurements were performed on 20 spots by means of Zeiss spectroanalysers MCS 501 and MCS511 NIR 1.7 in the 350-1700 nm spectral range (Figure 8). Some of these spots were also analysed by XRF. Table 2 shows for the analysed points the number of the FORS measurement, the exhibited colour, the description, the tentative pigment identification, and the elements detected by means of XRF analyses [11].

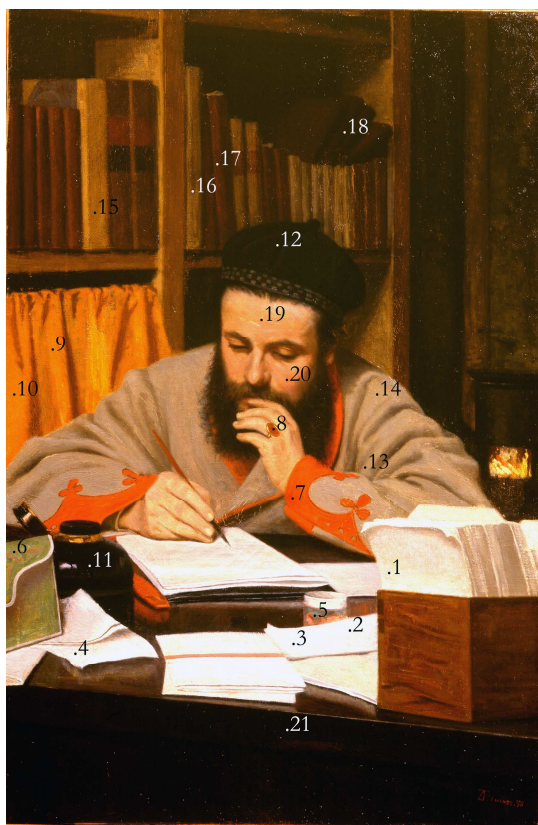


Figure 8: *Ritratto di Diego Martelli allo scrittoio*, F. Zandomenghi. Points of FORS measurements.

Name Place		Ritratto di Diego Martelli, Zandomeneghi PrivateConservation Laboratory – Muriel Vervat Restauro			
Device		Zeiss MCS501 and Zeiss MCS511 NIR 1.7			
Light source		Zeiss CHL500			
Fibre		n.1 visible optical fibre and n. 2 near infrared optical fibres			
Probe		AC3 0°/2x45°			
Range		350-1700 nm			
Point	Description	Colour		Pigment hypothesis	XRF
1	White sheet _1	White		Lead white, cobalt blue, iron oxides/hydroxides	Pb
2	White sheet _2	White		Lead white, cobalt blue	Pb
3	White sheet _3	White		Lead white, cobalt blue	Pb Zn Fe, Co
4	White sheet _4	White		Lead white	Pb
5	Jar	Grey		Lead white, Schweinfurt green, Prussian blue, Schweinfurt green, iron oxides/hydroxides	Pb Cu Fe As Zn
6	Envelope	Green		Lead white, Schweinfurt green, Prussian blue, Schweinfurt green, iron oxides/hydroxides	Pb As Cu, Fe Zn
7	Cuff	Red		Lead white, vermilion, iron oxides/hydroxides, strontium yellow (?)	Pb Hg Fe Sr Cu
8	Ring stone	Red		Lead white, vermilion, iron oxides/hydroxides (burnt earth)	Pb Fe Hg Cu Mn
9	Curtain_1	Orange		Lead white, vermilion, iron oxides/hydroxides (raw Sienna earth)	Pb Zn Fe Hg Cd Cu
10	Curtain_2	Orange		Lead white, vermilion, iron oxides/hydroxides,	Pb Fe Hg Zn
11	Inkwell	Black		Lead white, cobalt blue, Prussian blue, iron oxides/hydroxides (umber earth), black pigment	Pb Fe Cu Zn Co Ba Mn
12	Cup	Black		Lead white, Prussian blue, iron oxides/hydroxides, black pigment	Pb Fe Zn Cu Ca Ba
13	Sleeve_1	Gray		Lead white, iron oxides/hydroxides	
14	Sleeve_2	Gray		Lead white, iron oxides/hydroxides	Pb Zn Fe Cu
15	Book	Brown	Yellow	Lead white+ iron oxides/hydroxides	
16	Book	Brown	Yellow	Lead white+ iron oxides/hydroxides	
17	Book	Brown	Red	Iron oxides/hydroxides, vermilion, black pigment	
18	Book	Red	Red	iron oxides/hydroxides, vermilion, black pigment iron	
19	Forehead	Flesh		Lead white, iron oxides/hydroxides, vermilion	
20	Cheek	Felsh	Red	Lead white, iron oxides/hydroxides, vermilion	Pb Hg Zn Fe Cu Mn Co
21	Desk	Brown	Dark	Lead white+ iron oxides/hydroxides (umber earth), black pigment	Pb Zn Fe Cu Sr Mn Ba Ca

Table 2: Points analysed with the descriptions, the colour, the hypothesis of pigment, and the elements revealed by XRF analyses reported.

White areas were obtained by using lead white (point 4, Figure 9) recognisable for the absorption band at 1450 nm and, in some cases a cobalt blue (points 1, 2 and 3, Figure 9). In fact XRF analysis revealed in point 3 the presence of lead and cobalt together with zinc and iron (Table 2). This latter can be assigned to an earth-based pigment, as was suggested by the reflectance maximum at 450 nm and the absorption at around 950nm, but the presence of a Prussian blue, which contains both iron, cannot be completely excluded.

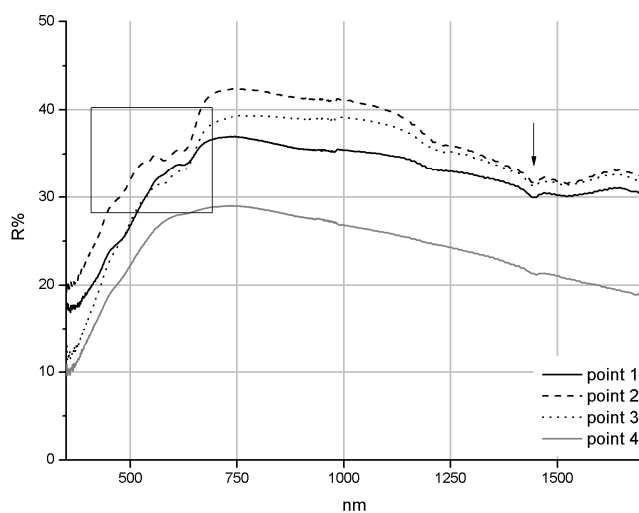


Figure 9: Reflectance spectra of white areas characterised by lead white and cobalt blue.

The spectrum 6 was acquired on a green area and it exhibits the typical behaviour of a copper based green probably mixed with lead white (point 6, Figure 10). As a confirmation XRF analysis detected lead, copper, arsenic, and iron. If the iron cannot be unequivocally linked to one pigment, the detection of arsenic is very important because it identifies that the copper based green as a Schweinfurt green,  $\text{Cu}(\text{CH}_3\text{COOH})_2 \cdot 3\text{Cu}(\text{AsO}_2)_2$ .

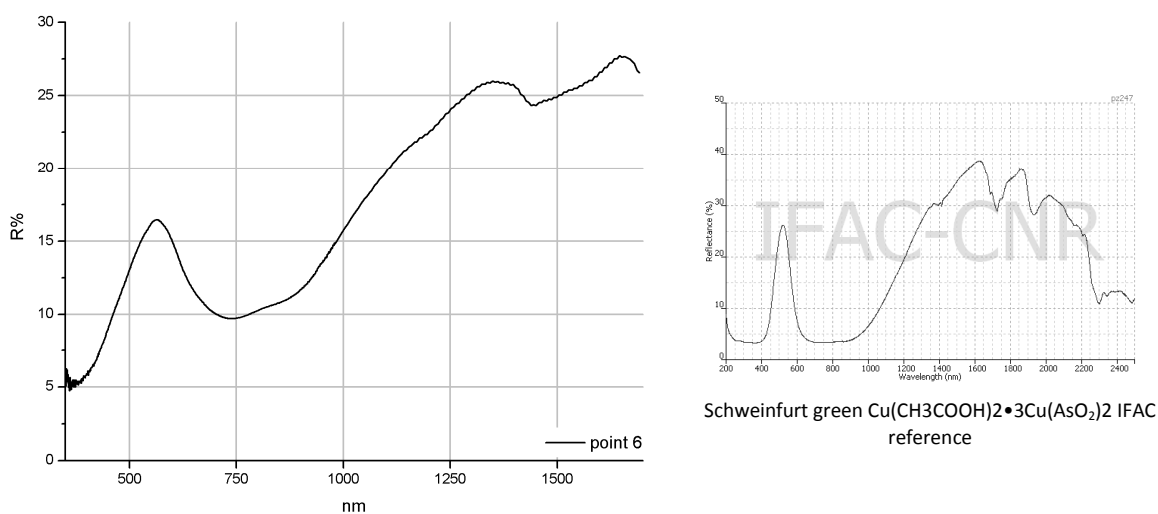


Figure 10: Reflectance spectra of a green area.

The spectral behaviour of the red areas (points 7 and 8, Figure 11) is due to lead white, vermilion, because of the S shape of the curves after 580 nm, and iron oxides/hydroxides, because of the absorptions of the Fe

(III) localised at 650 nm and 850 nm. It should be stressed that even if the absorption at 1450 nm is more emphasised in point 8 than in point 7, the former shows lower reflectance values. This means that in point 8 the reflectance due to the ground layer was detected together with the spectral information due to the pictorial layer. XRF results confirmed the use of vermilion, thanks to the detection of mercury.

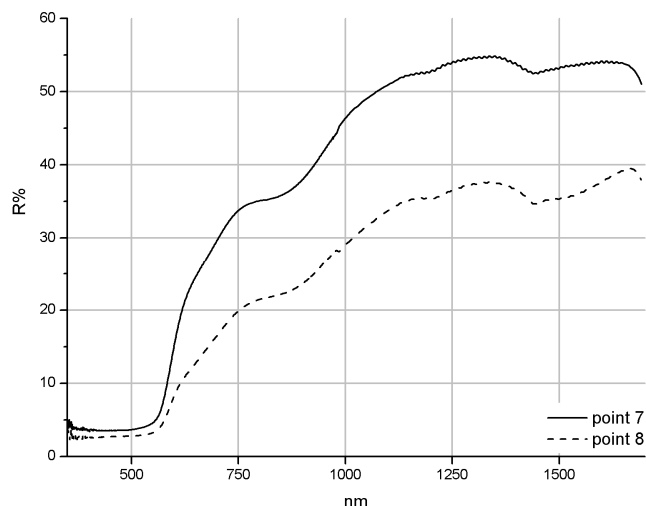


Figure 11: Reflectance spectra of red areas.

The flesh tone was made by mixing lead white, vermilion and a raw earth-based pigments (points 19 and 20, Figure 12) as suggested by the reflectance maximum at 450 nm, typical of raw earth-based pigments characterised by the presence of iron hydroxides. The XRF analysis of point 20 (Table 2) revealed lead, iron, mercury and zinc. Other elements in traces are present, such as manganese, cobalt, and copper attributable to umber earth, cobalt based blue, and copper-based green respectively.

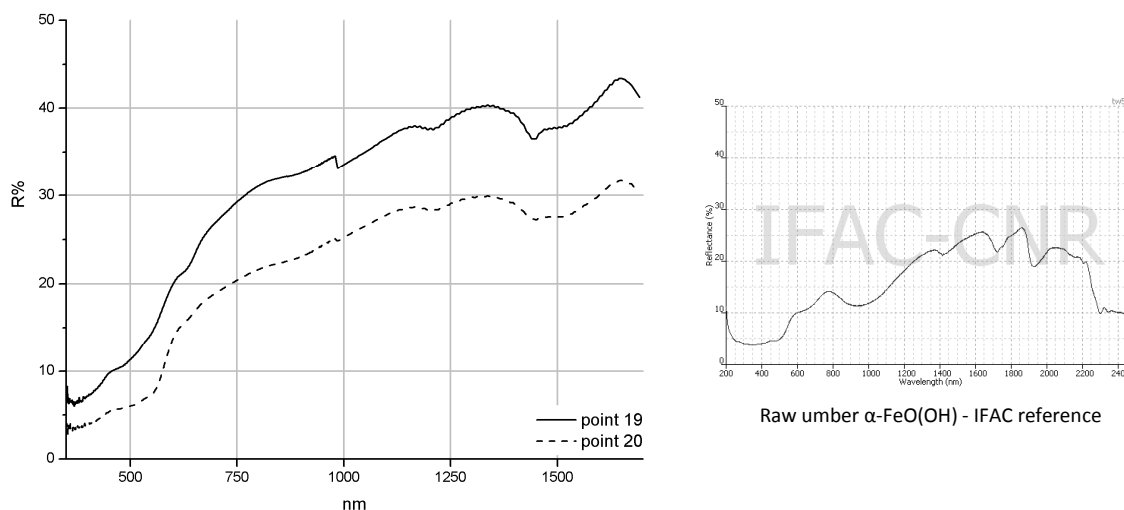


Figure 12: Reflectance spectra of flesh coloured areas.

Grey areas present low reflectance values (Figure 13) and the absorption due to lead white is not clearly visible, probably because of the presence of a black pigment, which absorbs in the NIR. On the other hand, features typical of an earth-based pigment are also detectable (points 13 and 14, Figure 13). The XRF analysis on point 14 confirmed the use of lead white (lead) and an earth-based pigment (iron).

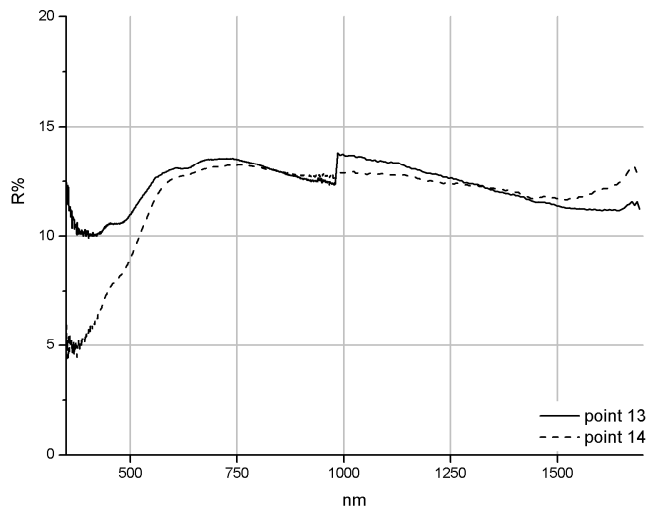


Figure 13: Reflectance spectra of grey areas.

FORS analysis does not yield significant results on black areas, because of the absence of characterising absorptions and the very low reflectance values in all the spectral range considered (points 11 and 12, Figure 14). XRF analyses revealed that lead is present in points 11 and 12, which is probably due to the ground layer, as well as iron, referable to Prussian blue and earth-based pigments. Cobalt and traces of mercury and nickel were detected in point 11. Since the colour of the zones analysed is black, it is reasonable to admit the presence of an organic black which cannot be detected because it is made using light elements. For instance, lamp black, which is amorphous carbon, cannot be revealed with this methodology.

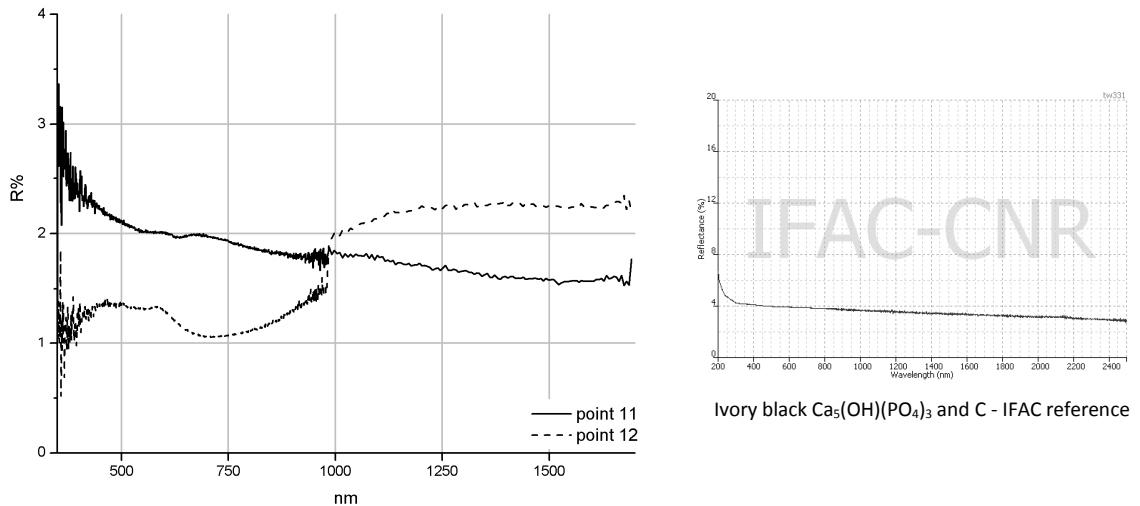


Figure 14: Reflectance spectra of black areas.

### 3.2.3- *Luna di miele*

Oil on panel, 16x29 cm

Signed

Provenience: Diego Martelli's collection, Galleria d'arte moderna of Florence

This painting, known also by the name *Senna's Riversides*, was sent to Florence in 1878 for the exhibition of the Società Promotrice. The value of the work was L. 500 and it came down to L. 400 for the second exposition at the *Esposizione Solenne* in Florence the following year.

*Luna di miele* is defined as the first French production of Zandomeneghi painted in an international manner [3, 5].

The analyses was conducted using a the hyperspectral scanner in order to obtain detailed documentation of the paint in the visible (Figure 15) and in the NIR ranges (Figures 16 and 17) and to investigate further aspects revealed by FORS analysis.

The study of the IR images did not reveal the presence of a preparatory drawing. On the contrary, in the IR image (Figures 16) it was possible to study the artist's brushwork which appears very fast and not dense, particularly in the sky and in the river where the white reflectance of the ground layer emerges. In both IR images a retouching on the female figure close to the plinth seems to be present. Therefore, the application of the principal component analysis (PCA) was performed in order to clarify this detail. In fact, by studying the 5<sup>th</sup> component (Figure 18) it was possible to recognise an inhomogeneous area in the same position which appears particularly bright, possibly due to a different sequence in the paint layers. Moreover, the presence of an area strongly enhanced at the top of the painting was noted, which seems to delineate the varnish layer.

By studying the IR false colour image it is possible to make some considerations about the artist's palette. For example the blue violet colour of the vegetation suggests the use of the same material mixed differently like a copper based green or a cinnabar green [12, 13]. On the other hand, some brushstrokes in the foreground and the light blue line on the other side of the river have an orange-grey tonality. The yellow colour of the belt suggests the use of a vermilion or cadmium red while the red colour of the earring could be due to a blue pigment reflecting in the NIR such as an ultramarine blue or a cobalt blue (Figure 19 and 20). In this point it was not possible to carry out a FORS acquisition because the probe used did not allow for analysis of the centre of the area of interest, therefore, the spectrum obtained by hyperspectral data was taken into account (Figure 20).



Figure 15: Luna di miele, F. Zandomenighi. Visible.



Figure 16: Luna di miele, F. Zandomenighi. IR - 880 nm.



Figure 17: Luna di miele, F. Zandomenighi. IR false colour.



Figure 18: Luna di miele, F. Zandomeneghi. Image obtained by PCA5.

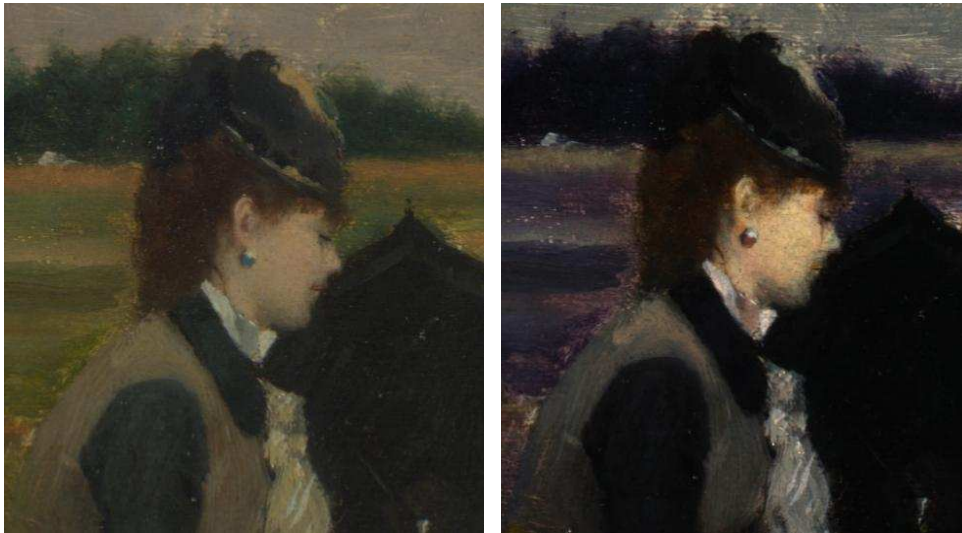


Figure 19 and Figure 20: Luna di miele, F. Zandomeneghi. Detail, visible and IR false colour.

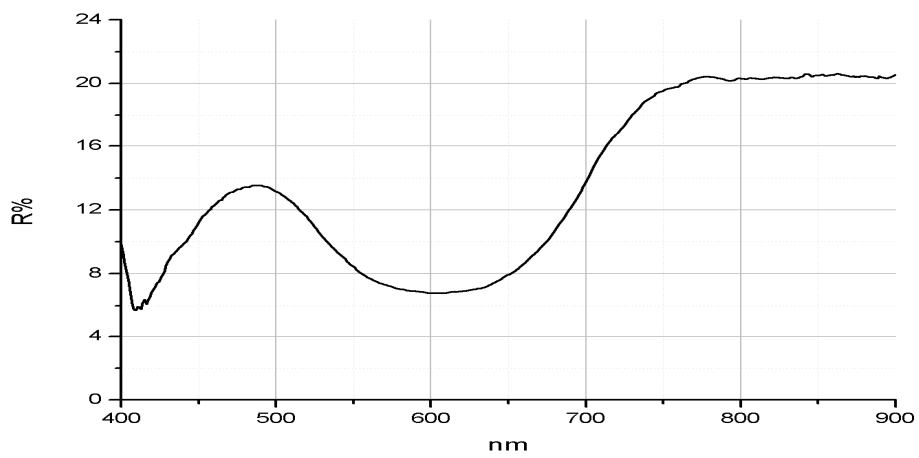


Figure 21: Reflectance spectrum obtained by hyperspectral data on the blue earring.



The reflectance maximum at around 480 nm and the minimum in the red region, centred at 600 nm can be attributed to a blue pigment like ultramarine blue ( $\text{Na}_{8-10}\text{Al}_6\text{Si}_6\text{O}_{24}\text{S}_{2-4}$ ). In fact, this material is characterised by an absorption in the red region due to a charge transfer transition on the sulfur ion [14] and its reflectance increases from 650 nm by determining a shoulder at 740 nm. Unfortunately indigo, which is a colorant often used as a pigment, exhibits a similar spectral curve. Therefore discerning the two pigments could be problematic when using only FORS data.

FORS measurements were carried out on 40 spots by means of Zeiss spectroanalysers MCS 601 and MCS 611 NIR 2.2 in the 350-2100 nm spectral range (Figure 22). Some of these spots were also analysed by XRF. Table 1 shows for the analysed points the number of the FORS measurement, the exhibited colour, the description, the tentative pigment identification and the elements detected by means of XRF analyses.

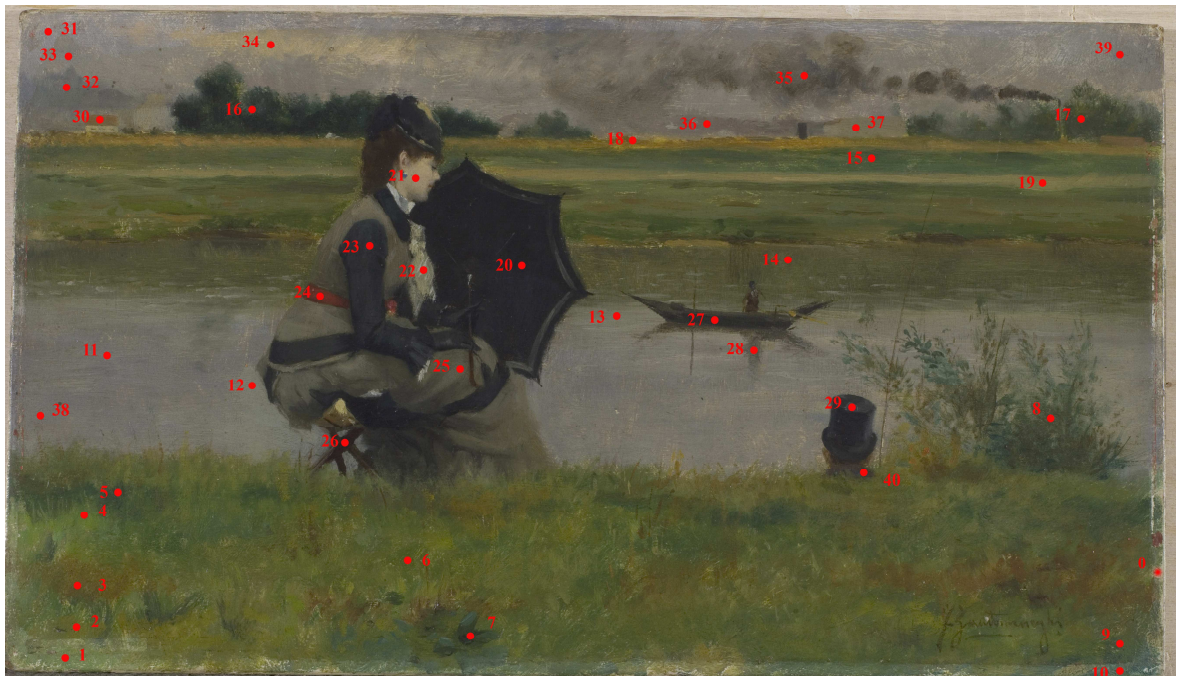


Figure 22: Luna di miele, F. Zandomeneghi. Points of FORS measurements.

Name	Luna di Miele				
Place	Private Conservation Laboratory – Muriel Vervat Restauro				
Device	Zeiss MCS601 and Zeiss MCS611 NIR 2.2 WR				
Light source	Zeiss CHL500				
Fibre	n.1 visible optical fibre and n. 2 near infrared optical fibres				
Probe	AC3 0°/2x45°				
Range	350-1700 nm				
Point	Description	Colour		Pigment hypothesis	Notes
0	Preparation	White			Pb
1	Grass bottom side under the frame	Green		Lead white, Prussian blue, chrome yellow	
2	Grass on the left	Green		Lead white, Prussian blue, chrome yellow	Pb Zn Fe Cr Ca Cd?
3	Grass on the left	Yellow	Dark	Lead white, Prussian blue, chrome yellow	Pb Zn Fe Cr Ca Cd?
4	Meadow on the left	Green		Lead white, Prussian blue, chrome yellow	
5	Meadow on the left	Green		Lead white, Prussian blue, chrome yellow	
6	Meadow in the middle	Green		Lead white, Prussian blue, chrome yellow	
7	Meadow in the middle	Green	Dark	Lead white, Prussian blue, chrome yellow	
8	Bush on the right	Green		Lead white, Prussian blue, chrome yellow	
9	Grass bottom side, on the right	Green		Lead white, Prussian blue, chrome yellow	
10	Grass bottom side, on the left under the frame	Green		Lead white, Prussian blue, chrome yellow	
11	River	Blue	Purple	Lead white, Prussian blue, chrome yellow, vermilion	Pb Fe Zn Cr Hg
12	River	Blue	Grey	Lead white, Prussian blue, chrome yellow	
13	River under the boat	Blue	Purple	Lead white Prussian blue, chrome yellow, vermilion, iron oxides/hydroxides	
14	River	Green	Grey	Lead white, Prussian blue, chrome yellow, iron oxides/hydroxides	
15	Meadow upper side, on the right	Green		Lead white, Prussian blue, chrome yellow, cadmium yellow	Pb Fe Zn Cr Ca Cd
16	Bush	Green	Dark	Lead white, Prussian blue, chrome yellow	Pb Fe Zn Mn Cr
17	Bush upper side, on the right	Green	Dark	Lead white, Prussian blue, modern yellow, iron oxides/hydroxides	
18	Meadow	Yellow		Lead white, iron oxides/hydroxides (umber earth), chrome yellow,	Pb Fe Zn Cr Mn Ca
19	Meadow	Yellow	Light	Lead white , Prussian blue, modern yellow, iron oxides/hydroxides	
20	Umbrella	Black		Black pigment, blue pigment?	Pb Fe Ca Zn
21	Cheek	Flesh		Lead white, iron oxides/hydroxides, Prussian blue, modern yellow	Pb Fe Zn Cr Hg?
22	Jabon	White		Lead white on black layer	
23	Sleeve	Black/blue	Dark	Black pigment, blue pigment?	Pb Fe Zn Mn Cr Ca Co
24	Woman's belt	Red		Lead white, vermilion, red lake	Pb Fe Zn Mn Hg Ca
25	Gown	Grey		Iron oxides/hydroxides, black pigment, Prussian blue/green?	Pb Fe Zn Ca Cr?
26	Stool	Brown		Lead white, iron oxides/hydroxides (raw umber earth)	
27	Boat	Black	Dark	Black pigment, iron oxides/hydroxides, blue pigment?	Pb Fe Zn Mn Ca
28	Shadow reflected in the water	Blue	Grey	Lead white, iron oxides/hydroxides	
29	Man's hat	Black		Black pigment, blue pigment?	
30	Roof of the house on the left	Red		Lead white, red ochre, black pigment	
31	Sky - upper side, on the left	Blue		Lead white, iron oxides/hydroxides, red pigment, blue pigment?	
32	Cloud on the left	Blue	Dark	Lead white , Prussian blue, modern yellow, vermilion	
33	Sky on the left	Blue	Grey	Lead white , blue pigment?	
34	Cloud	White		Lead white, Prussian blue, vermilion, iron oxides/hydroxides	
35	Smoke cloud	Blue	Grey	Lead white, iron oxides/hydroxides	
36	Sky	Grey	Blue	Lead white, blue pigment?	
37	House	Grey		Lead white, iron oxides/hydroxides, green pigment from the layer below?	
38	River left side	Blue	Blue	Lead white, Prussian blue, vermilion, chrome yellow,	Pb Fe Zn Cr Hg Mn?
39	Sky upper side, on the right	Blue	Blue	Lead white , red pigment?, iron oxides/hydroxides? Black pigment?	
40	Man's jacket	Grey	Dark	Lead white , iron oxides/hydroxides (umber earth)	Fe Mn Zn Pb Cd

Table 3: Points analysed with reported the descriptions, the colour, the hypothesis of pigment, and the elements revealed by XRF analyses.

The painting *Luna di miele* has a ground layer obtained with lead white. This was confirmed by both XRF and FORS analyses. In fact, XRF revealed the presence of lead in all the areas analysed (Table 3) and in point O carried out on the surface of the painting where the ground layer was visible. In addition, FORS analyses revealed lead white in all the measurement points, except for points 20, 23 and 29, because of the presence of a black pigment absorbing the NIR which masks the absorption of lead white at 1450 nm.

Moreover, in several spectra a small absorption at 1388 nm can be seen, which suggests the presence of clay materials, such as kaolinite [15], usually used in 19<sup>th</sup> century for the preparation layers.

The blue hues of the river (points 11, 12, 13, 28 and 38, Figure 23) were characterised by a mixture of several pigments difficult to identify by FORS analysis alone. It is possible to hypothesise the presence of a blue pigment, such as Prussian blue characterised by iron, which was detected by XRF (points 11 and 38, Table 3), mixed with a yellow pigment that shift the reflectance maximum from 490 nm to around 525 nm and the reflectance minimum from 700 nm to 620 nm. Chromium was detected with XRF (points 11 and 38, Table 3) suggesting that the yellow pigment is a chrome yellow. However, the shoulder at 740 nm and the high reflectance values over this value can be explained, for example, by admitting the presence of a third blue pigment, such as ultramarine blue or indigo. Due to the specific equipment, the XRF system used was unable to identify light elements such as C, H, N, O, and Na elements, which could characterise one of these pigments. Mercury revealed in points 11 and 38 (Table 3) is due to vermilion which confers a purple tonality. Vermilion, present in small amounts, is also visible in the reflectance spectra because it causes a sort of shoulder at around 590 nm (Figure 23).

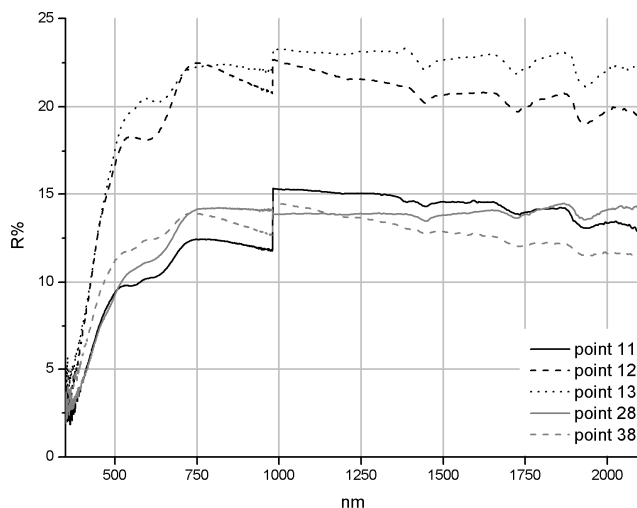


Figure 23: Reflectance spectra of blue areas of the river.

Green areas were made by using a mixture of Prussian blue and yellow pigment probably a chrome yellow as confirmed by XRF analyses (point 3, Table 3). In one point the presence of cadmium was also detected (point 15, Table 3), which can be linked to a cadmium yellow. The spectra acquired (points 1, 2, 4, and 7, Figure 24) show similar behaviour characterised by a reflectance maximum between 530 nm and 570 nm with an absorption localised at 700-720 nm, typical of Prussian blue. As a consequence, it is possible to conclude that for all the green areas of the pictorial layers the artist used the same combination of

pigments, just changing the percentages of blue and yellow, and by adding more or less lead white in order to make the tone lighter, as it is possible to note for example in point 6 (Figure 24).

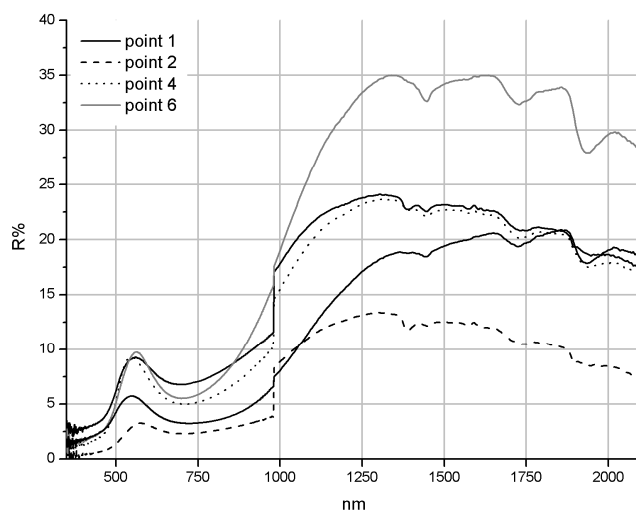


Figure 24: Reflectance spectra of green areas characterised by a mixture of Prussian blue and yellow.

A divergence map on point 4 was obtained in order to localise the green areas made with a mixture of Prussian blue and yellow. The image obtained (Figure 25) made it possible to extend point by point information achieved through FORS analysis to the whole pictorial surface. In fact, comparing the visible image (Figure 15) with Figure 25 it was possible to see that both the banks of the river were made with the same materials (a mixed green) except those areas where an earth based pigment was added, which appear brighter in Figure 25.

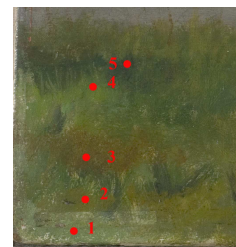


Figure 25: Luna di miele, F. Zandomeneghi. Divergence map on point 4.

The red pigments were vermilion and a red lake, detected together in the woman's belt (point 24, Figure 26). XRF analysis revealed in this point the presence of mercury, characterising vermilion, and iron, which can be due to an earth pigment, probably an umber earth tone because of the detection of manganese (point 24, Table 3). On the other hand, the red colour of the roof of the house on the left side seems to be due to red ochre (point 30, Figure 23).

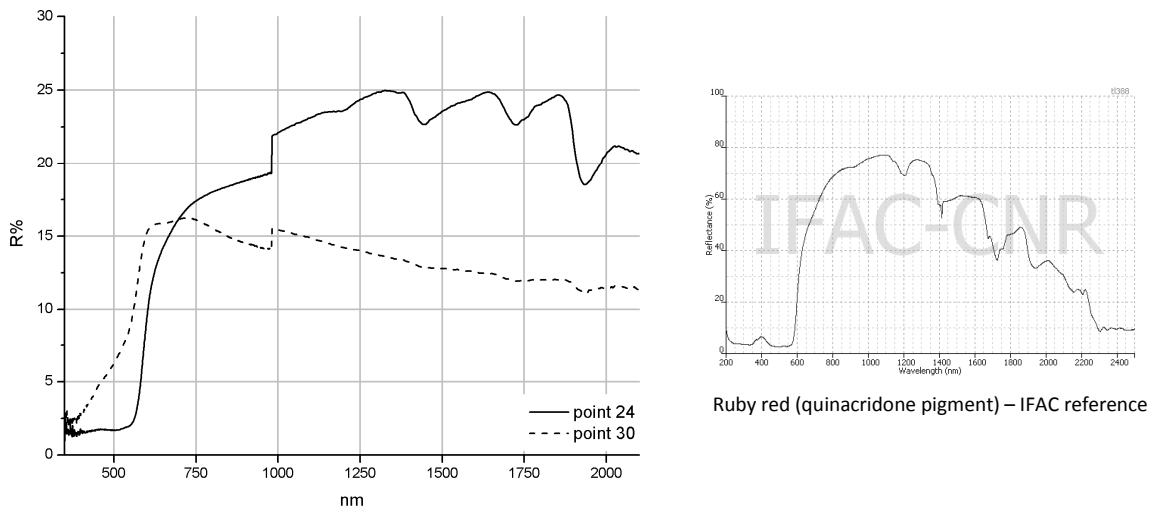


Figure 26: Reflectance spectra of red areas characterised by vermilion and red lake,

The yellow areas (points 3, 18, and 19, Figure 27) owe their colour to a yellow earth pigment and modern yellows. Point 3 exhibits the spectrum of a mixture of Prussian blue and modern yellow, probably a chrome yellow as confirmed by XRF analysis (point 3, Table 3) which detected chromium and iron. A similar spectrum characterises point 19, which probably contains also an earth pigment recognisable by the maximum at 450 nm. Concerning point 18, XRF results confirmed the presence of a chrome yellow together with a yellow-brown earth, such as a raw umber because of the detection of iron and manganese (point 18, Table 3) [16, 17].

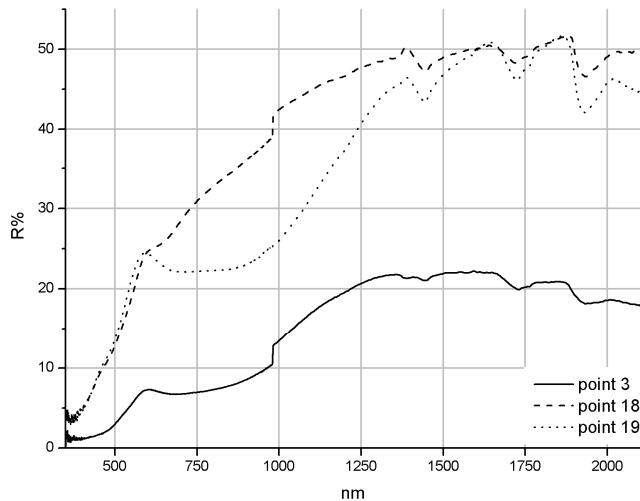


Figure 27: Reflectance spectra of yellow areas.

A divergence map on point 18 was calculated in order to localise the presence of earth pigments (Figure 28). The black areas are formed by the set of points characterised by a divergence angle close to 0°, which indicate a spectral similarity with the curve of point 18.



Figure 28: Luna di miele, F. Zandomenighi. Divergence map on point 18.

A point was also acquired on the face of the woman that was made with lead white, earth based pigments and vermilion (point 21, Figure 29); in fact XRF revealed on this point lead, mercury, iron and manganese (point 21, Table 3).



Figure 29: Reflectance spectrum of a flesh area.

Black areas (points 20, 23, 27, and 29, Figure 30) exhibit curves characterised by low reflectance values included between 2% and 6% in the visible and in the near infrared range, typical spectral behaviour of black pigments. Even if the curves seem to be the result of a mixture including a blue-green pigment, no more information can be given just by studying FORS results. On the other hand, XRF analyses (point 20, 23, and 27, Table 3) detected the presence of calcium in a considerable amount that could be related to the ivory black,  $\text{Ca}_5(\text{OH})(\text{PO}_4)_3 + \text{C}$ . Iron can be linked to Prussian blue or to an earth-based pigment, while the co-presence of iron and manganese suggest the use of an umber. In point 23 the detection of chromium, probably linked to a chrome yellow, and cobalt in traces, suggesting the use of a cobalt-based blue was quite interesting.

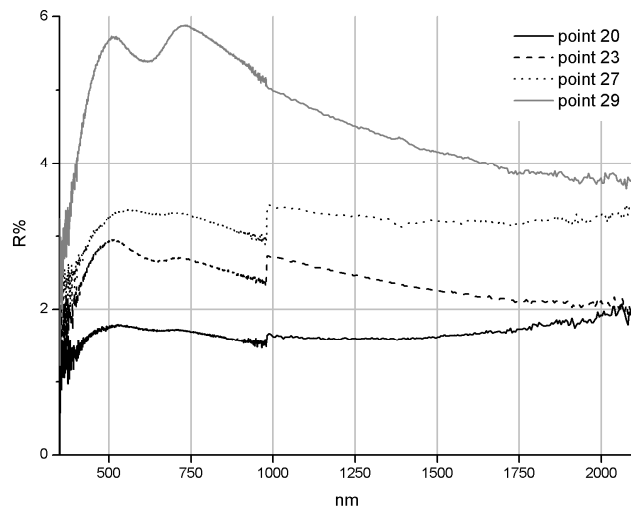


Figure 30: Reflectance spectra of black areas.

Finally, the brown colour of the plinth (point 26, Figure 31) was analysed and the spectrum acquired exhibits the typical behaviour of a raw umber.

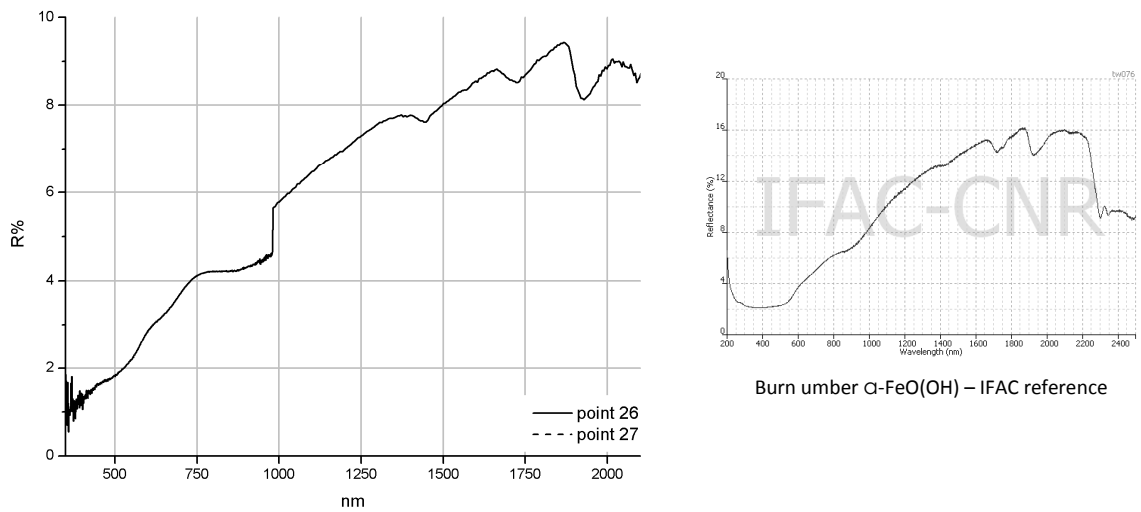


Figure 31: Reflectance spectrum of a brown area.

### 3.2.4- *A letto*

Oil on canvas, 60.5x74.5 cm

Signed and dated 1878

Provenience: Diego Martelli's collection, Galleria d'arte moderna of Florence

*A letto* was presented at the *Promotrice Fiorentina* in 1878 and at the *Esposizione Solenne della Società di incoraggiamento di Belle Arti* in 1879 remaining unsold probably because of the subject represented, a young woman in her bedroom, and the position assumed which was considered too intimate. As a consequence it entered Martelli's collection. This painting is one of the most important of Zandomeneghi's production and it is considered the perfect mix between a Tuscan building scheme and Parisian chromatism [3, 5].

Hyperspectral scanner analyses were used in order to obtain detailed documentation of the paint in the visible (Figure 32) and in the NIR ranges (Figure 33 and 34) and to investigate further some aspects brought to light by FORS analysis.

Even if there is no information about the presence of a preparatory drawing, IR images highlighted a mark around the central figure. This drawing, visible also in the RGB image, was probably made with the brush in order to create the outline of the body and the arm. A thinner line was also used to define the ear (Figure 35).

IR false colour images showed that the wall of the room has a patchy pictorial layer, in fact, in the proximity of the vertical lines it is possible to observe an orange tone probably due to the presence of pigments characterised by high reflectance values in the NIR. The same behaviour is evident in the flower decorations, blue in visible image and in their outline, which is characterised by a red colour in IR false colour image (Figure 36). As a consequence, it is possible to hypothesise for these areas that a blue pigment such as an ultramarine blue, or indigo, or a cobalt-based blue is present [12, 13]. Similar considerations can be made for the blanket, where the intensity of the cherry-red increases with the increasing of the intensity of the blue in RGB image.

The yellow colour of the flowers on the wall and the blanket (Figure 34) is probably due to the same red pigment, which could be vermilion.





Figure 32: A letto, F. Zandomenighi. Visible.



Figure 33: A letto, F. Zandomenighi. IR – 880 nm.



Figure 34: A letto, F. Zandomenghi. IR false colour.



Figure 35: A letto, F. Zandomenghi. IR – 880 nm, detail.



Figure 36: A letto, F. Zandomenghi. IR false colour, detail.

FORS measurements were performed after the cleaning intervention on 81 spots by means of Zeiss spectroanalysers MCS 601 and MCS611 NIR 2.2 WR in the 350-2100 nm spectral range (Figure 37). Some of these spots were also analysed by XRF. Table 4 shows for the analysed points the number of the FORS measurement, the exhibited colour, the description, the tentative pigment identification, and the elements revealed by XRF analysis.



Figure 37: A letto, F. Zandomeneghi. FORS analysis points.

Name Place	A letto Private Conservation Laboratory – Muriel Vervat Restauro				
Device	Zeiss MCS601 and Zeiss MCS611 NIR 2.2 WR				
Light source	Zeiss CHL500				
Fibre	n.1 visible optical fibre and n. 2 near infrared optical fibres				
Probe	AC3 0°/2x45°				
Range	350-1700 nm				
Point	Description	Colour		Hypothesis of pigment	Notes
1	Nightdress	White	Blue	Lead white, cobalt blue	Pb
2	Sheet	White		Lead white, cerulean blue	Pb
3	Pillow	Blue	Light	Lead white, cerulean blue	Pb Co
4	Pleat of the nightdress	White	Blue	Lead white, cerulean blue	
5	Pleat of the nightdress	White	Blue	Lead white, cerulean blue, yellow pigment?	
6	Pleat of the nightdress	White	Blue	Lead white, cerulean blue, yellow pigment?	
7	Pleat of the nightdress	White	Blue	Lead white, cerulean blue, yellow pigment?	
8	Pleat of the nightdress	White	Blue	Lead white, cerulean blue, yellow pigment?	
9	Pleat of the pillow	White	Blue	Lead white, cerulean blue, yellow pigment?	
10	Shirt	White		Lead white, cerulean blue, yellow pigment?	
11	Sheet	White	Grey	Cerulean blue, yellow pigment, black pigment	
12	Sheet	White	Blu	lead white, cerulean blue, iron oxides/hydroxides (yellow earth)	Pb Fe
13	Sheet	White		Lead white, cobalt based blue?, black pigment?	
14	Sheet	White		Lead white, cobalt based blue, iron oxides/hydroxides (yellow earth)	Pb Fe
15	Pleat of the sheet	White	Blue	Lead white, cobalt based blue, iron oxides/hydroxides (yellow earth)	XRF Pb Fe Ca
16	Pleat of the sheet	White	Blue	Lead white, cobalt based blue, iron oxides/hydroxides (yellow earth)	
17	Sheet	White		Lead white, cerulean blue, iron oxides/hydroxides (yellow ochre?)	
18	Sheet	White		Lead white, cerulean blue, iron oxides/hydroxides (yellow ochre?)	
19	Sheet	White	Blue	Lead white, cerulean blue, iron oxides/hydroxides (yellow ochre?)	
20	Sheet	White		Lead white, cerulean blue	
21	Fitted Sheet	White	Grey	Lead white, cobalt based blue, iron oxides/hydroxides (yellow ochre?), black pigment?	
22	Fitted Sheet	White		Lead white, cobalt based blue, iron oxides/hydroxides (yellow ochre?)	
23	Pillow	Blue		Lead white, cobalt based blue, iron oxides/hydroxides	
24	Pillow	White	Blu	Lead white, cerulean blue	
25	Pleat of the pillow	Blue		Lead white, cerulean blue	
26	Pillow	Blue	Light	Lead white, cerulean blue	
27	Pillow	White		Lead white, cerulean blue, black pigment?	
28	Fitted Sheet	Grey		Lead white, cobalt based blue, yellow pigment, ultramarine blue?	
29	Pleat of the fitted sheet	Grey		Lead white, iron oxides/hydroxides, black pigment	
30	Fitted Sheet	White		Lead white, cobalt blue	
31	Bed	Grey	Dark	Lead white, cobalt blue, ultramarine blue	
32	Pillow	Blue	Light	Cobalt based blue, iron oxides/hydroxides	
33	Pillow	Blue	White	Cerulean blue, black pigment	
34	Large Pillow Cover	Grey	Light	Cobalt based blue(?), yellow pigment?, black pigment	
35	Large Pillow Cover-shadow	Grey		Cobalt based pigment, black pigment, yellow pigment?	
36	Pillow	Blue	light	Cerulean blue, black pigment, yellow pigment?	
37	Bed	Brown	Light	Lead white, iron oxides/hydroxides (raw earth?)	
38	Bed	Brown	Light	Lead white, iron oxides/hydroxides, vermilion	Pb Fe Hg Ca
39	Bed	Brown	Dark	Lead white, iron oxides/hydroxides, vermilion, black pigment	
40	Canvas – lower and outer side,			Copper based green	XRF Pb Fe Hg Zn Cu Ba Ca (XRF point 84)
41	Bed	Grey	Dark	Ultramarine blue, black pigment	
42	Bed	Brown	Dark	Iron oxides/hydroxides, black pigment	Pb Fe Ca
43	Blanket	Blue	Dark	Lead white, cerulean blue	
44	Bed	Brown	Dark	Iron oxides/hydroxides (Burnt Sienna Earth)	
45	Bed – bright side	Brown	Light	Iron oxides/hydroxides (Raw/Burnt Umber Earth?), vermilion	Pb Fe Hg
46	Bed – bright side	Brown	Light	Iron oxides/hydroxides, blue pigment?	
47	Bed – bright side	Brown	Light	Lead white, cobalt base blue on iron oxides/hydroxides layer	
48	Blanket	Blue	Light	Cerulean blue, lead white?	
49	Blanket	Blue	Light	Cerulean blue	
50	Blanket	Blue	Light	Lead white, cerulean blue	
51	Blanket	Blue	Light	Lead white, cerulean blue	
52	Blanket	Blue	Light	Cerulean blue	Pb Fe Co Sn

53	Blanket	Blue	Dark	Cerulean blue, black pigment	
54	Blanket	Blue		Cerulean blue	
55	Blanket	Blue		Cerulean blue	Pb Fe Co Sn Ni
56	Blanket	Blue		Lead white, cerulean blue	
57	Cheek	Flesh		Lead white, iron oxides, cobalt based blue	Pb Fe Co
58	Armpit	Flesh- Brown	Light	Lead white, iron oxides/hydroxides, cobalt based blue(tr)	Pb Fe Co Cu
59	Arm	Flesh	Blue	Lead white, Cobalt blue, iron oxides/hydroxides	Pb Fe Co Cr Cu
60	Arm	Flesh	Light	Lead white, iron oxides/hydroxides , cobalt based blue	
61	Wall	Red	Dark	Red ochre on cobalt based blu , vermilion	Pb Fe Co Zn Ba
62	Wall	Red	Light	Lead white, red lake, iron oxides/hydroxides	Fe Zn Ba
63	Blanket - decoration	Red		Red ochre, iron oxides/hydroxides	Pb Fe Co Cu
64	Wall - decoration	Red	Light	Lead white, iron oxides/hydroxides on cobalt based blu layer	
65	Blanket - decoration	Yellow		Lead white, iron oxides/hydroxides (raw Sienna earth) , cerulean blue	
66	Hair	Brown		iron oxides/hydroxides (umber earth)	Pb Fe Mn Ca
67	Hair	Brown		iron oxides/hydroxides (raw umber earth))	Pb Fe Mn Ca
68	Wall	Grey	Light	Lead white, iron oxides/hydroxides, black pigment?	Pb Fe Ca
69	Canvas- outer side			black pigments , ?	Pb Fe Ca Zn
70	Wall	White		Lead white, iron oxides/hydroxides	
71	Wall	Purple	Grey	Lead white, cobalt based blue, umber earth	Pb Fe Mn Co
72	Wall - decoration	Green	Light	Lead white , green earth	
73	Wall - decoration	Green		Lead white, green earth, iron oxides/hydroxides	
74	Wall - decoration	White	Blu	Lead white , cerulean blue	Pb Fe Co
75	Wall - decoration	Brown	Light	Lead white , cobalt based pigment, iron oxides/hydroxides	
76	Wall	Brown	Light	Lead white, iron oxides/hydroxides , cobalt based blue?	
77	Wall - decoration	Purple	Light	Lead white, cobalt based blue, iron oxides/hydroxides	Pb Fe Mn Co Ca
78	Canvas – outer and upper side			Lead white , iron oxides/hydroxides, ?	Pb Fe Co Ca Cu Hg
79	Wall	Brown - grey	Light	Lead white, iron oxides/hydroxides,	
80	Canvas – outer, upper and left side			iron oxides/hydroxides	
81	Canvas – outer, bottom and left side			Lead white, iron oxides/hydroxides	Pb Fe Co Cu

Table 4: Points analysed with reported the descriptions, the colour, the pigment hypothesis, and the elements revealed by XRF analyses.

Five spectra were acquired from the canvas sides, two on the left side (points 80 and 81, Figure 38) and one on each remaining side (point 78, on the upper side, point 69 on the right side, and point 40 on the bottom side, Figure 38). These spectra are not similar to each other. This means that the painter's brushwork is not contained within the painting's surface but it has gone beyond or that the external edges of the canvas were used to 'clean' the brush from the colour. The absorption at 1450 nm and the presence of lead revealed by XRF in all points analysed (Table 4) suggests the presence of a sort of lead white based preparation layer (ground layer). Zinc was also detected in several points (points 40, 61, 62, 69, Table 4) together with barium (points 40, 61 and 69,) probably linked to form Lithopone ( $ZnS+BaSO_4$ ), which was developed in the 1870s as a substitute or supplement for lead carbonate [18]. Unfortunately the FORS methodology is not able to detect pure Lithopone because it does not exhibit specific absorption in the working spectral range. On the other hand, the use of zinc white was excluded because in the spectra acquired the absorption between 350 nm and 370 nm characteristic of this pigment is not present.

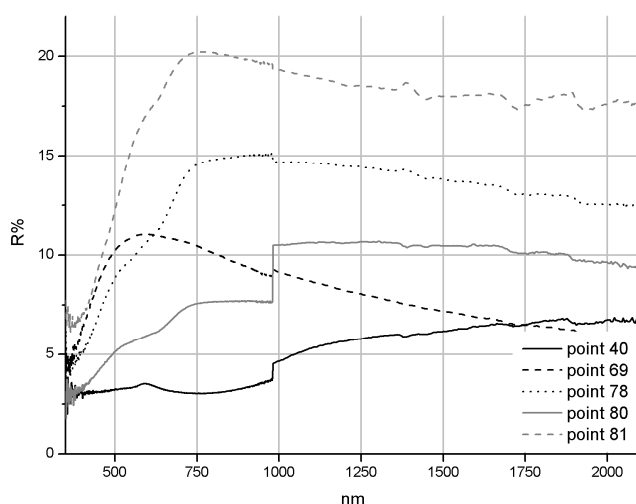


Figure 38: Reflectance spectra acquired on the canvas.

The bedclothes were obtained with lead white and a cobalt-based pigment. For the nightdress, cerulean blue (point 7, Figure 39) and cobalt blue (point 1, Figure 39) were revealed. Cerulean blue ( $CoO \cdot nSnO_2$ ) and cobalt blue ( $CoO \cdot Al_2O_3$ ) can be distinguished by FORS because they exhibit an absorption band divided into three absorptions in the visible range due to *d-d* transition of the Co (II) ion [10] shifted 20 nm toward higher wavelengths for the cerulean blue (Figure 40). Also the pillow was made with cerulean blue (points 26, 33 and 36, Table 4), even if in some cases the attribution of the blue pigment is not certain because the absorptions are localised in an intermediate position between those characterising cerulean blue and those characterising cobalt blue (point 27, Table 4). The blue blanket was made with cerulean blue, both pure or mixed with lead white (points 48, 49, 50, 51 and 52, Figure 41), as confirmed by XRF analyses which revealed cobalt and tin, elements characterising cerulean blue (points 52, 55, Table 4). In the spectra showed in Figure 41, the absorption band at 1200-1800 nm divided in three sub-bands characteristic of the cobalt (II) ion in a tetrahedral symmetry are clearly visible [10]. Regarding the bed-sheets, FORS analyses indicated the use of lead white with cerulean blue (points 18, 20, Figure 42), while cobalt blue was clearly detected only in point 30 (Figure 42). In several points a cobalt-based blue not clearly identified was

present. The problematic interpretation can be explained admitting that the blue pigment is present in small amounts. In these cases, XRF analyses did not yield any additional information; they did not reveal the cobalt probably because it is present in small amounts (points 12, 14 and 15, Table 4). Obviously, where the presence of a cobalt-based blue pigment has been hypothesised a co-presence of cobalt blue and cerulean blue cannot be excluded.



Figure 39: Reflectance spectra acquired of white-blue areas characterised by cobalt based blues and lead white – nightdress.

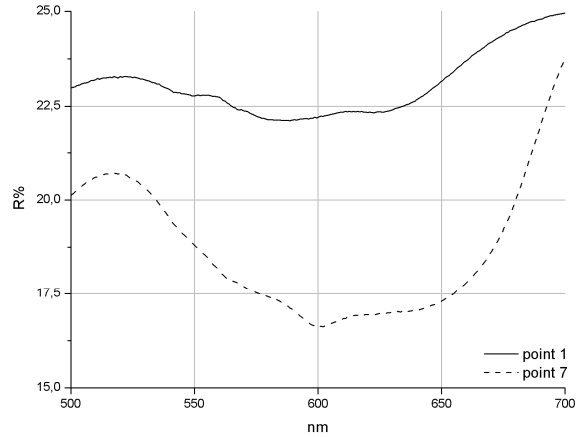


Figure 40: Reflectance spectra acquired of white-blue areas of the canvas focused on the 500-700 nm spectral range.

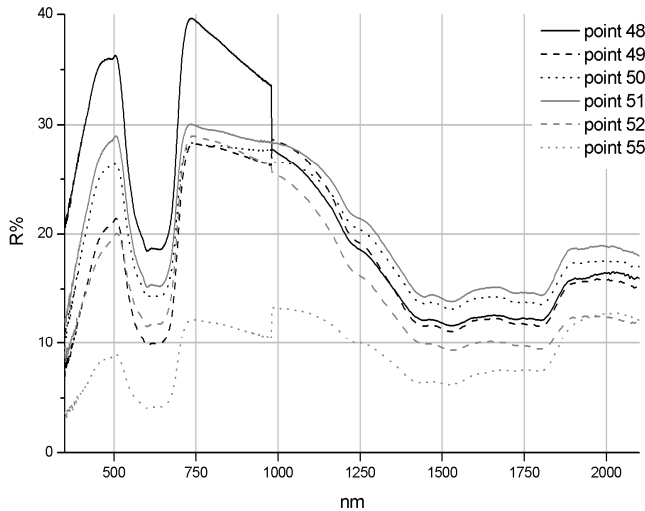
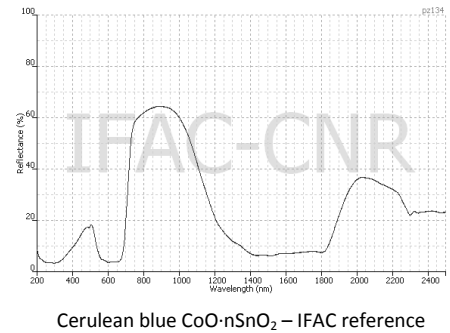


Figure 41: Reflectance spectra acquired of blue areas characterised by cerulean blue – blanket.



Cerulean blue  $\text{CoO}\cdot n\text{SnO}_2$  – IFAC reference

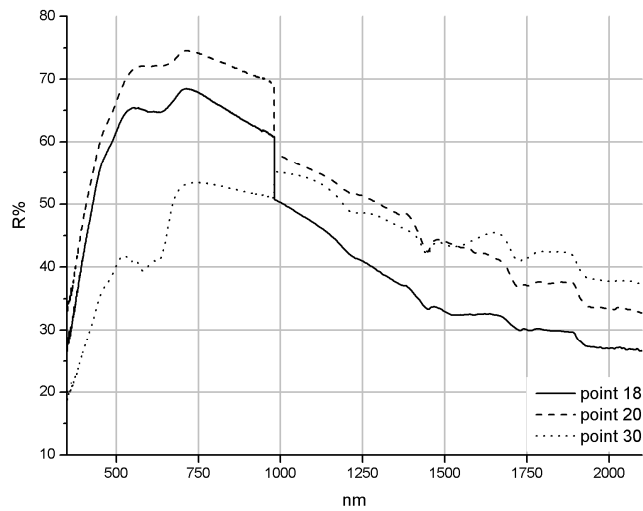


Figure 42: Reflectance spectra acquired of blue areas characterised by cerulean blue – sheets.

Several computation methods were applied to the multi-spectral sequence of images in order to distinguish cobalt blue from cerulean blue. At first, a divergence map on point 1, where cobalt blue was clearly detected, was obtained (Figure 43). Dark areas are formed by points with reflectance spectra similar to the reference spectrum (point 1). Even if the blanket is clearly differentiated from point 1, it is reasonable to admit that the evaluation of the divergence is influenced by the average behaviour of the reflectance curve, which can sometimes give more weight than the small differences between cerulean blue and cobalt blue. Interestingly, there were black areas on the arm (where FORS point 59 was collected, Figure 37) of the figure which allowed to hypothesise that cobalt blue was present; also the non homogeneous grey levels of the blue blanket proved the non-uniformity of that pictorial surface.



Figure 43: A letto, F. Zandomenighi. Divergence map on point 1.

A second try was done analysing the curvature of the spectra collected in the 580-620 nm spectral range, where cerulean blue and cobalt blue can be better differentiated thanks to the absorption at 600 nm of cerulean blue (Figure 44) which determines a positive value of the curvature visualised as light spots. The



map obtained was a distribution of cerulean blue, which is clearly present in the blanket but not in the bedclothes (light grey result). While in the arm, the dark-grey result observable in Figure 44 seems to confirm the presence of cobalt blue .



Figure 44: A letto, F. Zandomenighi. Curvature map focused on the 580-620 nm range.

In fact, FORS analyses reveal that the flesh tone was made with lead white, an earth-based pigment, probably a raw one, mixed with a cobalt based blue (points 57, 58, 59 and 60, Figure 45), which for point 59 is cobalt blue. Except for point 59, the cobalt-based blue was not easily recognisable by studying the visible range but it is clearly evident in the near infrared. The previous observation can provide interesting suggestions on the pictorial technique, for example that flesh tones were obtained starting from a blue tinted ground subsequently covered by brushworks of lead white and earth-based pigment. Lead, iron and cobalt revealed by XRF analyses seems to confirm the previous hypothesis. Vermilion (characterised by mercury) was not revealed (points 57, 58 and 59, Table 4). In addition, in points 58 and 59 small amounts of copper and chrome were detected (Table 4), the former probably linked to a copper-based green pigment while the latter to a chrome yellow.

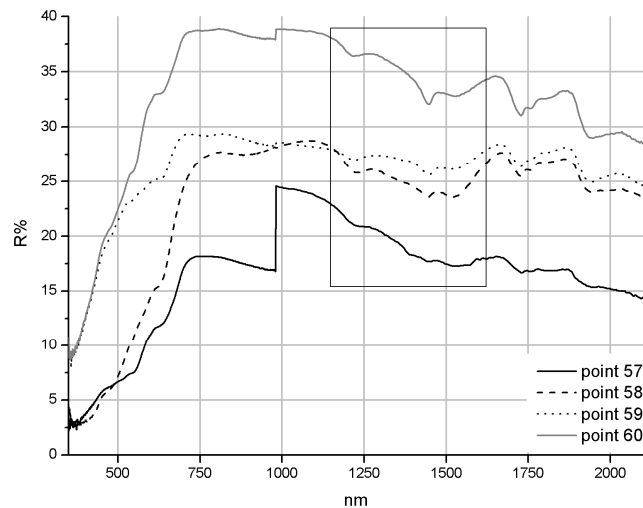


Figure 45: Reflectance spectra of Flesh-coloured areas.

For the brown zones mainly earth based pigments were used. The girl's brown hair was probably done with an umber as confirmed by the presence of iron and manganese (points 67 and 68, Table 4 and Figure 46). The bed frame was obtained with dark earth pigments (points 37 and 45, Figure 45). In some points cobalt-based blue (point 37, Figure 46) and an unidentifiable black pigment (point 42, Figure 46) were added. The presence of vermilion was hypothesised in a few cases (points 38 and 45, Figure 46), and confirmed by XRF analysis which revealed mercury (Table 4).

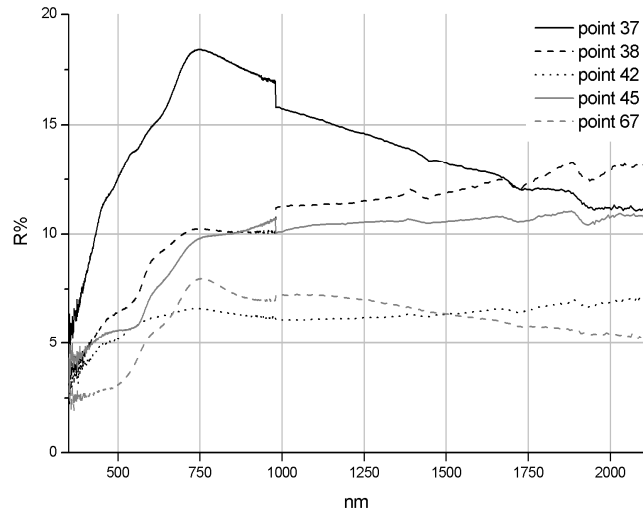


Figure 46: Reflectance spectra of brown areas.

It is very interesting to note that it was hypothesised that ultramarine blue or indigo were used in points 31 and 41 (Figure 47) in order to obtain a dark grey tonality, but unfortunately this hypothesis cannot be verified by XRF because the device used is not able to detect the elements characterising ultramarine blue (Si, Al, Na and S).

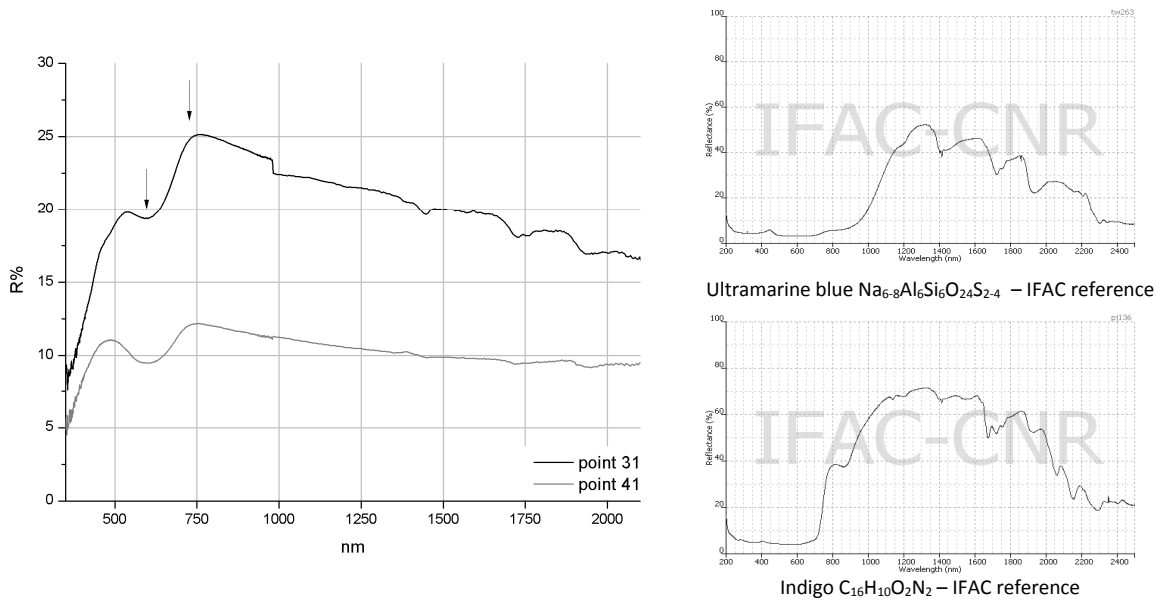


Figure 47: Reflectance spectra of grey areas.

By studying the hyperspectral data acquired by the scanner, it was possible to analyse a blue outline drawing present on the wall, which was too small to be analysed by FORS because of the dimension of the probe. The reflectance result of the point analysed (Figure 48) revealed a blue pigment characterised by an absorption band at 600 nm and a shoulder at 740, as well as ultramarine blue or indigo as previously shown. So, a divergence map was obtained to verify if it was possible to select points with a similar spectral behaviour. The image obtained clearly showed the presence of the reference blue pigment in all the blue lines of the wall (Figures 49 and 50) and in some areas of the blanket (Figure 49). In the latter cases, FORS analysis was not able to differentiate ultramarine blue/indigo because their spectral features get confused with the features of cerulean blue.

The presence of ultramarine blue or indigo was also detected in points 31 and 4, which appear darker than the surrounding areas (Figure 51).

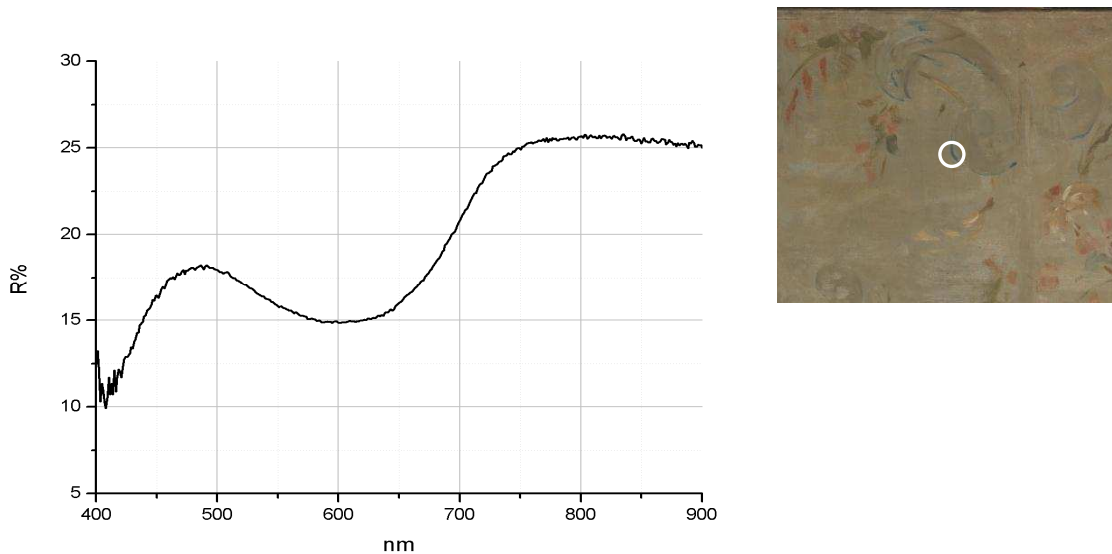


Figure 48: Reflectance spectrum obtained by hyperspectral data on a blue line.



Figure 49: A letto, F. Zandomenighi. Divergence map on the blue point shown in Figure 48.

Figure 50 and Figure 51: A letto, F. Zandomenighi. Divergence map on the blue point shown in Figure 48. Details.

Red areas (the flowers on the blanket and the wall of the room) owe their colour to red ochre (points 61, 62, 63, and 64, Figure 52). The cobalt detected by XRF (points 61 and 63, Table 4) is probably localised in the underlying pictorial layer. As a confirmation, FORS spectra exhibit the absorption due to a Co (II) ion tetrahedral symmetry (absorptions between 1250 nm and 1750 nm), mainly in point 64. The spectrum of point 62 owes its red colour to a mixture of vermilion, or cadmium red, or red lake with a black and an earth-based pigment. The absence of mercury and cadmium, not revealed by XRF, suggests that the painter used a red lake (Table 4).

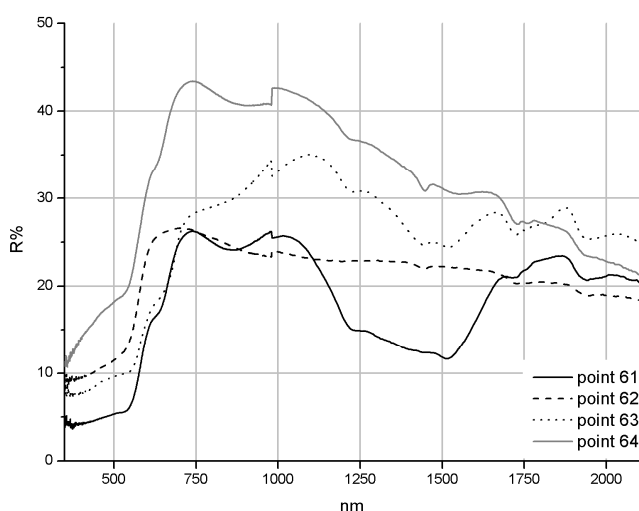


Figure 52: Reflectance spectra of red areas.

The green decorations on the wall were probably obtained with lead white and a green earth pigment (points 72 and 73, Figure 53). This latter pigment is easily recognisable in the measurement point 72, while it is partially hidden in point 73.

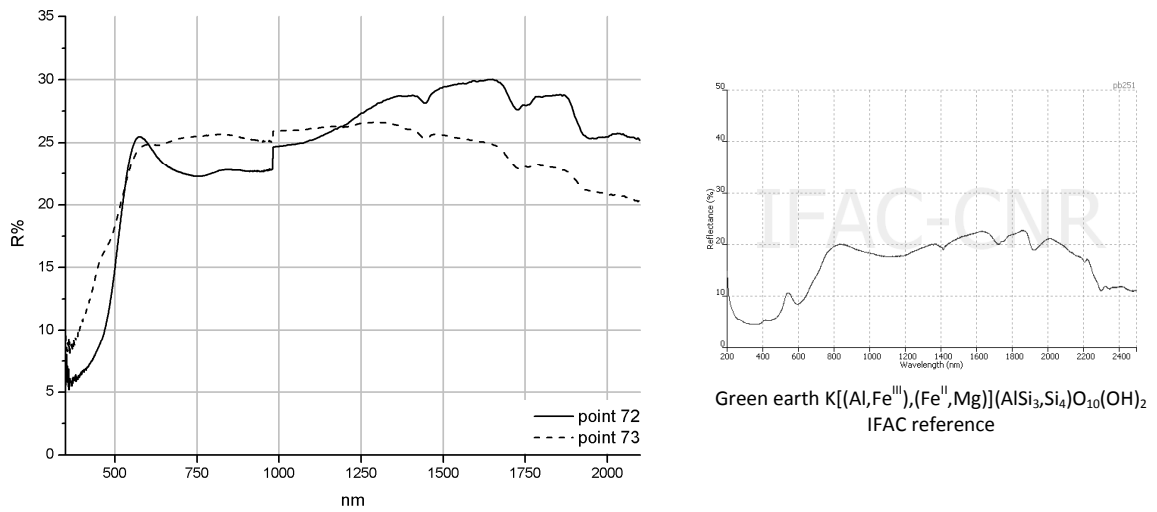


Figure 53: Reflectance spectra of green areas characterised by green earth.

Finally, the purple hues on the right wall are mixtures of lead white, earth pigments, and cobalt based blue, (points 71 and 77, Figure 54), as previously hypothesised after studying IR false colour images (Figure 36).

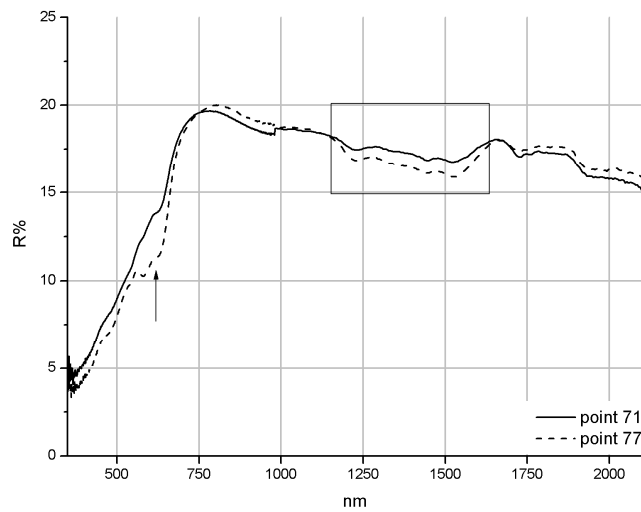


Figure 54: Reflectance spectra of purple areas.

### 3.3- Silvestro Lega (Modigliana, 1826 – Florence, 1895)

In 1843 Lega moved to Florence from Modigliana, a small town in the current province of Forlì-Cesena. In Florence he enrolled in the Accademia and then attended the school of Mussini, who trained him in Tuscan purism. In 1848 he enlisted as a volunteer in the first Italian war for independence. Upon his return to Florence he entered the school of Ciseri. He also frequented Caffè Michelangelo and he began to approach the group of artists who usually met there. Even when he started to paint outdoors using the new chromatic technique called *macchia*, he did not entirely abandon the purist influences of Mussini.

His first work painted in this new manner was *Imboscata di bersagliere in Lombardia*, presented at the Florence International Exhibition in 1861. In that year Lega visited Piagentina where, starting in the beginning of 1862, he stayed for a long period and began with Borrani, Serensi and Abbati a series of studies on the representation of nature. He became friends with the Batelli Family and in particular with the oldest daughter of Spirito Batelli Virginia. This period spent in the Batelli house was fundamental for the artistic production of Lega, who in these years painted some of his masterpieces such as *La curiosità* (1866), *Il canto dello stornello* (1868), and *La visita* among the best works of 19<sup>th</sup> century Italian art.

In 1870, after the death of Virginia Batelli, he came back to Modigliana and fell into a period of depression made worse by an eye disease. He gradually used brighter and brighter pigments in his pictures culminating in the dramatic use of colour of the Gabbro period, mainly characterised by the production of portraits and landscapes painted in the inland area of Leghorn where he spent long periods as a guest of the Bandini family. He died in poverty in 1894, at Florence's Ospedale San Giovanni di Dio [1, 2, 3].

### 3.3.1- *Passeggiata in giardino*

Oil on canvas, 35x22 cm

Dated 1864

Provenience: Diego Martelli's collection, Galleria d'arte moderna of Florence

*Passeggiata in giardino* belonged to Diego Martelli, who left the painting to the Municipality of Florence. In an inventory made in 1896 this artwork was named *Bozzetto di Paese*. The spiritual hues and the natural affection are predominant in Lega's poetry, as well as in this paintings that was set close to Batelli's home in Piagentina. The same background could be recognised in *La visita*, the most famous work by Lega [19, 20].

The analyses conducted by using the hyperspectral scanner resulted in detailed documentation of the paint in the visible (Figure 55) and in the IR ranges (Figure 56 and 57), and permitted the further investigation some aspects revealed during FORS analysis.

The study of IR images (Figure 56 and 57) did not uncover the presence of a preparatory drawing. The pictorial layers appear compact, without any trace of *pentimenti* or retouchings. The brushwork is elegant and refined and the surface seems to be polished. By magnifying the images it is possible to observe how the features of the paint were constructed using only colour stains. For example the details of the facial features were obtained using light brushstrokes which disappear in IR images (Figure 58 and 59). This characteristic is clearly evident also in the road surfacing, where the stones were created with homogeneous close layers of complementary colours – light blue and yellow-orange-, which appear grey to the eye (Figure 60 and 61).



Figure 55: *Passeggiata in giardino*, S. Lega.

The IR false colour image is characterised by a red tonality, particularly in the sky, in several points of the paving and in the grey areas, such as the shadows of the central figures and the creases of the dress of the woman on the right. By focusing on the shadows in the RGB images it is clear that Lega did not use black pigments to obtain the chiaroscuro but he instead exploited the *cangiantismo*.

As a consequence, it was reasonable to exclude the use of a Prussian blue for the sky, which has a dark appearance in IR false colour, and hypothesise a pigment reflecting the NIR, such as a cobalt based blue, or an ultramarine blue, or indigo.



Figure 56: Passeggiata in giardino, S. Lega. IR – 880 nm.



Figure 57: Passeggiata in giardino, S. Lega. IR false colour (enhanced).





Figure 58: Passeggiata in giardino, S. Lega. IR – 880 nm, detail.



Figure 59: Passeggiata in giardino, S. Lega. IR false colour, detail.



Figure 60: Passeggiata in giardino, S. Lega. Visible, detail.

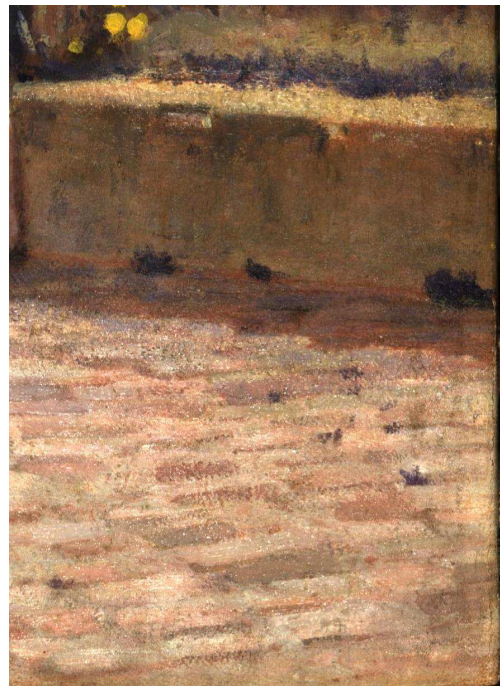


Figure 61: Passeggiata in giardino, S. Lega. IR false colour, detail.

FORS measurements were performed on 37 spots by means of Zeiss spectroanalysers MCS 601 and MCS611 NIR 2.2 WR in the 350-2100 nm spectral range (Figure 62). Table 5 shows for the analysed points the number of the FORS measurement, the exhibited colour, the description, and the tentative pigment identification.



Figure 62: Passeggiata in giardino, S. Lega. Points of FORS measurements.

Name Place	Passeggiata in giardino Private Conservation Laboratory – Muriel Vervat Restauro			
Device	Zeiss MCS601 and Zeiss MCS611 NIR 2.2 WR			
Light source	Zeiss CHL500			
Fibre	n.1 visible optical fibre and n. 2 near infrared optical fibres			
Probe	AC3 0°/2x45°			
Range	350-1700 nm			
Point	Description	Colour		Pigment hypothesis
1	Embroidery - dress	Green		Lead white, Prussian blue, yellow pigment, ultramarine blue/indigo
2	Grass	Green		Lead white, Prussian blue, yellow pigment
3	Grass	Green		Lead white, Prussian blue, yellow pigment
4	Greenery	Brown		Lead white, iron oxides/hydroxides, ultramarine blue/indigo
5	Greenery	Green		Lead white, copper based green, Prussian blue, yellow pigment
6	Greenery	Green		Lead white, copper based green, Prussian blue, yellow pigment
7	Greenery	Green	Light	Lead white, Prussian blue, yellow pigment, ultramarine blue/indigo
8	Leaves	Green		Lead white, ultramarine blue/indigo
9	Grass	Green		Lead white, ultramarine blue/indigo, yellow pigment
10	Grass	Green		Prussian blue, yellow pigment on lead white, ultramarine blue/indigo layer
11	Greenery	Green	Dark	Prussian blue, yellow pigment on lead white, ultramarine blue/indigo layer
12	Background	Green	Blue	Prussian blue, yellow pigment, lead white?
13	Fruit	Orange		Lead white, iron oxides/hydroxides on green layer
14	Tree leaves	Green	Light	Prussian blue, yellow pigment, ultramarine blue/indigo
15	Tree leaves	Green		Lead white, Prussian blue +modern yellow
16	Dress - woman on the right	White		Lead white, iron oxides/hydroxides, ultramarine blue/indigo
17	Dress - woman on the left	White		Lead white, ultramarine blue/indigo, ?
18	Foulard	Yellow		Lead white, iron oxides/hydroxides, yellow pigment?
19	Woman's dress on the right	White		Lead white, iron oxides/hydroxides, ultramarine blue/indigo
20	Cheek - woman on the left	Flesh		Lead white, iron oxides/hydroxides, vermilion/cadmium red
21	Parasol - right side	Orange	Light	Lead white, iron oxides/hydroxides
22	Parasol - right side	Orange		Lead white, iron oxides/hydroxides
23	Parasol on the left	Purple	Light	Lead white, iron oxides/hydroxides (red ochre?), ultramarine blue/indigo
24	Parasol on the left	Purple		Lead white, iron oxides/hydroxides (red ochre?), ultramarine blue/indigo
25	Tree trunk	White		Lead white, iron oxides/hydroxides (red ochre?), ultramarine blue/indigo
26	Sky on the left	White		Lead white, iron oxides/hydroxides (red ochre?), ultramarine blue/indigo, yellow pigment
27	Sky on the left	Blue	Light	Lead white, ultramarine blue/indigo
28	Tree trunk - shadow	Grey	Dark	Lead white, iron oxides/hydroxides, ultramarine blue/indigo, yellow pigment
29	Background	Grey		Lead white, ultramarine blue/indigo, yellow pigment?
30	Background	Blue	Light	Lead white, ultramarine blue/indigo
31	Flower	Red		Lead white, iron oxides/hydroxides, vermilion/cadmium red?
32	Wall	Orange		Lead white, iron oxides/hydroxides
33	Floor - shadow	Grey		Lead white, iron oxides/hydroxides, ultramarine blue/indigo
34	Floor - light	Brown	Light	Lead white, iron oxides/hydroxides, ultramarine blue/indigo
35	Book cover	Blue		Lead white, ultramarine blue/indigo, yellow pigment
36	Tree trunk on the right	Brown	Light	Lead white, iron oxides/hydroxides, ultramarine blue/indigo
37	Left side edge	White		Barite?

Table 5: Points analysed with the descriptions, the colour, the hypothesis of pigment, and the elements revealed by XRF analyses reported.

The spectrum acquired on a white area, on the left side of the painting can be referred to as the ground layer (point 37, Figure 63). The absorption bands around 1450-1600 nm and 1940 nm are due to the presence of a hydroxyl group, while the double absorption localised between 1.7-1.8  $\mu\text{m}$  is linked to the carbonyl/carboxyl group due to the presence of a binder. The absence of features ascribable to specific artistic pigments or materials suggests the presence of barium sulfate which does not show specific absorption in the spectral range considered.

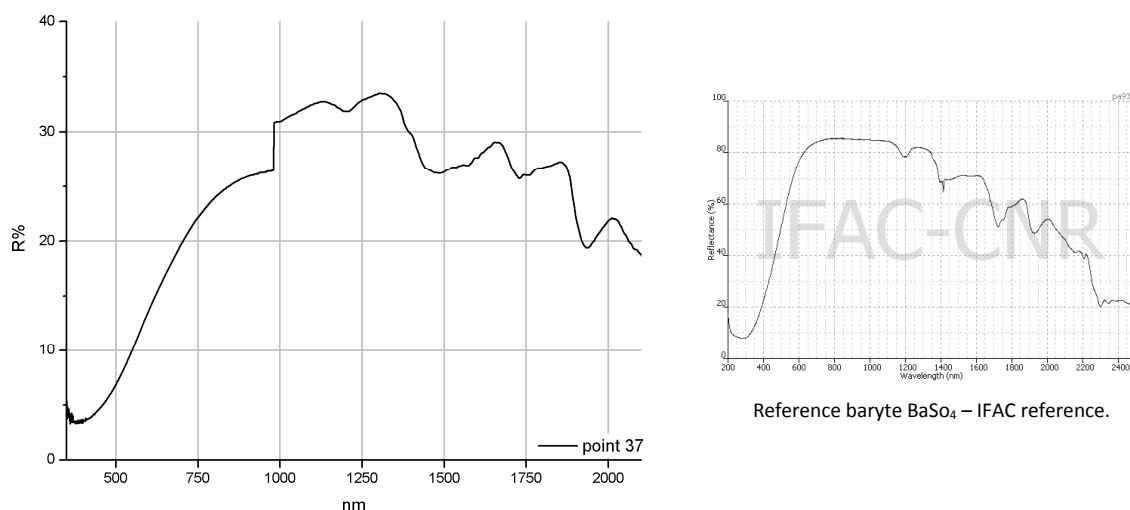


Figure 63: Reflectance spectra of the ground layer.

In this painting there are no areas strictly definable as white, in fact the white pigment used (lead white) was never found to be pure but mixed with iron oxides/hydroxides or ultramarine blue/indigo (points 16, 19, 26, Figure 64). Earth-based pigments are recognisable because of a small maximum at around 585 nm, while the shoulder at 740 nm is due to a blue pigment. It is particularly interesting to compare the spectrum of points 16 and 19, which are basically from the same area, the dress of the woman on the right side. In fact spectrum 19, which represents grey zone, was obtained from the same mixture of point 16 adding more blue in order to achieve the shadow of the dress.

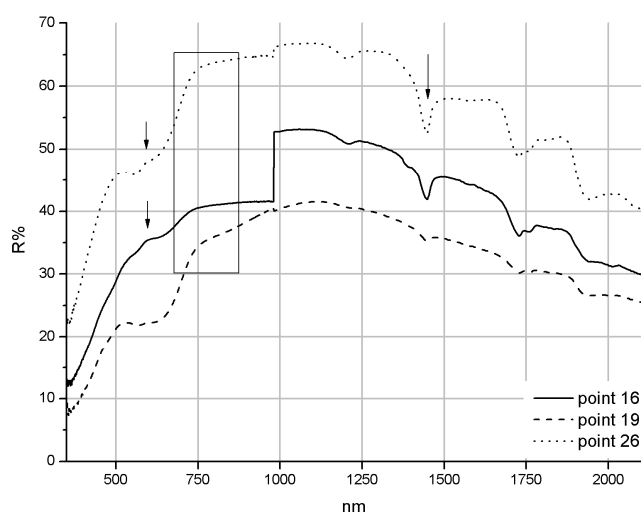


Figure 64: Reflectance spectra of white areas.

The blue areas were made with a mixture of lead white that is probably present in the pictorial layer and a blue pigment characterised by a reflectance maximum at around 490 nm, a minimum centred at 600 nm and a shoulder at around 750 nm (points 27, 30 and 35, Figure 65). Unfortunately with this kind of technique it is not possible to identify clearly this blue material as ultramarine blue or indigo. The spectrum acquired on point 35 present small reflectance values in the NIR without any of the features visible in points 27 and 30. This could indicate the presence of a dark-black under layer.

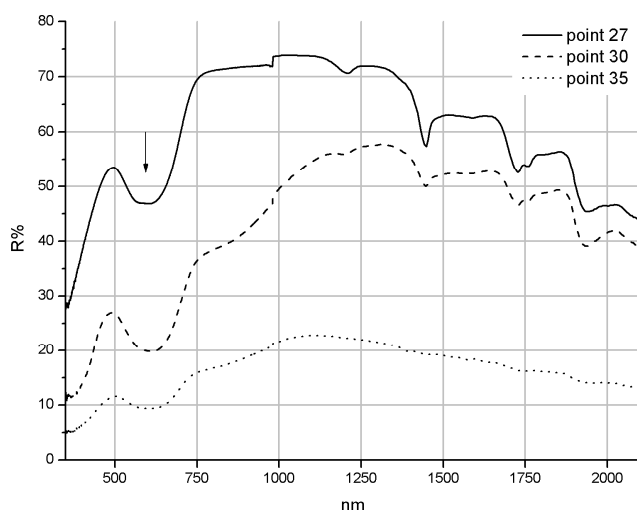


Figure 65: Reflectance spectra of blue areas.

Regarding the green areas, it was very interesting to discover how the painter was able to obtain different tonalities of green by mixing Prussian blue, a yellow pigment, and ultramarine blue/indigo (points 1, 2, 5, and 9, Figure 66). The presence of a copper based green was also hypothesised, mixed with Prussian blue and yellow, in points 5 (Figure 66) and 6 because of the large absorption band centred at 750 nm. The usual mixture of Prussian blue-yellow was detected in points 2 (Figure 66) and 3. As stated before, in some cases the ultramarine blue/indigo seems to completely replace the Prussian blue (point 9, Figure 66).

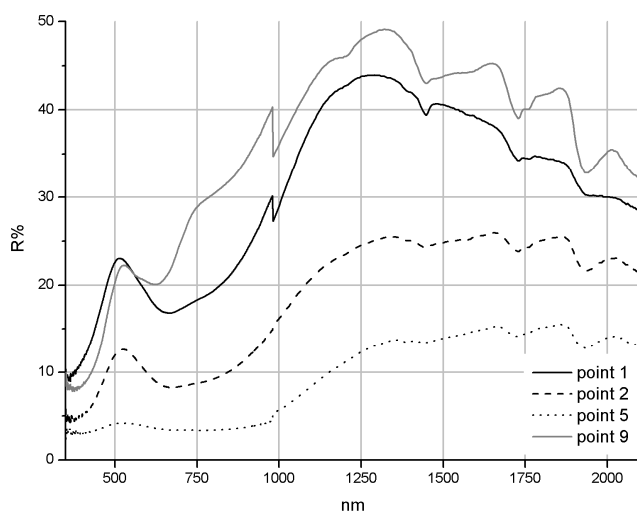


Figure 66: Reflectance spectra of green areas.

Yellow-orange tonalities were made using a mixture of earth based pigments (points 18, 22, and 32, Figure 67). If in point 18 the absorption under 400 nm suggests the presence of a yellow pigment, such as a

chrome yellow, mixed with earths, in points 22 and 32 the orange colour was probably achieved using a red ochre.

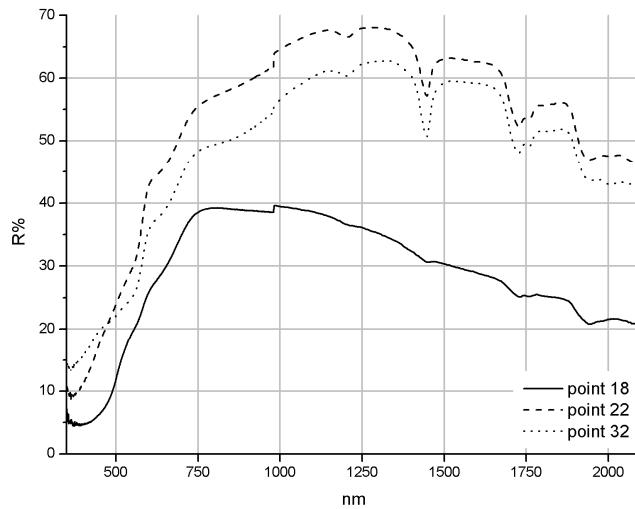


Figure 67: Reflectance spectra of yellow-orange areas.

The red point analysed (point 31, Figure 68) is characterised by the presence of vermilion or cadmium red, while the absorption at around 660 nm and the shoulder at 740 nm are probably due to the underlying green layer. The cheek of the woman (point 20, Figure 68) was made in the usual manner, mixing lead white and an earth-based pigment (probably raw Sienna) with vermilion or cadmium red.

Purples were made with a mixture of ultramarine blue/indigo and a red pigment that seems to be a red ochre, because of the shoulder at about 605 nm and the absorption at 670 nm (points 23, 24, Figure 69). However, the presence of vermilion/cadmium red cannot be excluded.

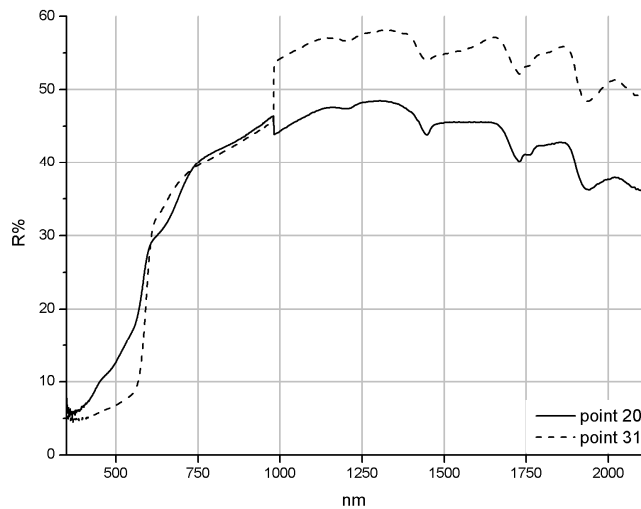


Figure 68: Reflectance spectra of a red area and Flesh-coloured area.

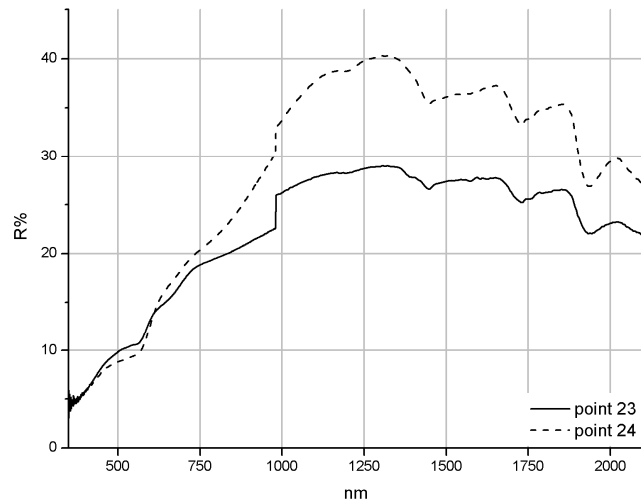


Figure 69: Reflectance spectra of purple areas.

Finally, grey zones were not obtained mixing white and black pigment, but using a blend made up of lead white and a blue component (ultramarine blue/indigo (points 28, 29, and 33, Figure 70). In some cases, the presence of an earth-based pigment can be detected because of a small reflectance maximum around 450 nm (points 28 and 33, Figure 70), while in point 29 the shift of the absorption band from 600 nm to around 620 nm suggests the presence of a yellow pigment such as a chrome yellow.

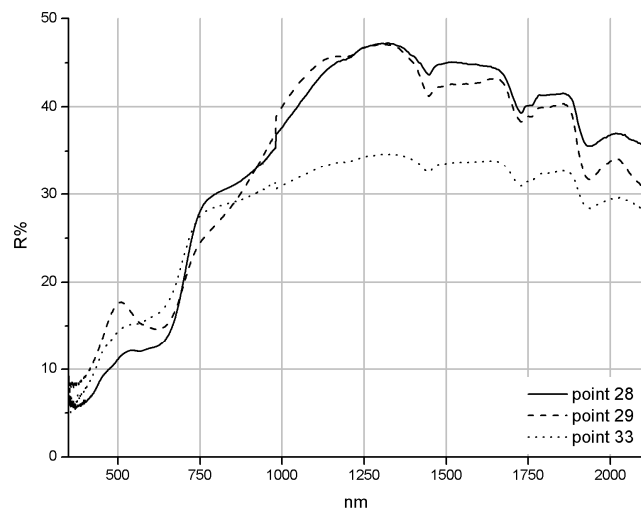


Figure 70: Reflectance spectra of purple areas.

The widespread presence of a blue pigment (ultramarine blue/indigo) detected in several reflectance spectra required the computation of different maps in order to try to localise its real presence on the pictorial layer. The first computation performed was a divergence map by selecting as a reference the spectrum of point 27, where the blue pigment was well detected. The image obtained (Figure 71) showed a high distribution of the pigment (dark spots), which was mainly used for the sky, for the 'grey' shadows of the dresses, for some areas of the vegetation, and finally for the floor. In order to have a second element of comparison, a curvature map was obtained by focusing the working spectral range between 700 nm and

800nm, in correspondence to the shoulder often revealed and attributed to the blue pigment of interest. The results are comparable enough, except for some details such as the tree trunk. In fact, even if the dark grey colour in Figure 72 seems to contain the blue pigment, other materials can present a reflectance maximum or a shoulder in the same spectral range, such as the yellow earth pigment present in the foulard or in the faces of the two women, which appear more grey than in Figure 71.



Figure 71: La passeggiata in giardino, S. Lega. Divergence map on point 27.

Figure 72: La passeggiata in giardino, S. Lega. Curvature map focused on the 700-800 nm range,



### 3.4- Conclusions

FORS analysis provided useful information about the artistic palette of the paintings taken into account. At the same time, image spectroscopy revealed itself as an important tool for mapping some of the pigments detected by FORS and for investigating details too small to be analysed with the FORS probe head. The opportunity to acquire several images of the painting at different wavelengths was useful in obtaining a complete documentation of the pictorial layer. By matching visible images with IR and IR false colour images, some further details on the nature of the materials can be acquired and the presence of inhomogeneous pictorial layers can be discovered. In this work, XRF analysis was performed mainly to confirm the interpretation of FORS spectra. Therefore, since the pictorial layers were particularly complex and multi-stratified, XRF provided telltale information about materials not spectroscopically revealed and on the nature of the ground layer.

Taking all of these results into account some conclusions about the artists' palettes can be drawn.

Zandomeneghi used a palette made up of essential pigments, such as lead white, Prussian blue, cobalt blue, earth based pigments, such as Sienna and umber, yellow and red ochres, vermilion, chrome yellow, and black pigments. However, for each painting some variations in the lists of the pigments discovered were noticed. For example in *Bastimento allo scalo* the presence of a second white pigment together with lead white and zinc white, was detected. In the painting *Ritratto di Diego Martelli* a copper based green was detected and thanks to XRF analyses it was possible to confirm the presence of Schweinfurt green. Even if it was copiously used by Impressionists, Schweinfurt green was not revealed in the other paintings investigated where a mixture of blue and yellow pigments was the preferred choice for creating green areas. Regarding this last mixture, it is important to emphasise that a green made from Prussian blue and yellow chrome was commercially available starting in the second half of the 19<sup>th</sup> century [21]. In *Luna di miele* it was shown that all the green areas were made with different mixtures of Prussian blue and chrome yellow. Unfortunately, it is not possible to say if Zandomeneghi used a cinnabar green tube colour or if he mixed the blue and yellow pigments himself. Probably an invasive analysis on the chemical composition of the materials should be performed in order to answer this question.

A blue pigment not very well identified (ultramarine blue or indigo) was also detected in *Luna di miele* and in *A letto*. Unfortunately, the elements characterising these two materials are too light to be detected by XRF; as a consequence, in order to have a correct identification a chemical analysis on a sample should be conducted. In *Luna di miele* this pigment was clearly used just for a localised point (the woman's earring), while in *A letto* it was detected in the floral decoration of the wall and in some areas of the blanket. Particular to the painting *A letto* is the use of three blue pigments - ultramarine blue/indigo, cobalt blue and cerulean blue, which is the material most present - while Prussian blue does not seem to be utilised. Finally, a not very clearly identified red lake was revealed in the woman's belt in *Luna di miele*.

In Silvestro Lega's paintings, the pigments detected were lead white, iron oxides/hydroxides, Prussian blue, a modern yellow, copper based green and, similarly to the previous cases, a blue pigment not clearly

identified, which is assumed to be an ultramarine blue or indigo. The information provided by image spectroscopy revealed a large use of this blue pigment, which was detected in the sky, in the green areas, in the shadows, and in the blue book in the hands of the woman on the left.

In the paintings analysed with image spectroscopy, the presence of a preparatory drawing was not detected. This lack of a preparatory drawing seems to confirm the fast style of painting of the *Macchiaioli*, who paid more attention to colours than to shapes. This hypothesis can also be supported by the study of the brushworks which are particularly instant and not thorough. This characteristic is more evident in the French work by Zandomenighi than in Lega's paintings. Obviously, these considerations are not valid for the paintings *Bastimento allo Scalo* and *Ritratto di Diego Martelli*, characterised by a more traditional execution. The only retouch discovered concerns the painting *Luna di miele*, where the presence of a pictorial *pentimenti* was discovered with the PCA elaboration.

With regards to the ground layer, the XRF revealed the presence of zinc in all the paintings analysed. This element is present in several materials used for artistic purposes, such as zinc white ( $\text{ZnO}$ ), barite ( $\text{BaSO}_4$ ), and lithopone ( $\text{BaSO}_4 \cdot \text{ZnS}$ ). The presence of zinc white can be excluded because the pigment is easily identifiable with FORS and it was not revealed in the spectra acquired. Barite and Lithopone do not present specific features in the working spectral range so they cannot be identified with FORS, however, the detection of barium can be associated with barite present in the ground layer. In fact, beginning in the first half of the 19<sup>th</sup> century, natural or synthetic barite was used as an extender in lead white preparatory layers because of its stability and lower cost. Moreover, it has been reported that barite was also used in order to cut lead white; as a consequence several mixtures were traded that were made with different percentages of lead white and barite, for example 'Venice white' had a 1:1 lead white-barite ratio, while Hamburg white had a 2:1 lead white-barite ratio. Where XRF analysis detected zinc together with barium the presence of lithopone can also be hypothesised. Even the presence of calcium mainly detected in *Luna di miele e A letto* is probably due to calcium carbonate which could be added in the preparation layer, in the form of earth and black pigments in order to give a light coloration to the base layer [22].

## References

1. The City Art Gallery -Manchester-, and The City Art Centre -Edinburg-, The Macchiaioli, masters of Realism in Tuscany, De Luca Publisher, Roma, 1982.
2. P. Adorno, A. Mastrangelo, L'arte, Correnti, artisti, società. Itinerari di lettura paralleli, V. 3, G. D'Anna Press, Firenze, 2002.,
3. D. Bianco, L. Mannini, A. Mozzanti, La grande storia dell'arte, L'Ottocento, seconda parte. SCALA GROUP Firenze, Milano, 2005.
4. [www.800artstudio.com/en/macchiaioli](http://www.800artstudio.com/en/macchiaioli) last accessed 15<sup>th</sup> December 2010.
5. F. Dini, Federico Zandomenoghi, la vita e le opere. Edizioni il Torchio, Firenze.
6. M. Bacci, Modern Analytical Methods in Art and Archaeology, Chemical Analysis Series, E. Ciliberto, and G. Spoto (Eds.), John Wiley & Sons Inc., New York, 155, 2000, 321.
7. M. Elias, C. Chartier, G. Prevot, H. Garay, C. Vignaud, Materials Science and Engineering B, 127, 2006, 70.
8. R. B. Singer, Journal of Geophysical Research, 87, B12, 1982, 10159.
9. D. M. Sherman, T. D. Waite, American Mineralogist, 70, 1985, 1262.
10. M. Bacci, and M. Picollo, Studies in Conservation, 41, 1996, 136.
11. Master Thesis in Conservation and Diagnostic for Modern and Contemporary Artworks – Lara Boselli, Univesità degli Studi di Ferrara, A.A. 2006/2007.
12. T. Moon, M. R. Schilling, and S. Thirkettle, Studies in Conservation, 37, (1), 1992, 42.
13. M. Bacci, L. Boselli, A. Casini, M. Picollo, and B. Radicati, L. Stefani, "Infrarosso falso colore: tra mito e realtà", in Proc. of VII Congresso Nazionale IGIC, Napoli, 2009, 67.
14. K. Nassau, The Physics and chemistry of Color, J. W. Goodman (Ed.), John Wiley & Sons, New York, 1983.
15. G. R. Hunt, J. W. Salisbury, and c. J. Lenhoff, Modern Geology, 4, 1973, 85.
16. G. Bruno, M. Picollo, B. Radicati, and M. Bacci, in Proc. of AIAR Colore e arte: storia e tecnologia del colore nei secoli, Firenze, 2007, 159.
17. Bachelor Thesis in Technology for Conservation and Restoration of Cultural Heritage – Giulia Bruno, Univesità degli Studi di Firenze, A.A. 2004/2005.
18. F. Feller, Barium Sulfate – Natural and Synthetic, in Artists' Pigments, A Handbook of their History and Characteristics Vol. 3, R. L. Feller (Ed), Cambridge University Press, Cambridge, 1986, 47.
19. Silvestro Lega, I Macchiaioli e il Quattrocento, G. Matteucci, F. Mazzocca, and A. Paolucci (Eds.), Silvana Press, Milano, 2007.
20. <http://www.fondazione-menarini.it/minuti/pdf/328%20Silvestro%20Lega.pdf> last accessed 15<sup>th</sup> December 2010.
21. N. Eastaugh, V. Walsh, T. Chaplin, and S. Ruth, Pigment Compendium A Dictionary of historic pigments, Oxford University Press, Butterworth-Heinemann, New York, 2004
22. P. Bensi, La tecnica della pittura italiana nel Primo Ottocento, in Proc. of Effetto Luce, Materiali, Tecnica, Conservazione della Pittura dell'Ottocento, Firenze, 2008, 65.



## **Chapter 4**

### **Non-invasive spectroscopic analysis of green pigments**

The 19<sup>th</sup> century's industrial and scientific progress resulted in the rapid development of chemical manufacturing processes involving the production of new materials, such as synthetic pigments. As a consequence, a large number of new artists' materials became available to painters.

By studying a number of paintings by Giovanni Fattori, one of the most important members of the *Macchiaioli* movement, it became apparent how difficult it is to detect the pigments present in a complex paint layer using non-invasive spectroscopic analysis. In particular, attention was devoted to the identification of green pigments, lavishly used in *plain-air* paintings. A number of green pigments, all of which were available in the second half of the 19<sup>th</sup> century, were investigated, and reference samples were prepared and studied.

Firstly, mock-ups of green pigments (both pure and in admixture with one another) were prepared and analysed with a bench spectrophotometer in order to obtain high resolution reflectance spectra. Subsequently, the characterisation of the spectra and the identification of the main spectral features was undertaken.

This research has to be considered as a preliminary and non-exhaustive study on the detection of green pigments by means of non-invasive methodologies.

#### 4.1- Analysis and spectroscopic characterization of reflectance spectra of green pigments

The spectra reported in this chapter were obtained from mock-ups by using a Perkin-Elmer spectrophotometer Lambda 1050 UV-Vis-NIR. The mock-ups were prepared by mixing ground powder pigments and linseed oil. The substrate was an industrially-prepared white canvas in order to obtain a reference sample as similar as possible to a real 19<sup>th</sup> century painting specimen. Chemical identification of components of the white canvas will be given below. The pigments used in the mock-ups, their composition and chemical formula, as well as their manufacturer and producer's code, are reported in Table 1.

All reflectance spectra of the mock-ups were recorded in the 350-2500 nm range with a sampling step of 1 nm on an area measuring approximately 0.5 cm wide and 1 cm high. Calibration was performed by means of a 99% Spectralon<sup>®</sup> diffuse reflectance standard. The processing of the reflectance spectra was done using the OriginPro 8<sup>®</sup> software.

Particular attention was paid to the 350-860 nm range of the electromagnetic spectrum because the most important features (reflectance maxima, absorption bands) for many green pigments occur in the visible spectral region. The NIR region of the spectrum is characterised mainly by absorptions due to the preparatory ground layer. The measurements were performed by selecting a 1 nm sampling step for all the spectral range analysed.

With the aim of better defining the position of the absorption bands and the inflection points in the visible range, the first derivative of each spectrum was calculated. A smoothing function was applied to each spectrum in order to reduce the noise. For the smoothing process, the method 'Adjacent-Averaging' working on 10 points was selected: entering an even number  $m$ , then  $m+1$  points are used to calculate each averaged result. After this, the first and second derivative functions of the smoothed spectra were calculated by means of Origin's differentiation tool. The differentiated values were calculated by averaging the slopes of two adjacent points for each data point.

The first derivative is a measure of how a function changes: the absorption maxima and minima of a function go to zero in the first derivative, while the inflection points, the points where the function switches from being a convex function (reflectance) to being a concave function (absorption) or vice versa, are visualised as maxima and minima of the new function. Additionally, the inflection points can be defined as points where the second derivative of a function changes signs, so calculating the second derivative function can also be useful. Unfortunately, the derivation amplifies the noise of the initial function (spectrum) making the result occasionally unreadable. In this case, by using the smoothing operation, for wavelengths below 860 nm, the first derivative functions could easily be used to interpret the reflectance behaviour of the sample while the second derivative spectra were not always taken into consideration.

The spectra of the canvases and the pure green pigments are reported and described below.

Pigment	Composition	Manufacture	Chemical Formula	Image
Malachite	basic copper(II) carbonate	Zecchi	$\text{CuCO}_3 \cdot \text{Cu(OH)}_2$	
Verdigris	copper salts of acetic acid (copper acetates)	Zecchi	$\text{Cu(CH}_3\text{COOH)}_2 \cdot [\text{Cu(OH)}_2] \cdot 2\text{H}_2\text{O}$	
Ultramarine green	calcined kaolin with soda, sulphur and carbon	Zecchi	$2\text{Na}_2\text{Al}_2\text{Si}_2\text{O}_6 \cdot \text{Na}_2\text{S}_2$	
Schfeinfurt green	copper(II)-acetoarsenite	Zecchi	$3\text{Cu(AsO}_2)_2 \cdot \text{Cu(CH}_3\text{COO)}_2$	
Cinnabar green	prussian blue + chrome yellow (lead chromate)	Zecchi	$\text{Fe}_4[\text{Fe(CN)}_6]_3 \cdot n\text{H}_2\text{O} + \text{PbCrO}_4$	
Viridian	hydrated chromium oxide	Zecchi	$\text{Cr}_2\text{O}_3 \cdot \text{H}_2\text{O}$	
Chromium oxide	chromium oxide	Zecchi	$\text{Cr}_2\text{O}_3$	
Cobalt green	solid solution of zinc and cobalt oxides	Zecchi	$\text{CoO} \cdot n\text{ZnO}$	

Table 1: Reference green pigments analysed in this study.

#### 4.1.1- Canvas

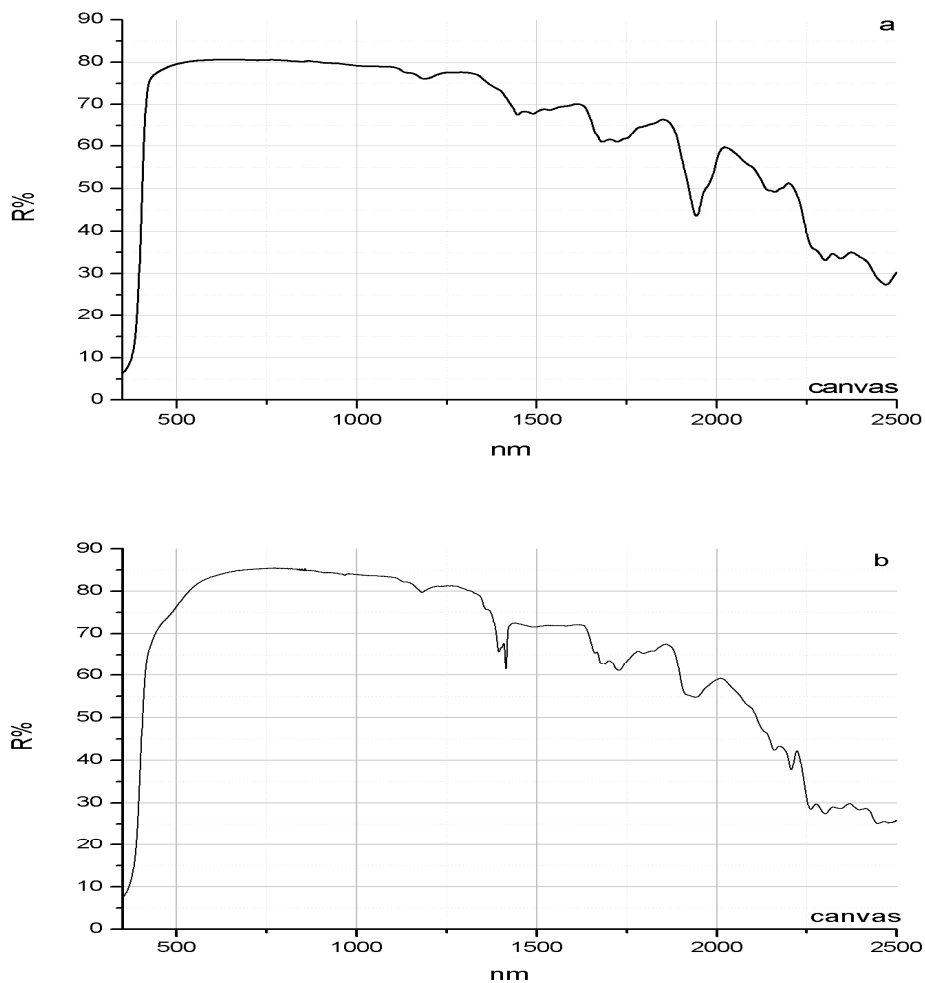


Figure 1: Reflectance spectra of the canvases used to prepare the mixtures' mock-ups (a) and the pure pigments' mock-ups (b).

Figure 1 (a and b) shows the spectra of the typical industrial primed canvases used to prepare the mock-ups. In Figure 1a the presence of both the bands at about 1.4  $\mu\text{m}$  and 1.9  $\mu\text{m}$  indicate water: the former is due to the first overtone of the asymmetric OH stretching, the latter is due to a recombination of the vibrational modes of the OH symmetric stretching and the H-O-H bending [1]. The sharp shape of the absorption also indicates that part of water molecules are present in the form of crystalline water located in defined positions within the molecular structure of the inert materials used for the preparatory layer, for example gypsum or a hydrated aluminosilicate/clay mineral. The absorptions at 1.2  $\mu\text{m}$  and from 1.45  $\mu\text{m}$  to 1.55  $\mu\text{m}$  are characteristic of vibrational water modes in the gypsum molecule: the former is due to the combination of the bending and the first overtone of the asymmetric stretching, while the latter contains the contribution of the first overtone of the asymmetric and symmetric stretching and a combination of the fundamental modes [2]. Gypsum is also characterised by features between 1.7  $\mu\text{m}$  and 2  $\mu\text{m}$ , due to combination tones involving librations of water; all these absorptions can be seen clearly in the spectrum in



Figure 1. Absorption localised in this range, mainly between 1.65-1.8  $\mu\text{m}$  can also be attributed to the carbonyl/carboxyl group due to the presence of a binder in the preparation layer of the support. The absorptions over 2.0  $\mu\text{m}$  can be attributed to carbonates, such as calcium carbonate, that have intense bands around 2.00  $\mu\text{m}$ , 2.35  $\mu\text{m}$ , and 2.5  $\mu\text{m}$ , due to the overtones and internal vibrations of the carbonate group [3].

In conclusion, the presence of all these features suggests that the support, made of canvas and cardboard, has a preparatory layer containing gypsum and calcite. Occasionally, a hydrated aluminosilicate such as kaolinite  $\text{Al}_2\text{Si}_2\text{O}_5(\text{OH})_4$  is added as in the second canvas shown. In Figure 1b the sharp absorption bands around 1.4  $\mu\text{m}$  are due to overtone and combination tones of the fundamental OH stretching modes, the weak water band around 1.9  $\mu\text{m}$  indicated the presence of absorbed molecular water, while the intense features around 2.2  $\mu\text{m}$  are caused by tone involving the AlOH bending fundamental [4]. The absorption band in the UV range is due to titanium oxide ( $\text{TiO}_2$ ), corresponding to the naturally occurring mineral rutile, which has a tetragonal crystalline system, showing an easily recognisable absorption located at 330 nm [5]. Figures 2-10 show the spectra of the green pigments. They all show absorption bands in the NIR region related to the preparatory layer. The intensity of these bands depends on the physical and chemical characteristic of each pigment.

#### 4.1.2- Viridian - $\text{Cr}_2\text{O}_3 \cdot \text{H}_2\text{O}$

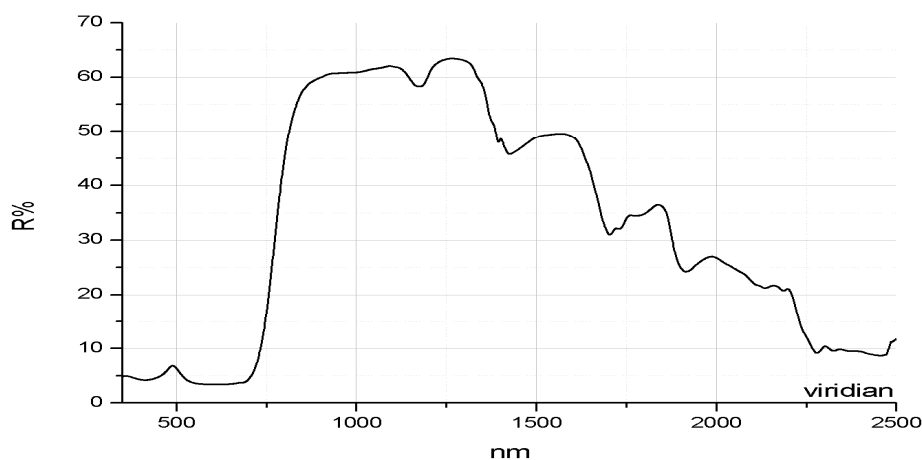


Figure 2: Reflectance spectrum of viridian.

Viridian, a hydrated chromium (III) oxide, was first prepared in 1838 by the colour maker Pennetier and his assistant in Paris, but the high price of the starting materials made the pigment prohibitively expensive. However, due to its highly valued characteristics, it was widely used by the Impressionists by the end of the 19<sup>th</sup> century. The earliest painting on which this pigment has been identified is dated 1863-1864 [6]. Viridian was included in the Winsor and Newton catalogue in 1869 [7]. Different processes to manufacture viridian are known; some produce materials similar to the hydrated chromium oxide, such as Arnaudonn's chrome green (a chromium phosphate). However, viridian is generally obtained by calcining a bichromate with boric acid and then hydrolysing this while washing to remove soluble matter [8].

The reflectance curve of viridian presents a reflectance maximum at about 500 nm [6] (in the spectrum shown in Figure 2 the maximum is at 490 nm and absorption bands centred at 460 and 610 nm because of a *d-d* transition due to the  $\text{Cr}^{3+}$  ion in an octahedral field of oxygen atoms) [9]. Another characteristic of the hydrated chromium oxide that has been reported in literature is the slight absorption (dip) in the high-reflection region at about 430 nm [10]. The absorption in the UV region at about 415 nm is probably due to a charge transfer transition involving the passage of an electron from the oxygen ion  $\text{O}^{2-}$  to the chromium ion  $\text{Cr}^{3+}$ . Some absorption bands in the infrared region at 1390 and 1420 nm are related to the hydrated silicate mineral in the preparatory (ground) layer.

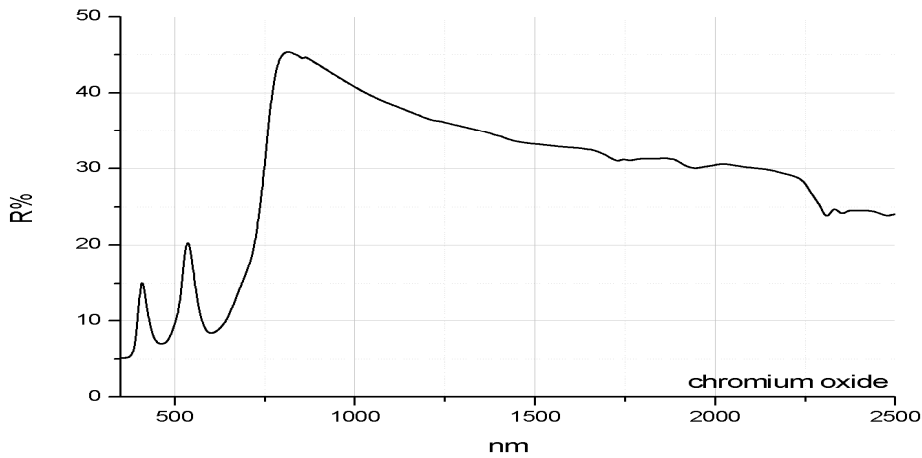
4.1.3- Chromium oxide -  $\text{Cr}_2\text{O}_3$ 

Figure 3: Reflectance spectrum of chromium oxide.

Chromium oxide is an opaque, deeply coloured green pigment, known also as chrome sesquioxide or chrome oxide. This pigment has been commercially available since 1862. Before this date, chromium oxide existed in nature in an impure state as the mineral eskolaite, but it was also artificially prepared for artistic purposes; the pigment seems to have been well known to artists and colour makers before 1862 [8]. For example, in his book “Chromatography” printed in 1835, George Field referred to a true chrome green, or Native green, as a lightfast pigment which held up well to pollution exposure [11]. Initially, the manufacturing of the pigment was achieved by decomposing iron chromate. Later, more inexpensive methods were developed which used the calcination of potassium chromate with sulfur. Modern processes are based on a reduction of sodium or potassium dichromates with carbon or sulfur<sup>1</sup>, or by heating ammonium dichromate<sup>2</sup>[8].

The reflectance spectrum of chromium oxide generally shows a much lower reflectance than that exhibited by viridian. Chromium oxide is characterised by a strong absorption band in the UV due to a metal-ligand charge transfer transition between the chromium and the oxygen anion and by a double absorption band with two absorption maxima at 460 nm and 600 nm due to *d-d* electronic transition typical of chromium (III) in an octahedral coordination. Another important characteristic shown in the spectrum is the high reflectance values of the pigment in the NIR region due to which it is impossible to obtain any information from the under layer [12].

---

<sup>1</sup>  $\text{Na}_2\text{Cr}_2\text{O}_7 + \text{S} \rightarrow \text{Na}_2\text{SO}_4 + \text{Cr}_2\text{O}_3$

<sup>2</sup>  $(\text{NH}_4)_2\text{Cr}_2\text{O}_7 \rightarrow \text{Cr}_2\text{O}_3 + \text{N}_2 + 4 \text{H}_2\text{O}$

#### 4.1.4- Cobalt Green – $\text{CoO}\cdot n\text{ZnO}$

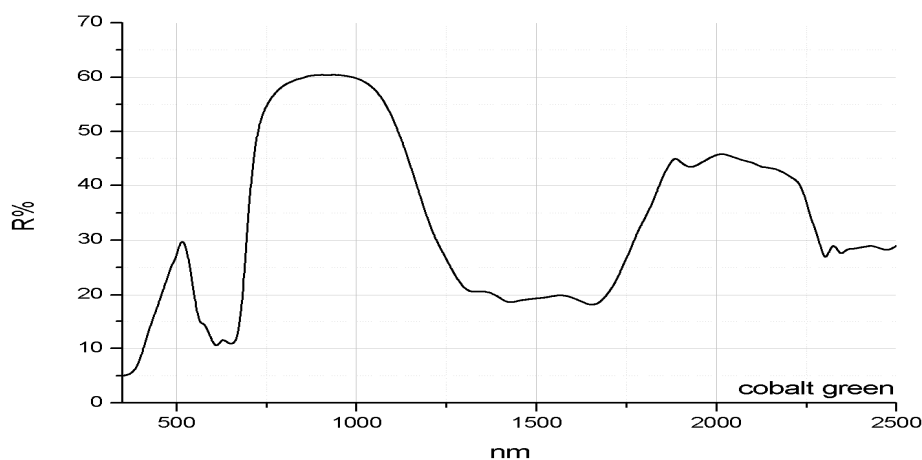


Figure 4: Reflectance spectrum of cobalt green.

Cobalt green is an inorganic pigment existing in nature. Its composition, very similar to cobalt blue, is characterised by a zinc oxide in which some of the  $\text{Zn}^{2+}$  ions are replaced by  $\text{Co}^{2+}$  ions [13]. It was first synthesised by Rinmann at the end of the 18<sup>th</sup> century (1780) but it was commercialised only around the middle of the following century, when it was simpler and cheaper to source zinc oxide. In 1901 Church wrote that cobalt green could be produced by adding a solution of a cobalt salt to a paste of zinc oxide and water. The result was then dried and calcined. In the final product there was just a small amount of  $\text{ZnO}$ , nevertheless the colour, a bluish-green, does not change with the variation of the cobalt-to-zinc ratio. This means that zinc and cobalt oxide do not form a well defined crystalline material, but a solid solution [8]. Like all cobalt-based pigments, cobalt green was a very expensive material. Its poor tinting strength and high cost kept it in limited use. Field called it "chemically good and artistically bad" [14]

The reflectance spectrum of cobalt green (Figure 4) is easily recognisable due to a strong absorption band in the visible range, divided into three sub-bands at around 560 nm, 610 nm and 670 nm. Additionally, it is possible to observe a strong increase in the reflectance values, up to 60% in the investigated pure pigment paint layer, from about 750 nm to 1100 nm followed by a second strong absorption in the NIR region, divided into three minor absorption bands at 1335 nm, 1430 nm and 1655 nm. Both the main absorptions, the first in the visible range and the second one in the NIR, are due to  $d-d$  transition of the cobalt ion  $\text{Co}^{2+}$  in a tetrahedral coordination. The charge transfer band is displaced into the blu-violet region [13].

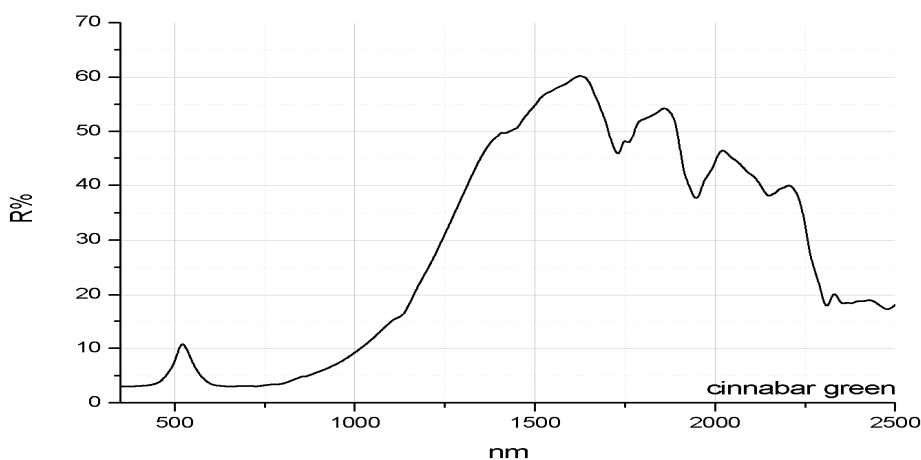
4.1.5- Cinnabar Green -  $\text{Fe}_4[\text{Fe}(\text{CN})_6]_3 \cdot n\text{H}_2\text{O} + \text{PbCrO}_4$ 

Figure 5: Reflectance spectrum of cinnabar green.

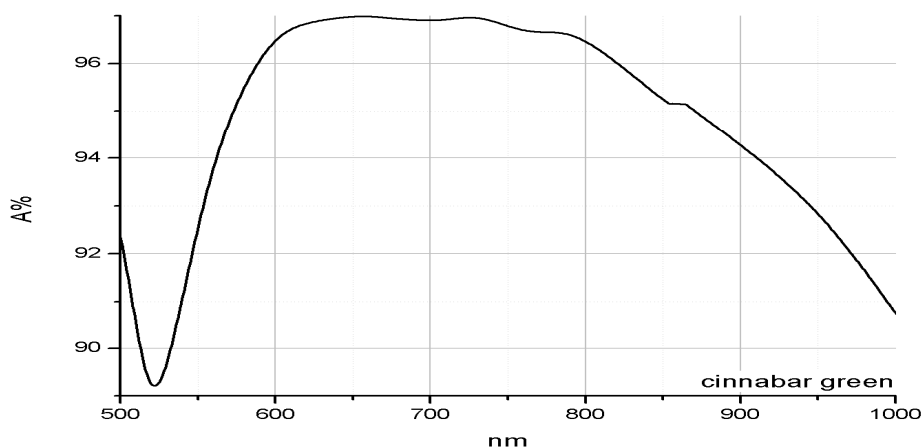


Figure 6: Absorbance spectrum of cinnabar green in the 500 nm – 1000 nm range.

The composition of this pigment has changed over time: it was a mixture of copper and arsenic, and subsequently a combination of Prussian Blue and lead chromate [8]. The latter formulation was analysed in the present section. Cinnabar green was one of the most widely used green pigments in the second half of the 19<sup>th</sup> century because of its distinctive opaque colour, varying from acid green to olive green, and for its low cost [15].

Cinnabar green does not present any characteristic absorptions that can be used to identify the pigment; it only exhibits a reflectance maximum centred at 520 nm, followed by a strong absorption at 700 nm. This last feature is due to the presence of Prussian blue, which can be distinguished by a minimum of reflectance among 700 nm due to a charge transfer transition between the two oxidation states of iron ( $\text{Fe}^{2+}$  and  $\text{Fe}^{3+}$ ). The presence in the mixture of a yellow pigment shifts the maximum of reflectance typical of Prussian blue from the violet-blue region (440-500 nm) to the green region (520-550 nm). The  $\text{CrO}_4^{2-}$  ion in lead chromate

causes a charge transfer absorption from the ultraviolet to green region [9] that has to be added to the absorption of Prussian blue. In the specific standard pigment used for this study, the presence of phthalocyanine green can also be detected because of the absorption bands localised at 650 nm, 730 nm and 780 nm, very evident in Figure 6 where the absorbance spectrum of the pigment is shown. Phthalocyanine green is a synthetic green pigment from the group of phthalocyanine dyes, a complex of copper (II) with a chlorinated phthalocyanine.

### 3.1.6- Malachite - $\text{CuCO}_3 \cdot \text{Cu(OH)}_2$

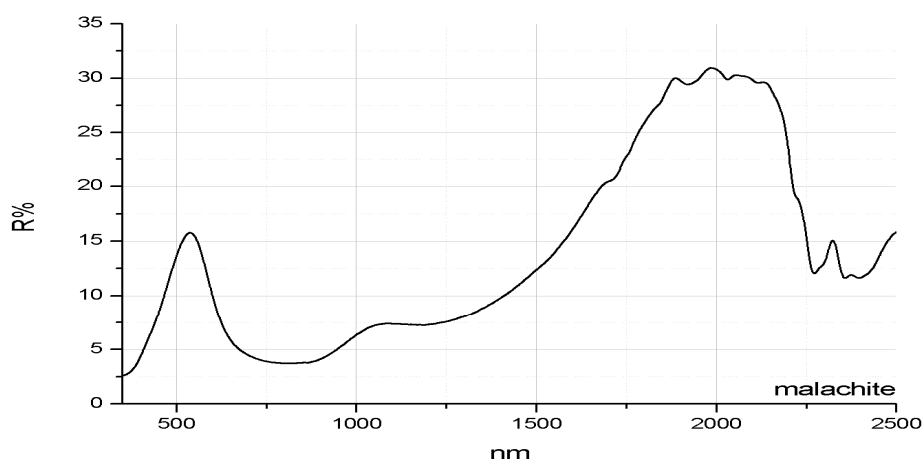


Figure 7: Reflectance spectrum of malachite.

Malachite was one of the first green pigments used in antiquity. Its use essentially ended in the 19<sup>th</sup> century, when it was replaced by modern green pigments [9], like Schweinfurt green or cinnabar green. Chemically it is a basic copper carbonate, very sensitive to acids and to heat which causes it to darken. It was obtained by grinding the malachite mineral. Different hues could be achieved just by varying the dimension of the granules [16]. It may be found as prismatic crystal but it is most commonly found as botryoidal<sup>3</sup> masses with an internal fibrous structure and a banded appearance [8].

The reflectance spectrum of malachite (Figure 7) is characterised by a maximum in the green region (~550 nm), followed by an absorption from about 600 nm to 1400-1500 nm due to a *d-d* transition of the  $\text{Cu}^{2+}$  ion. This band is divided into two sub-bands: the first band, very intense, is centred at around 800 nm while the second band is centred at about 1200 nm.

---

<sup>3</sup> A botryoidal texture is one in which the mineral has a globular external form. Each sphere in a botryoidal mineral is smaller than that of a reniform mineral, and much smaller than that of a mamillary mineral. Botryoidal minerals form when many nearby nuclei, specks of sand, dust, or other particles, are present. Layers of mineral material are deposited radially around the nuclei. As more material is deposited, the spheres grow larger and eventually overlap with those that are nearby. These nearby spheres are then fused together to form the botryoidal cluster.

4.1.7- Verdigris -  $\text{Cu}(\text{CH}_3\text{COOH})_2 \cdot [\text{Cu}(\text{OH})_2] \cdot 2\text{H}_2\text{O}$  basic or  $\text{Cu}(\text{CH}_3\text{COO})_2 \cdot \text{H}_2\text{O}$  neutral

Figure 8: Reflectance spectrum of verdigris.

Verdigris is a copper acetate, a synthetic pigment made since antiquity by exposing metallic copper to the acetic acid ( $\text{CH}_3\text{COOH}$ ) contained in vinegar [9]. There are different formulations of this pigment, which can exist as a basic or a neutral copper acetate. It was the most vibrant green available until the 19th century. It was often mixed with, or glazed over lead white or lead-tin yellow because of its transparency. It was also the most reactive and unstable of all the copper pigments and often changed colour to a dark brown or black as it aged. Today it is rarely sold as an artist's pigment because of its toxic nature.

As mentioned before, the pigment shows a high transparency and can be found used in paintings as a glaze. This property can be seen in the NIR region, where it is possible to detect the spectral features due to the preparation layer (Figure 8). In the UV region, the absorption is probably due to a charge transfer electronic transition among the metal (Cu) and the ligand, like in malachite and Schweinfurt green. In the visible region a very broad band from 550 nm to 1000 nm due to a  $d-d$  transition of  $\text{Cu}^{2+}$  can be detected [9]. In the NIR region, absorptions due to the canvas are also present: the sharp bands at 1350 nm, 1393 nm and 1414 nm can be attributed to a hydrated aluminosilicate, while the weak bands at 1666 nm and 1680 nm are due to the first C-H overtones of the methyl group [17].

#### 4.1.8- Schweinfurt Green (Emerald green) - $3\text{Cu}(\text{AsO}_2)_2 \cdot \text{Cu}(\text{CH}_3\text{COO})_2$



Figure 9: Reflectance spectrum of Schweinfurt green.

Schweinfurt green is a copper acetoarsenite produced in different ways and also known as emerald green. In the past, the name emerald green was used in various contexts, for example referring to a pigment obtained from a type of coffee berries [11]. Starting in the early 20<sup>th</sup> century 'emerald green' indicated copper acetoarsenite in the United Kingdom, while in France the same term was still being used for the hydrated oxide of chromium pigment (called viridian in the UK).

This pigment was first synthesised independently in two different laboratories: the paint manufacturer Sattler, with a pharmacist named Friederich Russ, studied and experimented reactions between verdigris and arsenic-containing compounds producing a new pigment, called Schweinfurt green, traded since 1814. In the second instance, Ignaz von Mitis in Vienna made the same pigment in 1814 and started its production in his factory in Kirchberg (Austria). By 1822 copper acetoarsenite was produced using various methods. Schweinfurt green was used as a pigment from 1830, especially by the Impressionists. Because of its toxicity, its employment declined drastically starting in the second half of the 19<sup>th</sup> century: the arsenic contents made the pigment extremely poisonous and it was blamed for deaths when employed as a wallpaper colour [14].

Like other copper-based green pigments, Schweinfurt green absorbs in the UV region with a reflectance maximum at 520 nm, followed by an absorption band centred at 735 nm (Figure 9). The manufacturing method can lead to some small variations in the spectral appearance of the pigment. In fact, it has been proven that the copper-to-arsenic ratio determines the hue of the pigment, with a higher arsenic value producing lighter colours [18]. In the visible region, a very broad absorption band from 550 nm to 1000 nm is due to a *d-d* transition on  $\text{Cu}^{2+}$  [9]. As reported for verdigris, in the NIR region, absorptions referable to the presence of a hydrated alumino-silicate in the underneath canvas can be detected: the sharp bands at 1350 nm, 1393 nm and 1418 nm. The weak bands at 1666 nm and 1680 nm are due to the first C-H overtones of the methyl group [17].



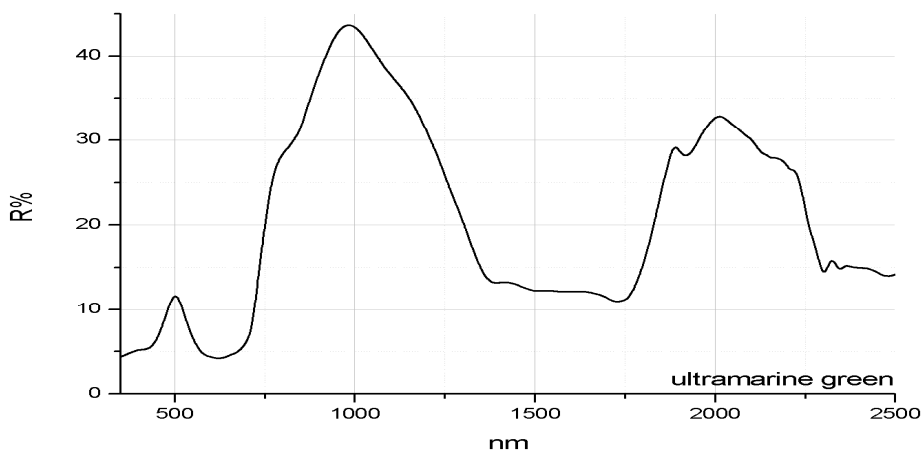
4.1.9- Ultramarine green -  $2\text{Na}_2\text{Al}_2\text{Si}_2\text{O}_6 \cdot \text{NaS}_2$ 

Figure 10: Reflectance spectrum of ultramarine green.

Ultramarine green is a sodium aluminosilicate with sodium and sulfur. It was produced for the first time by Kitting in Messein (France) in 1828 [8].

It is considered an intermediate product in the manufacturing of synthetic ultramarine: in other words the ultramarine green was an artificial ultramarine blue before the final roasting. Synthetic ultramarine blue is obtained by fusing kaolinite, soda ash, Glauber's salt ( $\text{Na}_2\text{SO}_4 \cdot 10\text{H}_2\text{O}$ ), sulfur, carbon and kieselguhr<sup>4</sup> in the absence of air at red heat for 7-10 hours. These compounds and this procedure determine the production of ultramarine green, which is cooled, ground and mixed with 7-10% of sulfur and then 'blued' by heating in a furnace. The hue of the final material can vary from greenish-blue to violet depending on the silica:alumina ratio. The pigment is particularly transparent and sensitive to acids and lead compounds, therefore it has never been very popular among painters, unlike ultramarine blue [19].

The reflectance spectrum (Figure 10) is characterised by two absorption bands: the first one in the UV-Vis region and the second one centred at about 650 nm. These features are probably due to a double metal-ligand charge transfer transition involving the ion  $\text{S}^{3-}$  and the ion  $\text{S}^{2-}$ . In fact, even if the  $\text{S}^{3-}$  ion predominates in ultramarine blue, both ions are present in comparable proportion also in ultramarine green: the  $\text{S}^{2-}$  is the yellow chromophore and the  $\text{S}^{3-}$  is the blue chromophore [20, 21].

In the NIR region, a broad absorption divided into three sub bands suggests the presence of a cobalt-based pigment added to the powder. The cobalt-containing material is probably responsible for other absorptions in the UV-Vis region, localised at about 580 nm and 680 nm.

<sup>4</sup> Kieselguhr is a diatomaceous earth (diatomite) and is a form of silica made up of the siliceous shells of unicellular aquatic plants of microscopic size. Kieselguhr is heat resistant and has been used as an insulator, as a component in toothpaste and as an abrasive in metal polishes. In the chemical industry, it is also used as a filling material in paper, paints, ceramics, soap and detergents (from [http://nobelprize.org/alfred\\_nobel/industrial/articles/krummel/kieselguhr.html](http://nobelprize.org/alfred_nobel/industrial/articles/krummel/kieselguhr.html)).

#### **4.2- Comparison of green pigments**

In order to verify better the differences between the various green pigments described above, a comparison between the reflectance spectra acquired on the experimental mock-ups was performed. Sometimes weak features cannot be observed very clearly by studying only spectra in reflectance mode (Figure 11). Therefore, in order to interpret the data in their entirety, including any weak features, first and second derivative functions of the spectra were calculated. Some of these pigments can be easily identified by their reflectance spectrum: for example chromium oxide exhibits a distinctive behaviour in the visible range and cobalt green has specific absorption bands both in the visible and in the infrared region that makes it simple to identify them. By contrast, differences between copper-based pigments, cinnabar green and ultramarine green are less clear, especially when the green pigment is present in admixture with other pigments. Even if small shifts in the reflectance maxima can be detected in the 350-650 nm range, more significant features are present at wavelengths above 650 nm (Figure 11). For example, above 650 nm, viridian and ultramarine green reflect the electromagnetic radiation more than other pigments, even if in ultramarine green this behaviour is probably influenced by the presence of cobalt blue in the manufactured formulation.

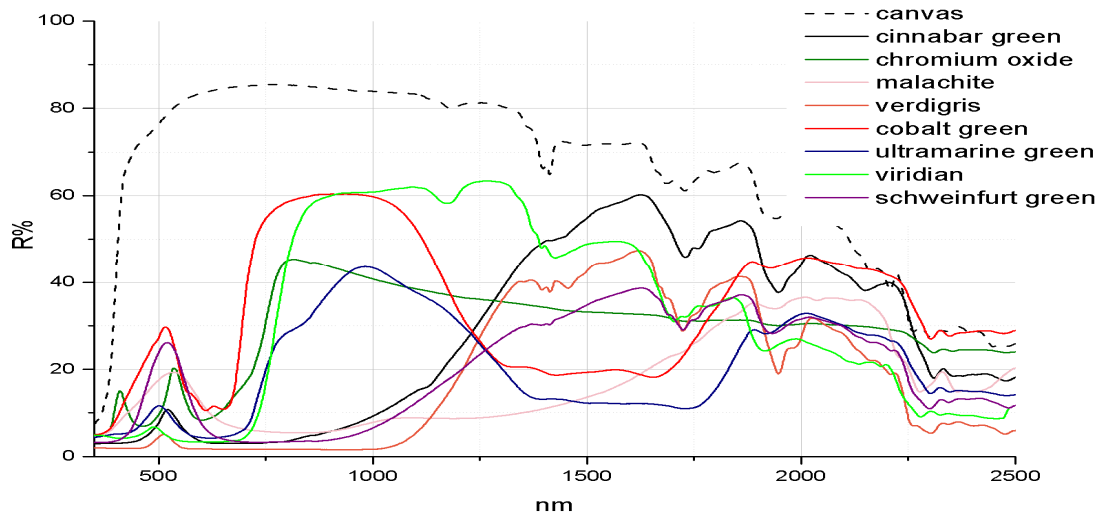


Figure 11: Reflectance spectra of the green pigments analysed: cinnabar green (black line), chromium oxide (dark green line), malachite (pink line), verdigris (orange line), cobalt green (red line), ultramarine green (blue line), viridian (green line) and Schweinfurt green (purple line). The spectrum of the canvas used for pure green pigments' mock-ups was also reported (dash black line)

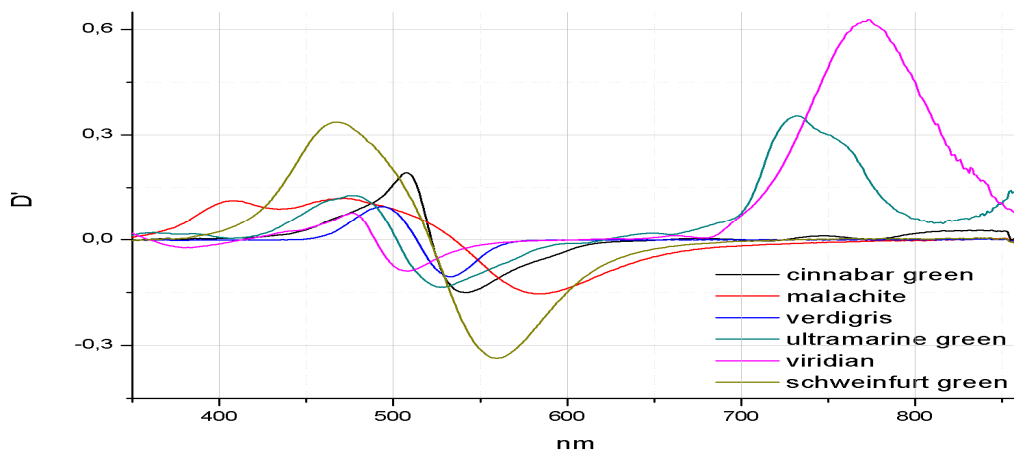


Figure 12: First derivative spectra of cinnabar green (black line), malachite (red line), verdigris (blue line), ultramarine green (green line), viridian (pink line) and Schweinfurt green (yellow line).

As mentioned above, in the first derivative the inflection points are amplified because they correspond to maxima and minima of the function and small absorptions not clearly visible in reflectance mode can be highlighted. In the 350–860 nm range, two of the pigments analysed could be clearly identified (Figure 12): the first is viridian (which was also identified in reflectance) because its reflectance increases in the red region; the second one is ultramarine green, which has a high reflectance between 700 nm and 800 nm with a relative minimum at 814 nm. In the blue-green region, the pigments present maxima between 450 nm and 500 nm: for example Schweinfurt green and cinnabar green, which exhibit comparable behaviours in the visible region (400-740 nm), can be differentiated in the first derivative spectra by means of their relative maxima positioned at 470 nm for Schweinfurt green and 507 nm for cinnabar green. Likewise, verdigris is characterized in the first derivative by a relative maximum at 495 nm. Otherwise, the relative minimum, localised for most of the materials analysed between 500 nm and 550 nm, can be useful in

detecting Schweinfurt green (560 nm) and malachite (585 nm). The latter presents a particular behaviour below 450 nm: in fact, a relative maximum at 408 nm makes it different from the others. It is important to emphasise that the elaboration performed here is related just to one brand of pigment. In order to have a complete analysis of the topic, pigments from various manufactures and with different physical characteristics (colour, particle size, etc.) should be taken into account.

In Table 2 the features characterising the pigments analysed are summarised.

Pigment	Reflectance minima (nm)	Reflectance maxima (nm)	Inflections point (nm)	Pigment	Reflectance minima (nm)	Reflectance maxima (nm)	Inflections point (nm)
Viridian	362	489	379	Malachite	820	535	408
	411	676	476				435
	620-640		507				472
			662				582
			679				
		773					
Chromium oxide	350	408	397	Verdigris	<445 >600	513	493
	460	536	420				533
	600	675	520				
			552				
			664				
			685				
			702				
			750				
Cobalt green	566	515	408	Schweinfurt green	350 735	522	470
	656		459				559
			409				
			503				
			543				
			571				
			591				
			619				
			639				
			693				
Cinnabar green	375	522	507	Ultramarine green	408 675**	500 622	475
	656*		542				528
	725*		673*				647**
	792*		715*				730
			746*				
			776*				

Table 2: Localisation of reflectance minima, reflectance maxima and inflection points in the reflectance spectra of the pigments analysed. The symbol (\*) reported for cinnabar green indicates the features due to the presence of phtalo-green, while the symbol (\*\*) reported for ultramarine green indicates the features due to the presence of cobalt-based pigment.

### 4.3- Green pigments in mixtures

In real cases, such as paintings or polychrome surfaces in general, pure green pigments are almost always used in admixture with other compounds, such as white and yellow pigments. In particular, with specific reference to paintings from the 19<sup>th</sup> century, paint layers are difficult to analyse by noninvasive spectroscopic methods because of the presence of very complex mixtures or multiple paint layers. As a consequence, the reflectance spectrum recorded in a specific point of the painted surface can be the result of the addition or subtraction of more than one reflectance spectrum, one for each material present in the sample. In order to study the reflectance behaviour of a mixture, binary mock-ups were prepared with some of the green pigments discussed in the previous paragraphs and the reflectance spectra of these standards were acquired.

The green pigments selected for this study were malachite, verdigris and chromium oxide green. Malachite and verdigris were selected because they are copper-based pigments and they are very hard to distinguish when mixed with other pigments. Even if Schweinfurt green is also a copper green pigment, it was excluded from this study because of its toxicity.

Chromium oxide green was not taken into account in the previous discussion because its features are very characteristic. However, if mixed with other pigments its reflectance characteristics could partially disappear making it difficult to identify it. The choice of the mixtures was made with reference to the pigments known to have been used by *Macchiaioli*. The aim of this study is to understand how the reflectance of these pigments changes and to try and isolate the spectral elements useful in identifying them. The focus will be mainly on the 350-860 nm range where specific absorption features can be detected.

### 4.3.1- Malachite and Verdigris

The first step is to study and to compare the reflectance spectra of pure malachite and pure verdigris in order to discover their similarities and differences.

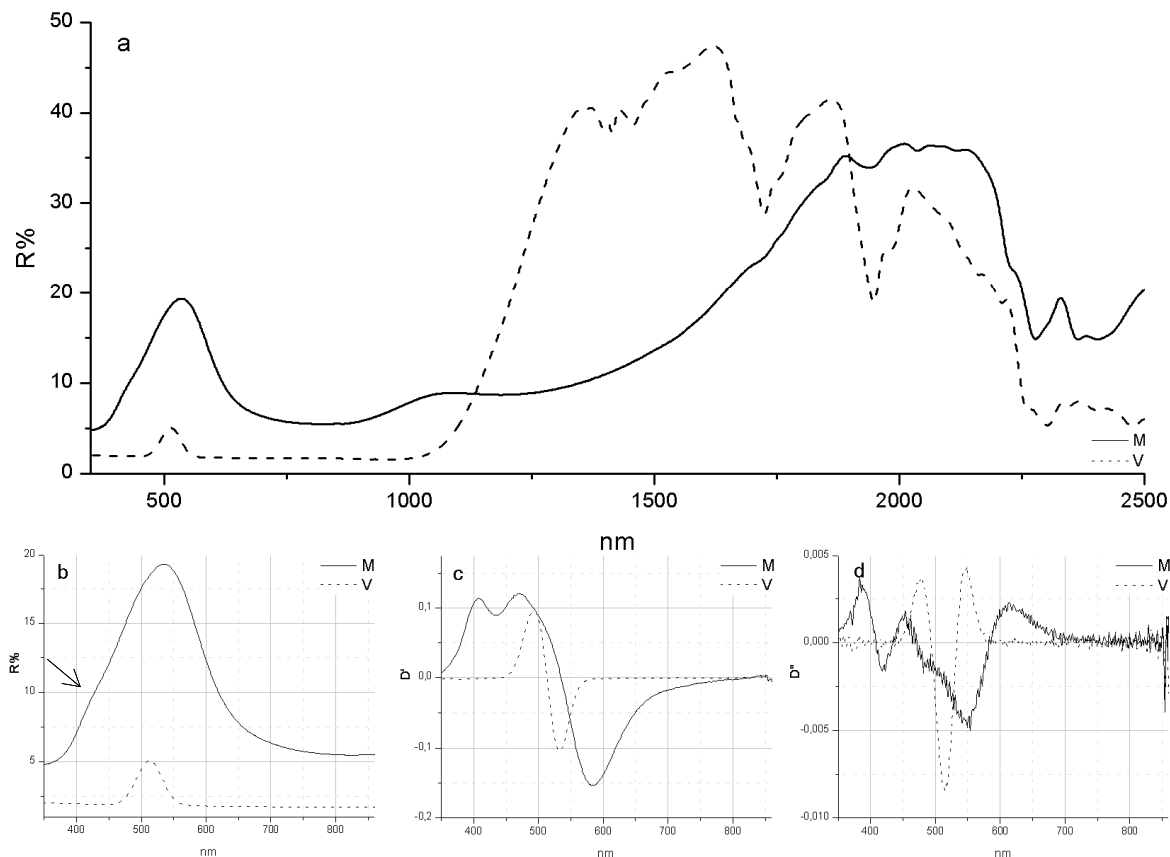


Figure 13: Reflectance spectra (a, b), first derivative spectrum (c) and second derivative spectrum (d) of malachite (M, solid line) and verdigris (V, dash line).

The reflectance spectrum (Figure 13-a, b) of pure malachite appears to be different from that of pure verdigris: in fact, the reflectance maximum for malachite is at 535 nm while for verdigris it is at 513 nm. Obviously, it is important to stress that values reported here have to be considered specific for the samples taken into account; in fact other factors can influence the colour of a pigment, such as dimension of the particles and the modality of application on the substrate. The absorption band in the yellow-red region is centred at 820 nm while in verdigris the absorption goes from 600 nm until about 900 nm. Looking at the first and second derivative (Figure 13-c, d) the presence of a minimum at 435 nm in the malachite first derivative spectrum is very interesting and only visible as a very small shoulder in reflectance mode (indicated by the arrow in Fig. 13b). In the NIR more differences can be noted (Figure 13-a): starting from 880 nm, the reflectance values of malachite increase until a maximum localised at 1100 nm. On the other hand, the spectrum of verdigris shows an intense rise from 1000 nm and absorption bands due to the acetate group. Moreover, in the NIR region, malachite has a greater hiding power than verdigris, which is relatively transparent and lets the backscattered radiation from the preparation layer through.

In Table 3 the pigments taken into account to prepare the binary mock-ups are reported.

Pigment	Manufacture	Code	Formulation	Abbr.
Malachite	Zecchi	0201	$\text{CuCO}_3\text{Cu}(\text{OH})_2$	M
Verdigris	Zecchi	0997	$\text{Cu}(\text{CH}_3\text{COO})_2 \cdot [\text{Cu}(\text{OH})_2] \cdot 3.2\text{H}_2\text{O}$	N
Lead white (Biacca)	Fluka Chemika	367410/1 54199	$2\text{PbCO}_3 \cdot \text{Pb}(\text{OH})_2$	B
Zinc white	Aldrich	23,794-9	ZnO	Z
Naples yellow	Zecchi	0772	$\text{Pb}_2\text{Sb}_2\text{O}_7$	N

Table 3: List of the pigments used for malachite and verdigris based mixtures. In the table, the name of the pigment the manufacture, the code, the formulation and the abbreviation are reported.

Different kinds of mixtures were prepared, changing the percentage of the materials used, as reported in Table 4.

Mixture	Green pigment	%	g	White pigment	%	g	Mixture	Green pigment	%	g	White pigment	%	g
MB01	Malachite	1	0.02	Lead white	99	1.98	MZ01	Malachite	1	0.02	Zinc white	99	1.98
MB05	Malachite	5	0.1	Lead white	95	1.91	MZ05	Malachite	5	0.11	Zinc white	95	1.88
MB10	Malachite	10	0.19	Lead white	90	1.8	MZ10	Malachite	10	0.2	Zinc white	90	1.79
MB20	Malachite	20	0.4	Lead white	80	1.6	MZ20	Malachite	20	0.4	Zinc white	80	1.59
MB50	Malachite	50	1	Lead white	50	1	MZ50	Malachite	50	1.02	Zinc white	50	0.98
VB1	Verdigris	1	0.02	Lead white	99	1.98	VZ1	Verdigris	1	0.02	Zinc white	99	1.98
VB10	Verdigris	5	0.1	Lead white	95	1.9	VZ10	Verdigris	5	0.1	Zinc white	95	1.9
VB20	Verdigris	10	0.2	Lead white	90	1.8	VZ20	Verdigris	10	0.2	Zinc white	90	1.8
VB5	Verdigris	20	0.4	Lead white	80	1.6	VZ5	Verdigris	20	0.4	Zinc white	80	1.6
VB50	Verdigris	50	1	Lead white	50	1	VZ50	Verdigris	50	1	Zinc white	50	1
Mixture	Green pigment	%	gr	Yellow pigment	%	Gr	Mixture	Green pigment	%	gr	Yellow pigment	%	gr
MN1	Malachite	99	1.98	Naples yellow	1	0.02	VN01	Verdigris	99	1.98	Naples yellow	1	0.02
MN05	Malachite	95	1.9	Naples yellow	5	0.1	VN05	Verdigris	95	1.9	Naples yellow	5	0.1
MN10	Malachite	90	1.8	Naples yellow	10	0.2	VN10	Verdigris	90	1.8	Naples yellow	10	0.2

Table 4: List of the mixtures prepared with the amount (in percentage and in weight) of green pigment and white/yellow pigment used.

First, the reflectance behaviour of malachite and verdigris in a mixture with the pigments used must be examined (Figure 14). The presence of lead white leads to an increase of the reflectance and the appearance of an absorption at 1450 nm due to the first overtone of the OH group in lead white (Figure 14-a, b). Moreover, in the mixtures with verdigris, the white pigment changes the shape and the intensity of the absorption in the red-region (Figure 14-b). Zinc white causes an increase of the reflectance, and the absorption at 370 nm due to a band-band transition on the zinc ion influences the position and the shape of the reflectance maxima that gets to 545 nm for MB01 and MZ01 as well (Figure 14-c, d). Naples Yellow shifts the reflectance maximum in the green region toward greater wavelengths (Figure 14-e, f). Obviously, this trend is more evident when the concentration of the yellow pigment augments. Looking at the last figure (Figure 14-f) it is interesting to note that the spectra of the pure pigments were probably acquired on mock-ups slightly yellowed because of their natural aging or due to the presence of too much binding medium in the paint layer. In fact, one of the consequences of chromatic spreading natural aging is the tendency to change colour, mainly due to the yellowing of the binding medium used. This phenomenon can

be seen, for example, in blu-green surfaces as a few nanometres shift of the reflectance maxima toward the yellow spectral region.

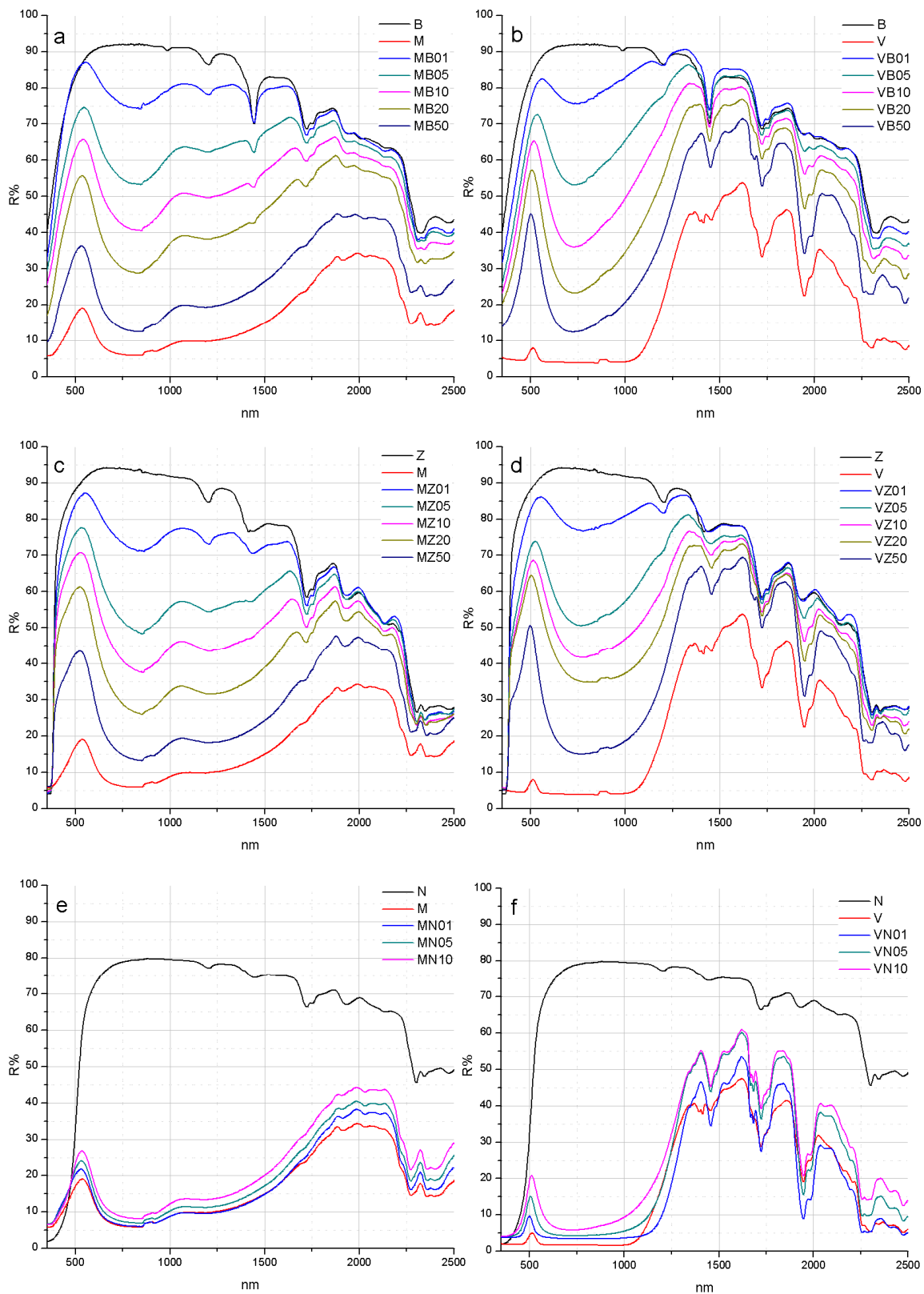


Figure 14: Reflectance spectra of malachite (left side) mixed with lead white (a), zinc white (b) and Naples yellow (c). Reflectance spectra of verdigris (right side) mixed with lead white (d), zinc white (e) and Naples yellow (f).



The discussion of the results will be developed focusing on the 350–860 nm range and considering the mixtures one by one (Figure 15 and Figure 16):

**-MB mixtures** (Figure 15- a, b): in the first derivative, malachite has two maxima at 408 nm and 472 nm (M) that shift to 388 nm and 448 nm (MB01). The reflectance maximum goes from 535 nm (M) to 575 nm (MB01). Even if the absorption band seems to be centred always in the same position, the inflection point moves from 582 nm (M) to 620 nm (MB01) leading to a shrinkage of the band.

**-MZ mixtures** (Figure 15- c, d): the presence of zinc white causes a strong maximum in the first derivative spectrum localised at 385 nm. The increase of the concentration of zinc white hides the maximum at 408 nm, the reflectance maximum moves from 535 nm (M) to 560 nm (MZ01) while the inflection points of the main absorptions move from 582 to 620 nm.

**-MN mixtures** (Figure 15- e, f): In reflectance mode, Naples yellow does not cause strong variations in the spectrum, except for the displacement of the reflectance maximum towards the yellow region (from 535 nm to 537 nm). Differently in the first derivative it influences the height of the second maximum that increases in intensity and shifts to 490 nm for mixture MN10.

**-VB mixtures** (Figure 16- a, b): in the first derivative the first maximum moves from 493 nm to lower wavelengths (450 nm) and seems almost to disappear in the mixture VB01. Contemporarily, the reflectance maximum goes from 513 nm to 595 nm and the inflection point of the absorption varies from 533 nm to about 635 nm. The absorption minimum is reached by the pure pigment at around 600 nm, while in the mixtures it moves to around 750 nm. Moreover, in pure verdigris the first derivative goes from zero until 860 nm, while for the mixtures the first derivative is positive for values greater than 750 nm. This means that the absorption band of pure verdigris is constant between 850 nm and 680 nm, while in the mixtures the absorption is centred at 750 nm and after this wavelength the reflectance increases.

**-VZ mixtures** (Figure 16- c, d): zinc white influences the reflectance behaviour of the mixtures because of its strong absorption at 370 nm that determines a maximum at 385 nm in the first derivative. The reflectance maximum moves from 513 nm (V) to 555 nm in mixture VZ01. The reflectance minimum is localised around 800 nm for all the mixtures, and as a consequence a shift in the centre of the absorption can be detected.

**-VN mixtures** (Figure 16-e, f): In reflectance mode a light shift of the maximum toward the yellow-red region is observed. The shape of the reflectance absorption in the red region changes, developing an absorption centre at about 715 nm (VN10) which is not seen in pure verdigris.

The next step involves the comparison of mixtures of malachite and verdigris in the same concentrations with lead white, zinc white and Naples yellow in order to verify if it is possible to tell which green pigment is present.

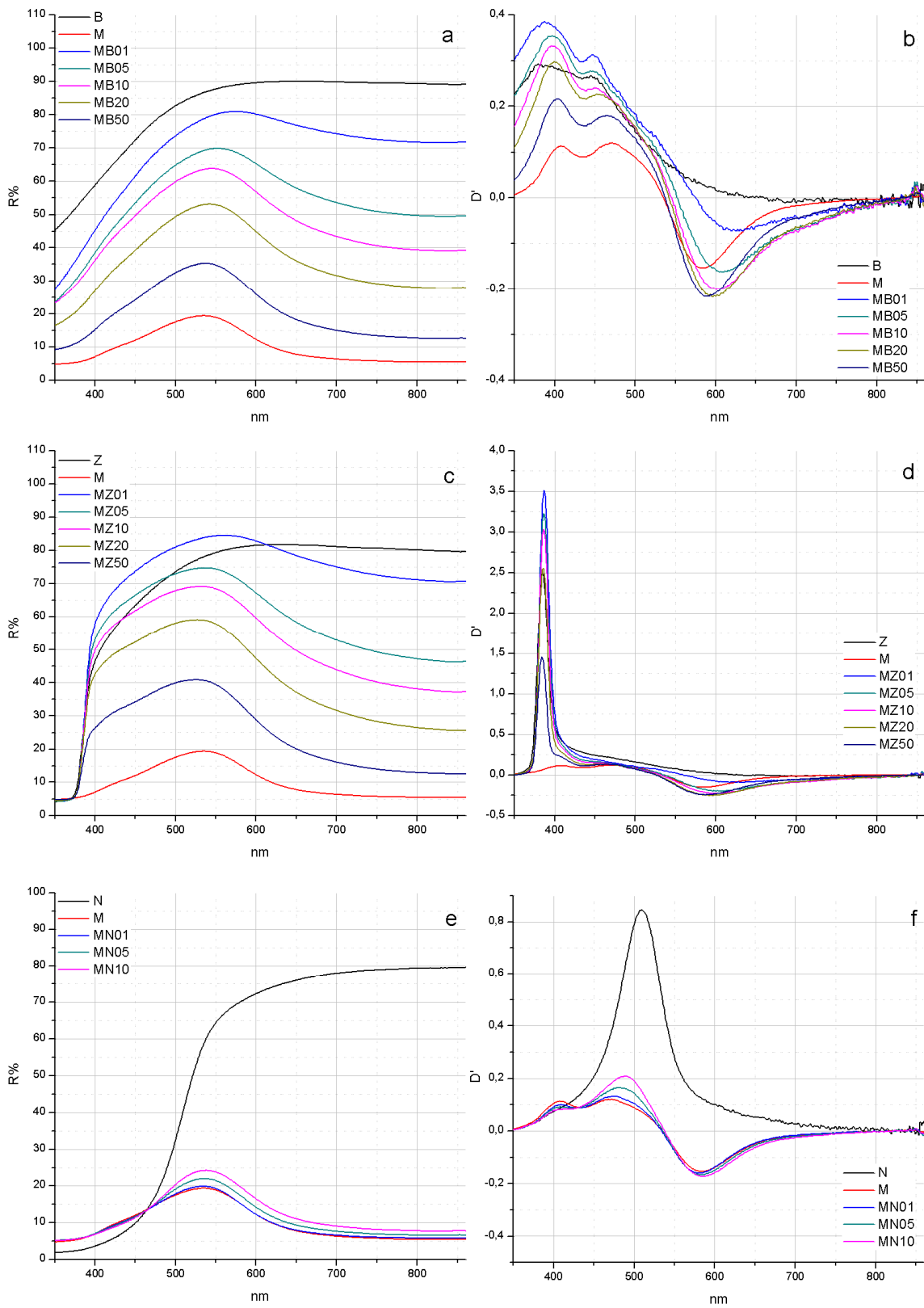


Figure 15: Reflectance spectra (left side) and first derivative spectra (right side) focused in the 350-860 nm range of the mixtures malachite-lead white (a, b), malachite-zinc white (c, d) and malachite-Naples yellow (e, f).

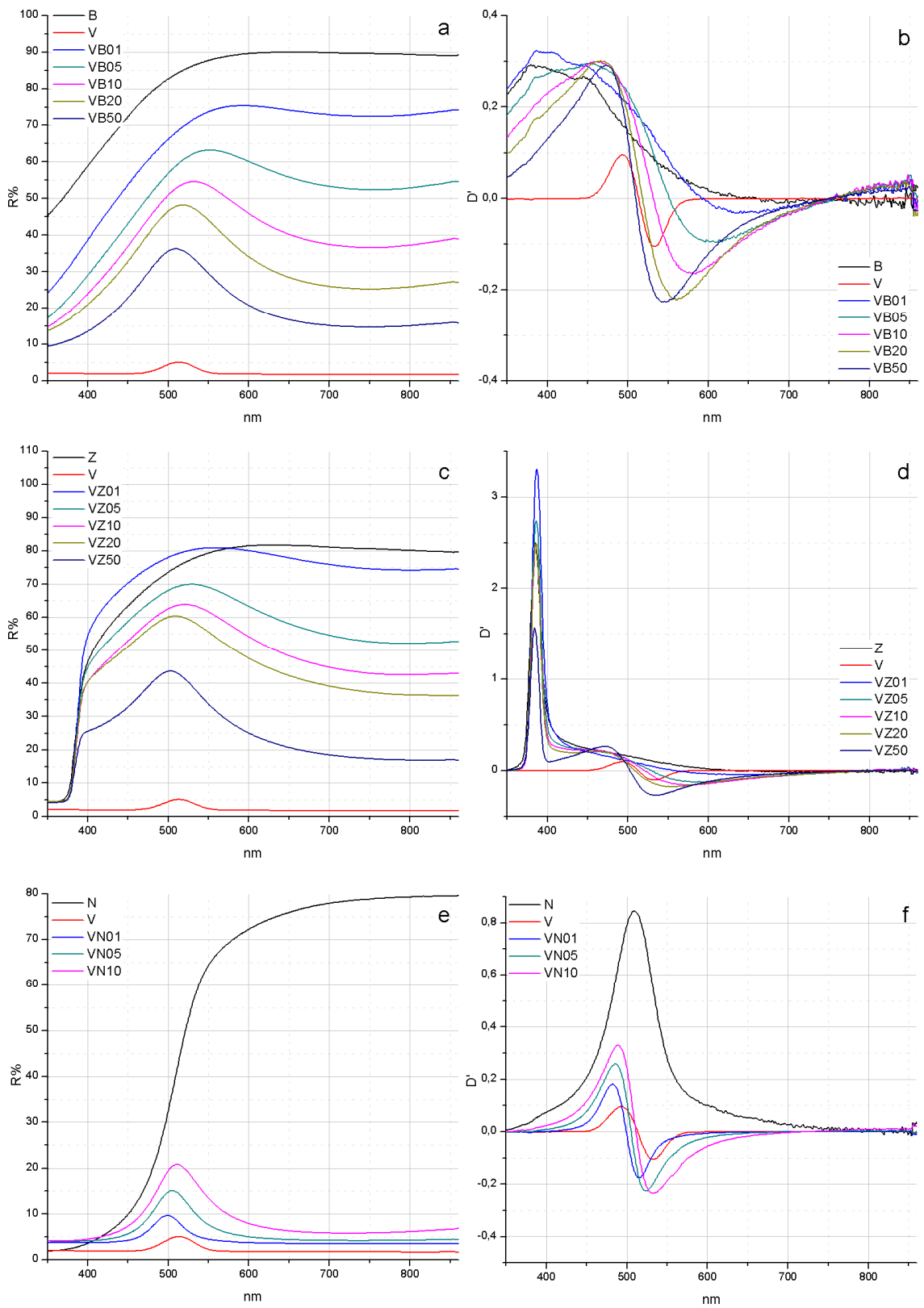


Figure 16: Reflectance spectra (left) and first derivative spectra (right) in the 350-860 nm range of the mixtures verdigris-lead white (a, b), verdigris-zinc white (c, d) and verdigris-Naples yellow (e, f).

#### *Mixtures with lead white and zinc white*

Even if zinc white causes a shift in the reflectance maximum of the two green pigments, verdigris and malachite are perfectly distinguishable in a 1:1 mixture with the white pigment (Figure 17-a, b). In particular, malachite can be recognised by the maximum at 408 nm present in the first derivative.

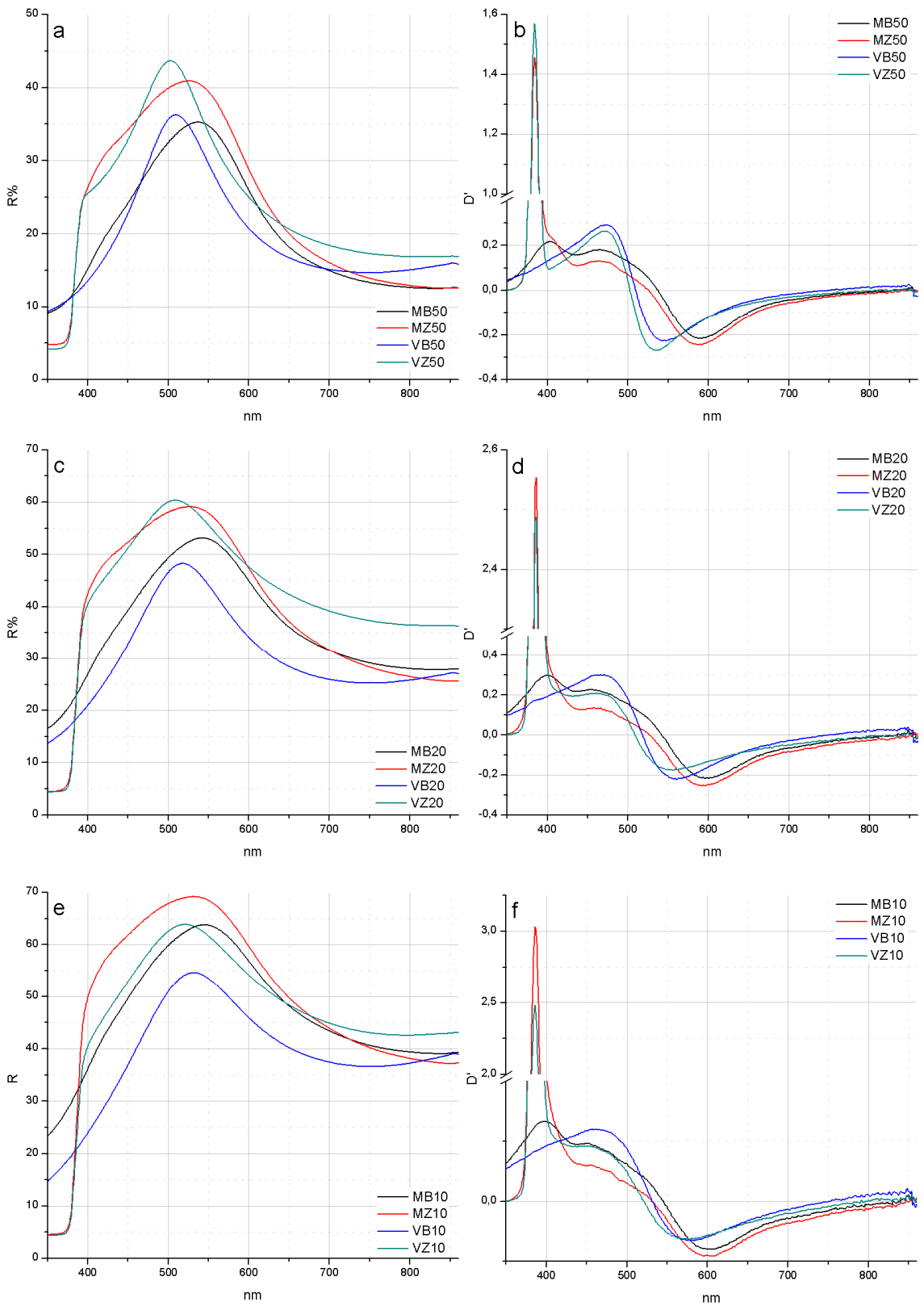
If the concentration of the green pigment decreases to 20% of the mixture (Figure 17-c, d), malachite is always identifiable because of its spectral behaviour but the maximum at 408 nm ( $D'$ ) decreases in mixture MZ20 because of the absorption band of zinc white. In fact, it can be noted that MB20 and MZ20 have a similar reflectance curve after 410 nm. At the same time, in the first derivative the minima of verdigris mixtures shift towards higher wavelengths, approaching the values typical of malachite minima.

When the concentration of the green pigment in the mixture is 5-10% (Figure 17-e, f, g, h), the spectral features of the white pigments prevail, and as a consequence in reflectance mode it is more difficult to distinguish which is the green component present just taking into account the reflectance maxima. On the other hand, in the first derivative MB10 retains the maximum between 400 nm and 410 nm due to the presence of malachite. The inflection point of the absorption in the red region is around 600 nm and around 580 nm for verdigris mixtures (except for MZ05 that is 600 nm) while the centre of the absorption is around 750-800 nm for verdigris and around 850 nm for malachite.

The presence of 1% of green pigment is not enough to identify the green substances. In fact, malachite could be recognised for the maximum at 390 nm only in the mixture MB01 (Figure 17-i, j).

#### *Mixtures with Naples yellow*

The presence of just 1% of Naples yellow does not influence the spectral features of the green pigments which are always distinguishable (Figure 18-a, b). The only difference noticed is that the second maximum in first derivative becomes the absolute maximum of the function, differently from the mixtures with white pigments. A higher concentration of Naples yellow (between 05-10%) does not influence the features of malachite which is still discernible from verdigris (Figure 18-c, d, e, f). However, studying the graphs some trends can be hypothesised: for example, reflectance maxima tend to approach each other, becoming non-distinguishable, while the maximum of malachite in first derivative at 408 nm disappears with the increase of the amount of the yellow pigment. In the mixtures studied, the presence of yellow does not considerably influence the shape and the intensity of malachite and verdigris absorption bands.



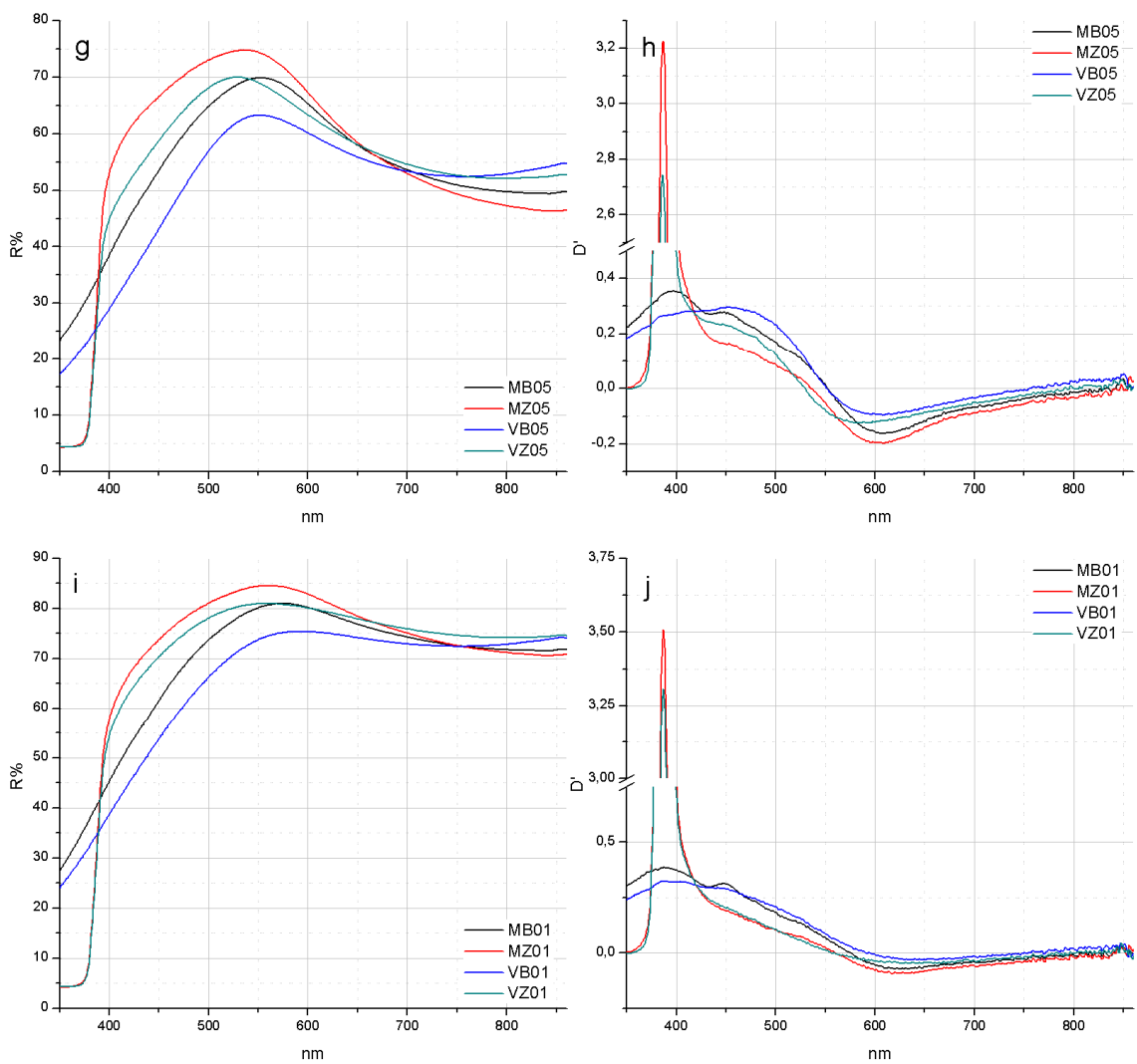


Figure 17: Reflectance spectra (left) and first derivative spectra (right) in the 350-680 nm range of white pigments mixed with the 50% of malachite and verdigris (a, b), 20% of malachite and verdigris (c, d), 10% of malachite and verdigris (e, f), 05% of malachite and verdigris (g, h), 1% of malachite and verdigris (i,j).

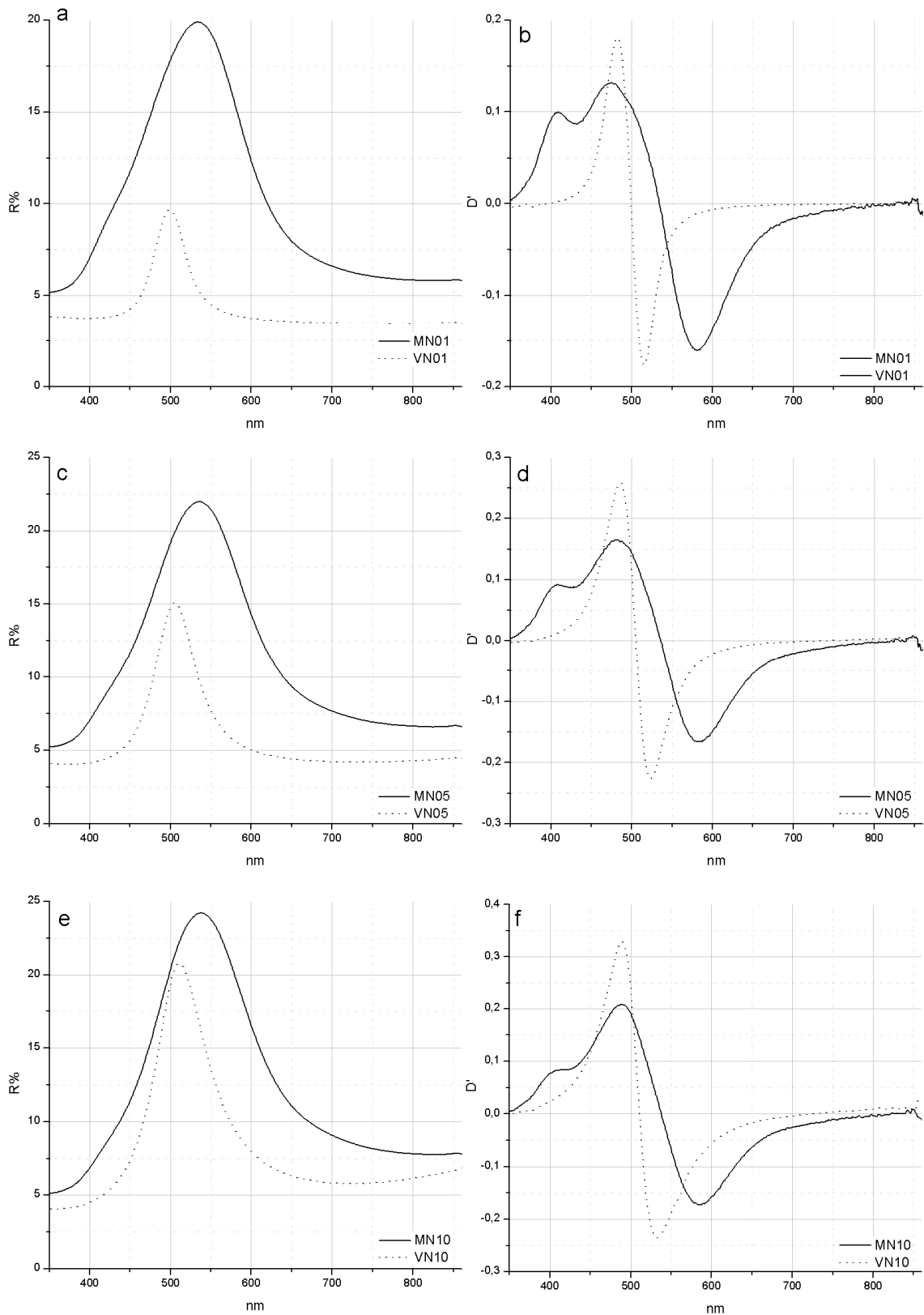


Figure 18: Reflectance spectra (left) and first derivative spectra (right) in the 350-680 nm range of Naples yellow mixed with 99% of malachite and verdigris (a, b), 95% of malachite and verdigris (c, d), 90% of malachite and verdigris (e, f).

In Tables 5 and 6 the features characterising the malachite-based mixtures and the verdigris-based mixture in the 350-860 nm range are summarised.

		Pure	50%	20%	10%	5%	1%	Shift
<b>Green</b>	<b>White/Yellow</b>	<b>Reflectance maxima (nm)</b>						
<b>M</b>	<b>B</b>	535	537	542	546	552	575	+40
<b>M</b>	<b>Z</b>	535	525	526	530	535	560	+25
<b>M</b>	<b>N</b>	535	/	/	537	535	535	+2
<b>Green</b>	<b>White/Yellow</b>	<b>Reflectance minima (nm)</b>						
<b>M</b>	<b>B</b>	820	828	830	840	840	840	+20
<b>M</b>	<b>Z</b>	820	840	850	850	850	840	+20
<b>M</b>	<b>N</b>	820			820	820	820	0
<b>Green</b>	<b>White/Yellow</b>	<b>Inflections point (nm)</b>						
<b>M</b>	<b>B</b>	408	403	400	398	398	388	-20
		435	435	435	435	439	434	1
		472	466	455	450	450	448	-24
		582	590	698	600	610	620	+38
<b>M</b>	<b>Z</b>	408	-	-	-	-	-	-
		435	435	440	442	-	-	-
		472	466	462	-	-	-	-
		582	588	594	600	605	625	+43
<b>M</b>	<b>N</b>	408	/	/	407	408	408	-1
		435	/	/	417	423	430	-18
		472	/	/	490	482	476	+18
		582	/	/	585	583	580	+3

Table 5: Location of reflectance maxima, minima and inflection points in the reflectance spectra of the malachite-based mixtures in the 350-860 nm range. The percentage for the malachite-Naples yellow mixtures refers to the amount of the yellow pigment. The symbol (-) means that the specific feature is undetectable.

		Pure	50%	20%	10%	5%	1%	Shift
<b>Green</b>	<b>White/Yellow</b>	<b>Reflectance maxima (nm)</b>						
<b>V</b>	<b>B</b>	513	510	518	533	552	594	+81
<b>V</b>	<b>Z</b>	513	502	510	520	530	555	+42
<b>V</b>	<b>N</b>	513	/	/	511	505	500	-2
<b>Green</b>	<b>White/Yellow</b>	<b>Reflectance minima (nm)</b>						
<b>V</b>	<b>B</b>	<445	-	-	-	-	-	-
		>600	750	750	750	755	755	+155
<b>V</b>	<b>Z</b>	<445	-	-	-	-	-	-
		>600	800	800	800	800	800	+200
<b>V</b>	<b>N</b>	<445	/	/	<355	<382	<392	-90
		>600	/	/	715	>700	>635	+115
<b>Green</b>	<b>White/Yellow</b>	<b>Inflections point (nm)</b>						
<b>V</b>	<b>B</b>	493	475	470	465	455	450	-43
		533	545	560	580	600	634	+100
<b>V</b>	<b>Z</b>	493	478	478	-	-	-	-
		533	535	555	575	585	650	127
<b>V</b>	<b>N</b>	493	-	-	488	486	482	-5
		533	-	-	533	524	515	0

Table 6: Location of reflectance maxima, minima and inflection points in the reflectance spectra of the verdigris-based mixtures in the 350-860 nm range. The percentage for the verdigris-Naples yellow mixtures refers to the amount of the yellow pigment. The symbol (-) means that the specific feature is undetectable.



## 4.3.2- Chromium oxide green

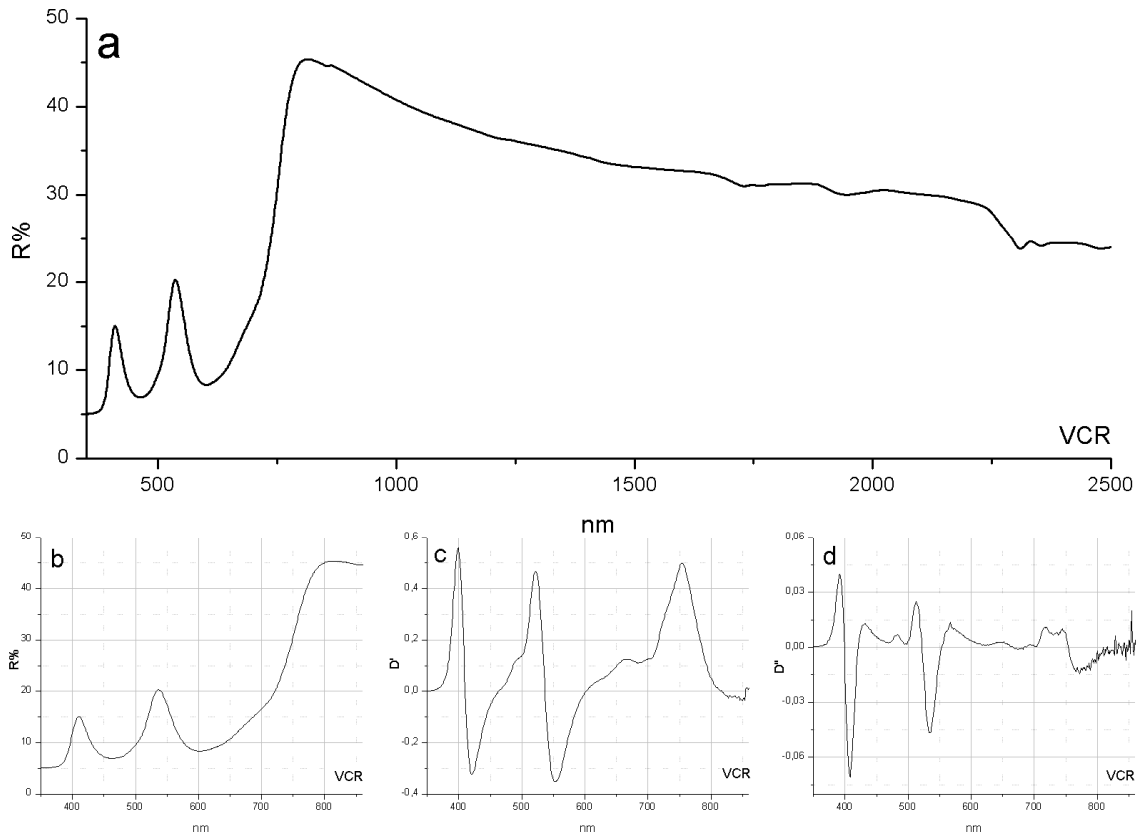


Figure 19: Reflectance spectra (a, b), first derivative spectrum(c) and second derivative spectrum (d) of chromium oxide (VCR).

Chromium oxide can be recognised by two reflectance maxima in the 400 nm to 535 nm visible range (Figure 19-a, b). Besides, the presences of weak reflectance minima at around 500 nm 700 nm are well visible in the first and second derivatives (Figure 19-c, d). As stated before, the aim of this study is to discover which absorptions best characterise chromium oxide and verify if they remain unchanged when the green pigment is mixed with white and yellow pigments.

In Table 7 and Table 8 the pigments and the mixtures studied are reported.

Pigment	Manufacture	Code	Formulation	Abbr.
Chromium oxide green	Zecchi	0405	Cr <sub>2</sub> O <sub>3</sub>	VCR
Lead white (Biacca)	Fluka Chemika	367410/1 54199	2PbCO <sub>3</sub> •Pb(OH) <sub>2</sub>	B
Zinc white	Aldrich	23,794-9	ZnO	Z
Naples yellow	Zecchi	0772	Pb <sub>2</sub> Sb <sub>2</sub> O <sub>7</sub>	N
Lead chromate	Aldrich	31,044-1	PbCrO <sub>4</sub>	CR
Lime Cadmium yellow	Zecchi	0591	CdS	CDL

Table 7: List of the pigments used for chromium oxide based mixtures. In the table, the name of the pigment, the manufacture, the code, the formula and the abbreviation are reported.

Mixture	Green pigment	%	g	White pigment	%	g	Mixture	Green pigment	%	g	White pigment	%	g
VCRB1	Chromium ox	1	0.02	Lead white	99	1.98	VCRZ01	Chromium ox	1	0.02	Zinc white	99	1.98
VCRB05	Chromium ox	5	0.1	Lead white	95	1.9	VCRZ05	Chromium ox	5	0.1	Zinc white	95	1.9
VCRB10	Chromium ox	10	0.2	Lead white	90	1.8	VCRZ10	Chromium ox	10	0.2	Zinc white	90	1.8
VCRB20	Chromium ox	20	0.4	Lead white	80	1.6	VCRZ20	Chromium ox	20	0.4	Zinc white	80	1.6
VCRB50	Chromium ox	50	1	Lead white	50	1	VCRZ50	Chromium ox	50	1	Zinc white	50	1
Mixture	Green pigment	%	g	Yellow pigment	%	g	Mixture	Green pigment	%	g	Yellow pigment	%	g
VCRN01	Chromium ox	1	0.02	Naples yellow	99	1.98	VCRCR01	Chromium ox	1	0.02	Lead chromate	99	1.98
VCRN05	Chromium ox	5	0.1	Naples yellow	95	1.9	VCRCR05	Chromium ox	5	0.1	Lead chromate	95	1.9
VCRN10	Chromium ox	10	0.2	Naples yellow	90	1.8	VCRCR10	Chromium ox	10	0.2	Lead chromate	90	1.8
Mixture	Green pigment	%	g	Yellow pigment	%	g							
VCRCDL01	Chromium ox	1	0.02	Cadmium yellow	99	1.98							
VCRCDL05	Chromium ox	5	0.1	Cadmium yellow	95	1.9							
VCRCDL10	Chromium ox	10	0.02	Cadmium yellow	90	1.8							

Table 8: List of the mixtures prepared with selected amounts (in percentage and in weight) of chromium oxide and white and yellow pigments.

The mixtures chromium oxide - lead white present an increase of the reflectance values in the visible and in the infrared range. No other variations were detected except for the absorption bands at 1450 nm due to lead white (Figure 20-a). Also zinc white does not seem to modify the reflectance features of the green pigment, except for the absorption band in the UV zone (378-385 nm), due to the band-band electronic transition on the zinc ion (Figure 20-b). On the other hand, the presence of a yellow pigment in the mixture can modify the features of chromium oxide, especially in the UV-Vis region, where the green pigment shows its characteristic absorption (Figure 20-c, d, e). In particular, a decrease of the absorption band localised at 460 nm can be noted, that is completely hidden by the absorption due to cadmium yellow.

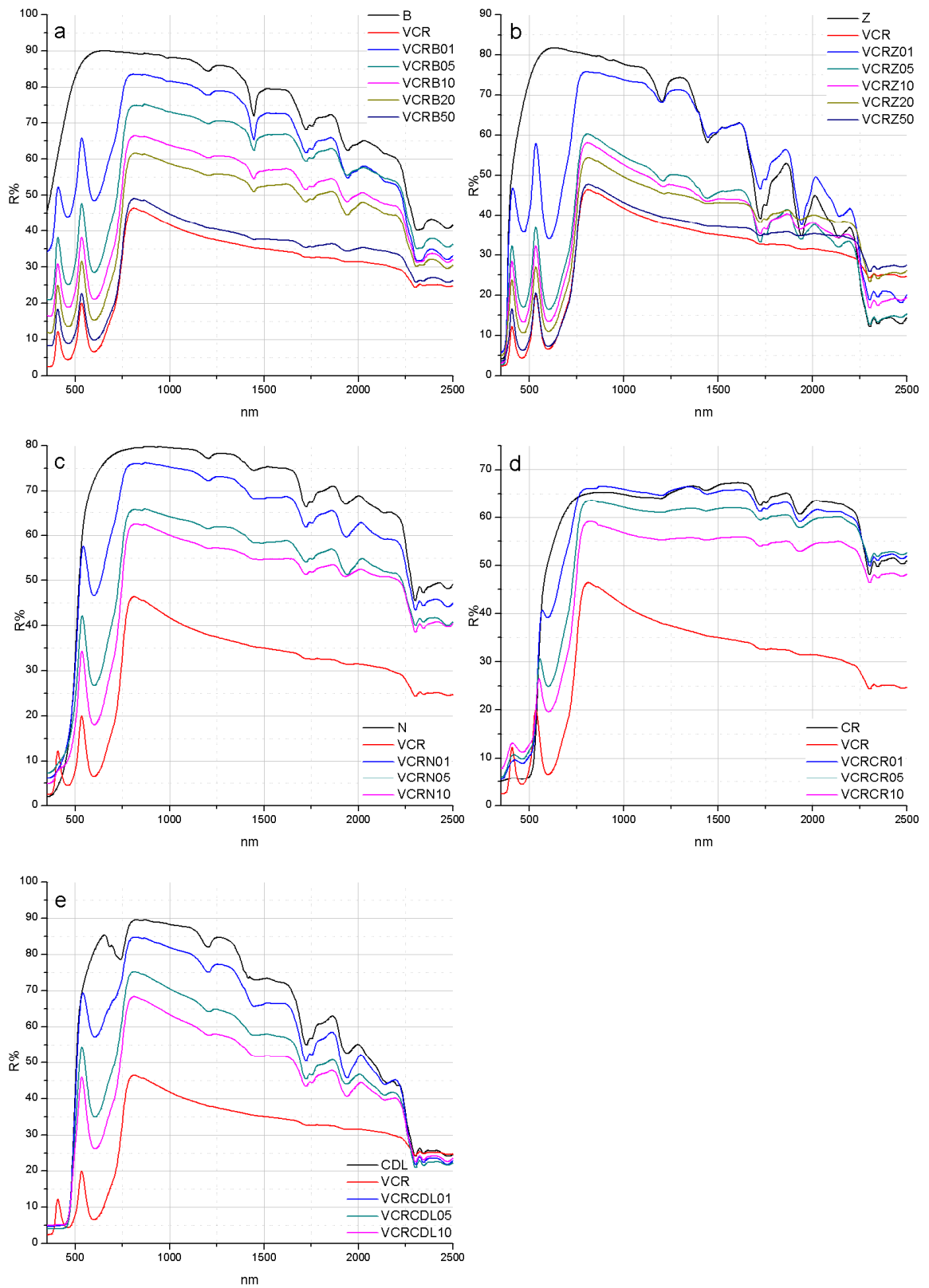


Figure 20: Reflectance spectra of chromium oxide mixed with lead white (a), zinc white (b) Naples yellow (c), lead chromate (d) and cadmium yellow (e).

The discussion of the results will be conducted focusing on the 350–860 nm range, considering the mixtures one by one and taking into account the first derivatives of the spectra acquired (Figure 21 and Figure 22).

**-VCRB mixtures** (Figure 21-a, b): The presence of lead white does not modify the position of the absorption bands, just their intensity. Some changes could be detected in the shape of the absorption because of a small shift in the inflection points. For example, in the first derivative the second minimum moves from 420 nm (VCR) to 425 nm (VCRB01) and the minimum at 552 nm goes to 557 nm.

**-VCRZ mixtures** (Figure 21-c, d): Not many changes in the absorption positions are recorded. The most significant variation is due to the absorption of zinc white characterised by an inflection point at 385 nm, easily recognisable in the first derivative spectra. As for chromium oxide-lead white mixtures, small differences in the position of inflection points are recorded, while reflectance maxima and minima are remain basically unchanged.

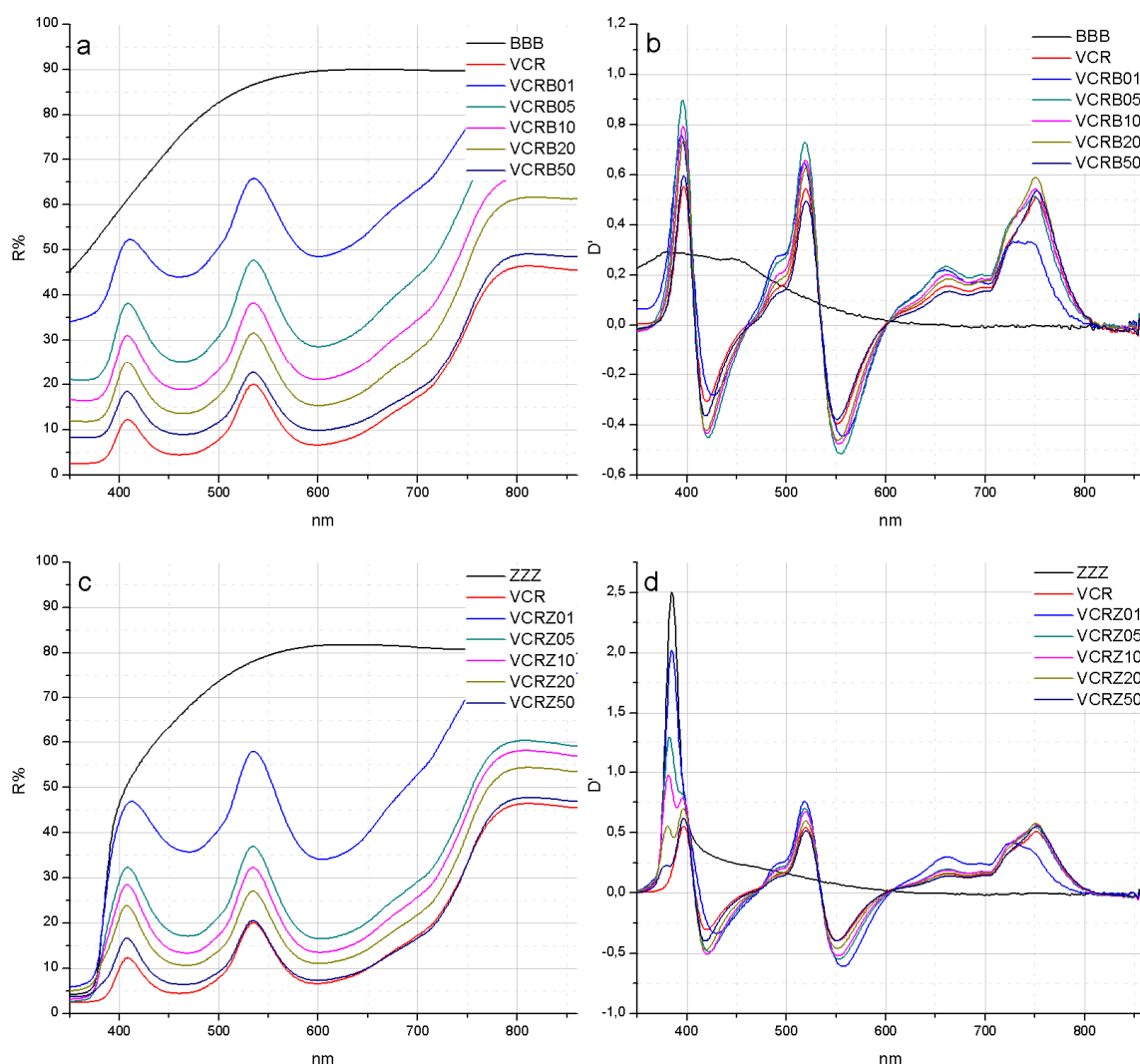


Figure 21: Reflectance spectra (left) and first derivative spectra (right) in the 350-860 nm range of the mixtures chromium oxide-lead white (a, b), chromium oxide-zinc white (c, d).

**-VCRN mixtures** (Figure 22-a, b): Naples yellow causes an increase in the reflectance of the green pigment's spectrum. The reflectance maximum at 408 nm disappears, as well as the absorption at 460 nm (they are

hardly visible in VCRN10sample). The reflectance maximum at 535 nm does not change in the mixtures but just moves to 543 nm in spectrum VCRN01. The inflection point localized at 520 nm in the green pigment remains constant enough, as well as the absorption band at 600 nm. The spectral features in the 650-700 nm range are unaltered: in the first derivative it is always possible to recognise two maxima at about 660-665 nm and the minimum at 700 nm, while the shoulder at 720 nm and the maximum at 750 nm, are only barely visible in spectrum VCRN01.

**-VCRCR mixtures** (Figure 22-c, d): As for Naples yellow, the increase of the concentration of lead chromate corresponds to an increase of the reflectance values for wavelengths higher than 550 nm; the reflectance maximum at 408 nm increases and shifts toward higher wavelengths and the inflection point at 397 nm shifts to 383 nm in sample VCRCR01. The strong absorption band at 460 nm does not change in position but decreases in intensity. The reflectance maximum at 535 nm undergoes a large shift to higher wavelengths to 570 nm (VCRCR01), after that the reflectance of the spectra increases very strongly for all the mixtures analysed. Obviously, this increase in reflectance is greater in mixtures containing a larger amount of yellow pigment. The absorption band at 600 nm can be seen in all the spectra but its intensity decreases gradually with the increase of the amount of yellow pigment. Also in the range 650-860 nm the spectral features are preserved. In fact, looking at the first derivative it is possible to verify that the position of the minima (685 nm and 702 nm) and that of the shoulder at 725 nm are the same for all the mixtures.

**-VCRCDL mixtures** (Figure 22-e, f): The spectrum of this cadmium yellow is characterised by a strong absorption divided in two sub-bands at 685 nm and 741 nm due to the presence of Co ions (II) in the yellow composition, in order to stabilise the colour. In the blue region the reflectance maximum at 408 nm disappears (in this spectral range the mixtures follow the spectral behaviour of the yellow pigments), and as a consequence an absorption is present from 350 to 450 nm in all the mixtures. In the first derivative it can be noted how the CDL trend at around 450 nm influences the spectral behaviour of the mixtures. In fact, the disappearance of the minimum at 474 nm, the increase of the maximum at 485 nm and the shift of the maximum from 520 nm to 505 nm are detected. Moreover, the reflectance minimum at 600 nm shifts to 605 nm in all the mixtures. In the 650-750 nm range, the presence of the double-absorptions due to the Co(II) ions in the cadmium yellow is very clear in the spectrum that show an intermediate behaviour between the green and the yellow pigment.

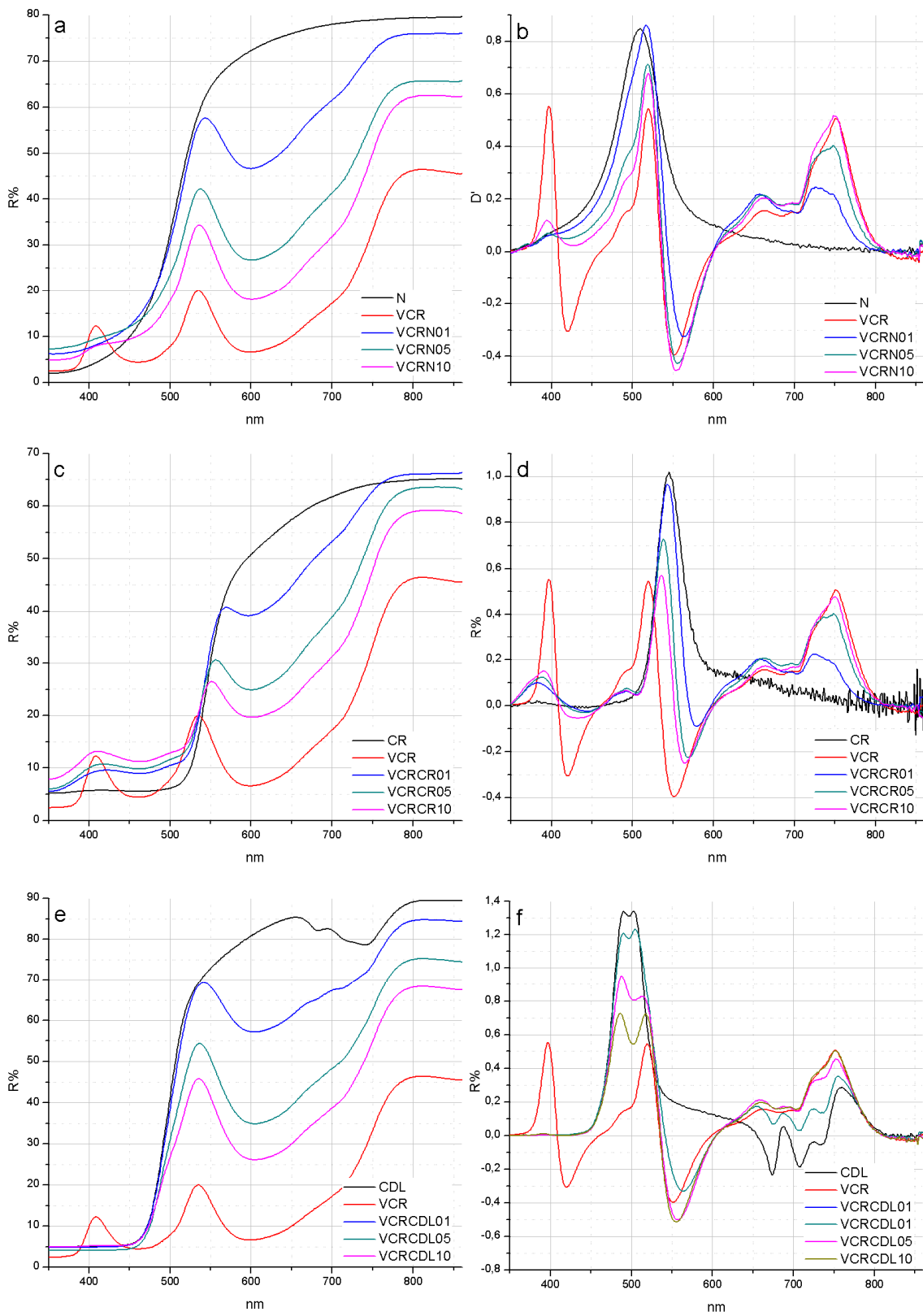


Figure 22: Reflectance spectra (left) and first derivative spectra (right) in the 350 nm-860 nm range of the mixtures chromium oxide-Naples yellow (a, b), chromium oxide-lead chromate (c, d) and chromium oxide-cadmium yellow (e, f).

From what has been discussed so far, it is clear that most of the variations in chromium oxide's spectral behaviour are due to the presence of yellow pigments, so it could be very useful to compare the different yellow-green mixtures having the same amount of green chromium oxide (Figure 23).

Mixtures with 10% of chromium oxide show mainly the spectral features of the green pigment (Figure 23-a, b). The CDL mixture is the only one that does not reflect in the 350-450 nm range, while in admixture with chrome yellow it has a reflectance maximum at 410 nm. This last mixture also has a reflectance minimum at 462 nm which is not present in the other curves. Both mixtures with chrome and Naples yellow have a minimum at about 425 nm in the first derivative. Looking at the spectrum for VCRCDL10, two relative maxima are visible between 485 nm and 515 nm, while the mixture VCRN10 has a shoulder at 490 nm and a very intense maximum at 519 nm. In VCRCR10 a relative maximum at about 490 nm and the maximum at 535 nm are recorded. In the VCrN10 and VCRCDL10 curves a reflectance maximum in the green region centred at around 535 nm is noted, while for VCRCR10 the maximum is localised at 552 nm. The same trend is detected for the inflection points of the absorption band at 600 nm: the inflection point is localised at 555 nm for VCRN10 e VCRCRL10 and at 565 nm for VCRCR10. So, even if the centre of the absorption is always at 600 nm, the shape of the absorption varies with the mixture. Over 600 nm, the reflectance behaviour of the samples is very similar and the only difference concerns the reflectance values, which is highest in VCRCDL10.

After halving the concentration of chromium oxide (Figure 23-c, d), the cadmium based mixture does not reflect in the 350-450 nm range and a weak reflectance is detected for VCRCR05 between 415nm and 420 nm. However, in the first derivative of VCRN05 a relative minimum can be seen at 380 nm which makes it different from the other spectra. In the first derivative of VCRCDL05 a strong maximum at 490 nm is detected, while in the other spectra just a shoulder (VCRN05) or a relative maximum markedly less intense (VCRCR05) is visible. The reflectance maximum is located at around 535 nm for VCRCDL05 and VCRN05, while it shifts to 557 nm for VCRCR05. Also the inflection points of the absorption band at 600 nm present different values: 555 nm for VCRCDL05 and VCRN05 and 565 nm for VCRCR05. For wavelengths greater than 600 nm, the behaviour of the curves is similar, especially for samples VCRCR05 and VCRN05, while in the first derivative functions of sample VCRCDL05 there are features linked with the presence of Co (II) ions. In the spectra acquired from the mixtures with 1% of chromium oxide, the spectral behaviour of the yellow pigments emerges as predominant (Figure 23-e, f); as a consequence, the mixture VCRCDL01 and VCRN01 absorb completely between 350 nm to 450 nm, while the mixture VCRCR01 has a reflectance maximum centred at 420 nm. After 450 nm all the curves start to increase in reflectance. In the green-yellow region the reflectance maxima are around 540 for VCRN01 and VCRCDL01 and 570 nm for VCRCR01. In the first derivative, the position of the maxima allows the mixtures to be distinguished: for VCRCR01 the maximum is at 543 nm, for VCRN01 it is at 517 nm, while VCRCDL01's spectrum has two maxima at 490 nm and 505 nm.

All the spectra show a reflectance minimum in the range from 595 nm to 605 nm. The following behaviour of the curves is more diversified than in the previous mixtures: in fact, the VCRCDL01 curve has the sharpest

reflectance increase while VCRCR01 has the slowest reflectance increase, and VCRN01 spectrum presents a behaviour intermediate between those taken into account. In the 650-750 nm range, the mixtures show the absorption due to the presence of the chromium oxide, even if the spectrum of the cadmium mixture is strongly influenced by the absorptions due to Co (II) ions.



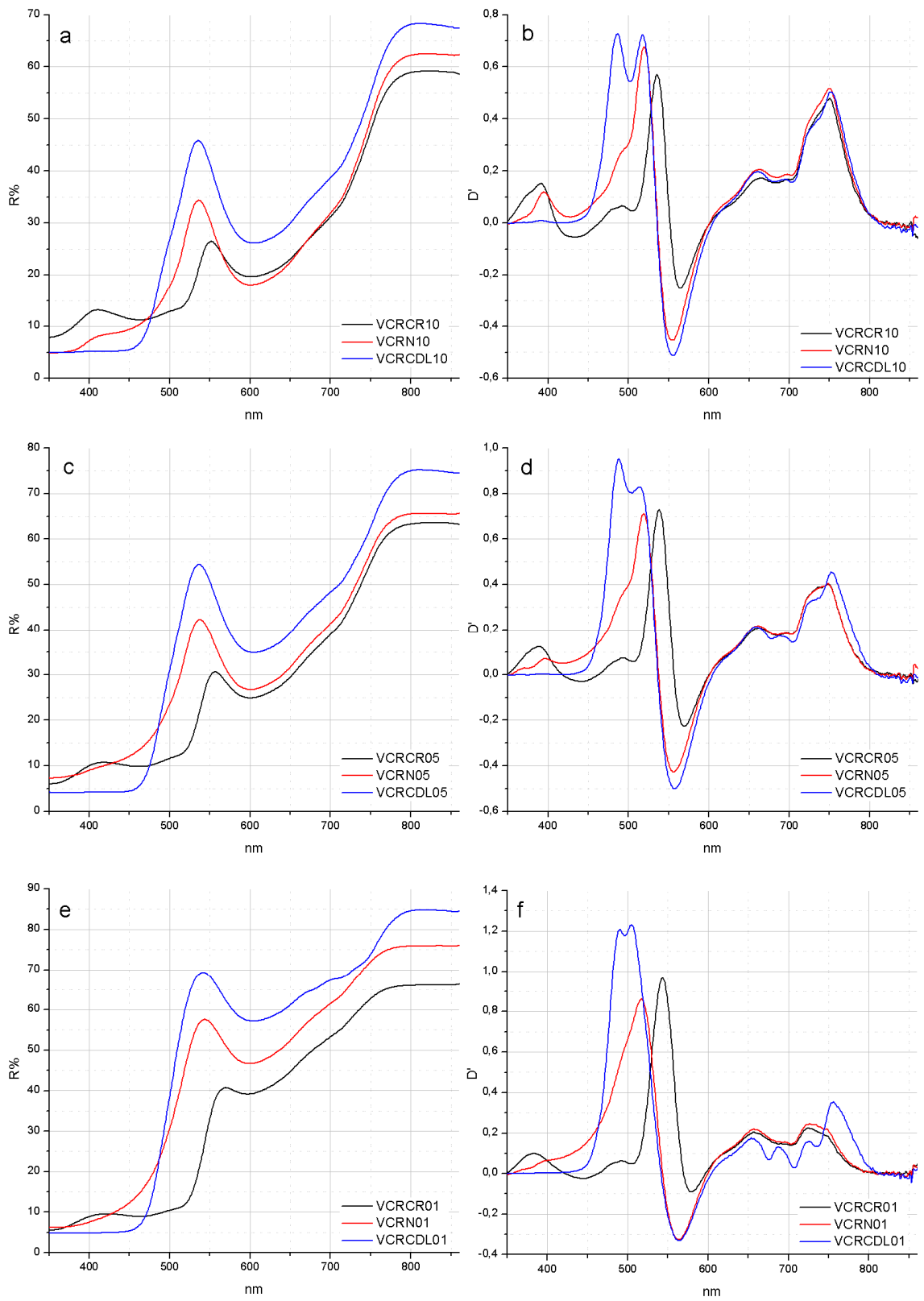


Figure 23: Reflectance spectra (left) and first derivative spectra (right) focused in the 350 – 860 nm range of chromium oxide mixed with 90% of the yellow pigments (a, b), 95% yellow pigments (c, d), 99% of yellow pigments (e, f).

In Tables 9, 10, and 11 the features characterising chromium oxide-based mixture are summarised.

	.	Pure	50%	20%	10%	5%	1%	Shift
Green	White/Yellow	Reflectance maxima (nm)						
VCR	B	408	408	408	408	408	408	+1
		535	535	535	535	535	535	0
		810	812	812	812	812	809	-1
VCR	Z	408	408	408	410	410	413	+3
		535	-	-	-	-	-	-
		810	810	810	809	809	809	-1
VCR	N	408	/	/	-	-	-	-
		535	/	/	536	537	543	+7
		810	/	/	810	810	810	0
VCR	CR	408	/	/	410	418	422	+14
		535	/	/	552	557	570	34
		810	/	/	810	810	810	0
VCR	CD	408	/	/	-	-	-	-
		535	/	/	537	535	541	+6
		810	/	/	810	810	810	0

Table 9: Location of reflectance maxima in the reflectance spectra of the chromium oxide-based mixtures in the 350-860 nm range. The symbol (\*\*\*) indicates the features due to the cadmium yellow. The symbol (-) means that the specific feature is undetectable.

	.	Pure	50%	20%	10%	5%	1%	Shift
Green	White/Yellow	Reflectance minima (nm)						
VCR	B	350	367	367	367	364	-	+14
		460	463	463	463	463	460	0
		600	600	600	600	600	600	0
VCR	Z	350	350	350	350	350	<350 (345)	5
		460	464	468	468	468	471	+11
		600	600	602	603	604	605	+5
VCR	N	350	/	/	355	355	355	+5
		460	/	/	-	-	-	-
		600	/	/	601	601	600	0
VCR	CR	350	/	/	350	350	350	0
		460	/	/	462	462	462	+2
		600	/	/	601	600	594	+4
VCR	CD	350	/	/	>425	>425	>425	+75
		460	/	/	-	-	-	-
		600	/	/	605	605	605	+5

Table 10: Location of reflectance minima in the reflectance spectra of the chromium oxide-based mixtures in the 350-860 nm range. The symbol (\*\*\*) indicates the features due to cadmium yellow. The symbol (-) means that the specific feature is undetectable.

	.	Pure	50%	20%	10%	5%	1%	Shift
Green	White/Yellow	Inflections point (nm)						
VCR	B	397	397	3997	396	396	394	-3
		420	419	419	420	421	425	+3
		520	520	520	519	518	517	-3
		552	551	551	552	555	557	+5
		664	664	663	662	662	660	-4
		685	685	685	685	685	685	0
		702	702	702	702	703	703	+1
		750	752	751	751	750	720-750	-30-0
VCR	Z	397	397	397	395	395	-	-2
		420	418	419	421	422	430	+10
		520	520	520	520	519	518	-2
		552	552	552	552	553	557	+5
		664	664	664	664	663	662	+2
		685	685	685	685	685	685	0
		702	702	702	702	702	703	+1
		750	751	750	750	750	-	0
VCR	N	397	/	/	395	396	-	+1
		420	/	/	427	418	-	-2
		520	/	/	519	519	517	-3
		552	/	/	554	555	564	+12
		664	/	/	663	660	657	-7
		685	/	/	685	685	685	0
		702	/	/	702	702	703	+1
		750	/	/	750	748	720-732	-30-(-22)
VCR	CR	397	/	/	392	389	383	+14
		420	/	/	433	442	444	+24
		520	/	/	535	538	543	+23
		552	/	/	565	570	580	+28
		664	/	/	684	684	687	+3
		685	/	/	684	684	687	+2
		702	/	/	702	702	702	0
		750	/	/	750	748	725	-25
VCR	CD	397	/	/	-	-	-	-
		420	/	/	-	-	-	-
		520	/	/	515	517	505	-15
		552	/	/	555	557	564	+12
		664	/	/	661	658	655	-9
		685	/	/	679	679	675**	-10
		702	/	/	703	705	706**	+4
		750	/	/	751	752	756	+6

Table 11: Location of inflection points in the reflectance spectra of the chromium oxide-based mixtures in the 350-860 nm range. The symbol (\*\*) indicates the features due to cadmium yellow. The symbol (-) means that the specific feature is undetectable.

#### 4.4- Conclusions

The comparison between the spectra of the pure green pigments and those of pigment mixtures allowed to particular features which can be used for the identification of specific green materials to be brought to light. As shown in the previous paragraphs, some modern green pigments can be identified easily, such as cobalt green and viridian, while others present similar spectral curves which differ just in small shifts in the absorption bands' positions. In particular, great difficulties are usually found when copper-based greens are taken into account or when multiple pictorial layers are examined.

Focusing the attention on malachite- and verdigris-based mixtures, even if the specific pigments were discernable in several of the situations studied, it was not possible to individuate characterising features not subject to shifts. In fact, by studying Tables 5 and 6, it is evident that the reflectance maxima, minima and inflection points detected strongly depend on the second component of the mixture and on the relative amount of green pigment used. However, some exceptions must be considered: for instance Naples yellow does not cause particular variations in the position of the reflectance maximum at 535 nm for malachite and the reflectance maximum at 513 nm for verdigris. On the other hand, zinc white is the material, among those considered, which affects the spectra the most. In fact, several features completely disappear when the concentration of zinc white increases, such as the first absorption of verdigris and the inflections points of malachite and verdigris. Lead white mainly determines a positive shift of reflectance maxima and minima, and moves the position of the inflections points toward higher or lower wavelengths as a function of the increasing or decreasing trend of the curve.

Very interesting results were achieved with mixtures containing chromium oxide. By considering the shifts detected in its reflectance maxima and minima (Table 9 and 10), it is evident that chrome yellow and cadmium yellow are responsible for the greatest variations. Concerning the inflection points, it is very important to note that three of the features taken into account (inflection points at 664 nm, 685 nm, and 702 nm) remain localised in the same position when considering a 10 nm shift acceptable.

In order to verify the possibility of identifying chromium oxide green in 19<sup>th</sup> century works of art by means of non-invasive spectroscopic methodologies, the painting *Carica di Cavalleria* by Giovanni Fattori was considered (Figure 24). In particular, this study considered green areas that had already been sampled for a previous project focused on Fattori's artistic technique [22]. For that occasion analysis on cross-sections of micro samples from the pictorial surfaces (Figures 25, 26, and 27) were conducted at the ICIS-CNR (Consiglio Nazionale delle Ricerche-Istituto di Chimica Inorganica e delle Superfici) in Padua [23]. The analysis was done by polarized optical microscopy (POM) in reflected white light in order to investigate the appearance and the possible composition of the pictorial layers. Moreover, Scanning Electron Microscopy with X-ray microanalysis (SEM/EDS) analysis was also performed in order to obtain qualitative and quantitative information about the elemental composition of the sample. The reflectance spectrum of the green area was acquired by means of a ZEISS spectroanalyser MCS 501 in the 350-1000 nm spectral range.

In the acquired spectrum where the sampling occurred (point 25, Figures 28 and 29), the inflection points localised at 660nm, 684 nm, and 702 nm are characteristic of chromium oxide (Table 11). However, the

reflectance maximum at 408 nm was not detected in spectrum 25, and the maximum at 535 nm is shifted to 525 nm, suggesting the presence of a second pigment absorbing in this spectral region. The reflectance maxima around 525 nm were detected in Schweinfurt green and cinnabar green (Table 2), and in the verdigris-lead white mixture (Table 6). Both these two green pigments could justify the absence of the maximum at 408 nm.



Figure 24: Carica di Cavalleria, G. Fattori. Spots of FORS measurements.



Figure 25: Carica di Cavalleria, G. Fattori. Spots of FORS measurements, detail.

Figure 26: Carica di Cavalleria, G. Fattori. Location of the sampling point.

Figure 27: Carica di Cavalleria, G. Fattori. Cross section – POM, magnification 520X.

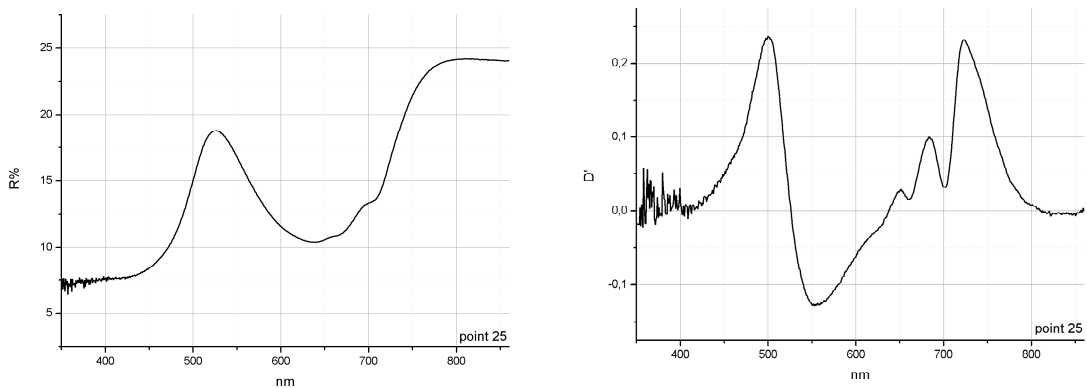


Figure 28 and Figure 29: Reflectance and derivative spectrum of the point 25 in the 350-860 nm spectral range – Carica di Cavalleria.

As a confirmation, EDS analysis and the study of the cross section at the polarized optical microscopy revealed the presence of chromium oxide green together with Schweinfurt green and lead white while sparse particles of vermilion and chrome yellow were identified in the deep green ground [23].

## References

1. G. R. Hunt, and J. W. Salisbury, *Modern Geology*, 1, 1970, 283.
2. G. R. Hunt, J. W. Salisbury, and C. J. Lenhoff, *Modern Geology*, 3, 1971, 1.
3. G. R. Hunt, *Geophysics*, 42 (3), 1977, 501.
4. G. R. Hunt, J. W. Salisbury, and c. J. Lenhoff, *Modern Geology*, 4, 1973, 85.
5. M. Bacci, M. Picollo, G. Trumpy, M. Tsukada, and D. Kunzelman, *Journal of the American Institute for Conservation*, 46, 2007, 27.
6. R. Newman, Chromium Oxide Greens in *Artists' Pigments, A Handbook of their History and Characteristics Vol. 3*, E. W. FitzHugh (Ed), Oxford University Press, New York, 1997, 273.
7. L. Carlyle, *The artist assistant. Oil Painting instruction Manuals and handbooks in Britain 1800-1900 with reference to selected 18th-century sources*, Archetype Publications, London, 2001.
8. N. Eastaugh, V. Walsh, T. Chaplin, and S. Ruth, *Pigment Compendium A Dictionary of historic pigments*, Oxford University Press, Butterworth-Heinemann, New York, 2004.
9. T. B. Brill, *Light, Its Interaction with Art and Antiquities*, Plenum Press, New York, 1980.
10. R. Johnston-Feller, *Color Science in Examination of Museum Objects, non Destructive Procedures*, The Getty Conservation Institute, Los Angeles, 2001.
11. G. Fields, *Chromatography or Treatise on Colours and Pigments and of their Powder in Paintings*, Mays and Barclay Printers, London, 1841.
12. M. Bacci, *Modern Analytical Methods in Art and Archaeology*, Chemical Analysis Series, E. Ciliberto, and G. Spoto (Eds.), John Wiley & Sons Inc., New York, 155, 2000, 321.
13. D. Patterson, *Pigments, an introduction to their Physical Chemistry*, Elsevier Publishing Co. England, 1967.
14. <http://www.webexhibits.org/pigments>, last accessed 25<sup>th</sup> November 2010.
15. B. Berrie, Prussian blue, in *Artists' Pigments, A Handbook of their History and Characteristics Vol. 3*, E. W. FitzHugh (Ed), Oxford University Press, New York, 1997, 191.
16. R. J. Gettens, and E. W. Fitzhugh, Malachite and Green Verditer, in *Artists' Pigments, A Handbook of their History and Characteristics Vol. 2*, A. Roy (Ed), Oxford University Press, New York, 1993, 183.
17. M. Shimoyama, S. Hayano, K. Matsukawa, H. Inoue, T. Ninomiya, *Journal of Polymer Science: Part B: Polymer Physics*, 36, 1998, 1529.
18. I. Fiedler, and M. Bayard, Emerald Green and Scheele's Green, in *Artists' Pigments, A Handbook of their History and Characteristics Vol. 3*, E. W. FitzHugh (Ed), Oxford University Press, New York, 1997, 219.
19. J. Plesters, Ultramarine blue, Natural and Artificial, in *Artists' Pigments, A Handbook of their History and Characteristics Vol. 2*, A. Roy (Ed), Oxford University Press, New York, 1993, 37.
20. R. J. H. Clark, D. G. Cobbold, *Inorganic Chemistry*, 17, (11), 1978, 3169-3174.
21. S. Kowalak, A. Jankowska, S. Zeidler, and A. B. Wieckowski, *Journal of Solid State Chemistry*, 180, 2007, 1119.
22. M. Bacci, L. Boselli, A. Casini, C. Cucci, M. Picollo, M. Poggesi, B. Radicati, L. Stefani, *Indagini spettroscopiche non invasive per la caratterizzazione delle opere pittoriche di Giovanni Fattori, Con la matita e col pennello*, G. Damiani, and M. Vervat (Eds), Mauro Pagliai Press, Firenze, 2009, 63.
23. M. Favaro, S. Bianchin, P. A. Vigato, and M. Vervat, *Journal of Cultural Heritage*, 11, 2010, 265.





## Chapter 5

# Spectroscopic analysis of 19<sup>th</sup> century Winsor & Newton watercolours

Within the framework of a collaborative research project between the Victoria and Albert Museum, London, (V&A) and IFAC a set of 19<sup>th</sup> century Winsor & Newton (W&N) watercolour cakes was analysed. The set of watercolours is part of the collections of the V&A. The aim of this study was to collect FORS data from original materials in order to create a spectral database of historical watercolours. This database could then be used as a set of references for the characterisation of pigments and dyes in works of art.

The watercolour cakes were still well kept in what is believed to be their original box (Figure 1 and 2). Table 1 shows the list of the cakes analysed as well as their position in the box.

In some cases, the presence of an external protective wax coating was noticed. Before acquiring any reflectance spectra, the coating, as well as surface dirt, was removed by abrading a small portion of the surface with silicon carbide paper. This operation was performed on the short side of the cakes, paying special attention in order not to ruin the bas-relief present on the front and the back of the cakes' sides.

In order to characterise the cakes, X-ray fluorescence (XRF), Raman spectroscopy, X-ray diffraction (XRD) and polarized light microscopy (PLM) analysis were also performed by the scientists at the V&A. This chapter will deal only with the FORS results.

In many instances, the name of the pigment embossed on the cakes does not correspond to the chemical composition of the cake. Primary sources were investigated to clarify this issue: 19<sup>th</sup> century Winsor & Newton's own catalogues [1, 2, 3], *A system of watercolour painting* by Penley [4], *The art of portrait painting in water-colours* by Merrifield [5], and *Chromatography* by Field [6]. In particular, the latter was

very useful for the present study because the author was one of the most eminent English colour-makers in the first half of the 19<sup>th</sup> century. Field is known to have provided his notebooks recording his pigment tests to William Winsor.



Figure 1: The Winsor & Newton box of watercolours from the V&A (external).

Figure 2: Winsor & Newton water colours cakes.

c	1	2	3	4	5	6	7	8	9	10	11	12		
A	Prussian green		Viridian	Terre verte	Emerald green	Green oxide of chromium	Bistre	Prussian blue	Raw umber	Payne's grey	Ivory black			
B	Purple madder	Light red	Const. white	Aureolin	Chinese white	Yellow Lake	Antwerp blue	Bronze	Brown madder	Violet carmine	Burnt pink	Warm sepia		
C	Vermilion	Indigo	smalt	Indian red	Rubens' madder	Cadmium orange	Olive green	Burnt umber	Mars yellow	King's yellow	Scarlet lake	Black lead		
D	Burnt ochre	French blue		Venetian red	Burnt Sienna	Blue black	Deep chrome	Burnt carmine	Carmine	Gallstone	Intense blue	Purple lake		
E	Hooker's green no. 2	Madder carmine	Crimson lake	Roman ochre	Raw Sienna		Neutral tint	Hooker's green no. 1	British ink	Mars orange	Van Dyke brown	Gamboge		
F	Pink madder	Dragon's blood	Scarlet vermilion	Ultramarine ash	Italian pink	Pink madder	Brown madder	Lamp black						
G	Rubens' madder	Mars yellow			Rose madder	Cologne earth		Sepia		Black lead	Purple madder			
	1	2	3	4	5	6	7	8	9	10	11	12	13	14
H	Oxide of chromium	Violet carmine	French blue	Smalt	Neutral tint	Orange de Mars		Aureolin	Ivory black	Cadmium orange	Crimson lake	British ink	Pale cadmium yellow	Madder carmine
I	Dragons' blood	Scarlet vermilion	Bronze	Burnt carmine	Indian purple			Gallstone	Cadmium yellow	Indian yellow	Carmine	viridian		
J			Purple lake	Italian pink	Yellow lake		Pure scarlet	Chinese white		A. Penley's neutral orange	Olive green			

Table 1: The watercolours analysed and their position in the Winsor & Newton box. Not all the slots in the box were actually filled with a cake.

### 5.1- Brief history of Winsor & Newton Watercolours

In 1832, William Winsor, a chemist, and Henry Newton, an artist, entered into a partnership as colourmakers for artists. The location of this activity was 38 Rathbone Place, London [7].

At first, the main goal of the company was to produce and trade watercolours made and studied by the partners themselves. However, very soon Winsor and Newton started to deal with all the materials that could be used for artistic purposes, such as brushes, canvases and oil colours [8]. In 1835, when Winsor and Newton introduced the first moist watercolours, their reputation increased and they became very popular in the art field, thanks to very famous artists such as Turner who started to use W&N products. The company also produced catalogues containing technical details about materials and prices. The first catalogue was published in 1835 and contains information about 49 colours; some of these had only recently been produced for the first time, such as cobalt blue, emerald green, lemon yellow and chrome [8]. The watercolours were prepared in full size cakes and half cakes (Figure 3). The price depended on the specific pigment and it ranged from 1 shilling for the cheapest materials to 21 shillings for ultramarine (10s. 6d. for the half cake). Different types of elegantly fitted boxes were also available including watercolours and tools such as brushes and pencils [1]. The historical catalogues do not contain any information about the manufacture of the moist watercolours; a carefully guarded trade secret. In fact, the following statement was found in all of the 19<sup>th</sup> century catalogues examined in this study [1, 2, 3]:

*“Winsor and Newton’s Moist Water Colours retain, from processes and treatment known only to themselves, their solubility and dampness for an unlimited period”*



Figure 3: As reported in W&N catalogues, the watercolours analysed have on one side the official logo of the company, a winged lion, and on the other side the name of the pigment as well as the name of the company.

Useful information about the introduction of new pigments was mentioned. This information can help in narrowing down the date of production of the cakes analysed in this study; for example, in the catalogue published in 1863 it is explained that a new pigment called aureolin was introduced. Aureolin is described as ‘a new primitive yellow’, ‘the latest and certainly one of the most important contributions of science to the artist’s palette’ [2].

Since aureolin was first made in 1851 but was not mentioned in any of the catalogues by W&N before the 1863 one, it can be inferred that the cakes in the V&A box were produced after 1863.

Another very interesting observation is linked to the presence of viridian. Since this pigment was included in a W&N catalogue only in 1869 [9], its presence further postpones the date of the whole box, assuming that all watercolours in the box are of the same date.

Basic information about the recipes is published on the W&N website, however, there are no details about the use of extenders. The available W&N literature reports that other compounds were added to the pigment in order to improve its performance. Generally the binding medium in watercolours is gum Arabic [10], but alum and glycerine can be found as well: the first is used to give more brightness to the hues, while the second delays the drying process, keeping the colours wet for longer. Glycerine was the secret ingredient of W&N watercolour cake recipes and its introduction set the company on the path to international fame [7]. Other materials such as wax, flavour glue, starch and sarcocolla etc., could be added to modify colour shades and give body to the pigments [10, 11]. Small ‘pans’ of colour were obtained, supplied in ceramic cups which could be held in a box and used directly by means of a wet brush. Obviously, the latter feature was mainly for artists who painted *en plain-air*.

Over the course of time, the W&N artist’s palette changed: some materials were replaced because of their toxicity or because new and more functional pigments became available. As an example, Table 2 shows the colours present in the box analysed at the V&A that were later discontinued. The reasons for discontinuation and the nearest equivalent material in the range are also shown. Knowing the year when these changes occurred could help us date the watercolours box. For example perylene pigments were used instead of purple madder from the 1920s, so the box analysed, which still contains purple madder, is likely to be from before the 1920s [7]. In conclusion, the suggested date for box lies between 1869 and the 1920s. It should be remembered the suggested date assumes that all watercolours in the box are of the same date and that no cakes were added at later stages during the life of the box.

Colour name	Reason for Discontinuation	Nearest Equivalent in Range
Blue black	Similar to lamp black	Lamp black
Purple madder	Replaced by the single pigment Perylene Violet	Perylene Violet
Alizarin Carmine	Similar to Alizarin Crimson	Permanent Alizarin Crimson
Carmine	Replaced by a more lightfast pigment	Permanent Carmine
Chrome Deep	Toxicity and lack of permanence	Winsor Yellow Deep
Crimson lake	Similar to alizarin lake	Permanent Alizarin crimson and Quinacridone magenta
Hooker’s Green Light	Replaced by a more lightfast pigment	Quinacridone gold + Winsor blue
Purple lake	Lack of permanence	Purple madder
Sap green	Replaced by a more lightfast pigment	Permanent Sap Green
Sepia warm	Close to sepia	Sepia and burnt Sienna
Scarlet Vermilion	Brighter variety now available	Permanent Alizarin Crimson + water Vermilion Hue
Vermilion		

Table 2: Discontinued Winsor and Newton materials.

## 5.2- FORS analysis

Non-invasive measurements were performed using two ZEISS spectroanalysers combined in a unique chassis. The working range was 350-2200 nm. The selected probe allowed the acquisition of spectra with a 0°/2x45° geometry using a system of optical fibres. In this configuration the area investigated is illuminated from a direction normal to the surface, and the backscattered light is detected at 45° to the normal on both the right and the left side. Optical fibres transfer the residual signal to a Si-photodiode array and InGaAs array detectors. The reflectance spectrum is displayed on the monitor of a computer linked to the instrument. Even if by using this probe the dimension of the investigated area is just 2 mm in diameter, it was necessary to reduce the probe-sample interface by partially covering the probe in contact with the sample, to avoid the interference of room lights (Figure 4).

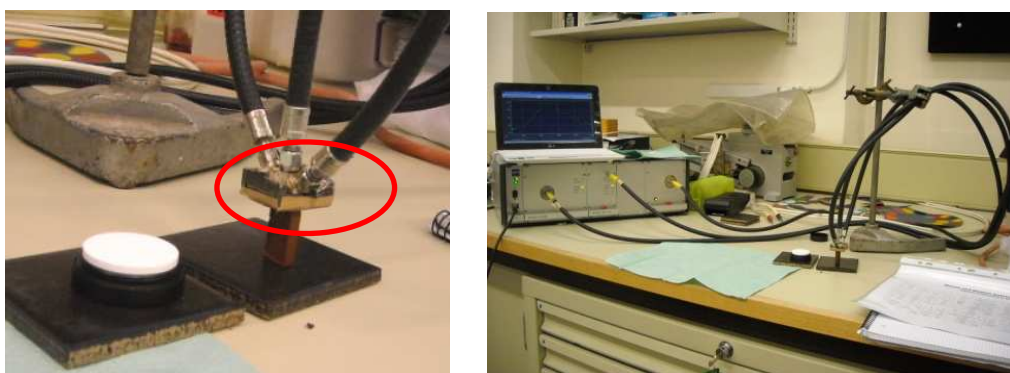


Figure 4 and Figure 5: Probe and standard reference used for the analysis; Instrumental set-up.

For each watercolour cake, three spectra were acquired and the average spectrum was calculated. A calibration on a white reflectance reference/standard (Spectralon<sup>®</sup> 99%) was made before changing the sample. The spectra acquired were reconstructed deleting the step at 980 nm caused by the change of the detector.

### 5.3- Results

This section reports the reflectance spectra of the cakes and the suggested chemical identification.

During the analysis of the data, recurring absorption bands were detected: these were due to the presence of the binder. As a consequence, in order to distinguish the features due to the pigments from those due to additional material, a sample of gum Arabic mixed with calcium carbonate was analysed. Calcium carbonate was selected instead of any other inert materials because it exhibits absorptions only over 2000 nm.

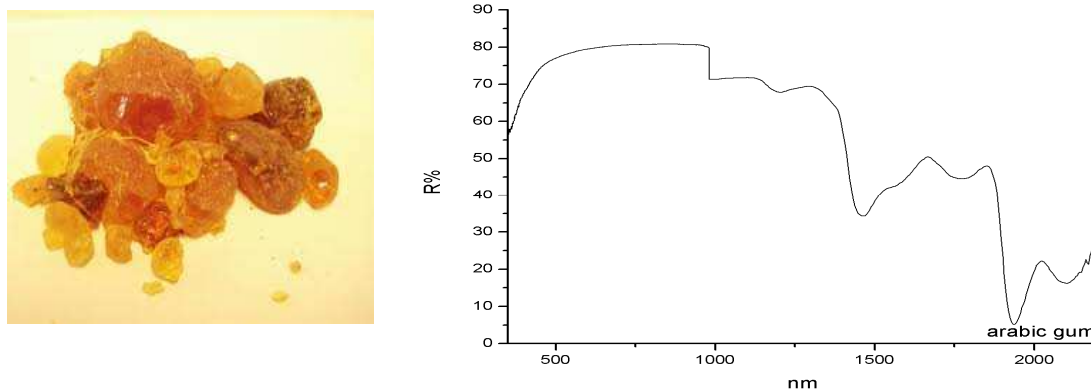


Figure 6 and Figure 7: A sample of gum Arabic; reflectance spectrum of gum Arabic and calcite.

Gum Arabic is obtained from the sap of trees of the *Acacia* species and is a complex polysaccharide containing galactose, arabinose, rhamnose and galacturonic acids (Figure 6). In the spectrum reported in Figure 7 the absorptions are due to water molecules and hydroxyl groups present in the chemical structure of the gum Arabic sample analysed and are localised at around 1200 nm, 1450-1650 nm, 1760 nm, 1940 nm and 2100 nm. These absorptions could mask any absorptions due to other substances and occurring in the same spectral range, such as those in gypsum or lead white.

Absorptions localised between 1650 nm and 1770 nm were found in several spectra from pigments such as Hooker's green (E8 and E1), madder carmine (H14 and e2), Prussian green (A1), purple madder (B1 and G11), Rubens' madder (C5) and violet carmine (B10 and H2). In this spectral region, absorption due to the first overtone of  $-\text{CH}_3$  (methyl),  $-\text{CH}_2$  (methylene) and  $-\text{CH}$  (methine) groups are present. In general, the first overtones of the CH stretching occur between 1700 and 1800 nm, the second overtones between 1150 and 1210 nm, and the third overtones between 880 and 915 nm [12]. Depending on the chemical environment, these features can shift by a few nanometres. Therefore, the absorptions recorded can be linked to the presence of fatty acids, contained in esterified forms of animal or vegetable fats, oils or waxes probably added to make the compounds more malleable (Figure 8).

Another recurring band is positioned at around 1380-1390 nm and it was detected mainly in dark or black pigments (Figure 8) such as bistre (A7), blue black (D6), British ink (E9 and H12), ivory black (A11 and H9), Payne's grey (H10), and sepia (G8) but also in bronze (I3), terre verte (A4), and ultramarine ash (F4). This absorption is probably correlated with a clay mineral added to give more body to the specific material.

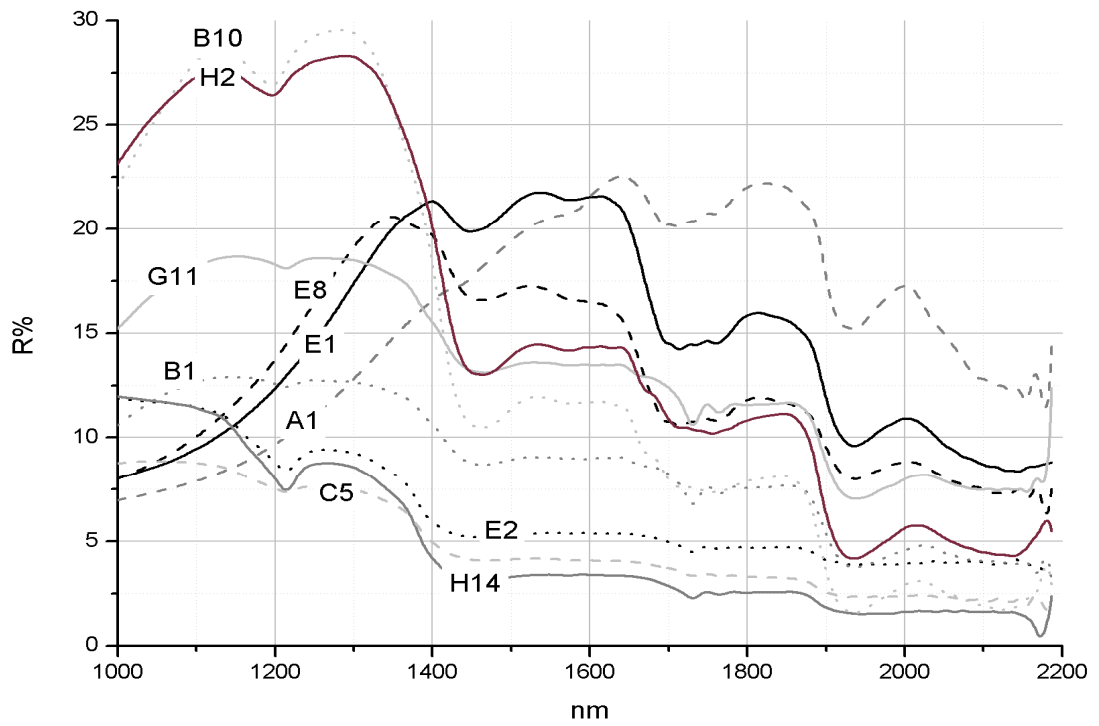


Figure 8: Reflectance spectra of watercolour presenting absorptions in the 1700-1800 nm spectral range.

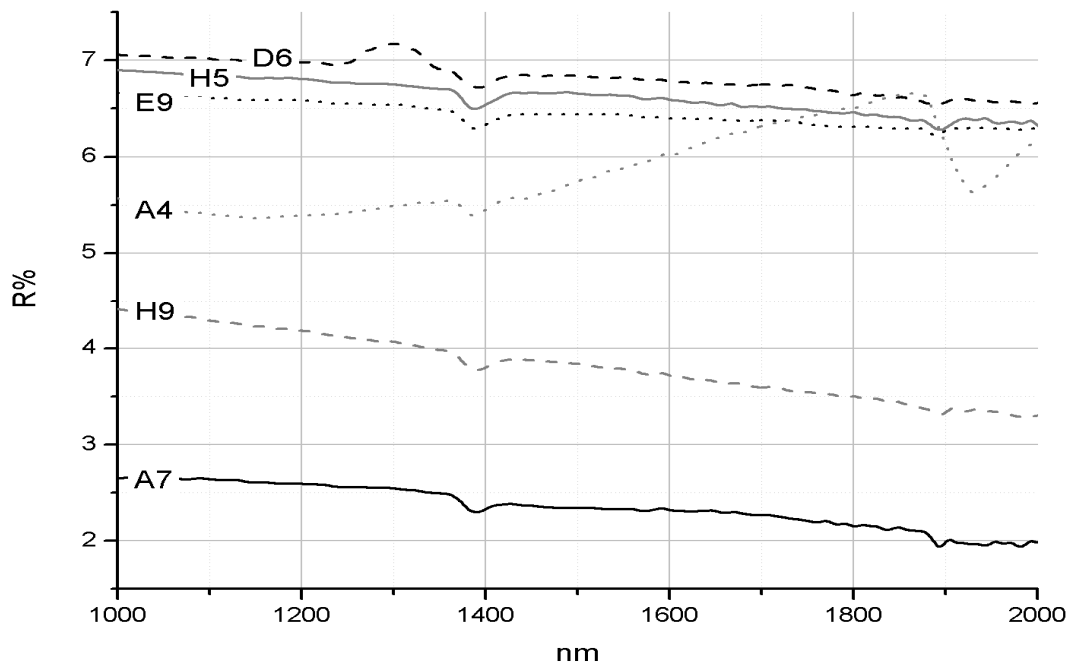
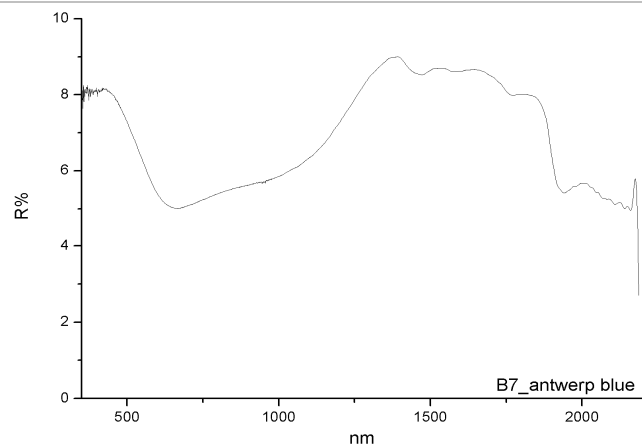
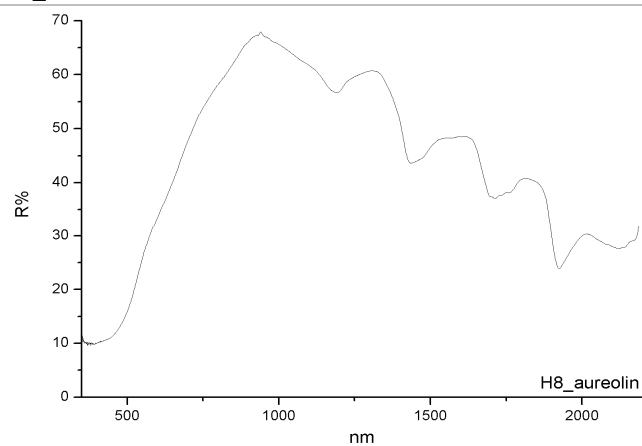
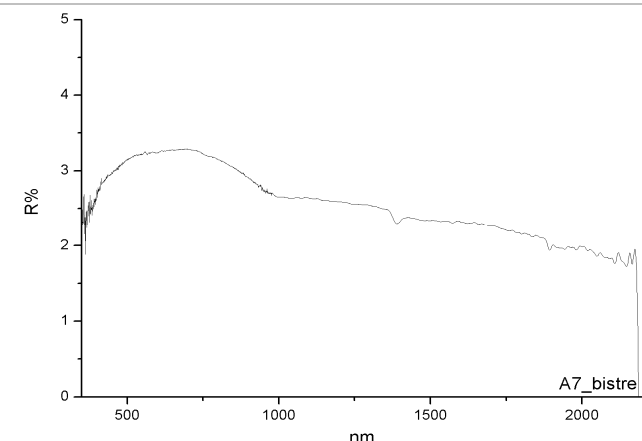
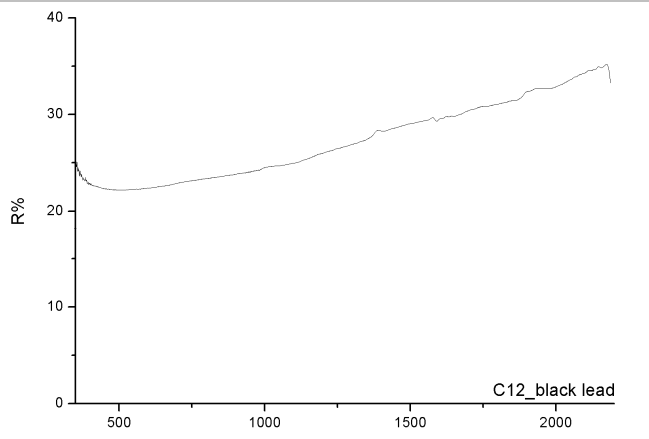
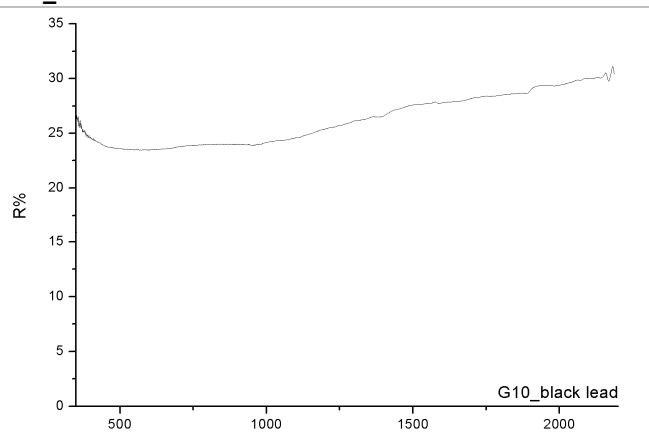
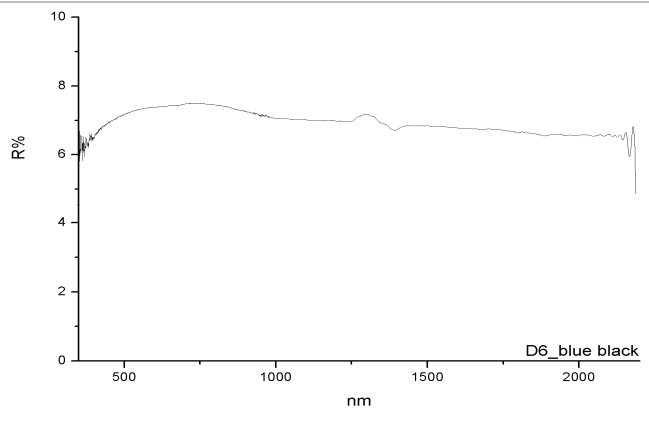
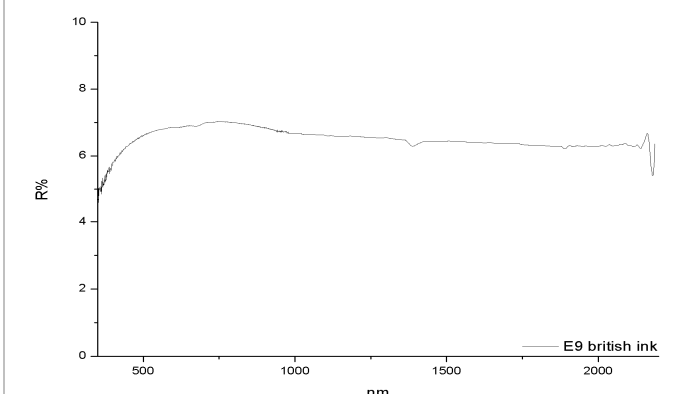
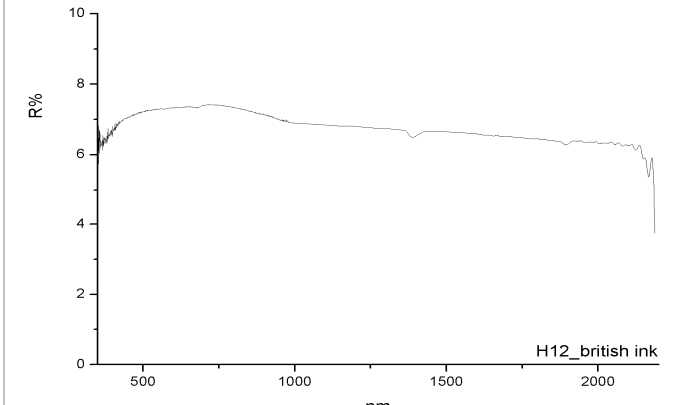

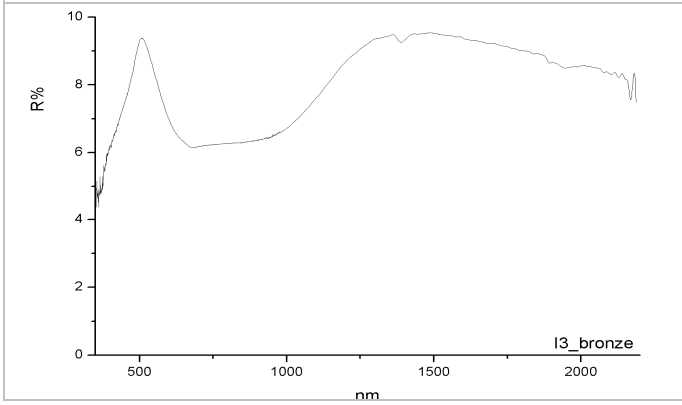


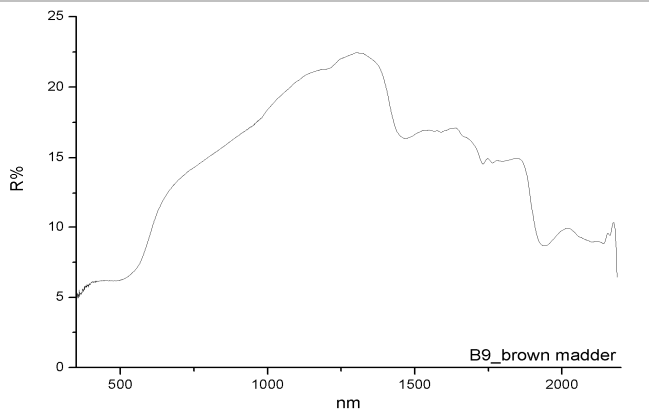
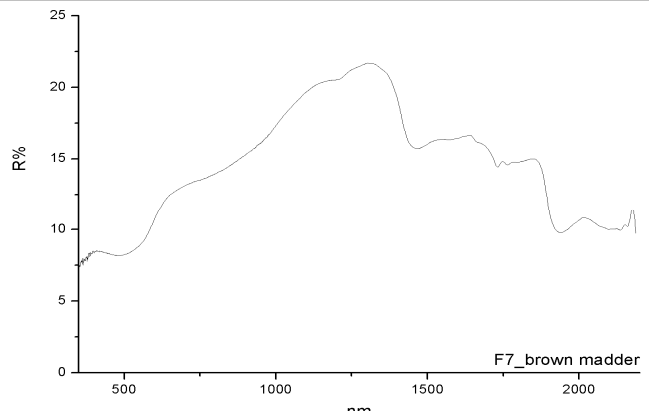
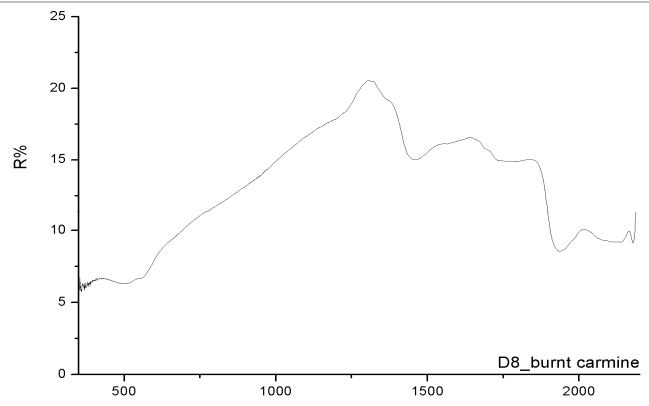
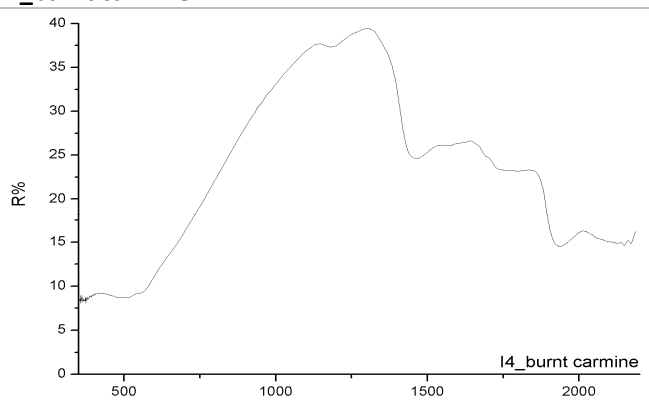
Figure 9: Reflectance spectra of watercolours presenting an absorption band at around 1380 nm.

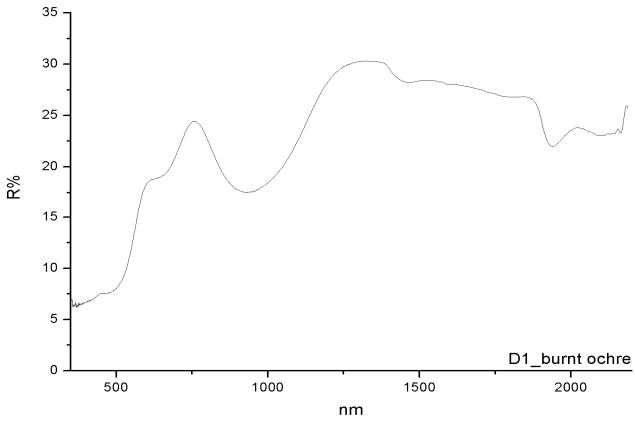
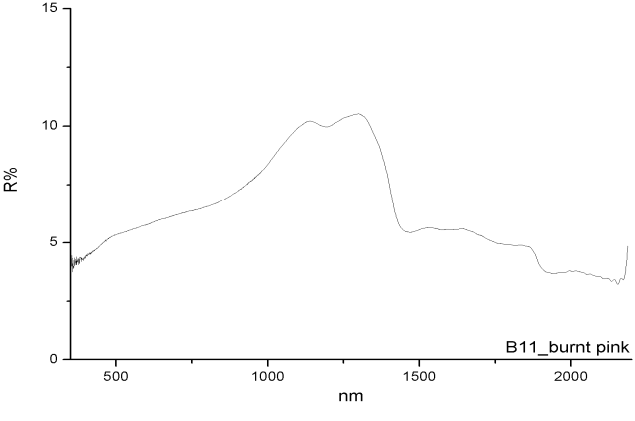
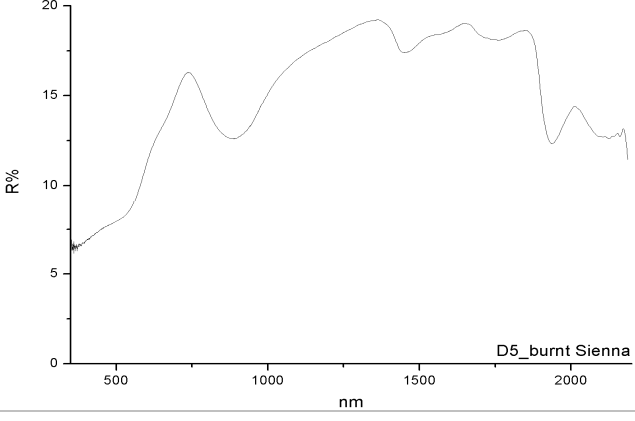
Reflectance spectrum	Hypothesis of identification
<p data-bbox="113 295 308 322"><b>B7_antwerp blue</b></p>  <p data-bbox="608 696 758 723">B7_antwerp blue</p>	<p data-bbox="799 324 1369 488">Antwerp blue is a bright Prussian Blue or 'ferro-prussiate of allumina', with 'terrene basis' [6]. This last term refers to the presence of clay materials, even if carbonates were also added [13].</p> <p data-bbox="799 501 1369 750">In the B7 spectrum the absorption band at 770 nm can be due to a metal-metal CT transition typical of Prussian blue. However, this spectrum is not totally comparable with Prussian blue's reference [14], because of the reflectance maximum at around 850 nm, which could be attributed to a second pigment.</p>
<p data-bbox="113 772 252 799"><b>H8_aureolin</b></p>  <p data-bbox="651 1171 758 1198">H8_aureolin</p>	<p data-bbox="799 801 1369 1232">Aureolin was first made in the mid-19<sup>th</sup> century; it was used in oil but much more as a watercolour. It is a potassium cobaltinitrite, a synthetic inorganic yellow [15]. Between 0 and 4 molecules of water are present in the structure of the pigment, depending on the concentration of the solution used for its precipitation [16]. The formula of the compound is therefore <math>K_3[Co(NO_2)_6] \cdot nH_2O</math> [15]. Regular octahedral coordination of Co (III) by six <math>NO_2</math> groups in the complex anion of cobalt yellow <math>[Co(NO_2)_6]^{-3}</math>.</p>
<p data-bbox="113 1249 225 1276"><b>A7_bistre</b></p>  <p data-bbox="671 1648 758 1675">A7_bistre</p>	<p data-bbox="799 1279 1369 1574">This brown pigment was mainly used as a watercolour in order to tint drawings [6] and on manuscripts in the 14<sup>th</sup> century. It was used until the end of the 19<sup>th</sup> century. Bistre is an artificial pigment obtained from the soot of burnt wood. The absence of specific absorptions typical of black materials prevents the pigment from being identified [17].</p>

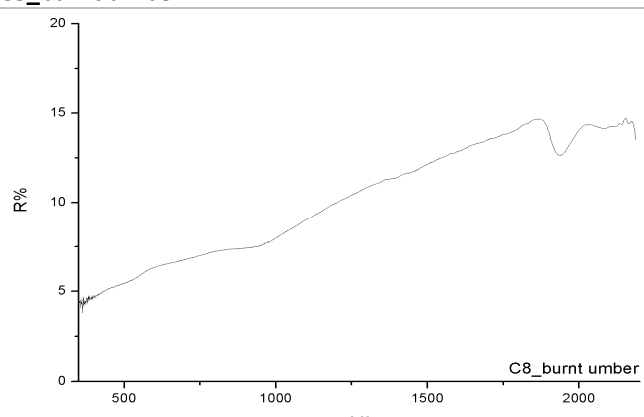
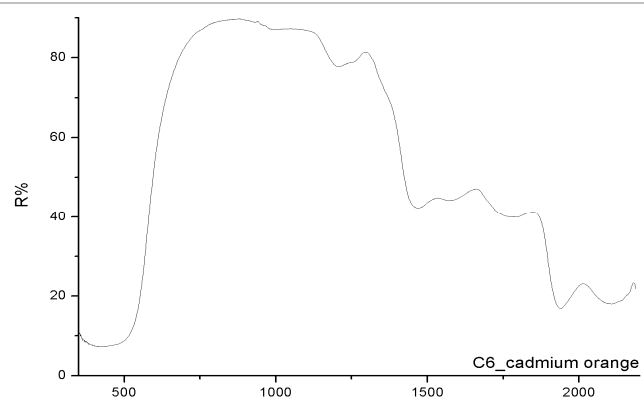
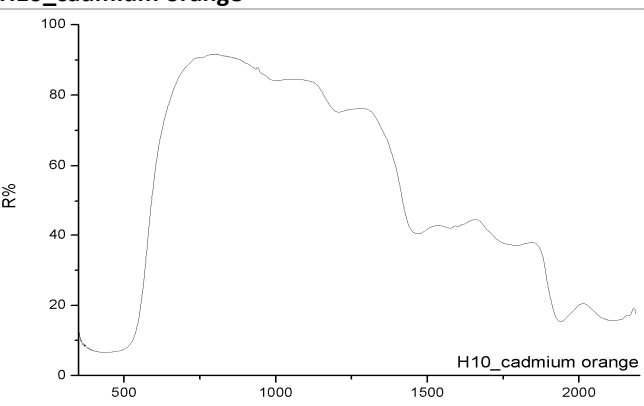



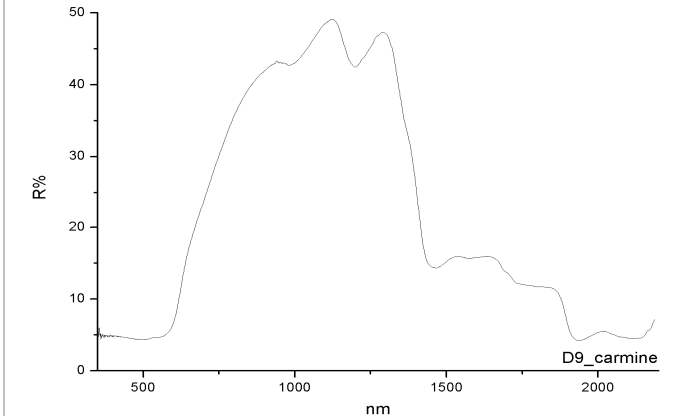
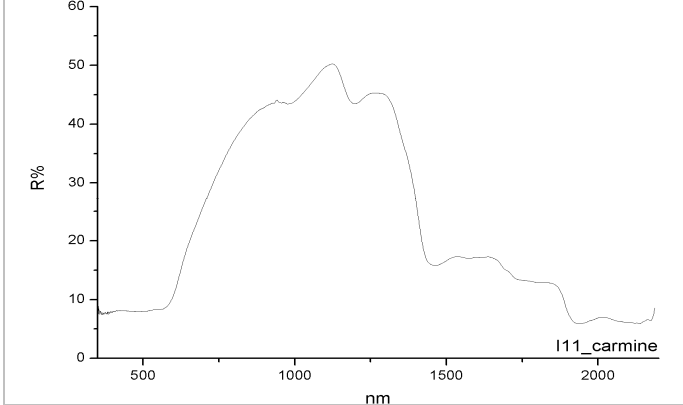
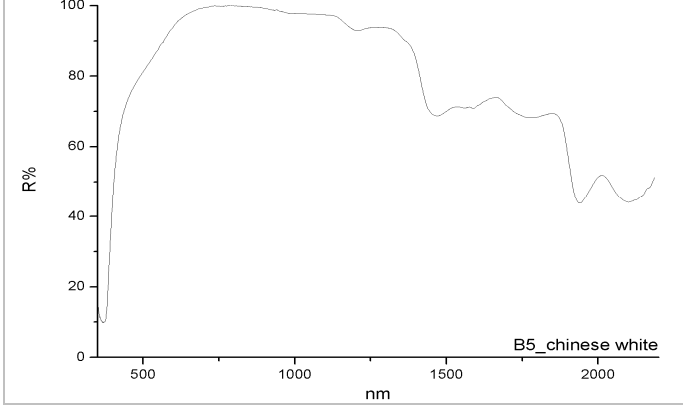
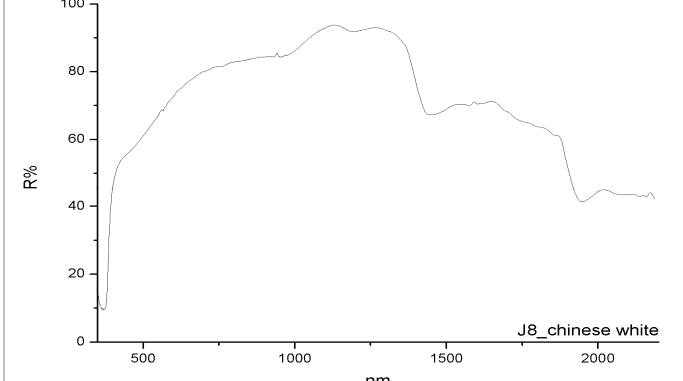
<p><b>C12_black lead</b></p>  <p style="text-align: right;">C12_black lead</p>	<p>Black lead is another name for graphite. The best graphite is obtained from mines in Borrodale, Cumberland (UK). It can be used as a watercolour, but could be useful also in oil [6].</p> <p>Because of the absence of specific spectral features in the UV-vis and in the NIR range as well, the C12 and G10 spectra suggest the presence of a black pigment.</p>
<p><b>G10_black lead</b></p>  <p style="text-align: right;">G10_black lead</p>	
<p><b>D6_blue black</b></p>  <p style="text-align: right;">D6_blue black</p>	<p>Some authors reported that this pigment could be a mixture of a black pigment (like ivory black) with a small amount of blue. Other recipes indicate that it was obtained from vine twigs or cocoa shells. In the first half of the 20<sup>th</sup> century it was listed as a carbon black [13].</p> <p>Low reflectance values suggest the presence of a non-identifiable black pigment. Differently from black lead, in the UV-Vis range a concavity in the spectrum was detected that could be due to the presence of a second pigment.</p>

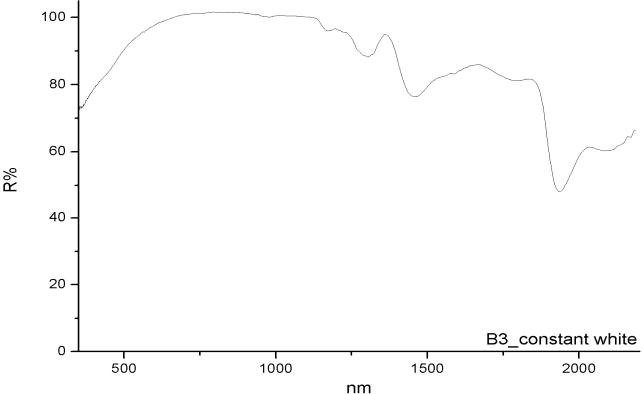
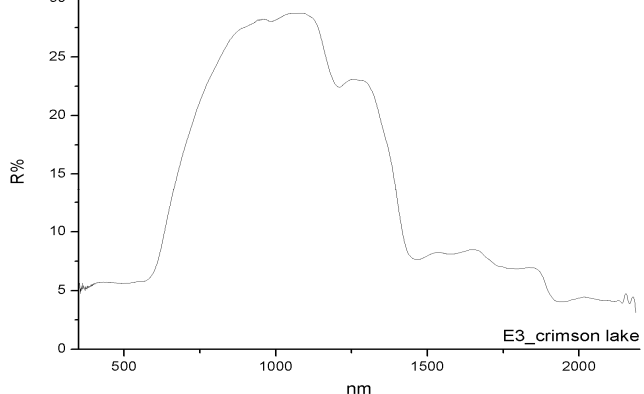
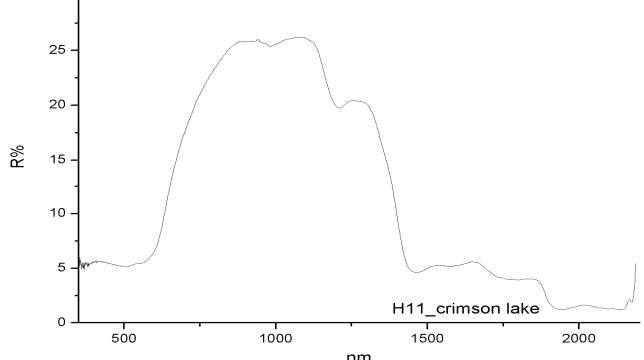

<p><b>E9_british ink</b></p> 	<p>Field reported about different kinds of ink: brown ink, china ink, Indian ink and red ink. No information was given about this pigment that was only listed in Winsor &amp; Newton catalogues. The low reflectance values are typical of a black pigment and the spectra E9 and H12 are very similar to D6's spectrum (blue black). An absorption band at 1387 nm is due to an extender, as previously stated, but the absence of other absorption is typical of a black pigment.</p> <p>In the H12 spectrum a little absorption at 670 nm was also detected.</p>
<p><b>H12_british ink</b></p> 	
<p><b>B8_bronze</b></p> 	<p>The name bronze is probably referred to a pigment also known as bronze green obtained by mixing Prussian blue with chrome yellow and zinc white. The literature reports that a pigment called Bronze green was included in W&amp;N catalogue in 1938, where it was apparently a 'mixed chrome green' [13].</p> <p>The absorption band at 370 nm is due to a band-to-band transition of the zinc white, while the absorption in the red region is probably due to a Prussian Blue. The reflectance maxima shifted towards the green region suggest the presence of a yellow pigment, probably a chrome yellow, confirming what reported above.</p>
<p><b>I3_bronze</b></p> 	


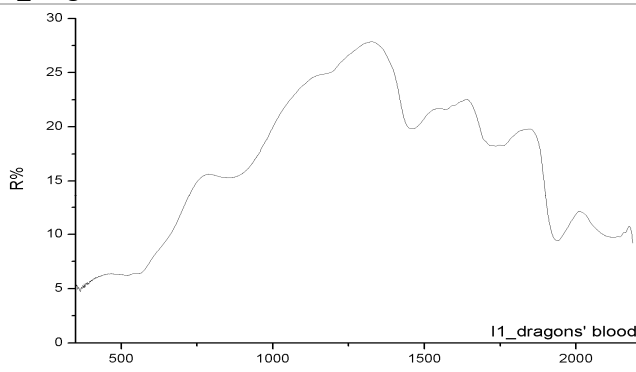
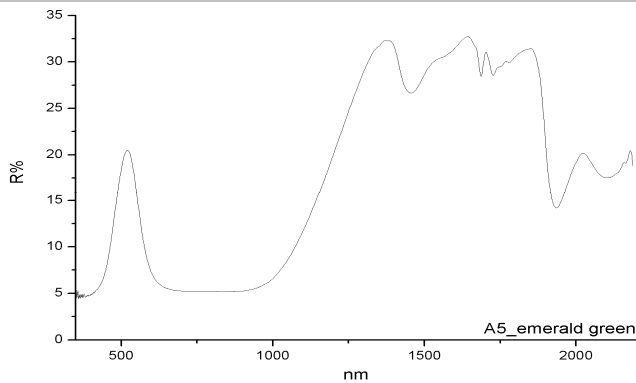
<p><b>B9_brown madder</b></p> 	<p>Madder is a lake pigment, a plant dye which has been fixed onto an inert substrate [7]. Madder brown (or Russet rubiate or Field's Russet) is prepared from the <i>rubia tinctoria</i> or madder root. This lake is reported to be a rich, transparent, deep colour very good for glazing [6]. The colour of madder pigments can vary from pink to brown depending on the concentration of the chromophores, in this case anthraquinone substances such as alizarin and purpurin. [17].</p> <p>The B9 and F7 spectra are characterised by an absorption band around 550 nm due to a <math>n \rightarrow \pi^*</math> transition, typical of the carbonyl group of the anthraquinones [18].</p>
<p><b>F7_brown madder</b></p> 	
<p><b>D8_burnt carmine</b></p> 	<p>From what Field reports it is unclear if the term carmine refers to tincture of kermes or of cochineal [6]. At the moment, carmine seems to better indicate a kermes-derived crimson lake [19]. However, both these dyes owe their colour to anthraquinone colorants such as carminic acid in cochineal and kermesic acid in kermes [17]. Since the chemical structure of these anthraquinones is similar, it is not possible to distinguish them with FORS technique [18].</p> <p>The burnt carmine was obtained by burning carmine in a cup over a spirit lamp in order to obtain a more lightfast compound [6].</p> <p>In the spectra D8 and I4 the presence of two absorption bands at 520 nm and 560 nm refer to a <math>n \rightarrow \pi^*</math> transition typical of the anthraquinones.</p>
<p><b>I4_burnt carmine</b></p> 	

<p><b>D1_burnt ochre</b></p>  <p>D1_burnt ochre</p>	<p>Ochre-based pigments contain clay and silica and owe their colour to the presence of iron oxide (hematite) and hydroxide (goethite). Usually, burnt ochres are produced by heating yellow ochres at temperatures below 800°C. In these conditions, any hydrated iron oxides become red, changing the colour of the pigment.</p> <p>Spectrum D1 is characterised by two absorptions due to Fe (III) – Fe (III) pair excitations and <i>d-d</i> Fe (III) transition typical of iron oxides and hydroxides at 500nm, 660 nm and 930 nm. A weak reflectance peak is also present at 450 nm [20, 21].</p>
<p><b>B11_burnt pink</b></p>  <p>B11_burnt pink</p>	<p>Field speaks about a brown pink which could be the burnt pink reported here. Brown pink is a vegetable lake precipitated from the decoction of French berries and dyeing woods, and is sometimes the residue of the dyer's vat. It is a transparent colour with an orange-green tonality [6]. Burnt pink can be the <i>Spinus Cervinus</i>, a flavonoid colour characterised by ramnetina, quercitina, and canferol which are the active principles of this yellow-green dye [19].</p> <p>In B11 spectrum no relevant absorptions can be detected referable to specific compounds.</p>
<p><b>D5_burnt sienna</b></p>  <p>D5_burnt Sienna</p>	<p>Sienna is a mixture of iron oxides, silica, clays and impurities. This pigment can be described as an ochre mixed with manganese dioxide.</p> <p>The spectrum presents the same absorptions already seen in D1_burnt ochre shifted by a few nanometres. Small variations in the shape and in the positions of the absorptions are always recorded and are due to the presence of impurities [20, 21].</p>

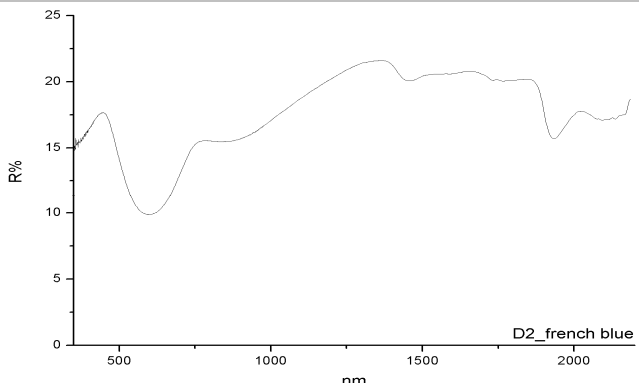
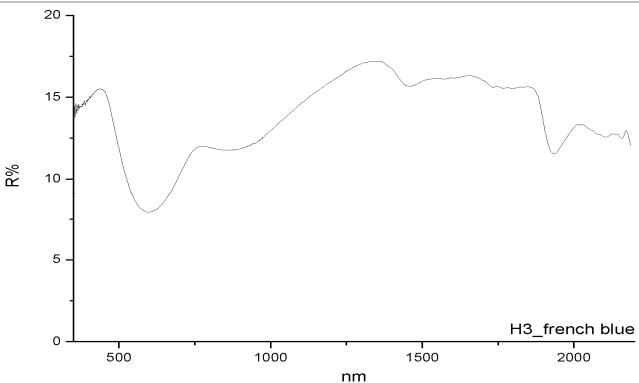
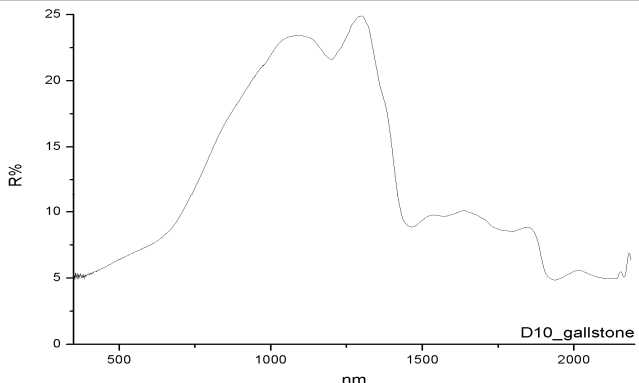
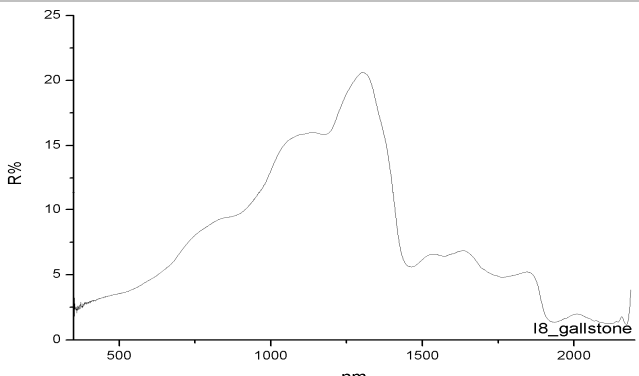
<p><b>C8_burnt umber</b></p> 	<p>Umber is a mixture of iron and manganese oxides and hydroxides. The presence of manganese dioxides makes this pigment darker than yellow/Sienna earths. When raw umber is calcined it becomes burnt umber, a darker pigment.</p> <p>The absorptions due to the iron oxides and hydroxides were detected in spectrum C8 and the low reflectance is a consequence of the dark colour of the pigment. These observations support the presence of a burnt umber.</p>
<p><b>C6_cadmium orange</b></p> 	<p>Cadmium-based pigments were discovered in 1817 but were not traded before 1820. Cadmium pigments exist in different colours from yellow to red [22, 23]. Cadmium yellow is a cadmium sulphide with some selenium added as a substitute for sulphur. The selenium:sulphur ratio and the preparation method determine the specific colour of the pigment [24].</p> <p>The C6 and H10 spectra present a strong absorption in the UV-Vis region centred at 440 nm due to a band-band transition in cadmium [25].</p>
<p><b>H10_cadmium orange</b></p> 	<p>In I9 the presence of CdS was confirmed because of the absorption at 440 nm. A small variation from the previous spectra was detected in the spectrum's shape between 550 nm and 950 nm. This behaviour could be due to a lower selenium:sulfur ratio.</p> <p>However, by studying these FORS spectra the presence of a vermilion red (HgS) cannot be excluded a priori because of the similarity between vermilion and cadmium red curves.</p>
<p><b>I9_cadmium yellow</b></p> 	

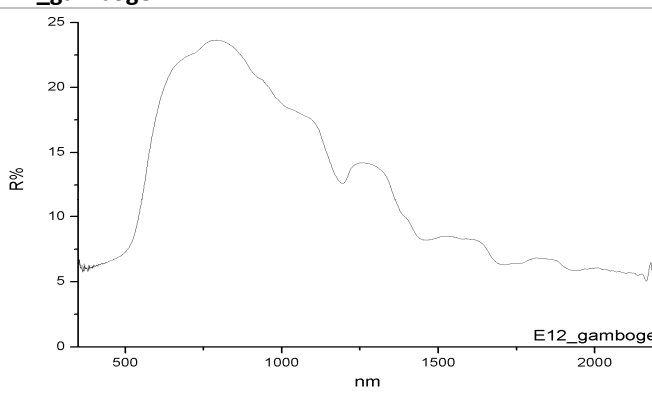
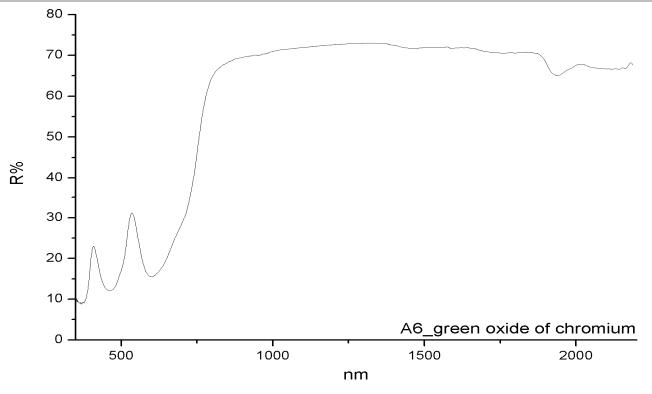
<p><b>D9_carmine</b></p> 	<p>In the first edition of his book, Field reported that the name carmine was originally given to kermes or cochineal tinctures, but subsequently it denoted any pigment characterised by a red-purple hue, similar to real carmine in beauty and texture [13]. Sometimes, vermilion could be added to the pigment.</p> <p>Contrary to burnt carmine (D8 and I4), D9 and I11 spectra present higher reflectance values. The absorptions due to the anthraquinone are always evident and allow the presence of an organic red/purple compound to be detected [18].</p>
<p><b>I11_carmine</b></p> 	
<p><b>B5_chinese white</b></p> 	<p>W&amp;N gave this name to a particularly dense form of zinc oxide (ZnO) introduced in 1834. It is different from previous zinc whites as the zinc was heated at much higher temperatures than the late eighteenth century variety. The name 'Chinese white' is said to have come from the oriental porcelain very popular in Europe in the 18<sup>th</sup> and 19<sup>th</sup> centuries [22].</p> <p>The Chinese white, by combining body and permanency, is far superior to those whites known as Constant or Permanent white' [4].</p> <p>The B5 and J8 spectra are characterised by an absorption at 370 nm due to a band-band transition of the zinc oxide [25].</p>
<p><b>J8_chinese white</b></p> 	

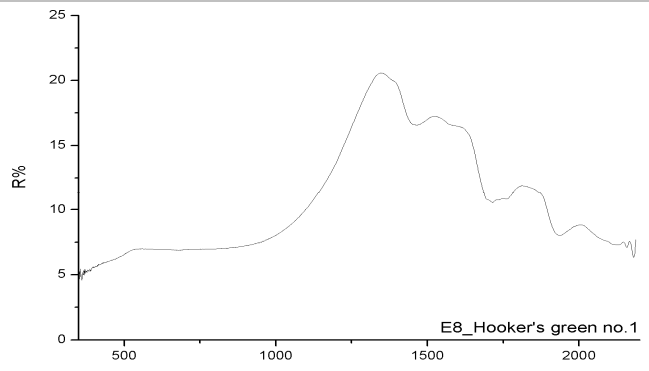

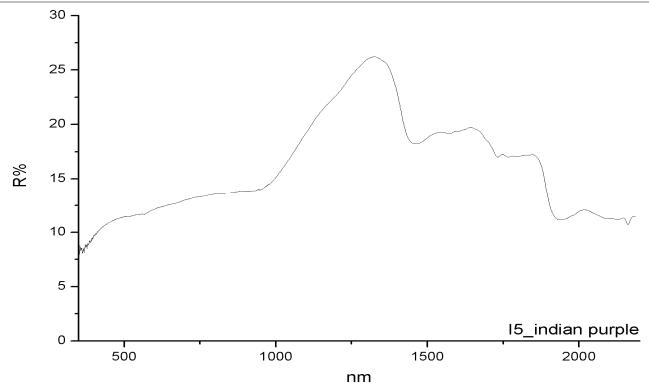
<p><b>B3_const. White</b></p>  <p>B3_constant white</p>	<p>Constant White or permanent white is a barium sulphate and when well prepared and free of acid was one of W&amp;N best whites for watercolour painting [6].</p> <p>The B3 spectrum does not show absorption bands due to the presence of specific white pigments. This behaviour suggests the presence of barite (barium sulphate) because this mineral by itself is spectrally featureless and has a high reflectivity in the working spectral range [26].</p> <p>The absorption band at 1170 nm remains unsolved.</p>
<p><b>E3_crimson lake</b></p>  <p>E3_crimson lake</p>	<p>Crimson lake or carmine (see burnt carmine D8 and D9) [6]. In the literature crimson lake is also reported as a synonym of kermes [19].</p> <p>Differently from carmine and burnt carmine, the reflectance values in the 350–1400 nm spectral range are relatively low, due to the fact that the colour of the pigment is darker than that of carmine and burnt carmine.</p> <p>The absorptions due to the anthraquinone are always clear and allow us to identify the presence of an organic red material.</p>
<p><b>H11_crimson lake</b></p>  <p>H11_crimson lake</p>	
<p><b>D7_deep chrome</b></p>  <p>D7_deep chrome</p>	<p>No information about this pigment was found.</p> <p>The D7 spectrum has the typical features (an absorption in the blue region) of a modern yellow pigment such as chrome yellow. Moreover, some features between 500 nm and 950 nm could be due to the presence of iron oxides and hydroxides.</p>

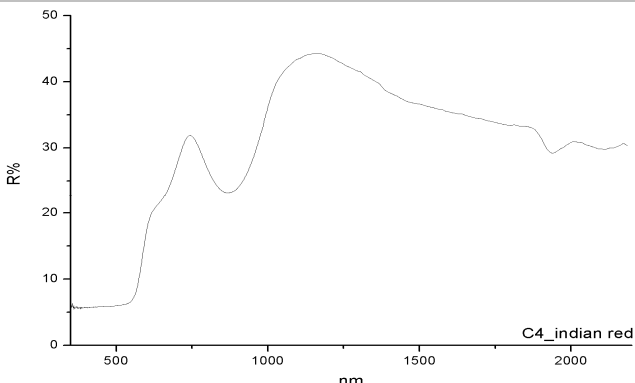
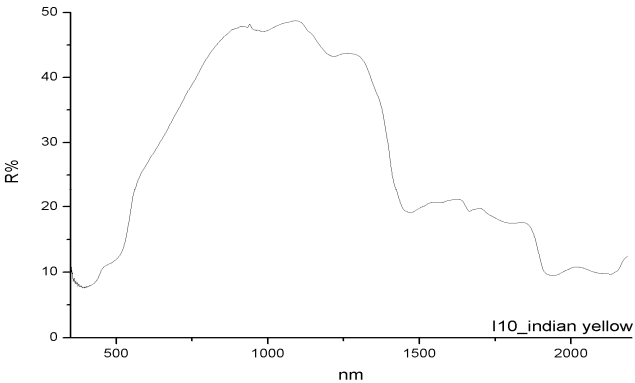
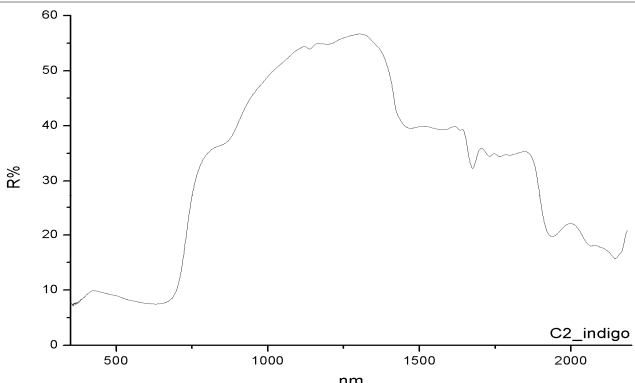
<p><b>F2_dragon's blood</b></p> 	<p>Dragon's blood was thought in ancient times in Europe to be the congealed blood of Dragons and Elephants mixed together as they fought to the death [6]. In reality it is a resinous substance from an Indian plant called <i>Calamus draco</i> [19] and in Europe a similar material was obtained from <i>Dracaena draco</i>, a plant from the Canary islands. The F2 and I1 spectra show the typical absorption in the blue-green region due to an organic red substance, but the presence of absorptions at 650 nm and 850 nm due to <i>d-d</i> transition in the iron ion of haematite was also detected.</p>
<p><b>I1_dragon's blood</b></p> 	
<p><b>A5_emerald green</b></p> 	<p>Differently from France, in the United kingdom the term emerald green refers to a copper-acetoarsenate known also as Schweinfurt green and available from 1814. The A5 spectrum is characterised by a broad absorption from 550 to 1000 nm due to a <i>d-d</i> transition in the copper ion [27]. Moreover, the absorption at 1685 nm can be linked to the first C-H overtones of the methyl group [28]. These features confirm that emerald green watercolour is a copper-acetoarsenate.</p>

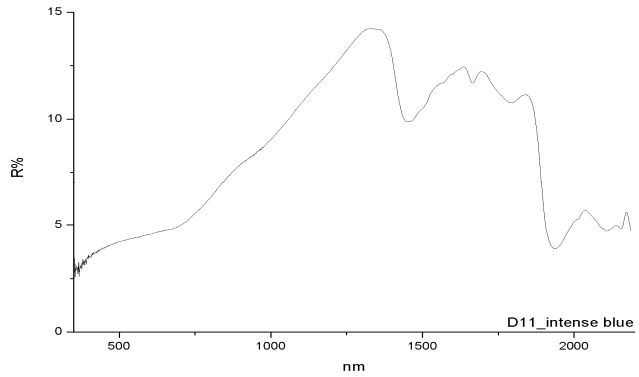
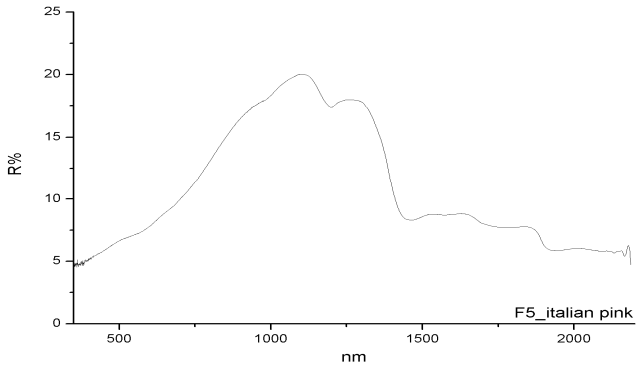
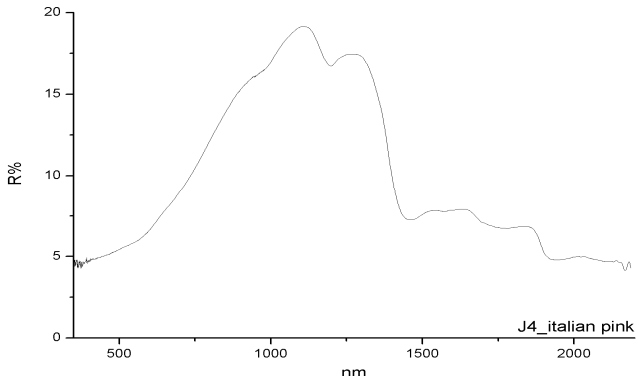


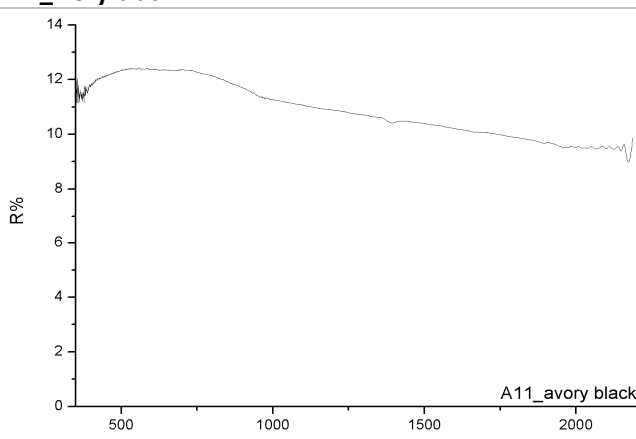
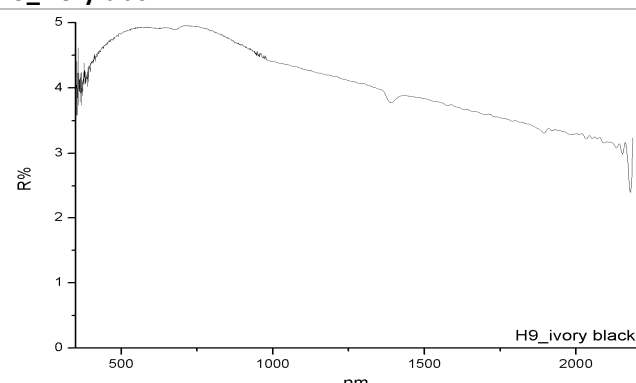
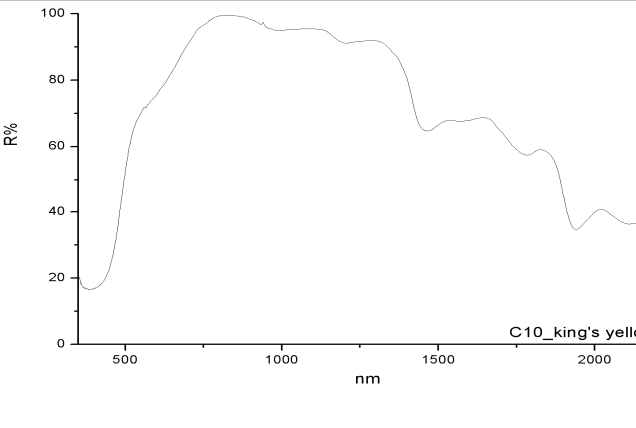
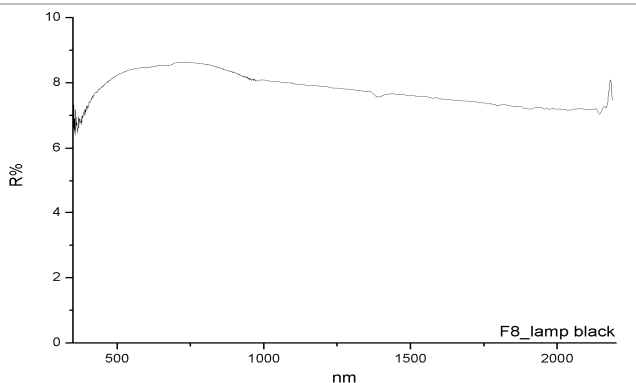
<p><b>D2_french blue</b></p> 	<p>The name French blue refers to ultramarine blue, a synthetic form of lapis lazuli, a complex sulfur-containing sodium aluminosilicate. It was manufactured from 1828 [24].</p> <p>Ultramarine blue is detected by the presence of a broad absorption band in the red region, centred at 600 nm due to a metal-ligand CT transition involving the ion <math>S^{3-}</math> [20].</p>
<p><b>H3_french blue</b></p> 	
<p><b>D10_gallstone</b></p> 	<p>Gallstone is an organic animal yellow-brown dye. The compound is obtained from animal calculus formed in gall-bladder, mainly of oxen. Literature indicated also the use of fish-bile or gall in order to produce bile yellow. Calcium bilirubinate complex is the major ingredient of so called brown-yellow pigments [13].</p> <p>In the I8 spectrum the absorption at around 950 nm suggests the presence of other materials, perhaps a earth-based pigment, that lower the reflectance in the UV-Vis range. Sometimes gallstone is confused with yellow quercitron lakes. In this specific case, the differences between gallstone's spectra with Italian pink (F5 and J4) and yellow lake's spectra (B6 and J5) seem to suggest a different source for these pigments.</p>
<p><b>I8_gallstone</b></p> 	

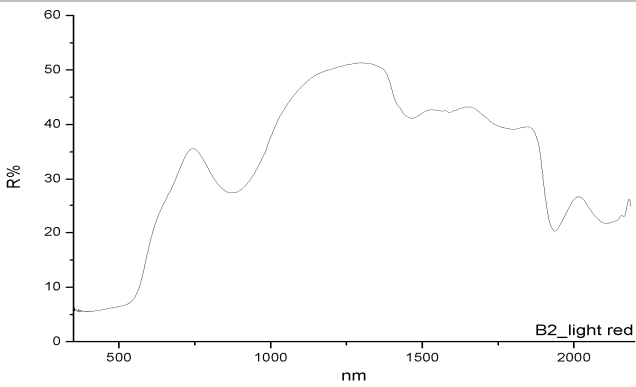
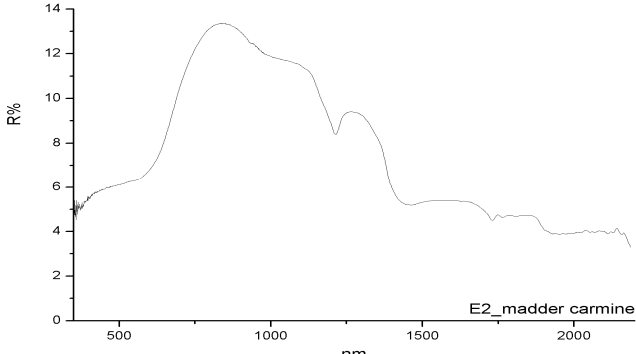
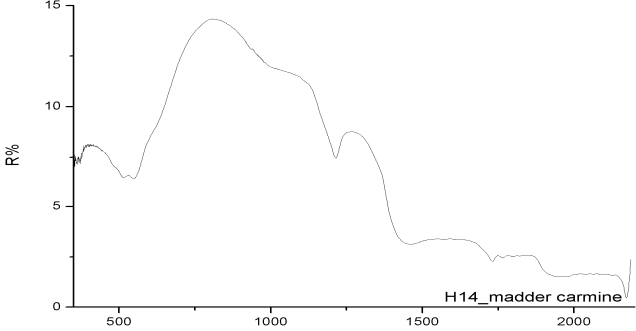
<p><b>E12_gamboge</b></p> 	<p>Gamboge is a resin-gum, an exudate obtained from some Asiatic plants belonging to the <i>Garcinia</i> species (<i>Clusiaceae</i> family). The principal chromophore of gamboge is gambogic acid which the substance gives an amber yellow colour. Well known in Asia, in Europe it was first used by the Flemish [19]. It was indicated as a good colour for drapery and backgrounds in portrait paintings thanks to the resinous materials it contained that produce a sort of natural varnish [5]. Spectrum E12 can be attributed to an organic yellow [29].</p>
<p><b>A6_green oxide of chromium</b></p> 	<p>Many of the pigments called as such were made up of a mixture of chrome yellow with Prussian and other blue colours (like Brunswick green). However, Field also wrote about a true chrome green (Native green) the colouring matter of which is the pure oxide of chrome [6]. The A6 spectrum is due to a chromium oxide, with a strong absorption in the UV due to a metal-ligand <i>C-T</i> transition between the chromium and the oxygen anion and by a double absorption with two absorption maxima at 460 nm and 600 nm due to <i>d-d</i> electronic transition typical of chromium (III) in an octahedral coordination.</p>

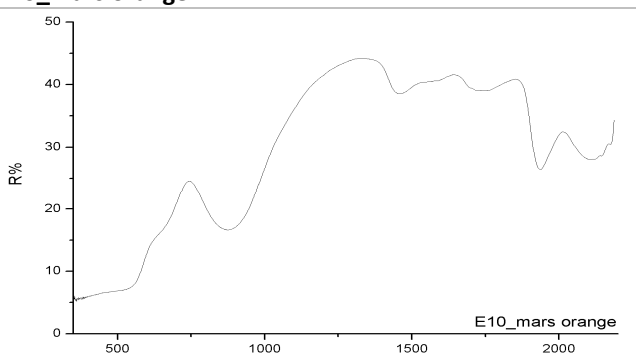
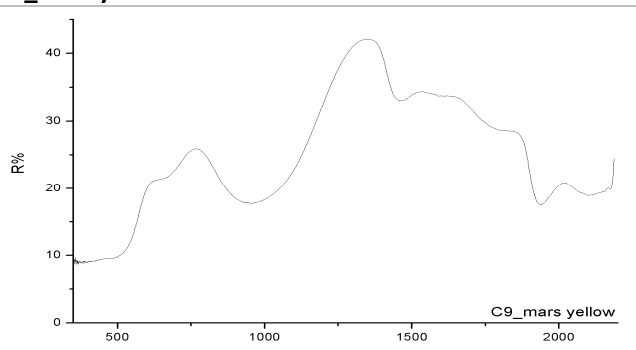
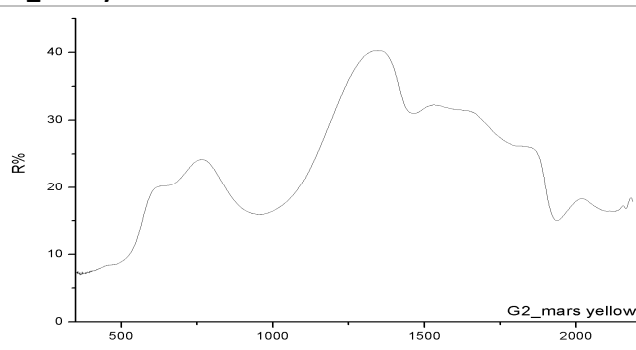
<p><b>E8_Hooker's green no. 1</b></p>  <p>E8_Hooker's green no.1</p>	<p>It is assumed to be a mixture of Prussian Blue and gamboge yellow [24]. Field reported that green obtained by mixtures of blue and yellow were often used in spite of green pigments. Obviously, it was necessary to use materials with similar features, such as chemical compatibility and the same degree of durability; and Prussian or Antwerp blue and gamboge seemed to satisfy these requirements [6].</p> <p>The FORS spectrum does not give information about the chemical composition of E8 and E1's samples. Because of the strong absorption in the 550-1000 nm range, the presence of a Prussian blue can be hypothesised, however it is not possible to confirm its mixture with a yellow pigment.</p>
<p><b>E1_Hooker's green no. 2</b></p>  <p>E1_Hooker's green no.2</p>	
<p><b>I5_indian purple</b></p>  <p>I5_indian purple</p>	<p>Obtained from an insect, Indian purple has a colour very similar to cochineal [6], and Salter described it as a precipitate of an extract of cochineal with a copper sulphate [13]. Another source reported the existence of an Indian lake, also called lac dye: an organic animal colorant from gumlac [24]. The main colorant principles are laccaic A and laccaic B acid that produce a deep red to brown colour depending on the mordant used [19].</p> <p>In the I5 spectra it is possible to recognise a small absorption 560 nm, referring to a <math>n \rightarrow \pi^*</math> transition on the anthraquinone.</p>

<p><b>C4_indian red</b></p> 	<p>Field reported that Indian red is an iron ochre from Bengal [6]. It seems to be a red of a purple hue with a good body.</p> <p>The C4's spectrum exhibits the typical behaviour of hematite.</p>
<p><b>I10_indian yellow</b></p> 	<p>It is a mixture of the calcium and magnesium salts of euxhantic acid. The euxanthone moiety is the active principle of mango leaves, and in the metabolic bovine process it is transformed into soluble salts attached to the oxidised carbohydrate moiety [30]. Field spoke about its beautiful, pure yellow colour, and light powdery texture [6].</p> <p>I10's spectrum suggests that iron oxides/hydroxides were used together perhaps with an organic (yellow) colour in order to obtain Indian yellow.</p>
<p><b>C2_indigo</b></p> 	<p>Indigo is the most commonly used organic blue pigment from antiquity. It is a vegetal organic pigment mainly extracted from <i>Indigofera Tinctoria</i>, a plant belonging to <i>Fabaceae</i> family. In order to obtain pure indigo, the powder extracted could be treated with sulphuric acid, potash (<math>KCO_3</math>) and alcohol [19]. Indigo was synthesised for the first time in 1880 by Adolf von Bayer, but Heumann made the first industrial synthesis in 1890.</p> <p>The C2 spectrum can be attributed to indigo thanks to its maximum in the blue region (425 nm) and the increase of reflectance in the NIR at 680 nm. However, it is necessary to stress that in the visible range the behaviour of indigo is not well discernible from that of ultramarine blue.</p>

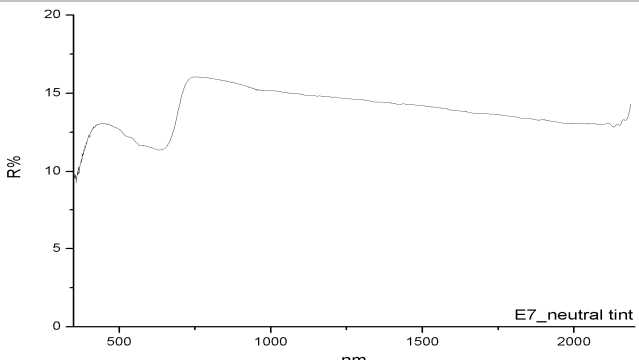
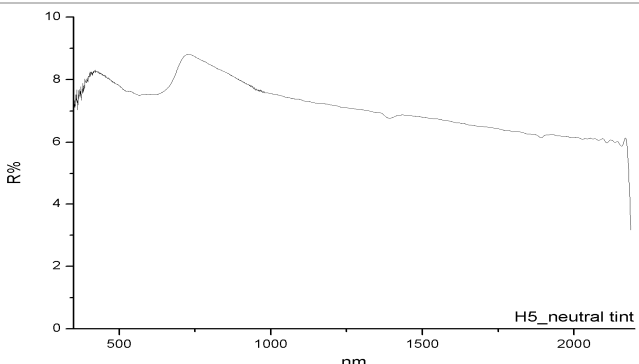
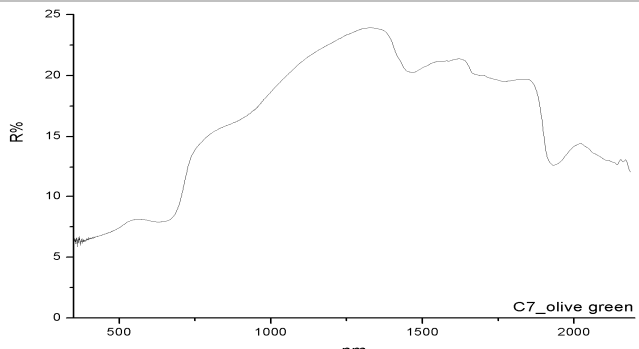
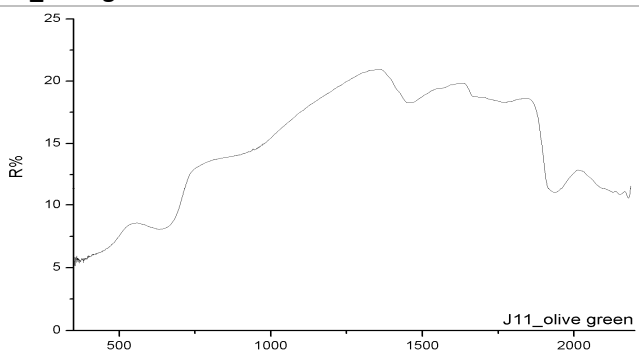
<p><b>D11_intense blue</b></p>  <p>D11_intense blue</p>	<p>Field reported that Intense blue is an indigo ‘refined by solution and precipitation’ [6] in order to obtain a more durable and resistant compound.</p> <p>The D11 spectrum exhibits some differences with respect to C2, mainly in the UV-VIS range. In detail, the reflectance maximum at 425 and the absorption at 640 nm are not so evident as in C2, probably because of the dark hue due to the purity of the material. Moreover, the reflectance values are lower in D11 than in C2, mainly in the NIR region.</p>
<p><b>F5_italian pink</b></p>  <p>F5_italian pink</p>	<p>Italian pink is an ‘absurd name’ [6] of an organic yellow lake made from berries, called <i>Stil de grain</i>. The latter is another name of the already discussed <i>Spinus Cervinus</i>. The source to make this pigment can also be dyer’s broom or weld [13]. If the attribution of burnt pink is correct, then Italian pink and burnt pink should be from the same organic source. In fact as reported by Field, brown pink is the darker version of Italian pink.</p>
<p><b>J4_italian pink</b></p>  <p>J4_italian pink</p>	<p>By comparing F5, J4 and B11 spectra it is possible to see that the reflectance values of burnt pink are lower than those visible in Italian pink. In particular, the former presents an absorption band centred at about 830 nm.</p>


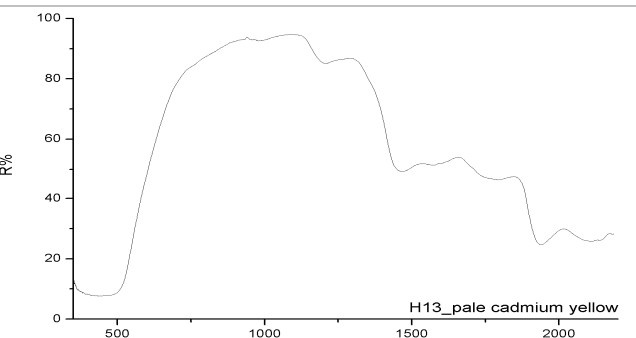
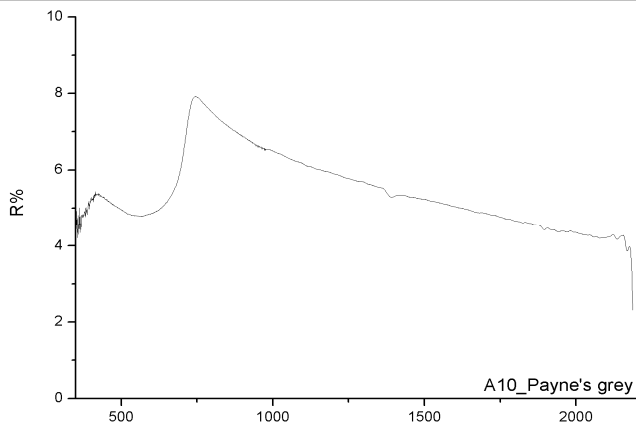
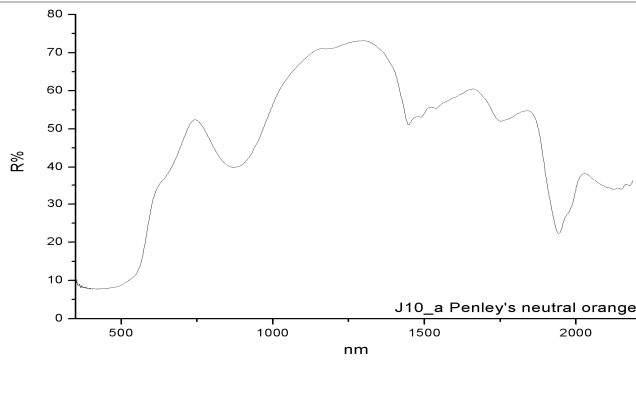
<p><b>A11_ivory black</b></p> 	<p>Ivory black is a black pigment obtained by charring bones or ivory. It has been well known and used since antiquity. Because of the data processing, the A11 spectrum shows spectral features not linked to the chemical composition of the compounds. However, black surfaces are not identified with this technique.</p> <p>Because of the low reflectance values which further decrease in the infrared the A11 and H9 spectra can be attributable to a black pigment.</p> <p>The presence of some small absorption in the 600-700 nm range can be due to small traces of cobalt-based pigment.</p>
<p><b>H9_ivory black</b></p> 	<p>King's yellow is yellow orpiment, an arsenic sulfide [6, 13]. This mineral yellow was used from Antiquity to the 20<sup>th</sup> century. Its disuse was due to the toxicity of the pigment which was then substituted by a combination of chrome yellow and zinc white [9].</p> <p>C10's spectrum shows an absorption band at 400 nm and the S-shape of yellow pigments characterised by a band-to-band transition, such as orpiment, Naples yellow or cadmium yellow. The absorption band at 370 nm due to zinc white was not detected.</p>
<p><b>C10_king's yellow</b></p> 	<p>Carbon black has been used as a pigment since the earliest of times. It was made by heating wood or other plant material, with a very restricted air supply.</p> <p>As it is possible to verify from the spectra F8, no specific absorption bands are detectable in the range analysed.</p> <p>As reported above for ivory black, the presence of low reflectance values which further decrease in the infrared suggest the presence of a black pigment.</p>
<p><b>F8_lamp black</b></p> 	

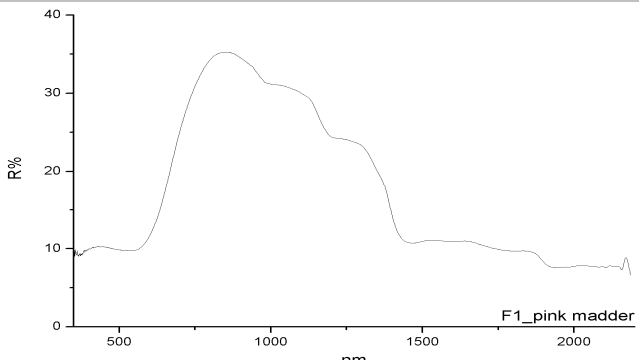
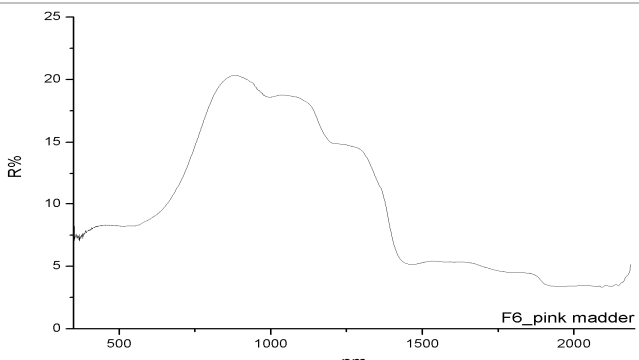
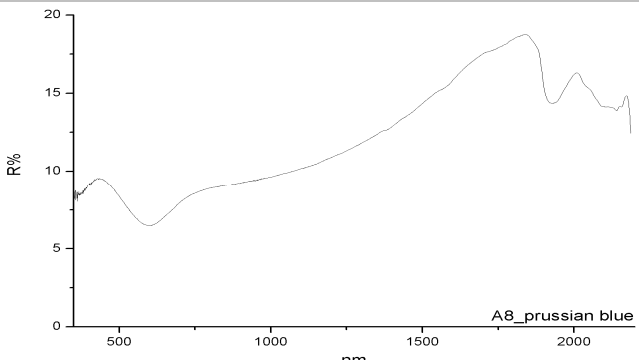
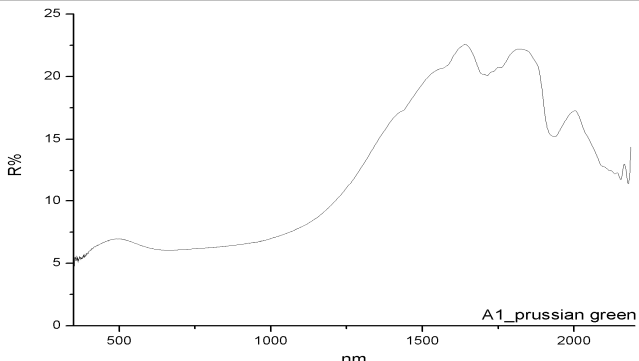
<p><b>B2_light red</b></p>  <p style="text-align: right;">B2_light red</p>	<p>Light red is an orange-brown ochre, the most common one is a brown burnt ochre, but there are also native ochres from India called with the same name [6].</p> <p>B2's spectrum shows the classical behaviour of red ochre characterised by hematite. The absorption band in the UV region is due to a metal-to-metal CT transition between iron ions, while the absorptions at 530 nm, 650 nm (weak) and 870 nm are due to <i>d-d</i> transition on the iron ion (III) in octahedral coordination with the ligands [20, 21]</p>
<p><b>E2_madder carmine</b></p>  <p style="text-align: right;">E2_madder carmine</p>	<p>Reported also as 'Field's carmine', this pigment is an organic madder red lake [6].</p> <p>In the 350-580 nm range, where anthraquinones present their absorption, a difference can be seen between E2 and H14 spectra. In fact H14's spectrum shows the typical features that allow an anthraquinone-based red lake to be recognized. In the E2 sample, the presence of a second pigment that masks the anthraquinones' absorptions can be assumed.</p>
<p><b>H14_madder carmine</b></p>  <p style="text-align: right;">H14_madder carmine</p>	<p>For wavelengths greater than 580 nm the spectra E2 and H14 show the same behaviour. In both the curves a sharp absorption at 1215 nm not previously detected can be noted.</p>

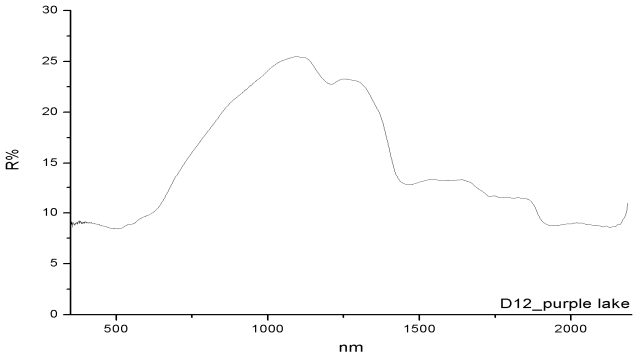
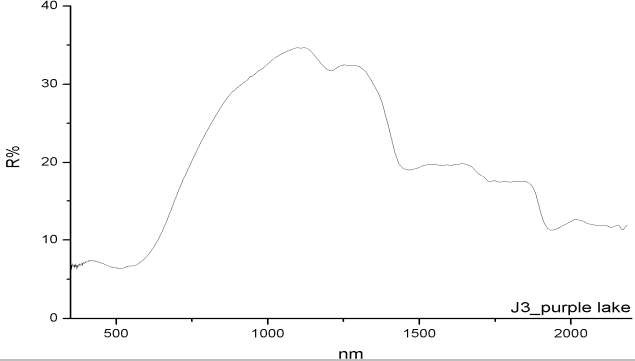
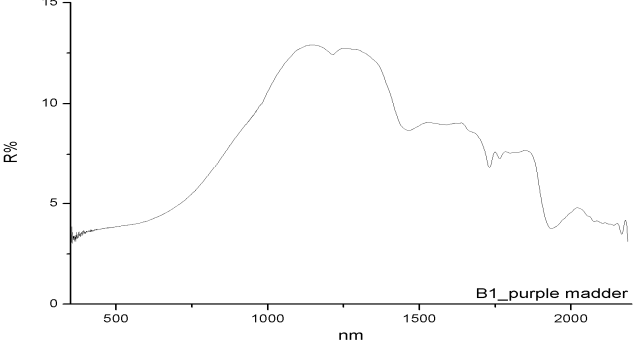
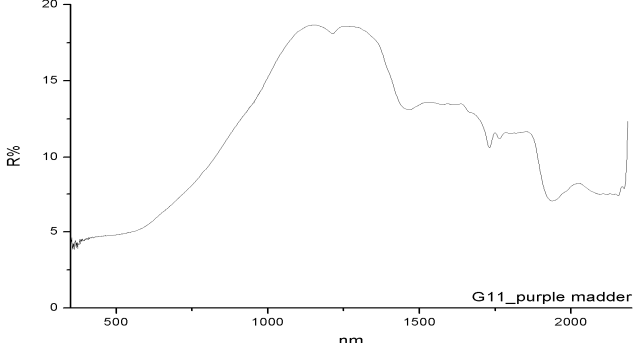
<p><b>E10_mars orange</b></p> 	<p>Mars pigments are synthetic versions of yellow and red ochres and earths, produced from the second half of the 19<sup>th</sup> century, and made of mixtures of iron oxides and hydroxides. Mars colours can show different hues, from violet to red and yellow [24]. Consequently, the reflectance curves of Mars pigments are similar to those given by ochre or earth materials.</p> <p>The E10 spectrum owes its features to a mixture of iron oxides and hydroxides, with a large concentration of hematite. As a confirmation of this interpretation, Rowbotham reported that Mars orange has a burnt Sienna character, without the tendency to brown typical of the latter [31].</p> <p>The spectra C9 and G2 can be referred to a mixture of iron oxides and hydroxides. Even if traditionally Mars yellow is defined as a brilliant yellow ochre, the spectra of these samples are more similar to a raw Sienna than a yellow ochre [14].</p>
<p><b>C9_mars yellow</b></p> 	
<p><b>G2_mars yellow</b></p> 	

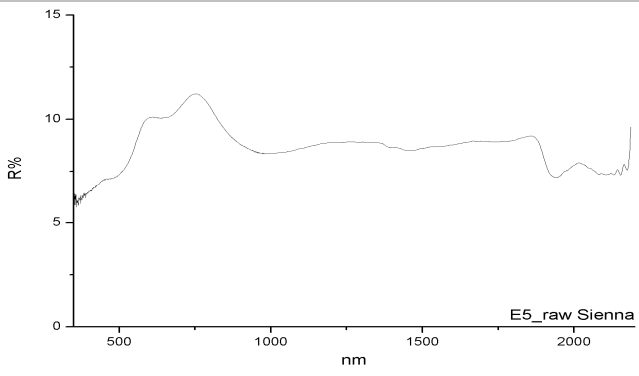
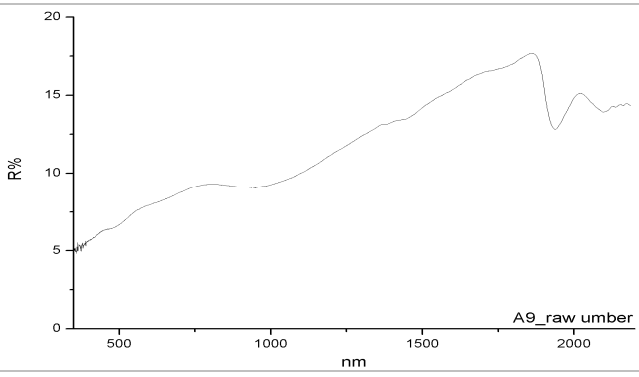
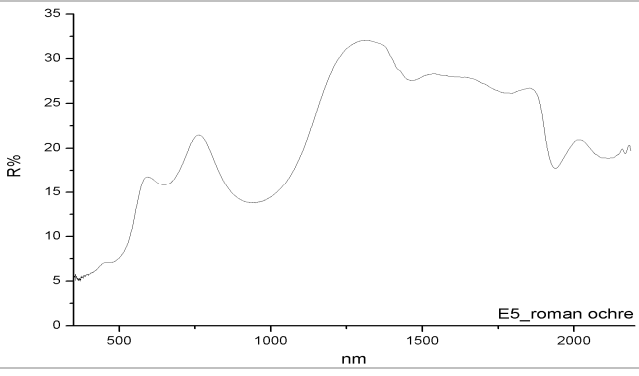
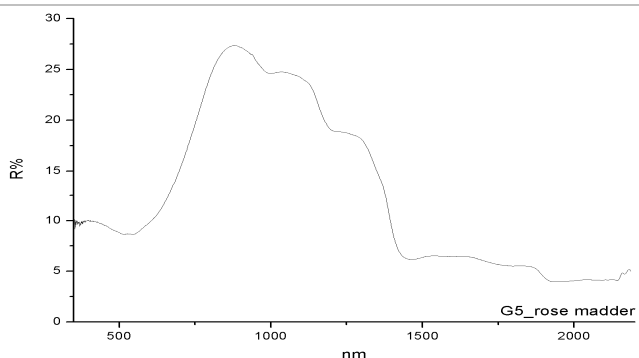


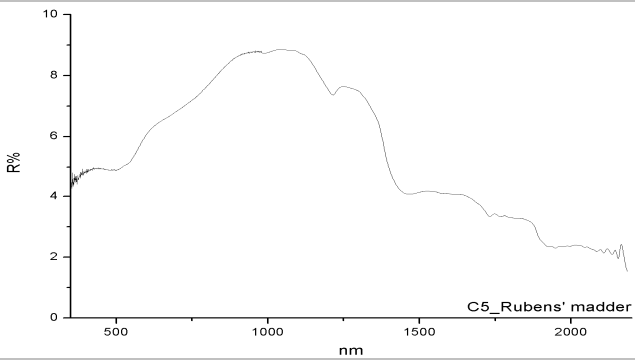
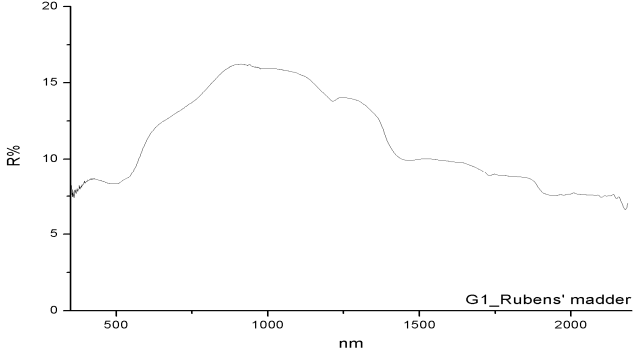
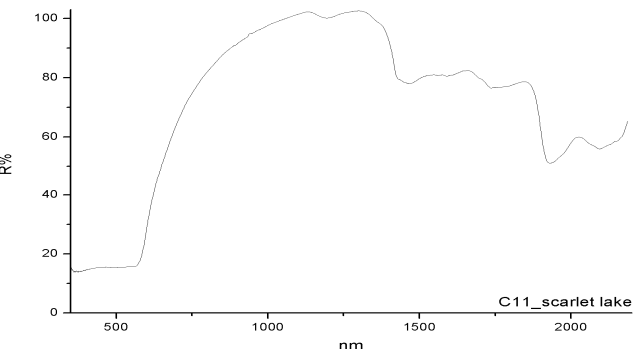
<p><b>E7_neutral tint</b></p> 	<p>Neutral tint is the name of a grey pigment made up of a mixture of sepia, indigo and other blues. It was mainly used as a watercolour [6]. In 1896, the Winsor &amp; Newton catalogue reported that neutral tint was 'an intimate combination of carbon black, ochre and French ultramarine' with indigo and red lakes [13].</p> <p>The E7 and H5 spectra are characterised by low reflectance values and no absorptions in the NIR region.</p> <p>This behaviour allows us to hypothesise the presence of a black pigment. Moreover, some interesting bands can be detected in the visible range between 500 nm and 650 nm probably linked to the presence of a cobalt (II) based pigment, such as cobalt blue [32].</p> <p>The study of these spectra does not exclude the use of other blue pigments such as ultramarine or indigo.</p>
<p><b>H5_neutral tint</b></p> 	
<p><b>C7_olive green</b></p> 	<p>Olive green is a mixed green, used in watercolours [6, 13].</p> <p>The C7 and J11 spectra have features referable to a mixture of a blue pigment, such as indigo or ultramarine blue (shoulder at 740 nm) and a yellow pigment which cannot be identified.</p>
<p><b>J11_olive green</b></p> 	

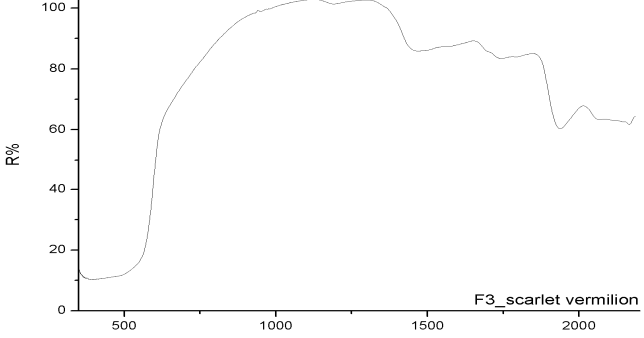
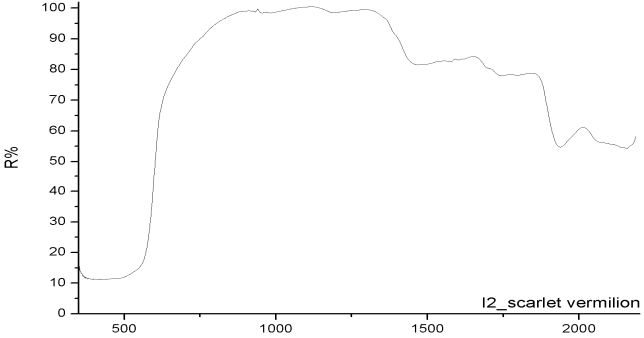
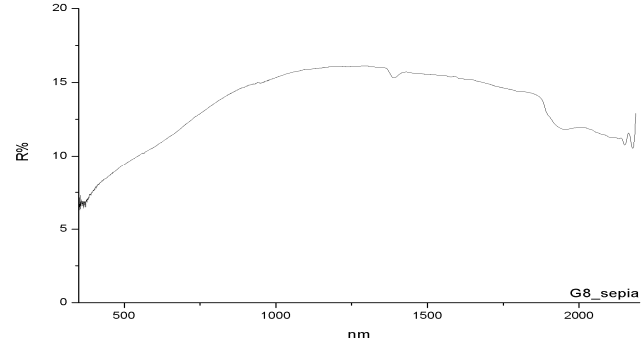
<p><b>H6_orange de Mars</b></p> 	<p>This watercolour belongs to the family of Mars pigments (E10). The H6 spectrum is similar to that given by hematite (See C2_light red).</p>
<p><b>H13_pale cadmium yellow</b></p> 	<p>The H13 spectrum is attributable to a cadmium yellow because of the absorption centred at around 450 nm (see C6_cadmium orange).</p>
<p><b>A10_Payne's grey</b></p> 	<p>Similar to neutral tint, but with different proportions of the compound pigments. It is a bluish, dark gray colour obtained by mixing a blue and a black pigment. Sometimes a touch of red was added to the mix [13]. The A10 spectrum exhibits low reflectance values in all the spectral range due to a black pigment which could not be identified. A blue pigment determines the reflectance maximum at around 420 nm. A10's spectrum is very similar to Neutral tint's spectra (E7 and H5), except for the cobalt blue which was not revealed here.</p>
<p><b>J10_a. Penley's neutral orange</b></p> 	<p>Salter reported that this pigment was done by mixing a yellow ochre with venetian red. In 1885 Taylor wrote that the yellow ochre was substituted with cadmium yellow. This latter composition was proposed also by Church [13]. The J10 spectrum exhibits the behaviour typical of a red ochre (see L2_light red). Moreover, the presence of gypsum can be seen thanks to the absorptions in the 1450-1550 nm range due to the first overtone of the OH stretching of the water molecules, plus other water combination bands [20].</p>

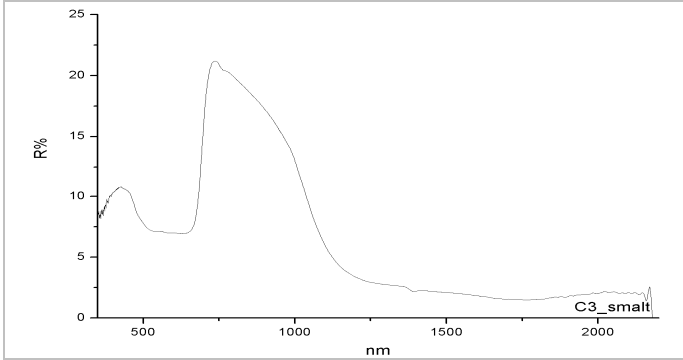
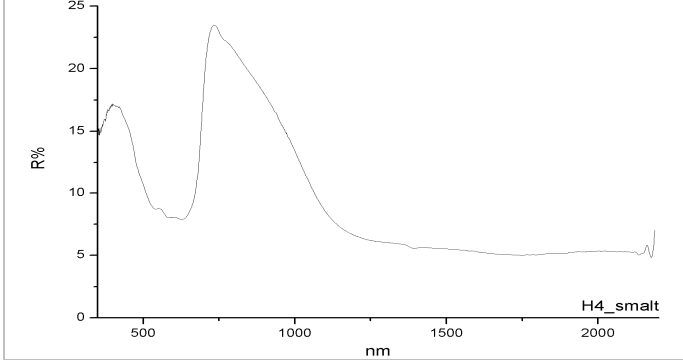
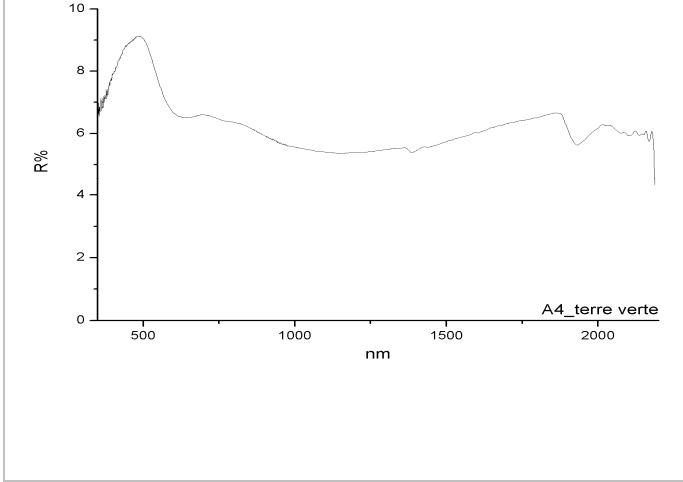
<p><b>F1_pink madder</b></p> 	<p>In spite of its name, this pigment is a yellow organic lake belonging to the flavonoid group [13]. It is not properly confirmed by Field, who reported that the pigments called pink madder were brick reds of dull ochre-like hues. Moreover, he did not distinguish this colour from the madder lake [6] characterised by anthraquinone substance. In fact madder can present also a yellow colour depending on the production of the organic colourants and the inorganic substrates [13].</p>
<p><b>F6_pink madder</b></p> 	<p>The F1 and F6 spectra are attributable to a yellow pigment since they reflect mainly in the yellow region of the visible spectrum. The absorption at around 530 nm is very similar to that already noted in several red-purple lakes due to the <math>n \rightarrow \pi^*</math> on the anthraquinone in the 450-550 nm range. This seems to confirm the second hypothesis previously introduced about the origin of the pigment.</p>
<p><b>A8_prussian blue</b></p> 	<p>Prussian blue has been one of the most used blue pigments since the second half of the 18<sup>th</sup> century. It was synthesised for the first time in 1704 by the colourmaker Diesbach in Berlin [24]. It is a ferric hexacyanoferrate and its spectrum is usually simple to identify because it is characterised by a broad absorption centred at 650-700 nm due to a charge transfer transition between <math>Fe^{2+}</math> and <math>Fe^{3+}</math> ions. The A8 spectrum presents a shoulder at around 750 nm that suggests the presence of a second pigment. In fact, it is reported that old water colour painters used to add crimson lake to Prussian blue in order to delete its green tone [31].</p>
<p><b>A1_prussian green</b></p> 	<p>Prussian green is a mixture of Prussian blue with a yellow pigment. Field reported that the latter could be a yellow ochre, as well as an organic yellow obtained from French berries. However, the best Prussian green was believed to be obtained with cobalt nitrate [6] (probably aureolin). The A1 spectrum presents the behaviour of a mixture of Prussian blue (see A8_Prussian blue) with a yellow pigment not clearly identifiable.</p>

<p><b>D12_purple lake</b></p> 	<p>Purple lake is an organic pigment, but the sources about its provenance are not very consistent [13]. In agreement with Field, Carlyle reported that it was made from cochineal lake [9, 13], while other authors wrote that purple lake is a crimson lake with a purple tone [13].</p> <p>In the spectra D12 and J3 it is possible to recognise the absorptions due to the <math>n \rightarrow \pi^*</math> on the anthraquinone in the 450-550 nm range.</p>
<p><b>J3_purple lake</b></p> 	
<p><b>B1_purple madder</b></p> 	<p>Also called Field's Purple, this pigment is an organic lake obtained from alizarin [6]. The lack of characterising absorptions in the UV-Vis range prevent make any comparison with the other spectra acquired difficult.</p>
<p><b>G11_purple madder</b></p> 	

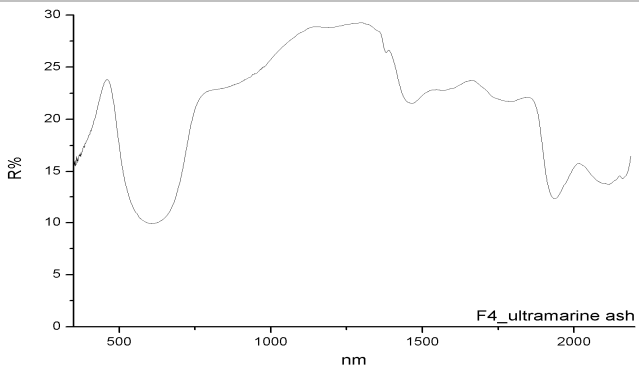
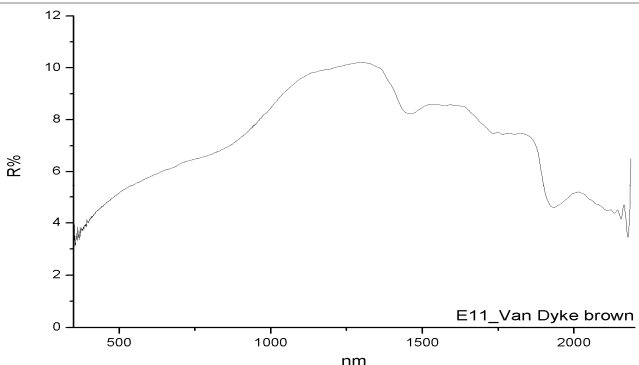
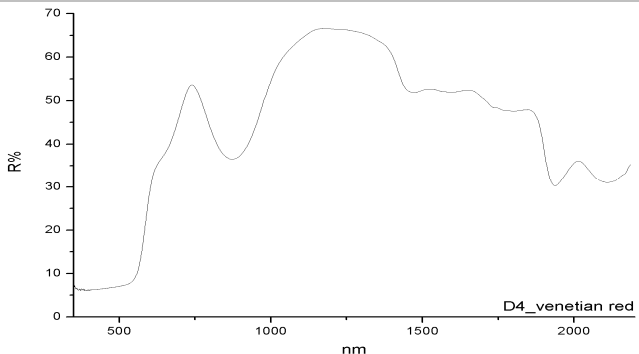
<p><b>E5_raw Sienna</b></p> 	<p>As reported for burnt Sienna (D5), raw Sienna is an earth pigment composed by a mixture of iron oxides and hydroxides. In spectrum E5 the absorption bands at 460 nm, 665 nm and 1000 nm due to iron (III) – iron (III) pair excitation and <i>d-d</i> iron transition are linked to goethite and hematite.</p> <p>The low reflectance values of the curve are not normally detected in raw Sienna, as well as the absorbing behaviour in the NIR region that could be related to the presence of another pigment [20, 21].</p>
<p><b>A9_raw umber</b></p> 	<p>As mentioned before (see C8_burnt umber), raw umber is a mixture of iron oxides and hydroxides with manganese oxides. The colour is lighter than that of burnt umber because of the greater presence of iron hydroxides.</p> <p>The absorptions due to the iron oxides and hydroxides were detected in the spectrum A9.</p>
<p><b>E4_roman ochre</b></p> 	<p>Roman ochre is a yellow ochre, characterised by the presence of goethite (iron hydroxide).</p> <p>In the E4 spectrum absorptions at 490 nm, 650 nm and 950 nm were detected. These features linked to iron (III)–iron (III) pair excitation and <i>d-d</i> iron transition are due to goethite [20, 21].</p>
<p><b>G5_rose madder</b></p> 	<p>Rose madder is an organic pink.</p> <p>In the G5 spectrum it is possible to recognise the absorptions due to the <math>n \rightarrow \pi^*</math> on the anthraquinone in the 450-550 nm range.</p>

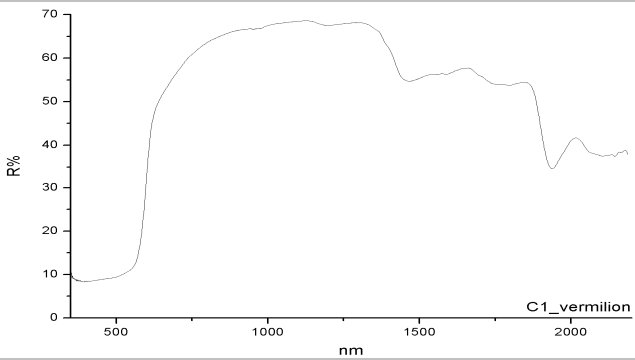
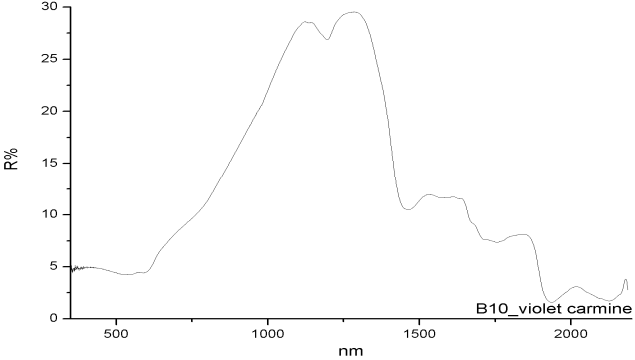
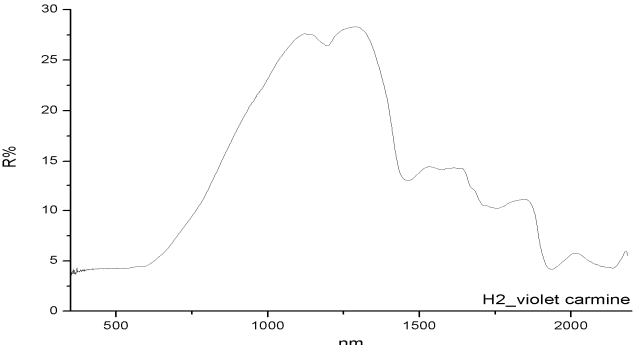
<p><b>C5_Rubens' madder</b></p>  <p>C5_Rubens' madder</p>	<p>Rubens' madder was originally prepared from madder root, but a recipe was found in one of Roberson's books which seems to include also burnt earth [13].</p> <p>The C5 and G1 spectra exhibit the absorption due to the anthraquinone guaranteeing the presence of an organic red. Also, a weak absorption at around 900 nm seems to confirm the presence of an earth pigment.</p>
<p><b>G1_Rubens' madder</b></p>  <p>G1_Rubens' madder</p>	
<p><b>C11_scarlet lake</b></p>  <p>C11_scarlet lake</p>	<p>Scarlet lake is usually refers both to a cochineal lake [6] and a crimson lake [29] prepared by adding vermilion [13].</p> <p>The C11 spectrum shows absorption due to the anthraquinone, so it confirms the presence of a red dye [14]. Moreover, a red pigment characterised by a band-to band transition seems to have been added in order to give more intensity to the colour. This is understandable thanks to the shape of the curve in the red region that exhibits an intermediate behaviour between a red lake and vermilion (F3). However, because of the limitation of FORS technique, the presence of a cadmium red cannot be excluded.</p>

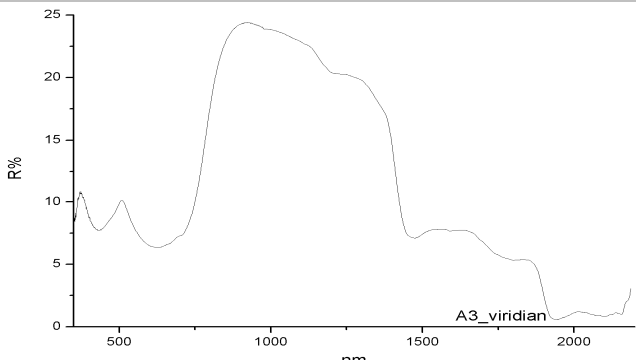
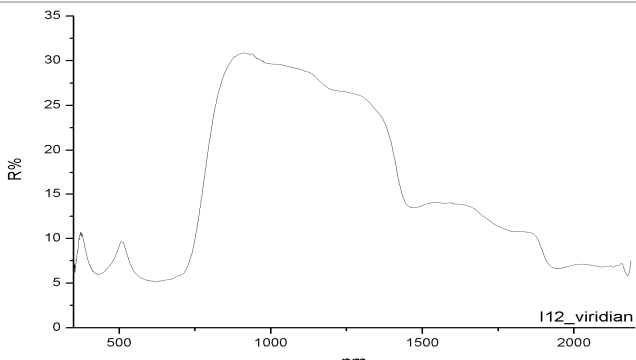
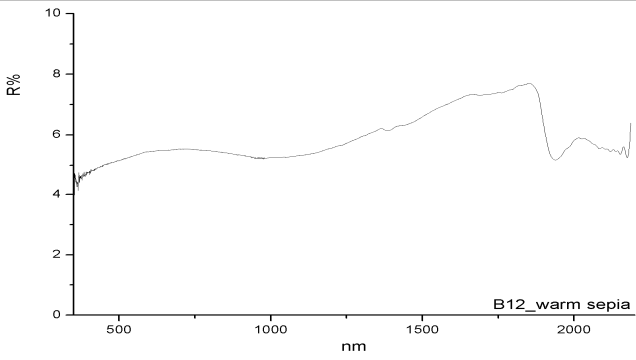
<p><b>F3_scarlet vermilion</b></p>  <p>F3_scarlet vermilion</p>	<p>Vermilion is a red pigment used from antiquity to the present. It was originally obtained from the red mineral called cinnabar (HgS). It was the principal red in paintings until the manufacture of synthetic cadmium red, available as a commercial product from the beginning of the 20<sup>th</sup> century [24].</p> <p>The spectra of F3 and I2 are characterised by a S-shape band due to a band-to-band transition typical of red pigments like vermilion or cadmium red. However, the inflection point localised at around 600 nm cannot be used to distinguish these two pigments, characterised by reflectance spectra which match each other closely [20].</p>
<p><b>I2_scarlet vermilion</b></p>  <p>I2_scarlet vermilion</p>	
<p><b>G8_sepia</b></p>  <p>G8_sepia</p>	<p>Sepia is a brown-blue-black pigment obtained from different species of <i>cephalopoda</i>, like <i>Sepia officinali</i>. It has been used since antiquity but became very important from the 17<sup>th</sup> century when it started to be used in drawings and watercolours on paper [6, 27].</p> <p>Since this dark compound does not present characteristic absorptions in the spectral range of work, it is quite difficult to make an identification of the material by FORS alone.</p>

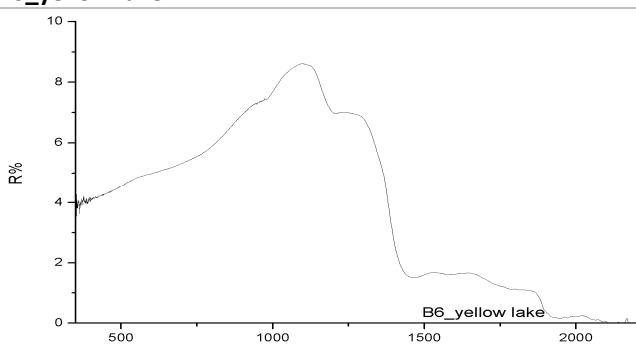
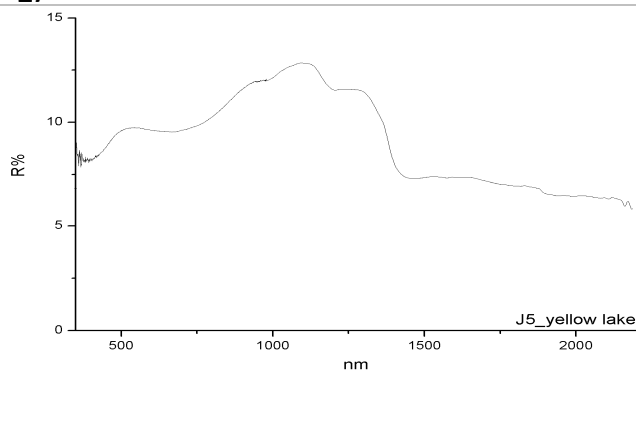
<p><b>C3_smalt</b></p> 	<p>Smalt is composed by potash silicate glass coloured by cobalt oxide (Artist Pigment). Known since the end of the 15th century, it was mainly used in 17<sup>th</sup> and 18<sup>th</sup> centuries.</p> <p>The presence of cobalt (II) in the spectra C3 and H4 is confirmed by the absorption divided into three sub-bands in the 550-650 nm range (better visible in H4's spectra) localised at 530 nm, 590 nm and 640 nm. The strong absorption in the NIR region is due to the tetrahedral coordination of the cobalt ion with respect to the ligands [32].</p>
<p><b>H4_smalt</b></p> 	
<p><b>A4_terre verte</b></p> 	<p>Field reported that terre verte was an ochre of a greenish colour. It was also called Verona Green. [6] Green earths are usually made up of two aluminosilicate minerals like glauconite and celadonite. [33]</p> <p>The A4 spectrum could not be referred to green earth [14] because the absorptions due to iron ions are not visible. Instead, the curve shows a behaviour very similar to that of a blue pigment, such as indigo or ultramarine, in the 350-680 nm range. The low reflectance values in the red and NIR region suggest that a black pigment was added.</p>



<p><b>F4_ultramarine ash</b></p>  <p style="text-align: right;">F4_ultramarine ash</p>	<p>Ultramarine ash is a pigment obtained by the refinement of Lapis Lazuli. The colour of this material is usually less intense than ultramarine blue, with a tendency to grey. Field added that by mixing ultramarine with a black and a white pigment the effect was the same as ultramarine ashes [6].</p> <p>The F4 spectrum shows the characteristic behaviour of ultramarine blue, with a reflectance maximum at 460 nm and an absorption at around 610 nm due to a CT transition on the ion <math>S^{3-}</math>. Moreover, the presence of a black pigment can be excluded because of the high reflectance of the curve in all the ranges analysed, typical of ultramarine blue.</p>
<p><b>E11_Van Dyck brown</b></p>  <p style="text-align: right;">E11_Van Dyck brown</p>	<p>Van Dyck brown is a sort of peat brown earth very similar to Cassel hearth [6]. It is an organic woody material obtained from plant decomposition [24].</p> <p>The E11 spectrum is characterised by a low reflectance value, typical of dark pigments.</p>
<p><b>D4_venetian red</b></p>  <p style="text-align: right;">D4_venetian red</p>	<p>Field reported that although Venetian red was supposed to be a natural ochre[6], it was often artificially prepared by calcining green vitriol copperas red [13].</p> <p>The D4 spectrum presents the absorptions typical of hematite (see B2, light red).</p>

<p><b>C1_vermilion</b></p>  <p>The graph shows the IR spectrum for C1_vermilion. The y-axis is labeled 'R%' and ranges from 0 to 70. The x-axis is labeled 'nm' and ranges from 500 to 2000. The spectrum shows a broad absorption band starting around 500 nm, reaching a maximum transmittance of about 65% between 1000 and 1500 nm. There is a sharp dip at approximately 1900 nm, and another smaller dip at about 2100 nm.</p>	<p>See Scarlet Vermilion (F3 and I2).</p> <p>The C1 spectrum exhibits the characteristic features of vermilion.</p>
<p><b>B10_violet carmine</b></p>  <p>The graph shows the IR spectrum for B10_violet carmine. The y-axis is labeled 'R%' and ranges from 0 to 30. The x-axis is labeled 'nm' and ranges from 500 to 2000. The spectrum shows a broad absorption band starting around 500 nm, reaching a maximum transmittance of about 28% between 1000 and 1500 nm. There is a sharp dip at approximately 1900 nm, and another smaller dip at about 2100 nm.</p>	<p>Violet carmine is an organic pigment prepared from the roots of <i>Anchusa tinctoria</i>. It seems that all the authors of the period agree with this definition, except for Sewar, who lists it as derived from cochineal [13].</p> <p>The B10 spectrum shows the absorption due to anthraquinone, as already reported for the D9 sample (brown madder). So, it suggests the presence of an organic red-purple dye.</p>
<p><b>H2_violet carmine</b></p>  <p>The graph shows the IR spectrum for H2_violet carmine. The y-axis is labeled 'R%' and ranges from 0 to 30. The x-axis is labeled 'nm' and ranges from 500 to 2000. The spectrum shows a broad absorption band starting around 500 nm, reaching a maximum transmittance of about 28% between 1000 and 1500 nm. There is a sharp dip at approximately 1900 nm, and another smaller dip at about 2100 nm.</p>	

<p><b>A3_viridian</b></p>  <p>R%</p> <p>nm</p> <p>A3_viridian</p>	<p>Viridian is a hydrated chromium (III) oxide and it was first prepared in 1838 by the colour maker Pennetier. Widely used by the Impressionists by the end of the 19<sup>th</sup> century, viridian was included in the Winsor and Newton catalogue in 1869 [9].</p> <p>Since the chemical nature of viridian is very close to the composition of green chromium oxide, the spectral curves of these pigments are very similar, (See A6_green oxide of chromium), but viridian can be recognised thanks to its lower opacity in the NIR region.</p>
<p><b>I12_viridian</b></p>  <p>R%</p> <p>nm</p> <p>I12_viridian</p>	
<p><b>B12_warm sepia</b></p>  <p>R%</p> <p>nm</p> <p>B12_warm sepia</p>	<p>Like Sepia, warm sepia is an organic brown-black pigment derived from the ink sac of different species of cephalopoda, like <i>Sepia officinalis</i>, that was the one most frequently used for this purpose [6, 13, 19].</p> <p>The B12 spectrum differs from G8_sepia spectrum because of the presence of a weak but broad absorption band centred at around 1000 nm. This behaviour can be due to the addition of an earth in order to create a specific colour effect or to give more body to the pigment.</p>

<p><b>B6_yellow lake</b></p>  <p>The graph shows the reflectance spectrum for B6_yellow lake. The y-axis is labeled 'R%' and ranges from 0 to 10. The x-axis is labeled 'nm' and ranges from 0 to 2000. The curve starts at approximately 4% reflectance at 400 nm, rises to a broad peak of about 8.5% at 1100 nm, and then drops sharply to near 0% by 1500 nm. A small label 'B6_yellow lake' is present in the bottom right corner of the plot area.</p>	<p>Yellow lake is an organic yellow pigment, reported both as Quercitron lake and Italian pink ([6, 13].</p> <p>If compared with Italian pink's spectra (F5 and J4), these can be considered similar except for the reflectance maximum at 520 nm, more evident in the J5 sample.</p>
<p><b>J5_yellow lake</b></p>  <p>The graph shows the reflectance spectrum for J5_yellow lake. The y-axis is labeled 'R%' and ranges from 0 to 15. The x-axis is labeled 'nm' and ranges from 0 to 2000. The curve starts at approximately 8% reflectance at 400 nm, rises to a broad peak of about 13% at 1100 nm, and then gradually declines to about 6% at 2000 nm. A small label 'J5_yellow lake' is present in the bottom right corner of the plot area.</p>	

#### 5.4- Conclusions

The production of a spectral database of historical materials could be very useful in studying works of art from the same period and made with the specific materials analysed.

Assuming that the pigments found in the box are all from the same period, and no pigments were added over time, it is possible to hypothesise an approximate date of the material analysed just using the well known information about the history of the pigments. For example, in this case, the presence of Aureolin, Viridian and Purple madder instead of Perylene Violet date the watercolours box between 1870 and the beginning of the 20<sup>th</sup> century.

FORS allowed to analyse the watercolours without sampling. From the spectra it was possible to verify or identify the chemical composition of many of the pigments. In some specific cases, FORS analysis was not capable of providing useful information: for example, it is not possible to identify black pigments because of the absence of any characteristic absorption bands. Moreover, several difficulties were met in the study of organic materials, such as red, purple and yellow colorants. In these cases, FORS does not provide additional information about the nature (whether vegetal or animal) of the substances.

FORS provided information on the presence of additional compounds such as hematite in Dragon's blood (F2 and I1 samples) and a cobalt-based pigment in Neutral tint (E7 and H5 samples). Gypsum was clearly detected only in Penley's neutral orange (J10).

Other interesting information achieved by FORS concern the presence of a binder different from vegetal glue, that probably was added in order to improve the performances of the watercolours, and the presence of a clay mineral, probably used to give more body to amorphous materials or materials characterised by a thinner granulometry, such as black-dark watercolours.

This spectral collection of specific and dated materials may allow the characterisation of 19<sup>th</sup> century watercolours by comparison of the reflectance spectra.

## References

1. Winsor and Newton, Catalogue of materials for water colours painting, and sketching, pencil and chalk drawing, London 1849.
2. Winsor and Newton, Manufacturing Artists' Colourmen, Trade catalogue, London, 1863.
3. Winsor and Newton, Manufacturing Artists' Colourmen, Trade catalogue, London, 1896.
4. A. Penley, A system of Watercolour Painting, Arliss and Tucher Printers, London, 1850.
5. M. P. Merrifield, Practical direction for Portrait Painting in water-colours, London, 1851.
6. G. Field, Chromatography or a Treatise on Colours and Pigments and of their Powers in Painting, Mays and Barclay Printers, 1941.
7. <http://www.winsornewton.com> last accessed 21<sup>th</sup> September 2010.
8. A. Gioli, Proc. of Effetto Luce, materiali tecnica e conservazione della pittura italiana del'Ottocento, Firenze, 2009, 51.
9. L. Carlyle, The Artist Assistant. Oil Painting Instruction Manuals and Handbooks in Britain 1800-1900 with reference to selected 18<sup>th</sup>-century sources, Archetype Publications, London, 2001.
10. B. A. Ormsby, J. H. Townsend, B. W. Singer, and J.R. Dean, Studies in Conservation, 50 (1), 2005, 45.
11. G. Piva, Enciclopedia-Ricettario per tutti gli artisti pittori dilettanti-allievi delle Accademie e Scuole di belle arti, ed. Hoepli, Milano, 1959.
12. L. G. Weyer, and S.-C. Lo, Spectra-Structure Correlations in the Near-infrared, in Handbook of Vibrational Spectroscopy, Vol.3, John Wiley & Sons (Eds.), U.K., 2002, 1817.
13. N. Eastaugh, V. Walsh, T. Chaplin, and S. Ruth, Pigment Compendium A Dictionary of historic pigments, Oxford University Press, Butterworth-Heinemann, New York, 2004.
14. <http://fors.ifac.cnr.it/> last accessed 20<sup>th</sup> December 2010.
15. M. Cornman, Cobalt Yellow (Aureolin), in Artists' Pigments, A Handbook of their History and Characteristics, Vol. 1, R. Feller (Ed), Cambridge University Press, Cambridge, 1986, 37.
16. A. H. Church, The chemistry of paints and painting, Seeley, Service & Co, London, 1915.
17. L. Campanella, A. Casoli, M. P. Colombini, R. Marini Bettolo, M. Matteini, L. M. Mignesco, A. Montenero, L. Nodari, C. Piccioli, M. Plossi Zappalà, G. Portalone, U. Russo, and M. P. Sanmartino, Chimica per l'arte, Zanichelli Editore, 2007.
18. C. Bisulca, M. Picollo, M. Bacci, and D. Kunzelman, UV-Vis-NIR reflectance spectroscopy of red lakes in paintings, in Proceedings of the 9<sup>th</sup> International Conference on Non-destructive investigations and microanalysis for the diagnostics and conservation of cultural and environmental heritage, Jerusalem, 2008.
19. A. Casoli, M. E. Darecchio, and L. Sarritzu, I coloranti nell'arte, Il Prato editore, Padova, 2010.
20. M. Bacci, Modern Analytical Methods in Art and Archaeology, Chemical Analysis Series, E. Ciliberto, and G. Spoto (Eds.), John Wiley & Sons Inc., New York, 155, 2000, 321.
21. M. Elias, C. Chartier, G. Prevot, H. Garay, and C. Vignaud, materials science and Engineering B 127, 2006, 70.
22. I. Fiedler, and M. Bayard, Cadmium Yellows, Oranges, and Reds, in Artists' Pigments, A Handbook of their History and Characteristics, Vol. 1, R. Feller (Ed.), Cambridge University Press, Cambridge, 1986, 37.

23. <http://www.webexhibits.org/pigments> last accessed 20<sup>th</sup> December 2010.
24. M. Matteini, and A. Moles, *La chimica nel restauro. I materiali dell'arte pittorica*, Nardini Editore, Firenze, 2003.
25. K. Nassau, *The Physics and chemistry of Color*, J. W. Goodman (Ed.), John Wiley & Sons, New York, 1983.
26. G. R. Hunt, J. W. Salisbury, and C. J. Lenhoff, *Modern Geology*, 3, 1971, 1.
27. T. B. Brill, *Light, Its Interaction with Art and Antiquities*, Plenum Press, New York, 1980.
28. .M. Shimoyama, S. Hayano, K. Matsukawa, H. Inoue, and T. Ninomiya, *Journal of Polymer Science: Part B: Plymer Physics*, 36, 1998, 1529.
29. J. Winter, Gamboge, in *Artists' Pigments, A Handbook of their History and Characteristics*, Vol. 3, E. W. Fitzhugh (Ed.), Oxford University Press, New York, 1997, 143.
30. N. S. Bear, A. Joel, R. L. Feller, and N. Indictor, Indian Yellow, in *Artists' Pigments, A Handbook of their History and Characteristics*, Vol. 1, R. Feller (Ed.), Cambridge University Press, Cambridge, 1986, 17.
31. T. Rowbotham, *The art of Landscape in watercolours*, London, 1850.
32. M. Bacci, and M. Picollo, *Studies in Conservation*, 41, 1996, 136.
33. C. A. Grissom, Green Earth, in *Artists' Pigments, A Handbook of their History and Characteristics*, Vol. 3, E. W. Fitzhugh (Ed.), Oxford University Press, New York, 1997, 141.





## Conclusions

The recent need to deal with 19<sup>th</sup> century works of art stems from a lack of knowledge about materials which results in an incomplete understanding of the artistic production of that period. Consequently, the development of effective conservative intervention can also be a particularly sensitive issue to address. The main goal of this thesis was to increase the amount of information of 19<sup>th</sup> century materials, by using a non-invasive scientific approach on the study of *Macchiaioli* artworks, expressly prepared laboratory muck-ups, and original pigments.

Non-invasive spectroscopic techniques in the Ultraviolet-Visible-Near Infrared spectral range showed themselves to be an excellent investigative tool for the study of 19<sup>th</sup> century works of art thanks to their capability to identify materials and provide useful information on artistic techniques. The multidisciplinary approach followed in this work during the analysis of *Macchiaioli* paintings allowed for clarification or confirmation of the hypotheses advanced by studying the spectral behaviour of the pictorial layers. The use of point by point techniques, such as FORS or XRF, together with imaging spectroscopy, allowed the results obtained in located spots to be extended to areas with similar reflectance behaviour. On the other hand, spectroscopy techniques cannot be used for the analysis of black-dark pigments, which present featureless reflectance curves. Equally, some identification problems were met when complex mixtures were taken into account. In these cases, spectroscopy usually can rightly detect some of the components, therefore, the personnel in charge of the painting and/or of the conservative treatment should evaluate if further analysis, such as chemical investigations, must be performed. In fact, the collaboration and an ongoing dialogue with various professionals, such as conservation scientists, conservators and art historians, is essential for a better understanding of the test piece and to direct the investigation.

In order to improve the results obtainable with FORS technique a detailed and rich reference database should be available. The database should contain both pure and mixed pigments' spectral curves in order to study how the pigments' features vary when they are mixed with other materials. In the present work the focus was on green pigments and in particular on copper-based green and chromium oxide. Regarding the latter, it was shown that the mixture with white and yellow pigments does not influence some spectral features, which was useful for the identification of the green compound. The databases should be diversified on the basis of the material taken into account (oil pigments, acrylic pigments, watercolours, inks, etc.) in order to be able to make a comparison between reflectance spectra as similar as possible to those acquirable on a case-study. In this context, the possibility to create a FORS database of historic watercolours became a wonderful research opportunity on original 19<sup>th</sup> materials not easily available. Where it was possible, a pigments' identification was also conducted in order to confirm the chemical compositions of the pigments.



## Acknowledgments

It is a pleasure to thank those who made this thesis possible: my tutors, Prof. Ferruccio Petrucci from the University of Ferrara and Prof. Marcello Picollo from IFAC-CNR in Florence for their continual support and advice throughout this PhD. A special thanks to Marcello who gave me several opportunities for my professional growth during my stay at the IFAC-CNR.

I would like to thank Muriel Vervat, the conservator who allowed me to analyse the Macchiaioli's paintings and taught me to really appreciate this artistic trend and Anna Maria Giusti, the current director of the Galleria d'arte moderna of Florence in Palazzo Pitti, who made the artworks available for analysis.

I owe my deepest gratitude to Lucia Burgio and all the staff of the Science Section - Conservation Department at the V&A for allowing me to analyse the 19<sup>th</sup> century W&N watercolour set. A special thanks to Lucia Burgio, who is a passionate researcher and a friend who was always available to read and correct this thesis and gave me interesting suggestions.

It is an honour for me to thank Mauro Bacci, Andrea Casini, Costanza Cucci, Bruno Radicati, Lorenzo Stefani, Marcello Picollo and Marco Poggesi from the IFAC-CNR for scientific discussions, advice and for the years spent working together. A special thanks to Bruno Radicati, who shared his office with me and always helped me solve my innumerable problems. I have appreciated the help from Alessandro Agostini and Saverio Priori in solving my never-ending computer problems.

I am also grateful to Monica Favaro from ICIS-CNR in Padua for making the image of the sample from *Carica di Cavalleria* available, Alessandro Migliori from INFN in Florence, Dario Vaudan from Regione Autonoma Valle d'Aosta, and Anna Piccirillo from Centro di Conservazione "La Venaria Reale" for acquiring the XRF data used in Chapter 3. I am grateful to Masaiko Tsukada from the Metropolitan Museum of Art, who made the pure pigment mock-ups, to Giulia Basilissi, Serena Carlesi, and Lorenzo Ciofi from the University of Florence who prepared the binary mock-ups analysed in Chapter 4. I would like to show my gratitude to Donata Magrini from ICVBC-CNR in Florence for providing me with the sample of gum Arabic analysed for the watercolour project reported in Chapter 5.

Furthermore, I would like to thank Mady Elias from Institut des NanoSciences de Paris and Sharon Cather from the Courtauld Institute in London, respectively my supervisors during my stay in Paris and my first stay in London. I would like to thank Giovanni Verri from University College London for providing very useful comments about my PhD work.

It is a pleasure to thank Fauzia Albertin, Virginia Pellicori, Eva Peccenini, Ferruccio Petrucci and Flavia Tisato for welcoming me into their research group at the INFN in Ferrara and giving me friendship and encouragement throughout the last months of this thesis.

Finally I would like to express my love and appreciation for my family for always supporting me.





Your E-Mail Address

lara.boselli@gmail.com

Subject

Dichiarazione di conformità con richiesta di embargo tesi

Io sottoscritto Dott. (Cognome e Nome)

Boselli Lara

nato a

Bentivoglio

Provincia

Bologna

il giorno

19/11/1982

avendo frequentato il corso di Dottorato di Ricerca in:

Scienze e Tecnologie per l'Archeologia e i Beni Culturali

Ciclo di Dottorato

XXIII

Titolo della tesi in Italiano

Studio spettroscopico non invasivo di materiali artistici del XIX secolo

Titolo della tesi in Inglese

Non-invasive spectroscopic study of 19th century artists' materials

Titolo della tesi in altra Lingua Straniera

Tutore - Prof:

Ferruccio Petrucci

Settore Scientifico Disciplinare (SSD)

FIS/01

Parole chiave (max 10)

non-invasive spectroscopy pigments Macchiaioli paintings

Consapevole - Dichiaro

CONSAPEVOLE --- 1) del fatto che in caso di dichiarazioni mendaci, oltre alle sanzioni previste dal codice penale e dalle Leggi speciali per l'ipotesi di falsità in atti ed uso di atti falsi, decade fin dall'inizio e senza necessità di alcuna formalità dai benefici conseguenti al provvedimento emanato sulla base di tali dichiarazioni; -- 2) dell'obbligo per l'Università di provvedere al deposito di legge delle tesi di dottorato al fine di assicurarne la conservazione e la consultabilità da parte di terzi; -- 3) della procedura adottata dall'Università di Ferrara ove si richiede che la tesi sia consegnata dal dottorando in 4 copie di cui una in formato cartaceo e tre in formato .pdf, non modificabile su idonei supporti (CD-ROM, DVD) secondo le istruzioni pubblicate sul sito : <http://www.unife.it/dottorati/dottorati.htm> alla voce ESAME FINALE – disposizioni e modulistica; -- 4) del fatto che l'Università sulla base dei dati forniti, archiverà e renderà consultabile in rete il testo completo della tesi di dottorato di cui alla presente dichiarazione attraverso l'Archivio istituzionale ad accesso aperto "EPRINTS.unife.it" oltre che attraverso i Cataloghi delle Biblioteche Nazionali Centrali di Roma e Firenze. --- DICHIARO SOTTO LA MIA RESPONSABILITA' --- 1) che la copia della tesi depositata presso l'Università di Ferrara in formato cartaceo, è del tutto identica a quelle presentate in formato elettronico (CD-ROM, DVD), a quelle da inviare ai Commissari di esame finale e alla copia che produrrà in seduta d'esame

finale. Di conseguenza va esclusa qualsiasi responsabilità dell'Ateneo stesso per quanto riguarda eventuali errori, imprecisioni o omissioni nei contenuti della tesi; -- 2) di prendere atto che la tesi in formato cartaceo è l'unica alla quale farà riferimento l'Università per rilasciare, a mia richiesta, la dichiarazione di conformità di eventuali copie. --- PER ACCETTAZIONE DI QUANTO SOPRA RIPORTATO

Dichiarazione per embargo

36 mesi

Firma Dottorando

Ferrara, lì \_\_\_\_\_ Firma del Dottorando

Firma Tutore

Visto: Il Tutore Si approva Firma del Tutore

\_\_\_\_\_